ANALYTICAL MODELLING OF THE PERFORMANCE OF A SNOW DEPOSIT UNDER PLATE LOADING

by

A.J. MURCIA

A Thesis submitted to the Faculty of Graduate Studies and Research in partial fulfillment of the requirements for the Degree of Master of Engineering

Department of Civil Engineering and Applied Mechanics
McGill University
Montreal, Quebec

October 1987

ABSTRACT

The purpose of this study is to develop an analytical technique for predicting the response of a deep snow layer under a rigid strip footing. The study is limited in scope to the verification of the validity of the application of an analytical/computer model to simulate the process of footing penetration into a deposit of deep snow.

The model is based on the finite element technique suitably adapted to take into consideration the high compressibility of the material and the progressive shear failure mechanism developed during the footing penetration process. The solution obtained using this model provides displacement fields and density distribution beneath the footing, the depth of shear along failure planes as well as the stress-sinkage relationship of the footing.

The validity of the proposed model is verified through a comparison of predicted and experimentally obtained results. Most results obtained from the finite element model are found to be in reasonably good agreement with the experimental data while some discrepancies are found to exist between specific types of results.

RESUME

L'objectif de cette étude est de trouver un moyen analytique rationnel pour prédire le comportement d'un dépôt de neige profonde soumis à une charge. La portée de cette étude se limite à la vérification d'un modèle analytique adapté pour l'ordinateur et utilisé pour l'analyse d'un socle rigide pénétrant le dépôt de neige.

Le modèle est basé sur la technique des éléments finis laquelle est adaptée pour le cas présent afin d'inclure l'effet de la grande compressibilité de cette substance et du mécanisme de cisaillement progressif, qui se développe sur deux plans verticaux pendant la pénétration du socle. La solution ainsi obtenue prédit les champs de déformation et la distribution de densité sous le socle, la profondeur du mécanisme de cisaillement vertical et enfin, la relation pression-pénétration du socle.

La validité du modèle proposé est vérifiée à travers d'une comparaison en général favorable des valeurs expérimentales et prédites par le modèle des paramètres mentionnés ci-haut.

ACKNOWLEDGEMENTS

The author expresses his sincere appreciation to:

1. Dr. R.N. Yong, William Scott Professor of Civil Engineering and Applied Mechanics, for his constant encouragement and sustained guidance which he so readily extended throughout this investigation.

2. Mr. N. Sciadas, Dr. P. Boonsinsuk for their helpful advice and stimulating discussions.

3. Mr. F. Caporuscio and Mr. K. Shikatani for their useful discussions and technical help.

4. Mr. J. Sellappah and Mr. C. Ludwig for their assistance in preparing this dissertation.

5. Mr. I. Metaxas for his help during the laboratory testing.

6. My wife for typing this dissertation.

7. My parents for their constant encouragement and help during the course of this study.

TABLE OF CONTENTS

LIST OF FIGURES

LIST OF TABLES

CHAPTER 1

INTRODUCTION

1.1 Nature of Snow

The mechanics of snow formation and precipitation is a complex subject involving many factors and is governed by the laws of physics, chemistry, thermodynamics as well as by meteorological conditions. In general, snow precipitation occurs provided sufficient atmospheric moisture is present in the air and that the climatic environment is suitable to initiate and maintain mechanisms by which this moisture is converted into snowfall. Condensation of water vapour in the atmosphere results into the formation of a cloud within which, provided the temperature drops below freezing, droplets joint to generate ice crystals. Continued growth of an ice crystal leads to the formation of a snow crystal, which is a particle sufficiently large to be visible to the naked eye. A snowflake is produced as a result of aggregation of several hundreds of snow crystals. Snowflake sizes vary from a fraction of a millimeter to several centimeters. Normally, larger snowflakes are generated when the ambient temperature is near 0° C and size decreases with decreasing temperature (Hobbs, 1973).

The accumulation of snow flakes on the ground leads to the generation of the snowcover. Evidently, characteristics of the snow-cover, such as crystalline structure and density, are highly controlled by the type of weather during precipitation (i.e, temperature, wind speed, humidity, etc) and are likely to change with time according to the meteorological conditions prevailing after deposition. Properties of the snow-cover such as strength, stiffness and density are of particular interest to transportation engineers concerned with travel over snow in northern countries. Transportation of supplies and goods to remote communities, mines, construction sites, etc, is heavily dependent on the efficiency of oversnow vehicles. Proper design of such vehicles requires not only a sound mechanical engineering basis but adequate understanding of the response of snow under loading. Since engineering design essentially and inevitably involves a mathematical idealization of the real problem at hand, the problem of analytically describing the behaviour of snow under loading arises. The present study addresses this problem and is a humble attempt to develop a technique for the mathematical/numerical simulation of the response of snow under set loading conditions.

1.2 Summary of the General Problem

1.2.1. The Scientific Problem

The scientific problem addressed in the present study consists in the prediction of the load-penetration response of a rigid footing penetrating into a deep snow deposit. The term "deep snow" generally applies when the thickness of the snow layer is greater than the largest dimension of the loaded area at the surface. The material is assumed to be a continuum exhibiting the following characteristics:

a) large deformation behaviour

b) highly compressible

c) weightless

d) the material fails according to the so-called local shear failure mode rather than the general shear failure mode

e) stress path dependent

f) strain rate dependent

g) compressibility is inversely proportional to density (i.e, stiffening type of stress-strain curve under purely axial compression loading)

h) negligible lateral expansion under purely axial compression loading (i.e, Poisson's ratio is approximately zero).

i) shear strength is governed by the strength of bonds between particles.

1.2.2. The Engineering Problem and its Complexity

Various subjects on snow mechanics have been studied over the years in order to develop a methodology to analyze and predict the stability of a snow mass and its response when subjected to external loading. Respective examples are avalanche prediction, which has been studied by Perla and Martinelli (1976) and Fraser (1978), and over-snow travel problems for which Harrison (1975), Yong (1979) and Brown (1979) have proposed approaches and solution techniques. Strength analyses of snow are difficult because of the nature of the material at hand but a theoretical evaluation has been proposed by Ballard and McGraw (1965).

In the proposed study, the problem is concerned with the evaluation of the response of relatively loose material which, when loaded by a rigid footing, fails according to a punching shear type of mechanism. The difficulties associated with such analysis pertain to both obtaining useful and reliable experimental data as well as to the theoretical formulation of the problem. Non-homogeneity is more severe for snow than for most soils due to the high thermodynamic activity of snow particles. Non-uniformity of grain packing and hence density complicates characterization. Experimental data, such as compressibility and shear strength, must be obtained from tests on samples whose replication is complicated by the variable nature of the material. Engineering properties of samples prepared for the different tests varied somewhat according to the ambient temperature, humidity and other factors that can potentially affect the formation of the material. In addition, non-uniform density distribution in the snow boxes arising from self-weight of the material may have been a factor against any kind of idealization of the problem.

As can be expected, the mathematical idealization of the problem is complicated by the fact that the desired objective is not ti calculate a limit state condition, such as the bearing capacity failure of soil under a footing, but rather to simulate the entire process of penetration of the footing into the snow. A lack of information, quantitatively describing the kinematics of the problem, exists and, although a qualitative description of the penetration mechanism is available from past experience, this is not sufficient to develop mathematical expressions representing the process from beginning to end. The approach adopted in this study was oriented in such a way that the kinematics of the problem would be a <u>result</u> (rather than an input) of a procedure developed to predict displacement fields, density distribution etc, as a function of footing penetration. Similarly, reaction forces on the footing and stress fields within the snow mass would also be quantified. The success of the analytical formulation used to represent the problem at hand would also heavily depend on the incorporation of appropriate material properties in the above procedure.

The step by step approach of the problem thus implied the need to adopt some kind of numerical simulation scheme designed to be easily handled by a computer. Some of the work accomplished in the present study was thus devoted to investigate possible variations of existing numerical methods that required input parameters which could be obtained through experiments specifically designed for the problem at hand but easily implemented in practice.

1.3 Purpose of the Study

Increasing interest in the evaluation of vehicle flotation capability and performance on snow covered terrain constitutes the main motivation for the present study. The behaviour of the snow material under static loading and transient vehicle tractive loads is the subject of study of a research program currently in operation at the

Geotechnical Research Centre of McGill University. The present work can thus be considered as the first step in the development of a rational method of analysis for assessing vehicle performance of snow. Its specific purpose is to predict the load-deformation behaviour of a snow deposit loaded by a rigid strip footing and to identify the engineering properties required for the analysis.

In addition, the value of the developed analytical/computer model can be further appreciated if one realizes that the applicability of the proposed general solution technique can be, in theory, extended to soil materials such as certain types of unsaturated clays, slurries, etc., exhibiting a significant degree of compressibility and a low value of Poisson's ratio.

Furthermore, it becomes obvious from the arguments presented in Chapter 2 that the present study considers a problem resemblant to that of the analysis of a footing failing by the local or "puching shear" mechanism (Fig. 1.1a) rather than by the general shear failure mode (Fig. 1.1b) proposed by Terzaghi which assumes the material to be incompressible. The solution scheme developed in the present work may therefore provide useful guidance on how to attack such a problem.

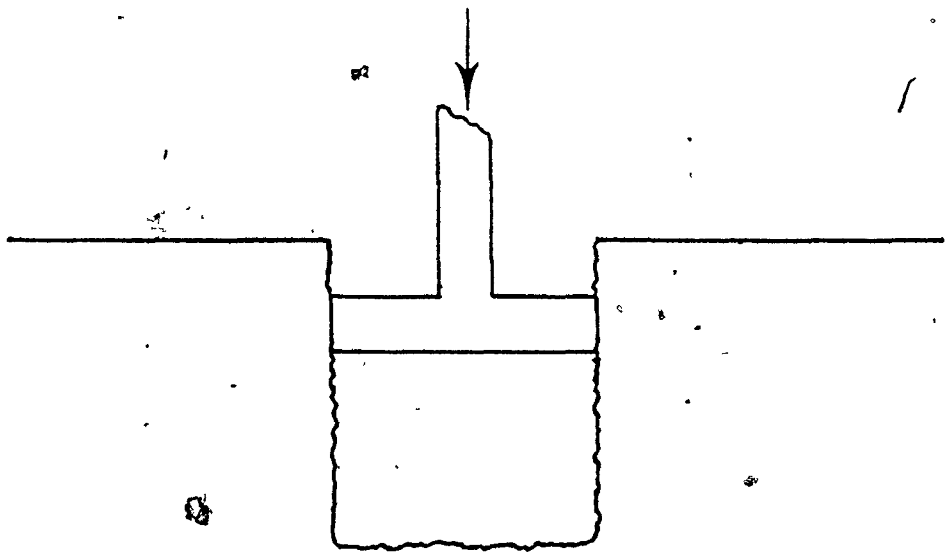

Fig. 1.1a Punching Shear Failure Mechanism

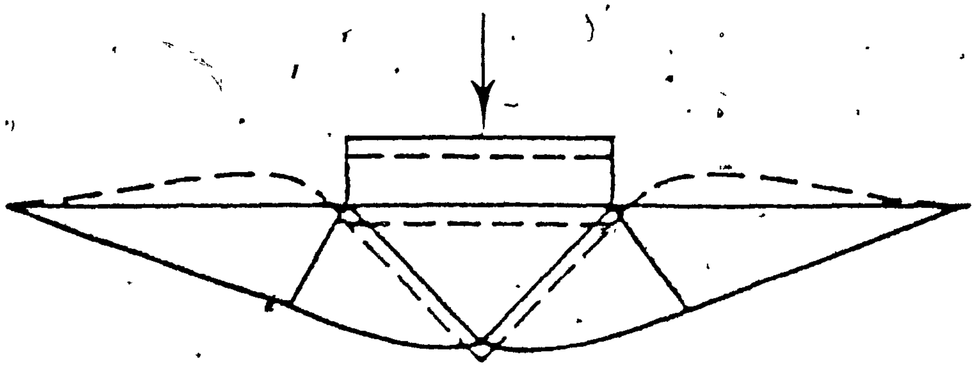

Fig. 1.1b General Shear Failure Mechanism

1.4 Scope of the Study

The scope of this study extends to the development and validation of a computerized mathematical model predicting the load-sinkage relationship of a rigid strip footing on deep snow. The creation of such a model focused on the volume change and shear characteristics of the material and their relationship to the overall behaviour under plate loading conditions. As shown in Fig. 1.2, it therefore became necessary to obtain information on the response of snow under the following conditions:

a) volume change only

b) shear only

c) combination of both volume change and shear occurring simultaneously.

The confined compression test was the obvious choice for investigating the volume change behaviour or compressibility of the snow (condition a above) whereas the direct shear test was selected to characterize the material response in pure shear (condition b above). The rigid plate, or footing test, was performed in order to assess the validity of the model through a comparison of experimentally obtained curves and those predicted by the computer model based on the properties of the snow material in compression and shear. The schematic diagram in Fig. 1.2 illustrates the relation between the method of analysis and the experimental program adopted in this study.

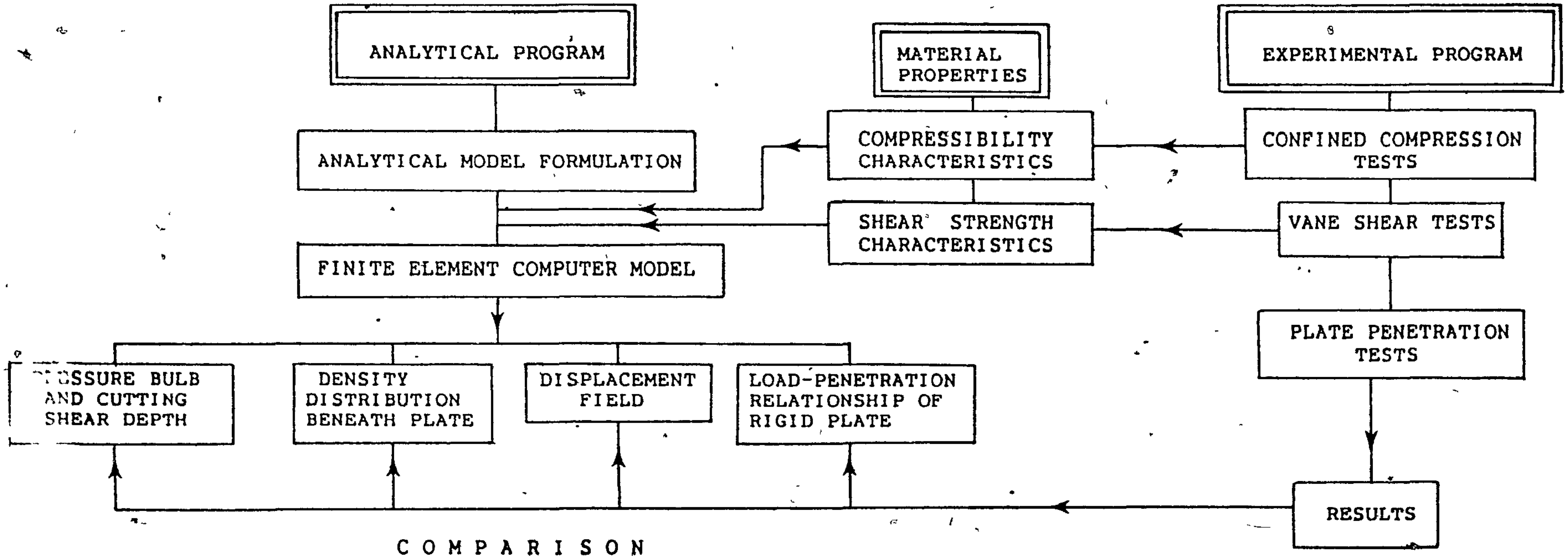

Fig. 1.2 Analytical and Experimental Programs in Present Study

For purposes of rationalization of the analysis as well as for minimization of unknown factors entering the problem, plate penetration tests were perfomed using a narrow box so that plane strain conditions could be assumed in the analysis and, consequently, to allow the development of the analytical/computer formulation and solution on a two dimensional basis. In addition, all tests were performed at the same (constant) rate so that a relationship between the three types of tests could be established. The strain rate selected for the tests was sufficiently high to cause the so-called brittle behaviour of snow described by Fukue (1977) and schematically represented in Fig. 1.1a.

The parameters pertinent to plate penetration performance in the present study solely concern snow material response; ageing time, density, stress-strain response in confined compression and shear. Rigid plate parameters such as size and penetration speed are kept constant.

1.5 Analysis of the Problem

The analytical prediction of the load-penetration curve of a rigid footing on snow is a complex problem involving a series of stress analyses of a highly compressible material under a given set of boundary conditions. The determination of stresses and deformations within a mass of material is a highly statically indeterminate problem, the solution of which requires statisfying the following conditions as dictated by basic mechanics of materials:

1) Equilibrium of the mass is maintained.
2) Compatibility of deformations (i.e, deformation field is continuous within the mass and is geometrically consistent with the imposed boundary conditions).
3) The constitutive relationship (or equations of material behaviour) is respected at any point within the mass.

In so far as the material is assumed to be a continuum, the solution of the problem can be investigated through continuum mechanics. The classical theory of linear elasticity constitutes a powerful tool for solving many of such problems. The method is purely analytical and consists in solving equations of stress with a particular set of boundary conditions. The above theory involves many assumptions regarding the behaviour of the material under study. The most significant are:

a) the material is isotropic and homogeneous
b) the material is linear elastic
c) small strain theory applies
d) the deformation field is continuous such that no gaps or relative displacements between parts of the body occur.

The analytical solution of continuum mechanics problems is only possible for simple cases of loading and boundary conditions. The problem of determining the load-sinkage response of a footing in the type of deep snow considered in this study is already complicated by the presence of shear stresses along the sides of the pressure bulb generated by the plate penetration process. Moreover, the deformation field along the sides of the bulb is not continuous due to the differential vertical displacement of points on either side of the planes of shear. Assumption "d" above therefore automatically rules out the possibility of using classical elasticity as a solution procedure. The fact that the material is highly compressible and that large deformations occur during the plate penetration process also opposes assumption "c". In addition, snow is a non-linear material whose stiffness increases with volumetric strain and therefore, in this case, assumption "b" is violated. Finally, it is also evident that no material is perfectly isotropic and homogeneous but assumption "a" is a justification always applied for idealization for these types of problems.

In light of the above, it is obvious that simulation of the plate penetration process cannot be performed by purely analytical means. The method required should be able to easily handle material non-linearity, as well as large and discontinuous deformations. The finite element method was thus judged best suited for the present problem. An incremental approach, according to which the rigid plate is displaced downwards in steps for each of which material properties and deformations are updated, is selected. Accordingly, the problem is divided into a series of linear elasticity problems (the material is not elastic but all elements are essentially undergoing loading such that rebound of the material is not allowed) for which a finite element solution is obtained. The method is elegant due to that the body analyzed (i.e, the snow beneath the penetrating plate) is assumed to be composed of series of triangular plates of material or elements for each of which stresses, strains, vertex displacements, etc, corresponding to each of the plate displacement increments introduced above, are known. Similarly, one-dimensional elements representing the shearing mechanisms developed along the vertical sides of the pressure bulb are also incorporated into the analysis. Stresses and displacements for these elements are also updated with plate displacement.

1.6 Organization of the Thesis

The present thesis is divided into two main parts:

1) The first part dealing with the statement of the problem, the development of the model used in the solution of the problem, the experimental program, a discussion analyzing and comparing experimental and predicted results

and, finally, conclusions. This part is subdivided into five chapters:

Chapter 1 - of which this section is a part, is an introductory chapter discussing the nature, scope and need for the solution of the problem at hand and presenting the adopted solution technique in a general way.

Chapter 2 - describes in detail the proposed analytical/computer model and corresponding algorithm developed.

Chapter 3 - describes the experimental work performed during the course of the study including a description of equipment, test procedure and results.

Chapter 4 - involves a presentation and discussion of the predicted rigid plate load-penetration behaviour versus the corresponding experimentally obtained relationships.

Chapter 5 - contains conclusions and recommendations for further work.

A list of references to previous work related to the present study is included at the end of this first part.

2) The second part consists of appendices and provides additional information useful to the reader for a more complete understanding of the techniques involved in the present study:

Appendix A - Photographs of experimental rigid plate penetration tests.

Appendix B - Computer Program Flowcharts.

Appendix C - Program input data.

Appendix D - Program output information

Appendix E - Program listing.

The organization of the thesis is schematically described in the block diagram shown in Fig. 1.3.

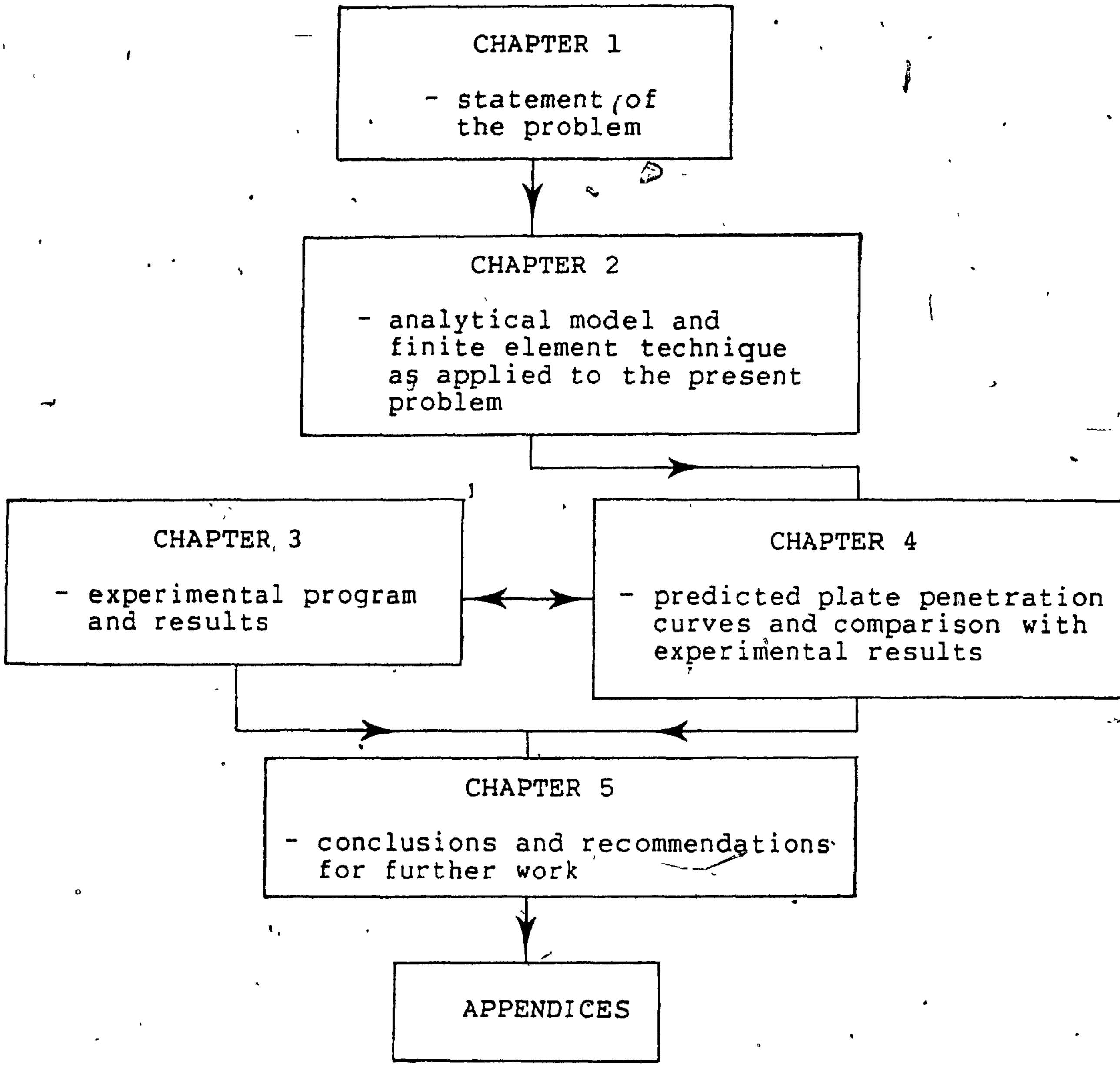

Fig. 1.3 Organization Of The Thesis

CHAPTER 2

GENERAL PROBLEM DEVELOPMENT AND APPLICATION OF THE FINITE ELEMENT METHOD

2.1 Introduction

The finite element method is a powerful numerical procedure for solving continuum mechanics problems. Originally developed for structural mechanics applications, the method has been extended to handle a great variety of problems often too complicated for a closed form mathematical solution. With the development of new algorithms and techniques designed to treat material non-linear stress-strain behaviour (material non-linearity) as well as large deformation problems (geometrical non-linearity), interest and confidence in using finite elements have grown amongst geotechnical engineers so that today, many geotechnical problems are solved by this tool rather than by conventional classical soil mechanics theories. In the present study, a special algorithm, based on the finite element method of analysis and designed to model the behaviour of snow material, is presented and discussed. The applicability of the finite element method to analyze a snow mechanics problem may, at first glance, appear questionable because of the nature of the material itself and its inelastic and large deformation behaviour. In the solution method, however, finite element analysis is simply a computational step in an algorithm specifically developed for the numerical simulation of the material at hand and emphasizing its characteristic non-linearity, high compressibility and stiffening behaviour. Evidently, success in proper modelling the responses of snow to the loading conditions considered in this study largely depended on the memory space and speed of the computing machine used. Fortunately, the availability and time efficiency of the computer utilized during the course of the present study confirmed the feasibility of the project.

2.2 Analytical Model Adopted In The Present Study

2.2.1 General Considerations

As the first step in the development of an analytical model for the prediction of snow behaviour under controlled rate plate penetration conditions, it is essential to identify the stress transfer mechanisms occurring within the snow mass and to approximately define the dimensions and shape of the pressure bulb generated by penetration of the plate in the material. Photographs taken during plate penetration tests showed the basic difference between the behaviour of snow and most soil materials (Fig. 2.1) when subjected to such loading conditions. As illustrated in Fig. 2.1, the deformation pattern in snow is characterized

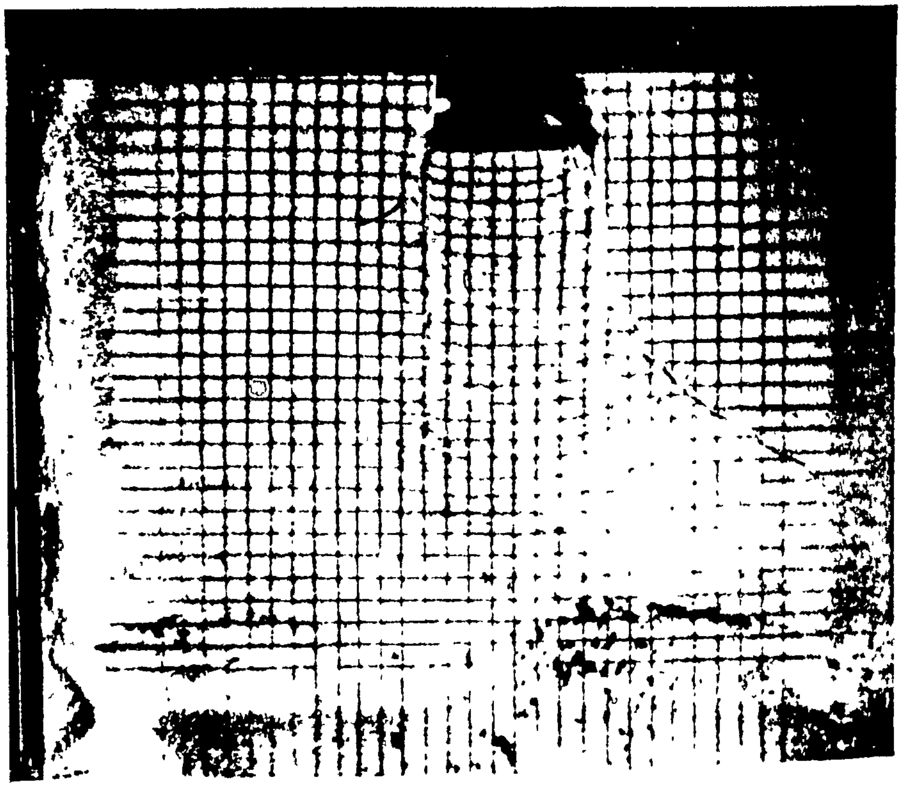

Fig. 2.1 Typical Photograph of a Plate Penetraiton Test

by the cutting effect of the edges of the penetrating plate causing the development of a pair of vertical shear planes which, with the plate-snow interface, define three boundaries of the pressure bulb induced by the penetration process. Furthermore, it can also be observed from the typical test photograph in Fig. 2.1 (also see Appendix A for more photographs) that snow material on the outside of the shear planes remains essentially unaffected by the penetration of the plate thus implying negligible lateral expansion of the snow as it deforms vertically. This, of course, is typical of a material with a low Poisson's ratio. The depth of the pressure bulb, implying a fourth boundary (the bulb is practically rectangular), is a function of the penetration of the plate and is mainly governed by the relative values of compressive and shear stresses developed within and along the sides of the pressure bulb, respectively (which in turn depend on the relative stiffnesses of the snow in compression and shear) and the shear strength. For a given plate penetration, a relatively high shear stiffness and snow strength causes a more shallow pressure bulb as a greater portion of the reaction load on the plate is carried by the shear stresses acting along both sides of the pressure bulb. Conversely, a decrease in shear stiffness and snow strength implies a deeper pressure bulb. The influence of the properties in shear of the material is analyzed through both experimental and predicted plate load-penetration behaviour and discussed in Chapter 4.

The simultaneous shear and volume change mechanisms that occur during plate penetration are schematically illustrated in Fig. 2.2 showing the shear and compression actions undergone by elements A and B, respectively. As mentioned earlier, the stresses associated with these actions are controlled by the stiffness and strength of the snow material which, in general and as proved by confined compression and vane shear test results (presented in Chapter 3), are a function of density. The success of the solution procedure thus relies on the ability to determine the density distribution beneath the plate, from which stiffness and strength values can be correctly assigned to any given point within and along the sides of the pressure bulb as a function of plate penetration. The knowledge of the resulting system stiffness at a given plate sinkage then permits the calculation of incremental reaction forces on the plate from which a load-penetration curve can be constructed. The resulting predicted curve can then be compared to experimental results for verification purposes of the proposed model.

The problem thus involves the determination of the load-deflection relationship of a non-linear system in which the total stiffness K is a function of deflection and deflection rate. As discussed earlier, the mechanics of the system suggest that the reaction force on the plate at a penetration z is composed basically of two parts (Fig. 2.3a):

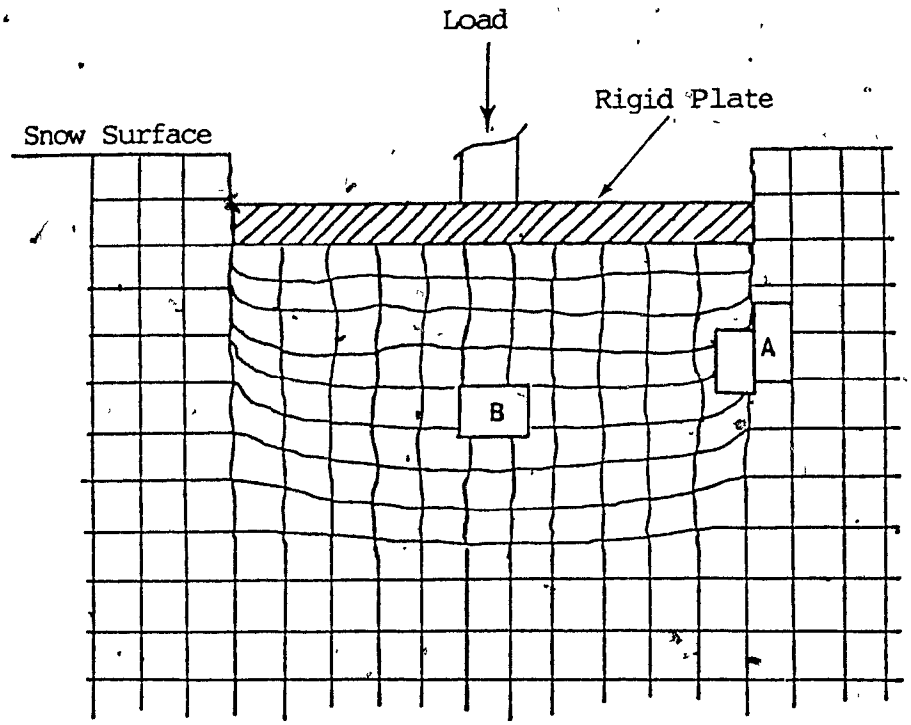

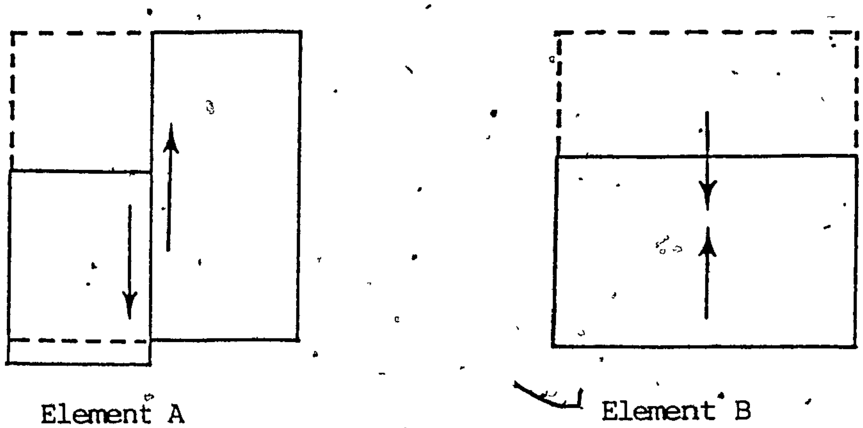

Fig. 2.2 Volume Change and Cutting Shear Mechanisms Under Plate Loading Conditions

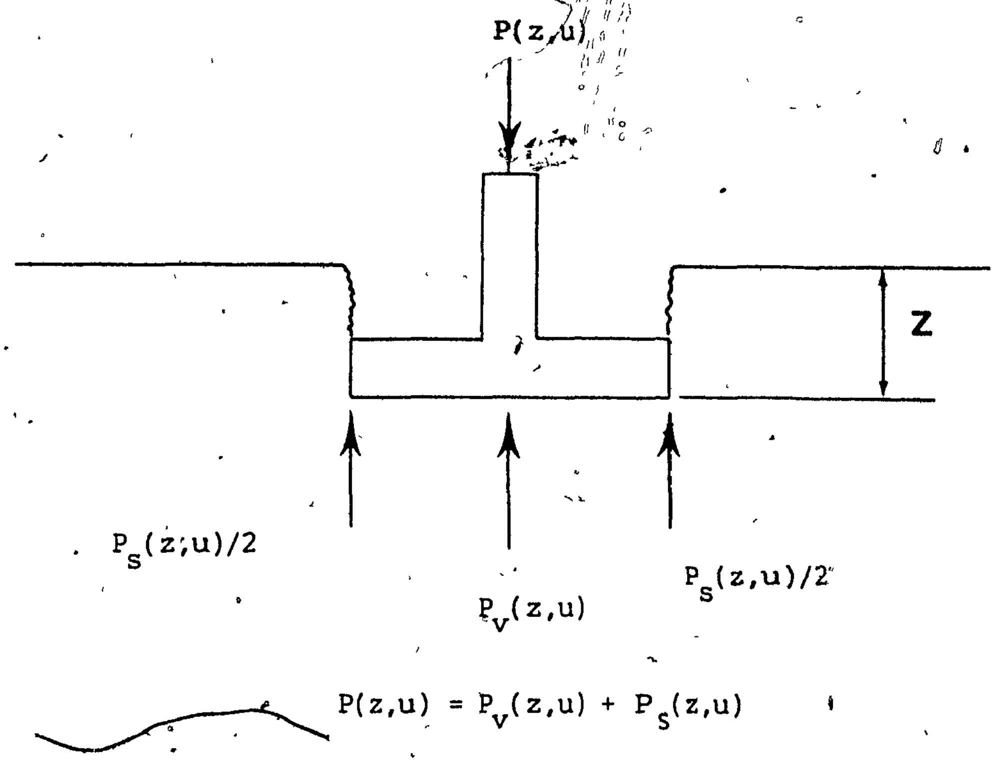

Fig. 2.3a Forces on Plate Due to Volume Change and Cutting Shear Mechanisms

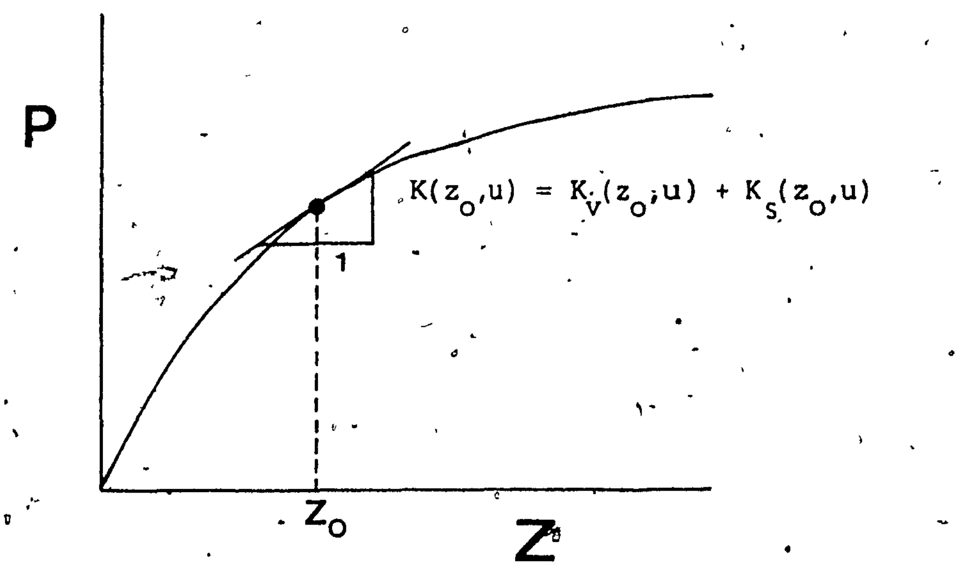

Fig. 2.3b Schematic Representation of Relationship Between Stiffness Function and Load (P) - Penetration (Z) Curve

a) a force P_v due to the volume change resistance of the snow within the pressure bulb.

b) a force P_s resulting from the resistance of the snow to shear along the failure planes.

The nature of the problem thus implies that, in fact, these forces are also a function of the plate penetration z, as a result of the variation of properties of the material (i.e, stiffening effect due to snow densification and softening effect due to local shear failures along the planes of cutting shear) as plate penetration progresses. In addition, the penetration speed of the plate u constitutes another parameter to consider since, for a viscous material such as snow, the velocity field generated has a direct effect on material properties and hence, on the reaction force. The total system stiffness can thus be expressed in terms of the volume change and shear components as follows:

$$P(z,u) = P_v(z,u) + P_s(z,u) \tag{2.1}$$

where $P(z,u)$ = total reaction force on the plate as a function of plate penetration z and plate penetration rate u.

$P_v(z,u)$ = reaction force on the plate due to volume change resistance of snow.

$P_s(z,u)$ = reaction force on the plate due to shear resistance of snow.

Differentiating the above expression with respect to plate penetration z and rewriting it in differential form:

$$dP(z,u) = \frac{\partial P_v(z,u)}{\partial z}\,dz + \frac{\partial P_s(z,u)}{\partial z}\,dz \tag{2.2}$$

$$dP(z,u) = (K_v(z,u) + K_s(z,u))\,dz \tag{2.3}$$

where $K_v(z,u)$ = tangent volumetric stiffness function (Fig. 2.3b)

$K_s(z,u)$ = tangent shear stiffness function (Fig. 2.3b)

Equation (2.3) is the basic relationship that mathematically represents the process of a rigid plate penetrating into a snow mass at a constant rate.

The solution of the problem thus requires knowledge of the volumetric and shear stiffness functions $K_v(z,u)$ and $K_s(z,u)$ both of which are essentially dependent on the plate penetration z and the penetration rate u. The load-penetration relationship can then be determined by integration of equation (2.3):

$$P(z,u) = \int_0^z (K_v(z,u) + K_s(z,u))\,dz \tag{2.4}$$

The following two sections discuss the above functions in more detail.

2.2.2 Volumetric Stiffness Function $K_V(z,u)$

For a given plate penetration rate, the volumetric stiffness function in the present model is controlled by density distribution within the stress bulb due to the variation of the compressibility of the snow material with density. Prior to any penetration of the plate, the snow deposit in the situation under study has a more or less uniform density. As penetration proceeds, the snow directly below the plate compresses somewhat more than that further below due to the simultaneous action of shear stresses along the pair of planes of cutting shear. A given plate penetration therefore yields a density profile in which density is highest near the plate and decreases with depth until the original value corresponding to the unloaded state. Therefore prior to any plate penetration, the snow exhibits uniform volumetric stiffness properties but as penetration increases, the stiffness at a given point in the snow mass changes and therefore affects the subsequent density distributions which, as a result, causes a change in the volumetric stiffness function $K_V(z,u)$ with plate penetration.

Consider an infinitesimal element of snow, of type "B" in Fig. 2.2, within the pressure bulb, after a plate penetration Z_p and having a volume dV in which the density is γ and the instantaneous strain rate is $\dot{\varepsilon}$ (Fig. 2.4). Also let the compressive modulus, defined herein as the ration of stress to strain under pure axial deformation

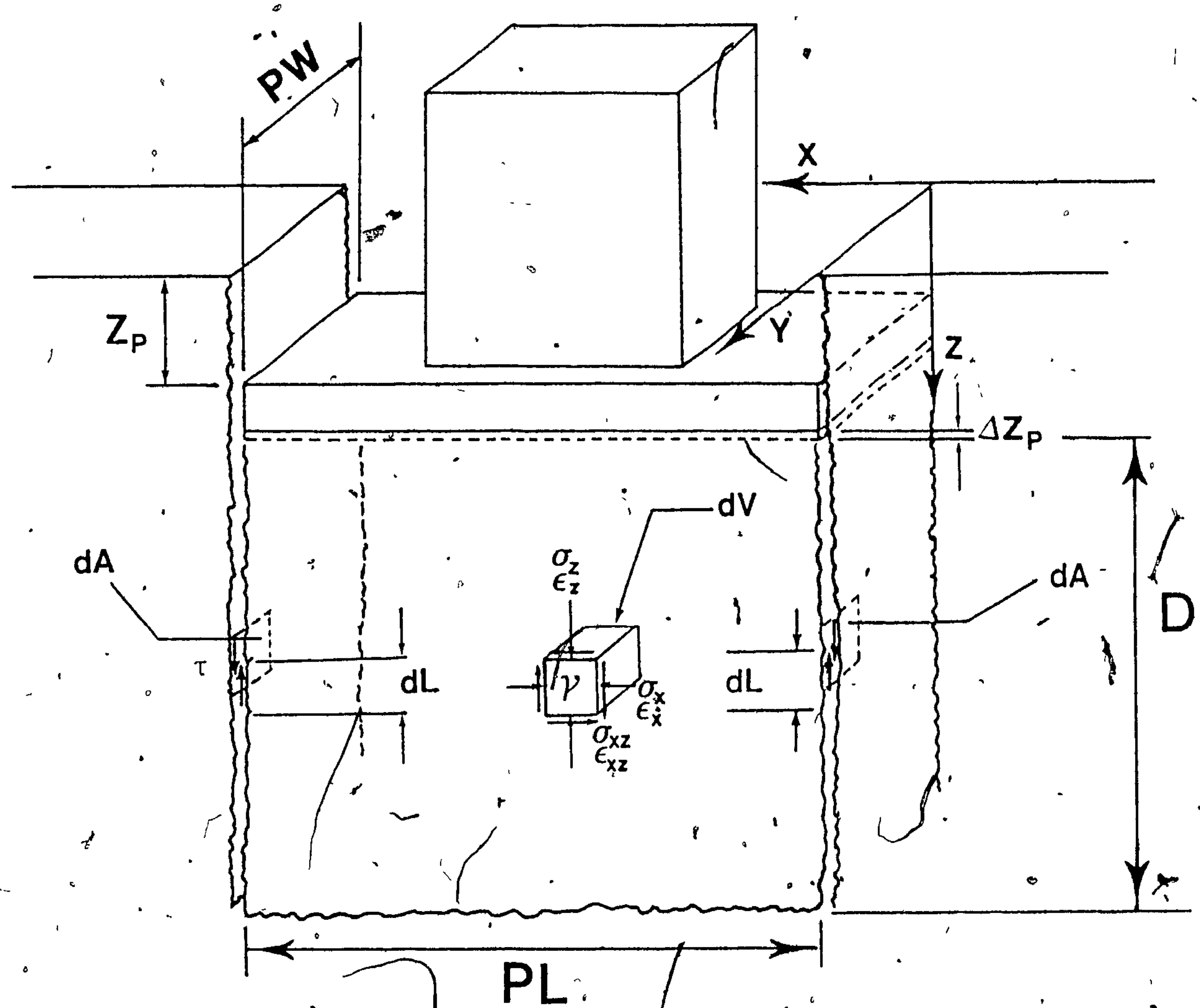

Fig. 2.4 Stresses Induced in Snow Mass Due to Incremental Plate Displacement

conditions, be $E_c(\gamma,u)$ for the density γ and the strain rate u. Upon an additional increment of plate displacement ΔZ_p, both axial and shearing strains ε_x, ε_y, ε_{xy} develop, the latter due to the distortion effect of shearing stresses generated along the planes of cutting shear. These strains are then related to stresses through the compressive modulus defined above and the Poisson's ratio of the material. The work done in deforming the given snow element is then:

$$dW = (\sigma_x\varepsilon_x + \sigma_y\varepsilon_y + \sigma_{xy}\varepsilon_{xy})\, dV \tag{2.5}$$

Integration of the above expression over the entire pressure bulb yields the total energy spent in compressing and distorting the snow for the given plate incremental displacement. Due to the particular boundary conditions of the present problem and the low Poisson's ratio of the material, the energy involved in the distortion of the snow mass within the pressure bulb is small relative to the volume change energy. It can therefore safely be stated that evaluation of the integral of equation (2.5) over the volume of the pressure bulb is basically equal to the volume change energy component due to an increment of plate penetration Z :

$$\Delta E_v = \text{volume change energy} = \int_0^D\int_0^{PW}\int_0^{PL} \sigma_x\varepsilon_x + \sigma_y\varepsilon_y + \sigma_{xy}\varepsilon_{xy}\, dx\, dy\, dz \tag{2.6}$$

Assuming plane strain conditions and realizing that the pressure bulb depth is, in general, a function of plate penetration Z_p:

$$\Delta E_v = PW\int_0^{D(Z_p)}\int_0^{PL}\sigma_x\epsilon_x + \sigma_y\epsilon_y + \sigma_{xy}\epsilon_{xy}\,dxdz \qquad (2.7)$$

The above quantity is equal to the work done by the incremental force P_v. Therefore;

$$\Delta E_v = \Delta P_v \Delta Z_p \qquad (2.8)$$

from which the volume change stiffness function evaluated at a plate penetration Z_p can be obtained:

$$K_v(Z_p,u) = \frac{\Delta P_v}{\Delta Z_p} = \frac{\Delta E_v}{(\Delta Z_p)^2} \qquad (2.9)$$

Substituting for E_v (eq. 2.6) in equation (2.9), the volumetric stiffness function is thus:

$$K_v(z,u) = \frac{PW}{(\Delta Z_p)^2}\int_0^{D(Z_p)}\int_0^{PL}\sigma_x\epsilon_x + \sigma_y\epsilon_y + \sigma_{xy}\epsilon_{xy}\,dxdz \qquad (2.10)$$

The key in the determination of the function $K_v(Z_p,u)$ thus lies in defining the following functional relationships:

1) Distribution of incremental stresses and strains, density, strain rate and pressure bulb depth as a function of plate penetration Z_p:

$$\begin{aligned} \text{i.e, } & \sigma_x(x,z,z_p)\ ,\ \epsilon_x(x,z,z_p) \\ & \sigma_y(x,z,z_p)\ ,\ \epsilon_y(x,z,z_p) \\ & \sigma_{xy}(x,z,z_p)\ ,\ \epsilon_{xy}(x,z,z_p) \\ & \gamma(x,z,z_p)\ ,\ \dot{\epsilon}(x,z,z_p)\ ,\ D(z_p) \end{aligned} \qquad (2.11)$$

These functions can be determined from the proposed finite element model and are thus obtained by numerical computation.

2) Compressive modulus of snow as a function of density and plate penetration u:

$$\text{i.e,} \quad E_c(\gamma, u) \tag{2.12}$$

This function is a characteristic describing the compressibility of the material and therefore needs to be obtained through tests. Confined compression tests (see Chapter 3) were carried out for such a purpose.

It should be noted that the above relationship allows the introduction of a material parameter in the stiffness matrix of elements in the finite element analysis and therefore controls the values of the above functions (i.e, eqs. 2.11).

2.2.3 Shear Stiffness Function $K_s(z,u)$

The shear stiffness function is linked with the effect of shear stresses supporting the stress bulb along the two planes of cutting shear described in section 2.2.1. As for the volume change component, the shear stiffness of the system is dependent on the amount of plate penetration, density distribution and penetration rate.

When the plate penetration process is initiated, high vertical shear stresses develop below both edges of the plate so that the shear strength of the snow material at these points is likely to be exceeded thus starting the cutting shear mechanism. At this point, it should be noted that the main difference between the proposed analytical model and the real situation is the question of the predetermination of the planes of cutting shear. The kinematics of the problem, as observed during actual plate penetration tests, imply a progressive development of the shearing planes. In the present finite element idealization (see section 2.3), these planes are defined prior to any penetration of the plate. However, it can be argued that since shear displacements further down the shearing planes, as computed by the model for a given plate penetration, may be very small then the difference between idealized and actual shear mechanisms becomes academic.

In any case, if one considers that the two planes of shear are composed of a series of elements of the "A" type in Fig. 2.2, it is clear that, as the plate begins to penetrate into the snow mass, such an element located immediately below one of the edges of the plate eventually undergoes a shear deformation sufficient to cause a shear stress build up and consequently, failure of the element. Other elements further below are subjected to smaller displacements which, depending on the stiffness and strength of the material in shear at the density across the plane of deformation, may also imply failure. However, at a certain distance below the edges of the plate, these displacements and stresses are eventually insignificant so that failure does not occur. Upon an additional increment of plate penetration, the shear elements may or may not fail depending on the respective cumulative shear stress and shear strength associated with them. The failure condition for snow in shear is therefore defined by consideration of the cumulative shear stress in a given element and the value corresponding to failure, determined by the shear resistance of the snow material at a density equal to that along the plane of shear:

i.e, failure occurs if $\tau_c > \tau_r(\gamma)$, where τ_c = cumulative shear stress in the given shear element.

γ = snow density along the shear plane of the element.

$\tau_r(\gamma)$ = shear resistance of the snow at a density equal to that across the plane of shear.

Failure in the present context refers to the point of breakage of bonds between snow particles, corresponding to the maximum or peak shear stress that the snow material can resist at a given density. At larger strains, the behaviour of the material is somewhat questionable. In the case of a relatively rapid shearing action (i.e, high strain rate) the material exhibits a strain softening behaviour with a steadily decreasing residual shear strength due to the self-polishing action (heat generated due to friction melts down particles) of the two surfaces rubbing against one another. Such post peak shear stress-strain behaviour of snow has been previously discussed by Yong and Muro (1981) who proposed a mathematical relationship describing the falling portion of the stress-strain curve, as obtained from vane shear tests. Such experiments were conducted on artificial snow at a rotational speed of 1.75 r.p.m., which for the diameter of the vane used, corresponds to a shearing velocity of 0.95 mm/sec. The proposed analytical expression is:

$$\tau = \tau_0 e^{-2y} \tag{2.13}$$

τ = shear stress for a given angular displacement of the vane.

τ_0 = peak shear stress or shear strength of snow.

y = angular displacement of the vane (in radians).

Results from controlled rate vane shear tests were made available by other researchers (Yong (1985)) during the course of this study and proved to be useful guidance in modelling. A typical curve from a vane shear test conducted on artificial snow at a rotational speed corresponding to a shearing velocity of 0.0073 mm/sec is shown in Fig. 2.5. It should be noted that in this case, the curve is characterized by a decrease in stiffness (probably due to bond breaking) at a vane rotation of approximately 2 degrees

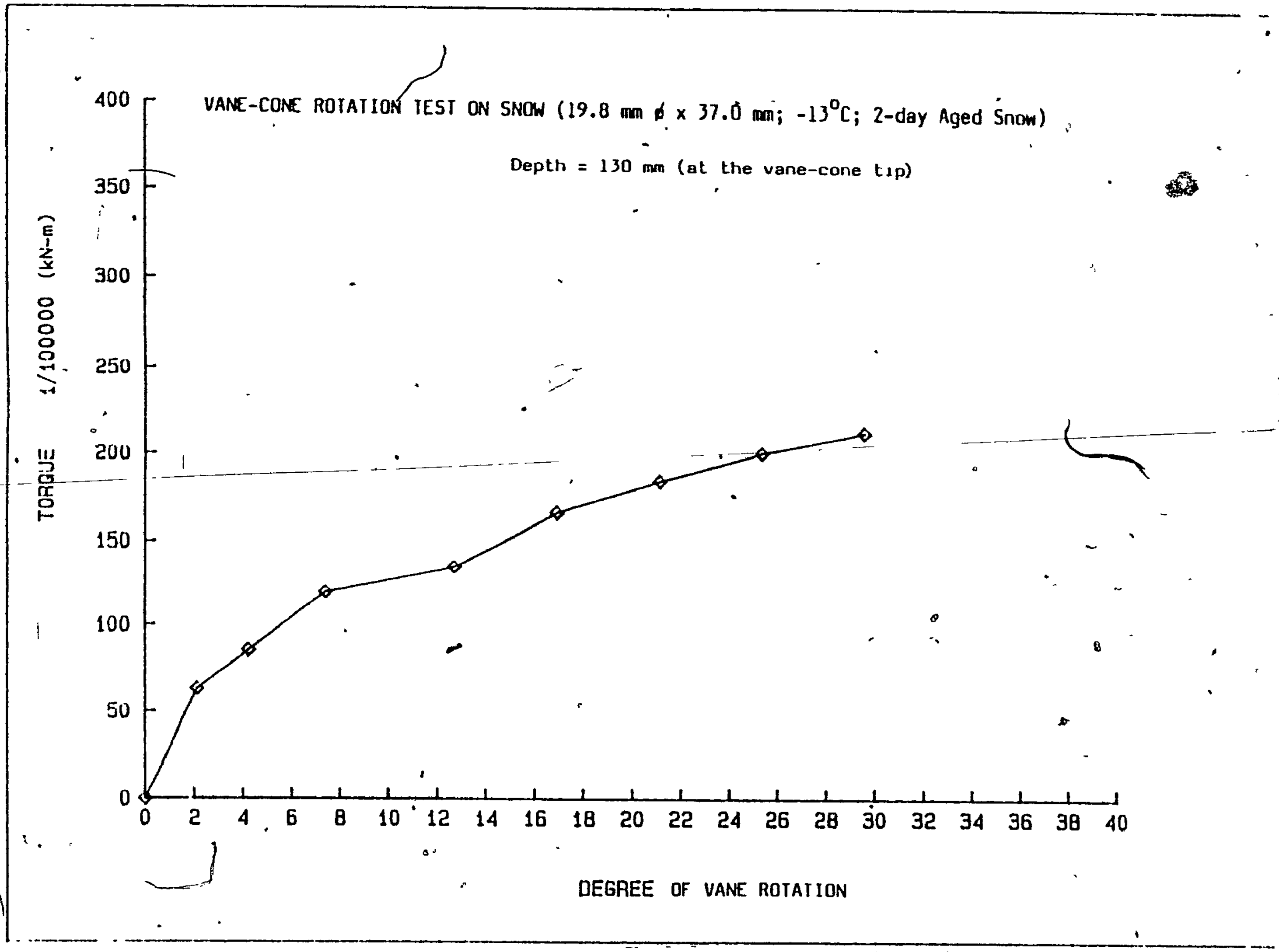

Fig. 2.5 Vane-Cone Rotation Test on 2 Day Old Artificial Snow (After Yong, 1985)

but that torque, and hence shear stress, increases, rather than decreases, as suggested in the previous case, with vane rotation. The difference between the two types of response seems to be due to the difference in shearing rate. A relatively rapid shear test yields a strain softening type of curve whereas for a slower test, a strain hardening behaviour is observed. In the light of this, the choice of the appropriate response for the purpose of modelling a plate penetration test is somewhat arbitrary and should be governed by the shearing velocity along the planes of cutting shear. Since, throughout the course of the study, a plate penetration speed of 0.58 mm/sec was used, which is not too dissimilar to the average of the shearing rates considered above, an intermediate condition, i.e, a constant stress post peak response (Fig. 2.6) was adopted. The author felt that this idealization is not unrealistic and is both practical and expedient to implement in the developed model since the type of vane shear tests performed to obtain shear strength-density curves (see Chapter 3) excluded any type of post peak analysis.

Having established the basic parameters describing the response of snow in shear, the shear stiffness function $K_s(z,u)$ is determined by the following analysis. Consider a shear element of surface area dA, as shown in Fig. 2.4, in which the snow density and instantaneous strain rate at its center are γ and ξ, respectively, when the total penetration

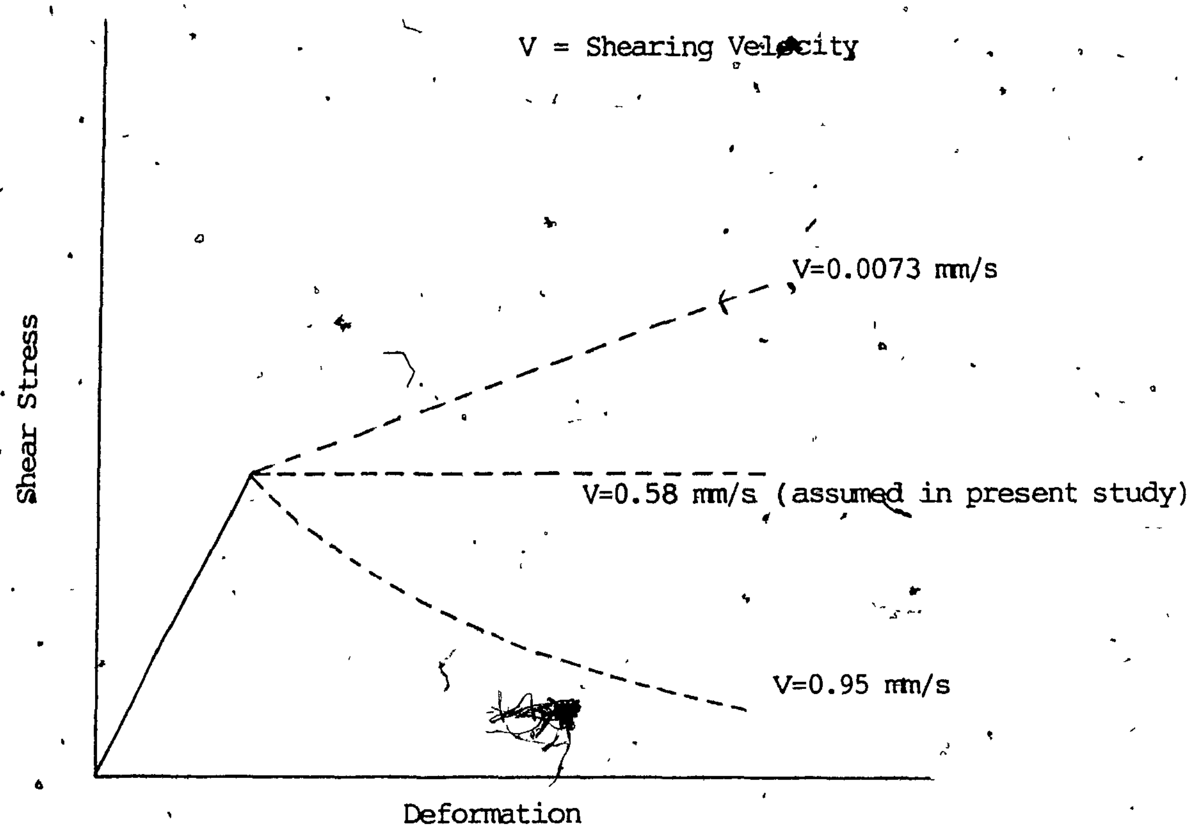

Fig. 2.6 Effect of Strain Rate on Shear Stress-Deformation Behaviour

of the plate is Z_p. If the plate is further displaced downwards by an amount ΔZ_p, a shear strain develops, whose value is related to a corresponding shear stress τ through the stiffness of the material in shear, which, in general, is a function of density γ, strain ξ and strain rate $\dot{\xi}$:

$$K_s = G(\gamma, \xi) \tag{2.14}$$

The total shear force developed in the process is:

$$dP_s = \tau dA = \tau dy dz \tag{2.15}$$

The total area of shearing consists of the two vertical planes of cutting shear passing through the edges of the penetrating plate. Therefore, integration of the above equation over this area yields the shear force due to an incremental plate displacement ΔZ_p:

$$\Delta P_s = 2\int_0^D \int_0^{PW} \tau \, dy dz \tag{2.16}$$

For plane strain conditions and setting the stress bulb depth D to be a function of the plate penetration Z_p:

$$\Delta P_s = 2\, PW \int_0^{D(Z_p)} \tau dz \tag{2.17}$$

The shear stiffness function evaluated at a plate penetration Z_p is then:

$$K_s(Z_p, \sigma) = \Delta P_s / \Delta Z_p = \frac{2PW}{\Delta Z_p} \int_0^{D(Z_p)} \tau \, dz \tag{2.18}$$

Again, as for the volume change stiffness function, the determination of the shear stiffness function thus requires investigation of two types of functions:

1) Distribution of shear stresses along the planes of cutting shear as a function of plate penetration Z_p:

$$\text{i.e,} \quad \tau(Z, Z_p) \tag{2.19}$$

This function is obtainable through the finite element form of analysis proposed in this study.

2) Parameters describing the shear stress-strain behaviour as a function of density γ, strain ξ and strain rate $\dot{\xi}$:

$$\text{i.e,} \quad \text{a) shear strength} : \tau_r(\gamma, u) \tag{2.20}$$

$$\text{b) shear modulus} : G(\gamma, \xi, \dot{\xi})$$

These functions are material properties requiring testing (i.e, shear tests) for their identification (see Chapter 3) and govern the above shear stress distribution function (eq. 2.19).

2.3 Finite Element Formulation and Solution in the Present Study

The mathematical relationships developed in the preceding sections constitute the basis for the solution of the plate penetration problem. The complex nature of the equations developed in the preceding section and the particular nature of the boundary conditions involved discourage a purely analytical solution. The finite element method of analysis not only provides a solution to the problem but the similarity between the actual physical process and the corresponding numerical simulation renders it attractive and justifies its choice as a solution technique.

2.3.1. Idealization of the Problem

The solution of engineering problems always implies a certain degree of idealization of the material considered. In the present study, snow is assumed to have the following properties:

a) The material is homogeneous and isotropic.

b) The material is weightless.

c) Poisson's ratio is 0.

d) The material exhibits a linear-plastic behaviour in pure shear such that stress increases linearly with strain until failure and remains constant afterwards.

e) The material is non-frictional (i.e, shear stresses and strength are independent of normal stresses).

In addition, the material is known to exhibit the following characteristics:

a) The material is non-linear and highly compressible thus implying large strain behaviour.

b) The material exhibits a stiffening type of stress-strain curve in compression such that its stiffness increases with strain.

c) The shear strength of the material depends on density and shearing velocity.

Techniques for modelling the idealized material having the properties described above are discussed in later sections of this chapter.

Further assumptions concern the solution scheme itself:

a) The plate penetration problem can be treated on a plane strain basis. This seems reasonable in the light of the loading conditions imposed during testing in which the snow deposit is constrained to deform in basically two directions (see Chapter 3 for details on experimentation).

b) Body forces due to gravity are neglected since stresses, strains, reactions, etc., due to external loading only are of interest.

c) The material fails in shear when the cumulative shear stress at a given point along the shearing planes exceeds the shear strength corresponding to the density at that same point.

d) The stiffness of snow in compression is directly dependent on accumulated volume change and, hence on density (details on how this is included in the finite element analysis is discussed in the next section).

e) The planes of cutting shear passing through the edges of the plate are vertical and symmetrical with respect to the plate.

f) The effect of strain rate is included in the analysis only through the use of material properties in compression and shear corresponding to a deformation velocity equal to that of the penetrating plate. In so doing, the effect of a non-uniform strain rate distribution throughout the snow mass and along the planes of shear is thus ignored. Although it is recognized that the inclusion of strain rate distribution as an additional parameter describing material response results into a more precise and realistic analysis, the author felt that the extra computer time required for convergence of an additional non-linear type of analysis would not justify the additional degree of accuracy obtained.

g) The shear stiffness parameter K_s is kept constant throughout the analysis although it is recognized that, as outlined earlier in section 2.2.3, K_s, is in general a function of density, strain and strain rate.

2.3.2 Finite Element Mesh and Boundary Conditions

The initial step in the finite element solution of a given problem is the design of a mesh physically representing the body under study with proper consideration of boundary conditions. In the present case, the body in question is the snow mass extending sufficiently far from the plate to cover the maximum pressure bulb depth and contained between the two shearing planes passing through the edges of the plate. In addition, a layer of snow just outside the shear planes is included for a more realistic representation. This body is divided into constant plate strain triangular elements and joint elements (Goodman et al (1968)) are used to model the effect of vertical shear stresses supporting the pressure bulb along its walls. Due to the symmetrical nature of the problem, only one half of the bulb is considered in the finite element analysis. The mesh used in this study is snown in Figs. 2.7 and 2.8 displaying node and element numbers respectively.

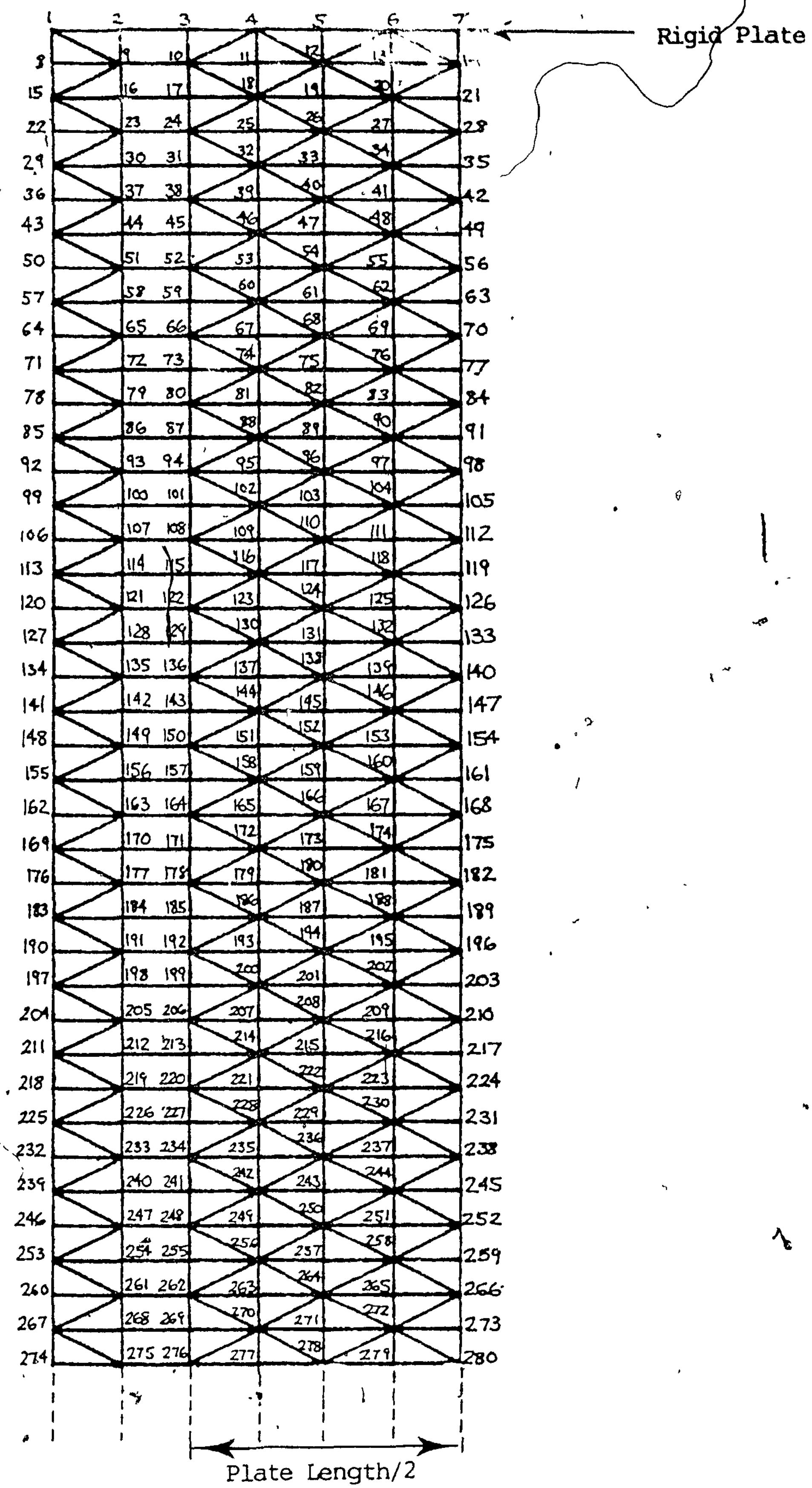

Fig. 2.7 Node Numbers

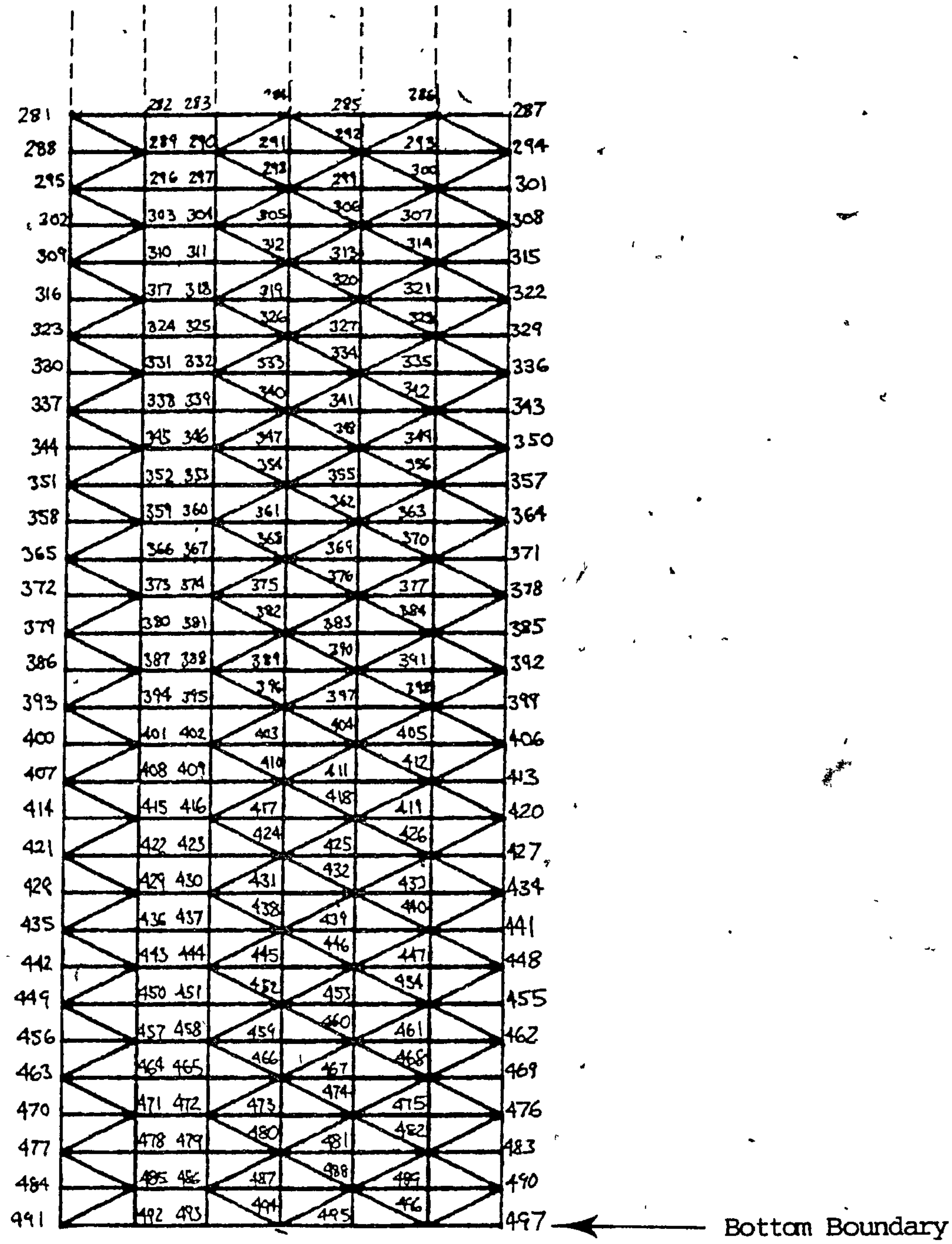

Fig. 2.7 Node Numbers (Continued)

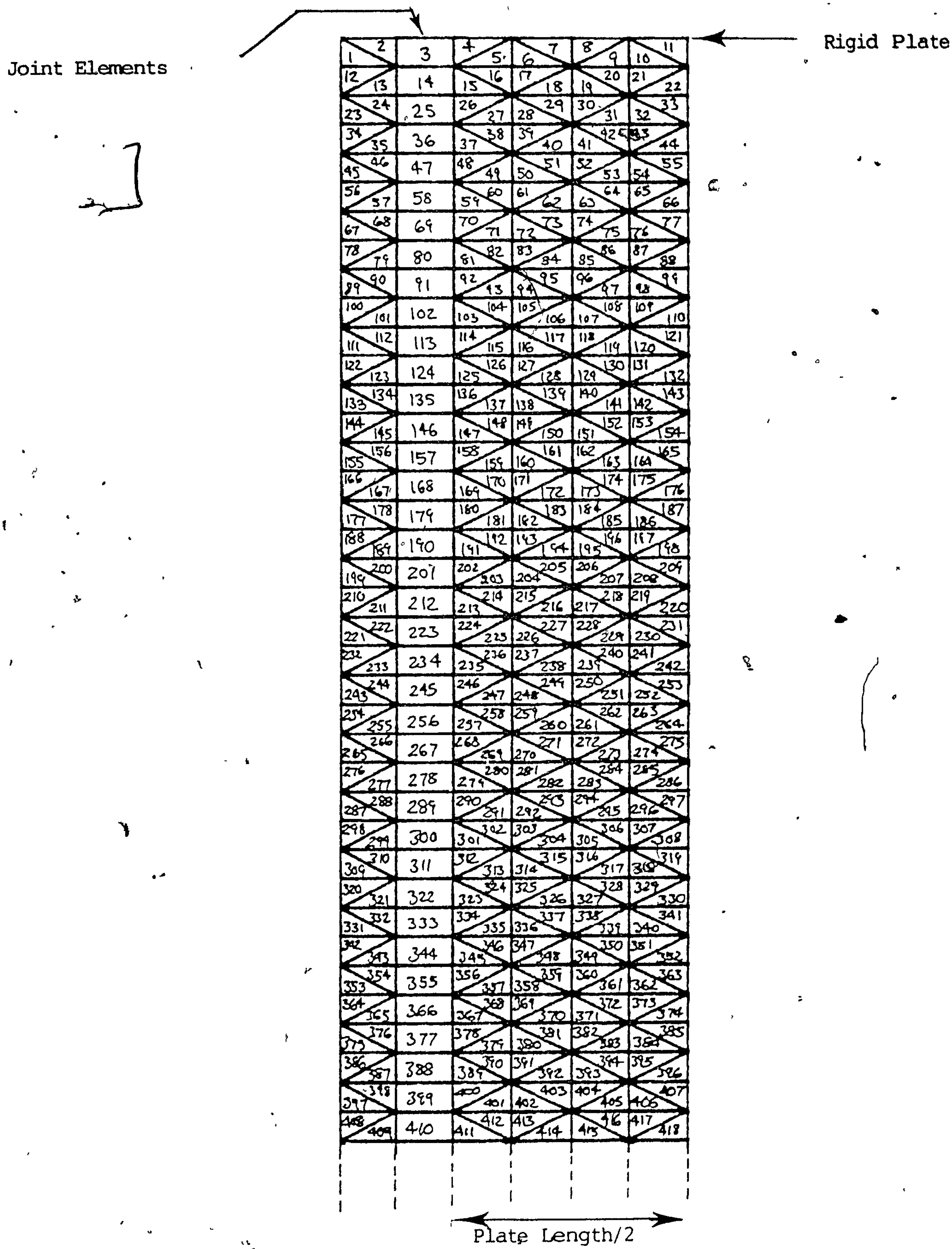

Fig. 2.8 Element Numbers

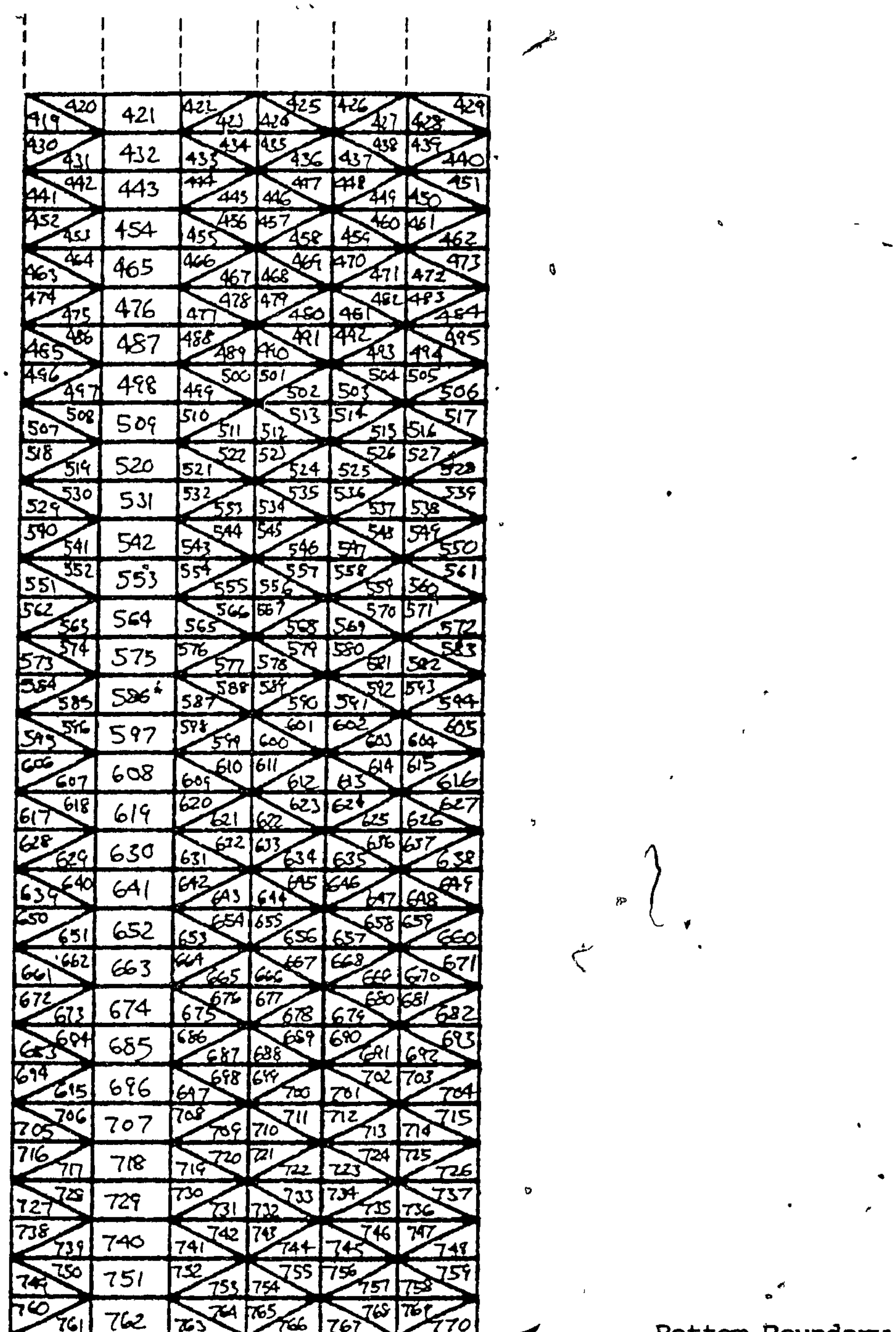

Fig. 2.8 Element Numbers (Continued)

The choice of displacement boundary conditions, rather than load boundary conditions, for the finite element analysis is motivated by two main factors pertaining to the nature of the problem at hand:

a) In the plate penetration tests, displacement of the plate is controlled by the constant penetration rate and the corresponding reaction force on the plate is measured. The use of displacement boundary conditions combined with the incremental finite element technique used in this study, in which the plate is progressively displaced into the snow material and corresponding reactions are computed from nodal displacements, therefore renders the numerical simulation that much more realistic.

b) A better control on the large strain behaviour of the material is achieved with the displacement boundary condition approah which, in addition, favourizes the constant updating of material properties (both in compression and shear) as plate penetration progresses.

As outlined in sections 2.2.2 and 2.2.3, point b) is a basic requirement of the solution technique used if a realistic analysis is to be performed. Furthermore, the selection of relatively small increments of displacement not only enables the handling of the brittle behaviour of the material in shear but also preserves the validity of the small strain assumption induced in the stiffness matrix formulation of the constant strain triangular elements. Consequently, the detrimental effect of geometric non-linearity is also diminished by the use of such an incremental procedure.

The boundary conditions assumed for the solution of the present problem are schematically described in Fig. 2.9. The top of the mesh, representing the snow surface, rigidly moves downwards, thus simulating penetration of the plate in the snow. These surface nodes are however free to displace horizontally thus implying a smooth plate. The left-hand side boundary, bounding one of the layers just outside the planes of cutting shear is fixed. Joint element nodes are allowed to move freely in the vertical direction while horizontal motion is prevented. The bottom boundary, which is located sufficiently far away from the plate in order to minimize bottom boundary effects, is also fully restrained. Motion of the nodes along the right-hand side (i.e, the plane of symmetry) is constrained to be vertical only due to considerations of symmetry of the problem.

2.3.3 Solution Procedure

The finite element algorithm used in the solution of the problem is derived from a computer program developed by Hanna (1975) and begins with the initialization of material properties according to the initial density of the snow,

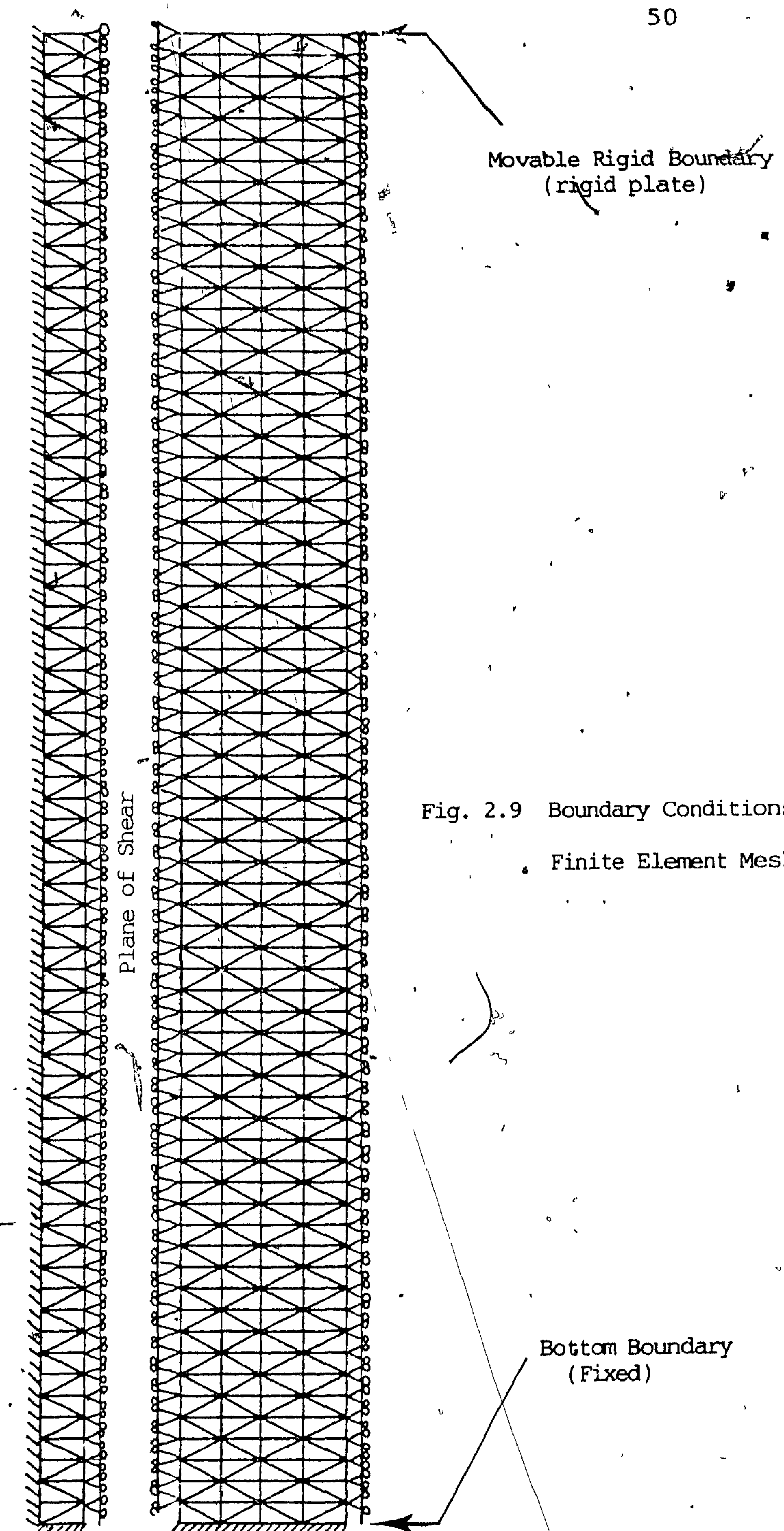

Fig. 2.9 Boundary Conditions For Finite Element Mesh

i.e. before any plate penetration occurs. As outlined in sections 2.2.2 and 2.2.3, the stress-strain properties of snow in compression and shear are functions of density and plate penetration speed so that the corresponding parameters;

$$E_c(\gamma, u) \quad \text{(compressibility)}$$
$$t_r(\gamma, u) \quad \text{(shear strength)}$$

obtained from confined compression and vane shear tests respectively, are all initially defined according to the results from tests performed on snow at the initial density. More specifically, the value of modulus of elasticity initially assigned to the triangular continuum elements is equal to the tangent modulus of the stress-strain curve in confined compression at zero strain. The value of Poisson's ratio is set to zero and is kept constant throughout the entire analysis. Similarly, the shear stiffness of joint elements is initially assigned a value which as outlined in section 2.3.1, is assumed to remain constant and the maximum stress tolerated by these elements corresponds to the shear strength of the snow at the initial density. The normal stiffness is irrelevant in the present analysis, since the normal displacement of joint elements is prevented according to the specified boundary conditions, but is arbitrarily given a value of 100000.

The size of the specified incremental plate displacement (i.e, 2 mm) used in the finite element analysis is determined simply by dividing the maximum plate penetration (approximately 70 mm) by the total number of increments, which, in the program presented in this study, is set to 35.

The proposed method of solution thus consists of a series of finite element analyses, each applying to an increment of plate displacement, for which material properties in the form of stiffness parameters, are obtained from characteristics derived from tests results. The non-linearity of the material implies the use of an iterative technique, developed for the triangular elements, which is discussed in section 2.3.4.

Following a particular increment of plate displacement, stresses and strains in triangular elements are computed from the resulting incremental nodal displacements and the non-linear analysis procedure mentioned above is undertaken and is carried through for a maximum of twelve iterations. Upon completion of the algorithm for material non-linearity, stresses in joint elements are examined. Failure in shear at various points along the vertical cutting shear planes is reflected, in the proposed model, by a total or cumulative shear stress in a given joint element greater than that tolerated by the snow material at a density equal to that across the plane of shearing. When failure does occur, a very small value (i.e. 0.0001) of shear stiffness is assigned to the element and shear stresses subsequently remain constant at the failure value according to the idealized stress-strain curve in shear introduced in section 2.2.3. As a result, after failure of a given joint element, the difference between the cumulative shear stress and the stress corresponding to failure must be "released" back into the snow mass on both sides of the plane of shear. This is done by converting the excess shear stress into an equivalent system of vertical forces (section 2.3.5) which are then applied on nodes on either side of the plane(s) of shear. A finite element analysis also including the non-linearity algorithm, is then performed for this loading situation while keeping the plate stationary. The resulting reactions on the plate prove to be opposite to those generated during increments of plate penetration. Ideally, the stress release cycle should be repeated until the excess shear stress in any joint element is zero but, because of computer time costs, additional analyses are undertaken only if the last incremental (negative) reaction load on the plate is of significant magnitude with respect to the value corresponding to the previous stress release cycle. Incremental reactions due to either plate penetration or excess shear stress release are determined by summation of the individual vertical reactions exerted on the nodes representing the plate-snow interface and multiplication of the result by the plate width PW (Fig.2.4) as a result of the assumed plane strain condition. The resulting value is then doubled since, as it can be recalled, the finite element analysis performed applies to only half of the plate. The equation for reaction load on the plate is thus:

$$RL = 2PW(RY(3) + RY(4) + RY(5) + RY(6) + RY(7) \tag{2.21}$$

where PW = plate width

RY(3) ... RY(7) = Vertical reaction for nodes 3,4,5,6,7 (i.e, the snow-plate interface nodes for either a plate displacement increment or excess shear stress analysis,

where RL = incremental reaction load on plate.

The total updated load on the plate is then computed by summation of the incremental reaction loads on the plate computed for each plate displacement increment or excess shear stress analysis.

At the end of every increment of either plate displacement or shear stress release cycle, the nodal coordinates are then updated simply by adding the incremental horizontal and vertical displacements to the coordinates at the of the previous increment. The density distribution beneath the plate can thus be obtained. The basis for computing density is the change in area of the triangular elements as deformations occur. The area of these elements at any stage of plate penetration is calculated from the updated coordinates of the nodes as schematically described in Fig. 2.10. Since the initial

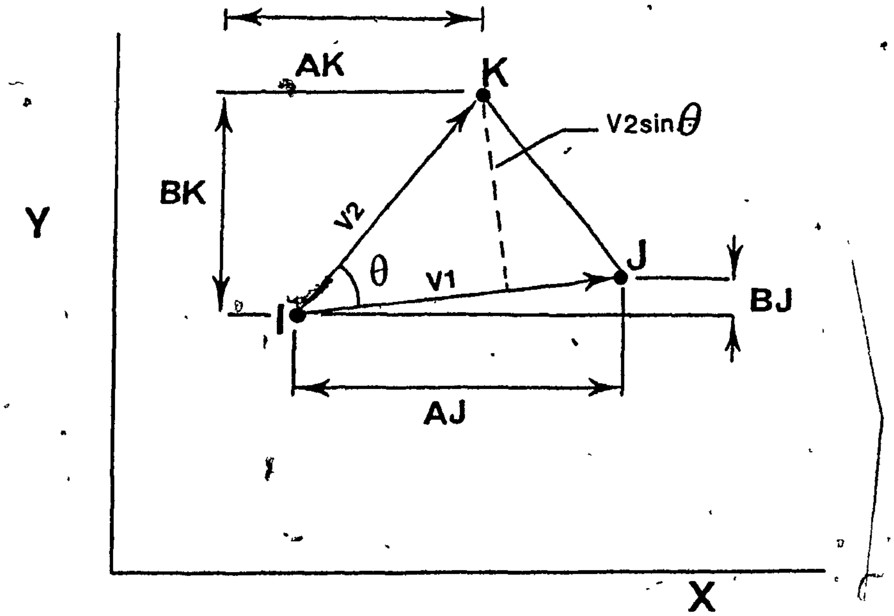

Vectors $\overline{V1} = (AJ,BJ)$

$\overline{V2} = (AK,BK)$

Cross product :

$$\begin{vmatrix} i & j & k \\ AJ & BJ & 0 \\ AK & BK & 0 \end{vmatrix}$$

$$AJ \cdot BK - AK \cdot BJ$$

$$|V1|\ |V2|\ \sin\theta = 2A$$

$$A = \frac{AJ \cdot BK - AK \cdot BJ}{2}$$

Fig. 2.10 Computation of Area of Triangular Elements area of each element in the original, undeformed finite element mesh is computed and stored in the finite element mesh generating subroutine INMESH, the ratio of deformed to undeformed element areas can be determined. Due to the plane strain condition imposed to the problem, these ratios are also the volume ratios from which density is obtained through the following expression:

$$\gamma = (A_0/A) \times \gamma_0 \qquad (2.22)$$

where γ = updated density in given element.

A_0 = initial area of undeformed element (i.e, area computed from initial undeformed mesh coordinates).

A = area of deformed element (i.e, area computed from updated nodal coordinates) (Fig. 2.10)

γ_0 = initial snow density (snow density prior to plate penetration)

From the resulting density distribution within the snow mass, an equivalent average strain in each triangular element is then determined in order to prepare the non-linear analysis in the next increment. The corresponding computational procedure and the motives justifying its incorporation in the proposed model are discussed in the next section.

The shear stress in failed joint elements is then recorded in order to maintain the bookkeeping on the updated state of shear stress in joint elements subjected to subsequent excess stresses which must then be removed leading to the stress release effect discussed earlier in this section.

The finite element algorithm then proceeds to another increment of plate displacement and the entire analysis is repeated, each time with proper consideration of the variation of material properties with density distribution, which is dependent on the total plate penetration. The procedure is terminated when the plate penetration equals a value selected according to the maximum plate penetration achieved in the experiments (about 70mm.).

2.3.4 Technique for Non-Linear Analysis - Triangular Elements

In the incremental type of finite element analysis of a non-linear material, the level of stress and strain of the material must be known at the beginning of each increment. For a non-linear "elastic" material undergoing relatively small volume change, such as saturated clayey soil, incremental stresses and strains are added to obtain cumulative values from which principal stresses and strains can be obtained at a particular stage of loading. These stresses and strains are then compared to a reference stress-strain curve obtained from tests on the material (e.g. triaxial texts) and an iterative non-linear analysis based on tangent elastic modulus can thus be performed. Examples of techniques for non-linear analysis which can be used with such an incremental procedure are illustrated in Fig. 2.11.

For a compressible inelastic material such as snow and for the type of test performed to determine its response to compression (i.e. confined compression test), the above procedure is not applicable because of the following arguments. The application of the finite element procedure using the small strain formulation and nodal coordinate updating approach implies the use of a true stress-strain curve as opposed to an ordinary engineering stress-strain curve. In obtaining a true stress-true strain curve from a given test, stresses and strains are calculated on the basis of constantly changing sample dimensions caused by the loading process whereas for an ordinary stress-strain curve, the values are calculated from original sample dimensions. Since, in the present incremental finite element procedure, strains in a given increment are computed on the basis of the deformed mesh corresponding to the end of the preceding increment, these values may be considered to be approximately true strains. For a material such as snow, tested in confined compression, true strains can be computed

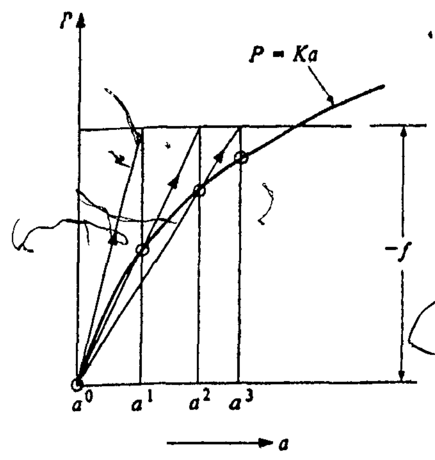

Direct iteration

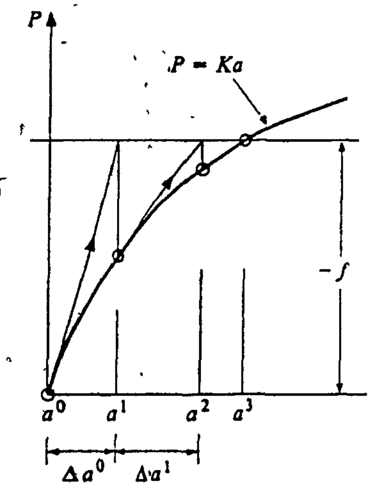

Newton–Raphson method

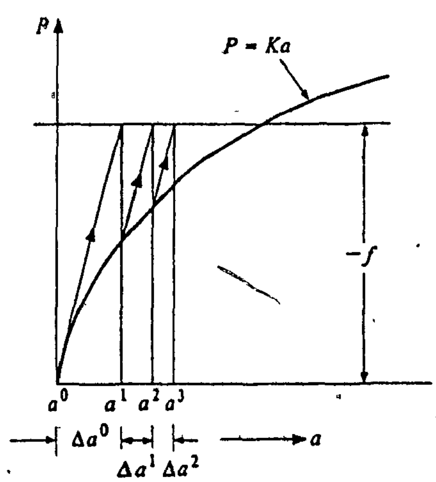

'Modified' Newton–Raphson method

Fig. 2.11 Examples of Non-Linear Analysis Solution Techniques
(After Zienkiewicz, 1977)

from ordinary strains from the following equation:

$$\varepsilon = \ln (\ell - \Delta / \ell) \tag{2.23}$$

where ℓ = original sample height

Δ = total sample compression

Similarly, true stresses are calculated from the original cross-sectional area and the lateral deformations occurring during the test. Since, in the present case, the cross-sectional area of the sample remains unchanged during the test, true stresses are thus equal to ordinary engineering stresses. The shape of the resulting true stress-true strain curve, as obtained from a confined compression test and shown in Fig. 2.12, exhibits an inflection point and thus misrepresents the actual stiffening behaviour of the snow material under these particular loading conditions.

A simple different procedure, combining incremental and direct iteration techniques and based on the volume change of the material, is adopted in the present model. As mentioned in the previous section, the updated density associated with each triangular element at the end of each plate displacement or shear stress release increment is calculated and recorded. Since, in a confined compression test, volume change can be directly related to axial strain, an "equivalent" axial strain for a given element can therefore be obtained (Fig. 2.13):

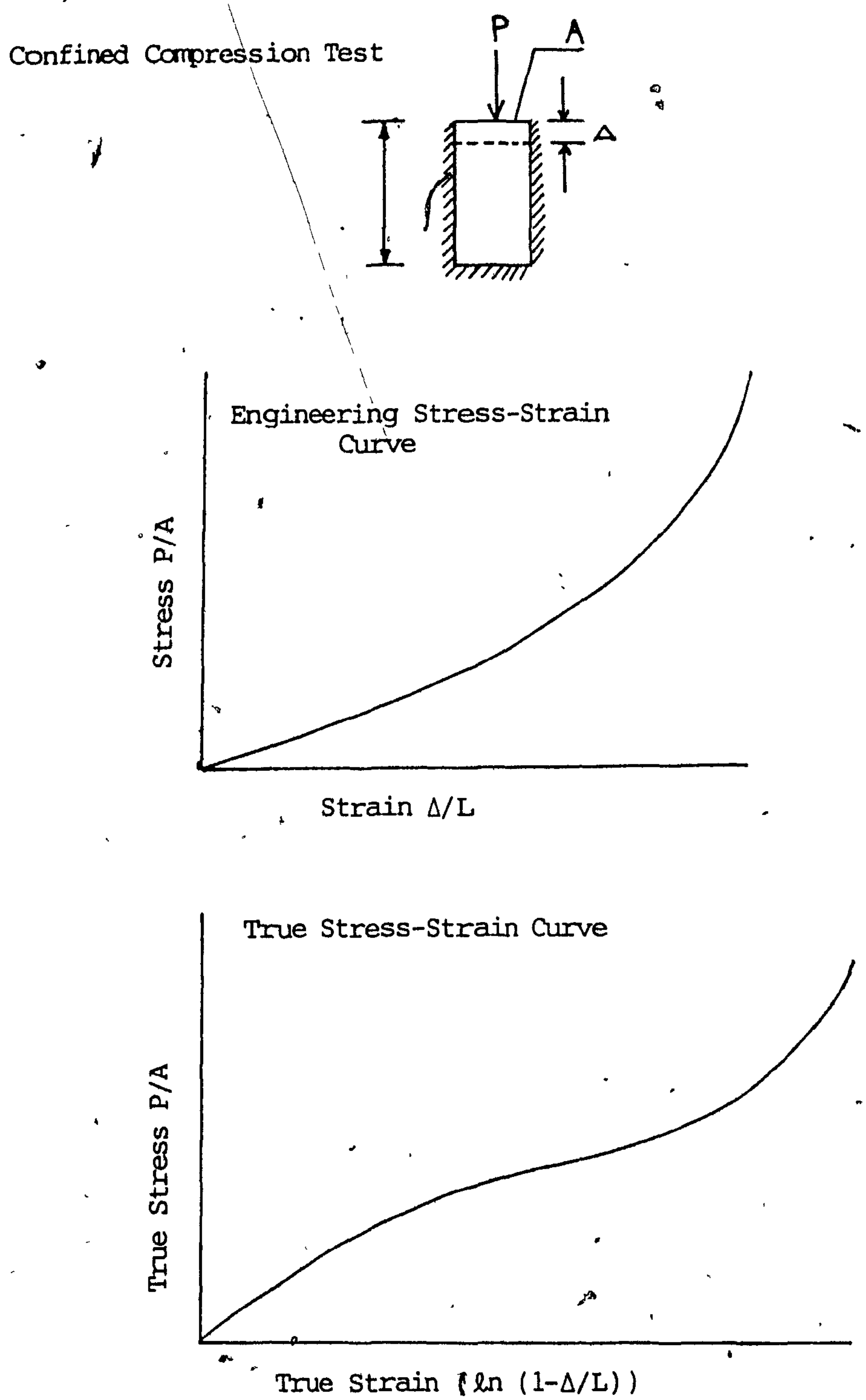

Fig. 2.12 Engineering and True Stress-Strain Curves

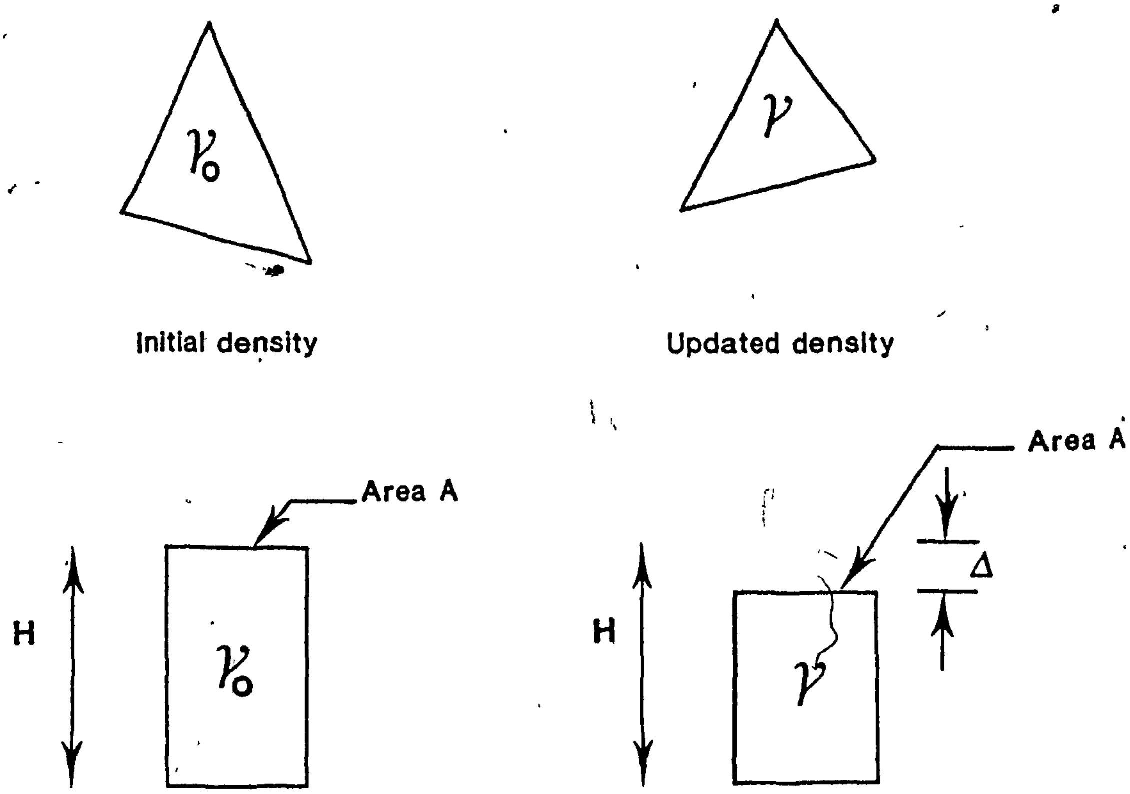

$$\gamma_o AH = \gamma A(H-\Delta)$$

$$\frac{\gamma_o}{\gamma} = 1-\Delta/H = 1-\epsilon$$

$$\epsilon = 1 - \gamma_o/\gamma$$

Fig. 2.13 Updating of State of Strain of Continuum Elements

$$\varepsilon_{eq} = 1 - \gamma_o / \gamma \tag{2.24}$$

where ε_{eq} = "equivalent" axial strain

γ = updated snow density for a given element

γ_o = initial snow density prior to plate penetration.

The corresponding stress value, σ_{eq}, can be obtained by interpolation from the confined compression curve. The quantities ε_{eq} and σ_{eq} are thus assumed to represent the average state of stress and strain within a given element at the beginning of a particular increment.

In the technique for the analysis of non-linearity adopted in the present model, the strain level (or "equivalent" axial strain discussed above) for each triangular element is first checked against a value of 0.1. If it is found that the strain level in all elements is less than this value, the iterative non-linear analysis procedure is omitted simply on account of the fact that for strains up to 0.1, the confined compression curve was found to be linear for the types of snow tested and for the loading rate used. When the non-linear analysis is required, an equivalent stress-strain curve is generated for every element and essentially depends on the state of strain within each element. The resulting curve represents the stress-strain behaviour at a particular level of strain of the snow (Fig.

2.14). Given the average state of strain and stress in a given element to be (ε_{eq}, σ_{eq}), the equivalent stress-strain curve is generated by taking the point (ε_{eq}, σ_{eq}) as the origin. ~~The~~ points describing the new curve for the given increment are thus:

$$\varepsilon_i = \text{STRAIN}_i - |\varepsilon_{eq}| \qquad (2.25)$$
$$\sigma_i = \text{STRESS}_i - |\sigma_{eq}|$$

(i = 1,2,3,....N)

where N = number of points describing the digitized confined compression stress-strain curve.

STRAIN $_i$ = strain (computed as the ratio of sample deformation to original sample height) coordinate of point i of the confined compression curve.

STRESS $_i$ = stress coordinate of point i of the compression curve.

ε_i, σ_i = strain and stress coordinates of point i of the new equivalent stress-strain curve.

ε_{eq}, σ_{eq} = "equivalent" strain and stress values of snow at the start of a given increment, as discussed earlier.

The non-linear analysis procedure is then based on the comparison between the value of stress corresponding to the maximum principal stress computed for the increment and that

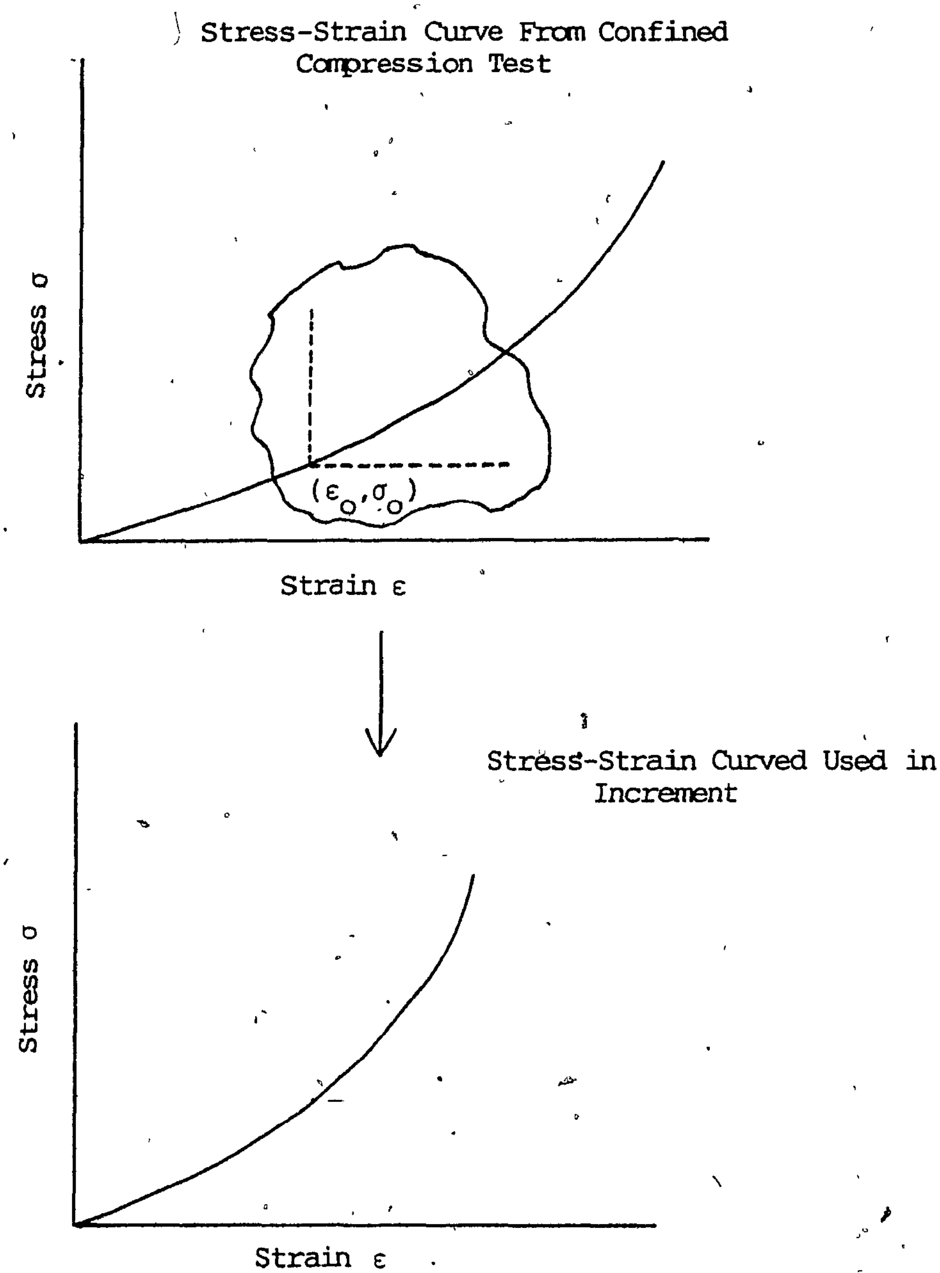

Fig. 2.14 Updating of Stress-Strain Curve for Continuum Elements

obtained by interpolation, at the same strain, of the new equivalent stress-strain curve derived as described above. For a given element, the discrepancy ERROR between these stress values can be expressed as a percent error:

$$\text{ERROR} = \left| 100 \times (\sigma_{calc} - \sigma_{int}) / \sigma_{int} \right| \qquad (2.26)$$

where σ_{calc} = calculated stress value corresponding to the maximum principal stress for a particular increment.

σ_{int} = interpolated value of stress from the new equivalent stress-strain curve corresponding to the average strain level or "equivalent" strain at the start of the particular increment.

The maximum error so computed for all triangular elements is taken as the degree of convergence associated with the proposed non-linear analysis technique. In the case when the error exceeds 5% for any element, the convergence is judged inadequate and a new value of elastic modulus is calculated and used in the next iteration:

$$E = \sigma_{int} / \varepsilon_{calc} \qquad (2.27)$$

where E = elastic modulus used in the next iteration.

σ_{int} = same as previously defined.

ε_{calc} = maximum principal strain computed for the particular increment.

The procedure is repeated until the maximum error value ERROR for any element is less than or equal to 5% or, in order to maintain a reasonable computer cost for a given program run, until twelve iterations have been performed. Convergence of the proposed technique for a given element is guaranteed, as schematically described in Fig. 2.15, but may sometimes be very slow particularly in the case where there is an abrupt change in slope of the confined compression stress-strain curve.

Once the desired degree of convergence has been achieved for a given increment, the non-linear analysis technique for the next increment begins with values of elastic modulus for each element equal to those used in the last iteration of the preceding increment.

The procedure developed for the non-linear analysis described in this section is approximate but considering the high compressibility of the material, its inelastic behaviour and the strong dependence of its stiffness properties on volume change, the author felt that the application of such a method was appropriate for such a material under the loading conditions imposed during the plate penetration tests.

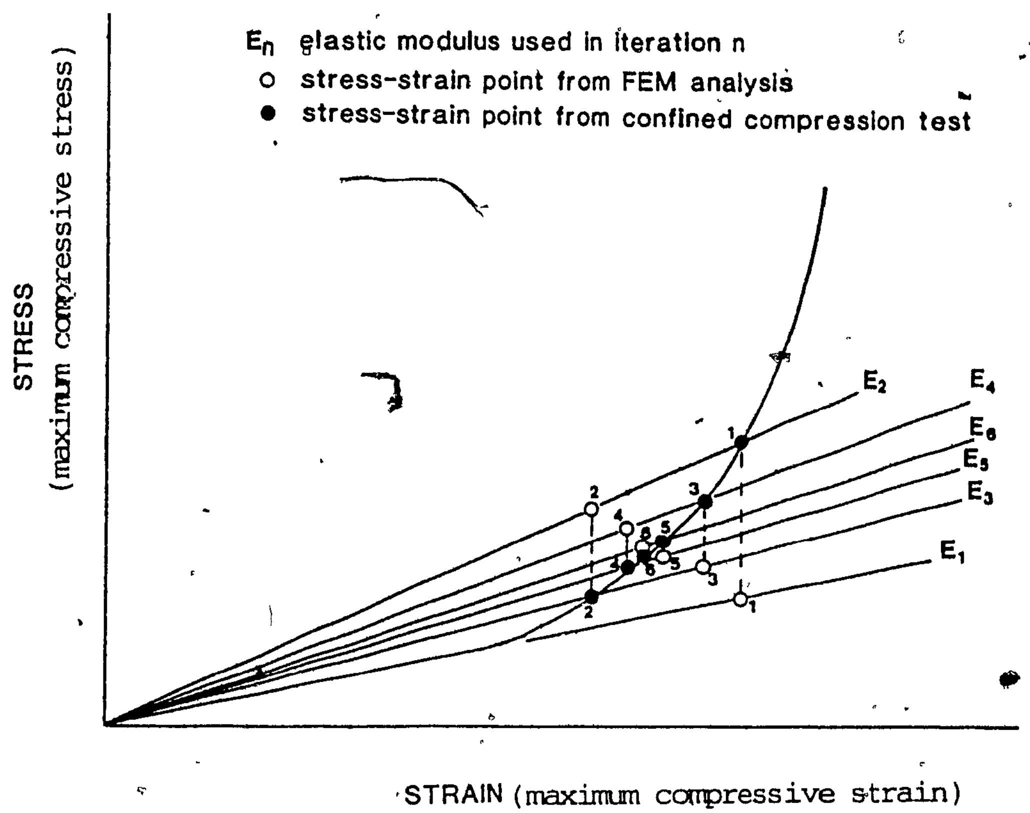

Fig. 2.15 Iterative Procedure for Non-Linear Analysis of Continuum Elements

2.3.5 Analysis For Failure In Shear Of Joint Elements

The analysis for failure of joint elements is performed for every increment of plate displacement. First, the average density across the plane of shearing of a given joint element is computed based on the area of the adjacent triangular element inside the pressure bulb. Area is computed from the resulting updated coordinates, as discussed in section 2.3.3 and shown schematically in Fig. 2.10. The shear strength of the snow material at that density is then computed by interpolation of the shear strength-density curve obtained from vane shear tests and inputted in the computer model as a material characteristic. The cumulative shear stress in a joint element resulting from the superposition of stresses from the present and previous increments is then computed. Shear stress in joint elements is obtained as the product of the shear stiffness per unit length and the average shear displacement, calculated as the average relative displacement of each pair of nodes.

As introduced in section 2.2.3, failure at any point along the planes of cutting shear occurs when the cumulative shear stress in the joint element representing a series of such points exceeds the shear strength of the snow at a density equal to that across the plane of shearing:

i.e. failure if $\tau_c > \tau_r(\gamma)$

where τ_c = cumulative shear stress in joint element.

$\tau_r(\gamma)$ = shear strength of snow at density γ across the plane of shearing.

Therefore, since the shear resistance of snow at any point along the planes of cutting shear varies with density and therefore is a function of the plate penetration (i.e, density distribution along the planes of shear changes with plate penetration), the analysis for failure consists in comparing the shear resistance function at any point and the corresponding cumulative shear stress function for the same point. Failure thus occurs when these two functions intersect as graphically described in Fig. 2.16.

After failure of a given joint element, the shear stress is assumed to remain constant according to the idealization introduced in section 2.2.3 and excess shear stresses must therefore be eliminated for a proper simulation. The procedure for doing so is inspired from finite element analysis of strain softening materials. The method of stress release and transfer was first used by Zienkiewicz et al (1968) for stress analysis in a no-tension material. Lo and Lee (1973) later addressed the problem of slope stability analysis in strain softening materials via a similar approach. According to this method, the difference between the maximum shear stress in a given element and the

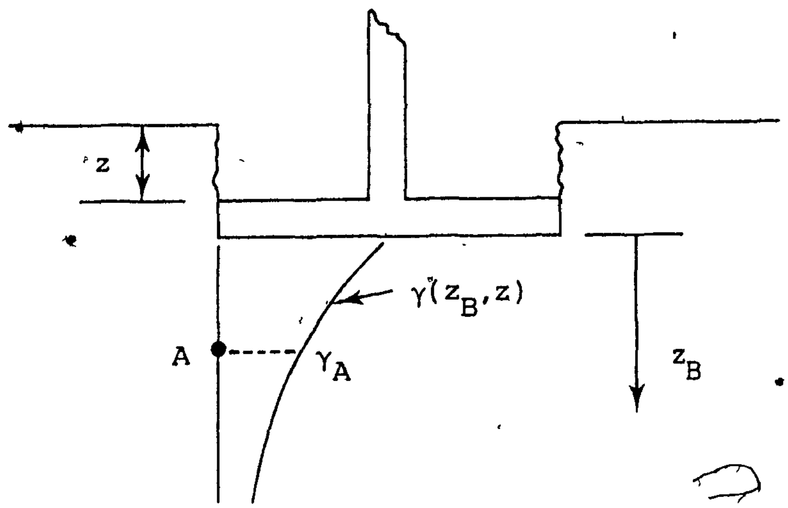

$\gamma(z_B,z)$ = density-depth function along plane of cutting shear

For Point A:

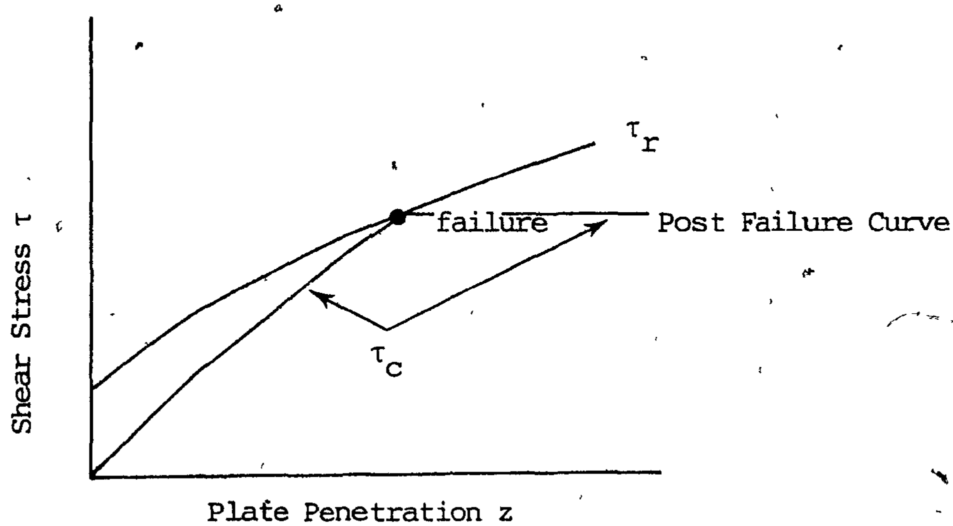

τ_r = shear resistance at Point A as a function of plate penetration

τ_c = total shear stress at Point A as a function of plate penetration

Fig. 2.16 Analysis for Failure of Joint Elements shear strength of the material is taken as an excess shear stress (i.e, the material cannot tolerate a shear stress greater than its shear strength) and must be thus released back into the assumed continuum. This is done by generating a set of equivalent nodal forces using the principle of virtual work. Equal and opposite forces are then applied at the element nodes so that the net effect is to transfer the excess shear stress to neighbouring elements.

In the present case, application of the above method consists of generating four nodal forces, equivalent to the difference $\Delta\tau_i$ (Fig. 2.17) between the cumulative shear stress τ_i in a given joint element at the end of a given increment i and the applicable shear strength $\tau_f(\bar{\gamma})$ along its plane of shear. These nodal forces are actually equal to one half of the load obtained from the product of the above excess shear stress and the shearing area of the element since it can be assumed that each node belonging to one side of the joint element carries an equal share of load.

Therefore consider a joint element for which an excess shear stress $\Delta\tau_i$ has been calculated and whose removal will subsequently lower the cumulative shear stress to the failure value $\tau_f(\bar{\gamma})$. The excess shear load is thus:

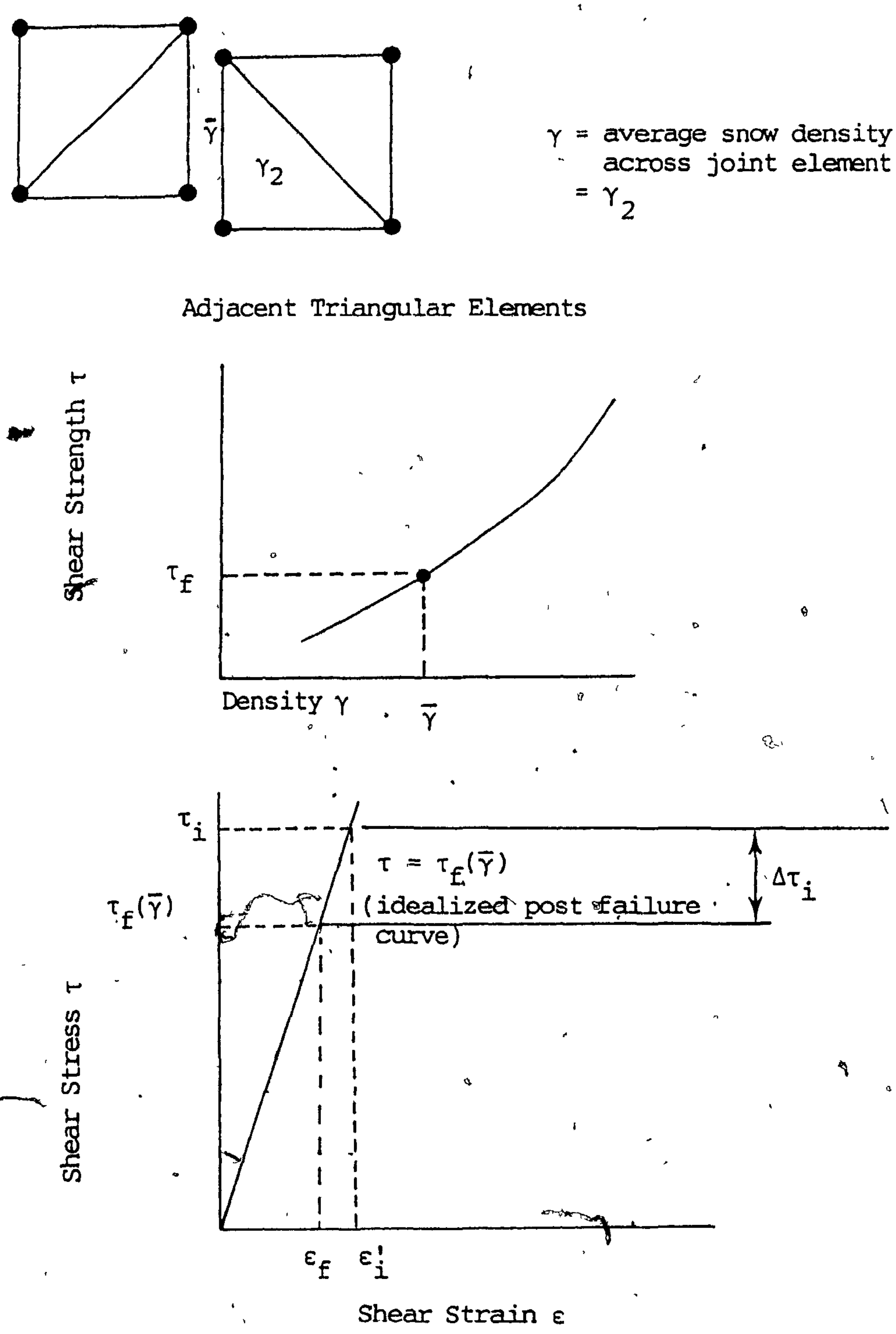

Fig. 2.17 Post Failure Analysis of Joint Elements

$$P_e = \Delta\tau_i \times \text{area of shear} \tag{2.28}$$

$$P_e = \Delta\tau_i \times \ell \times PW$$

ℓ = length of joint element

PW = plate width.

The equivalent forces to be applied at the four nodes of the element are thus equal to:

$$P = P_e/2 = (\Delta\tau \times \ell \times PW) / 2 \tag{2.29}$$

and their direction is opposite to those developed during a plate penetration increment, i.e. as shown in Fig. 2.18. Such a calculation is performed for every failing joint element and the excess shear stress analysis consisting of a finite element analysis with all appropriate vertical loads on joint element nodes is undertaken for every required cycle as outlined in the solution procedure described in section 2.3.3.

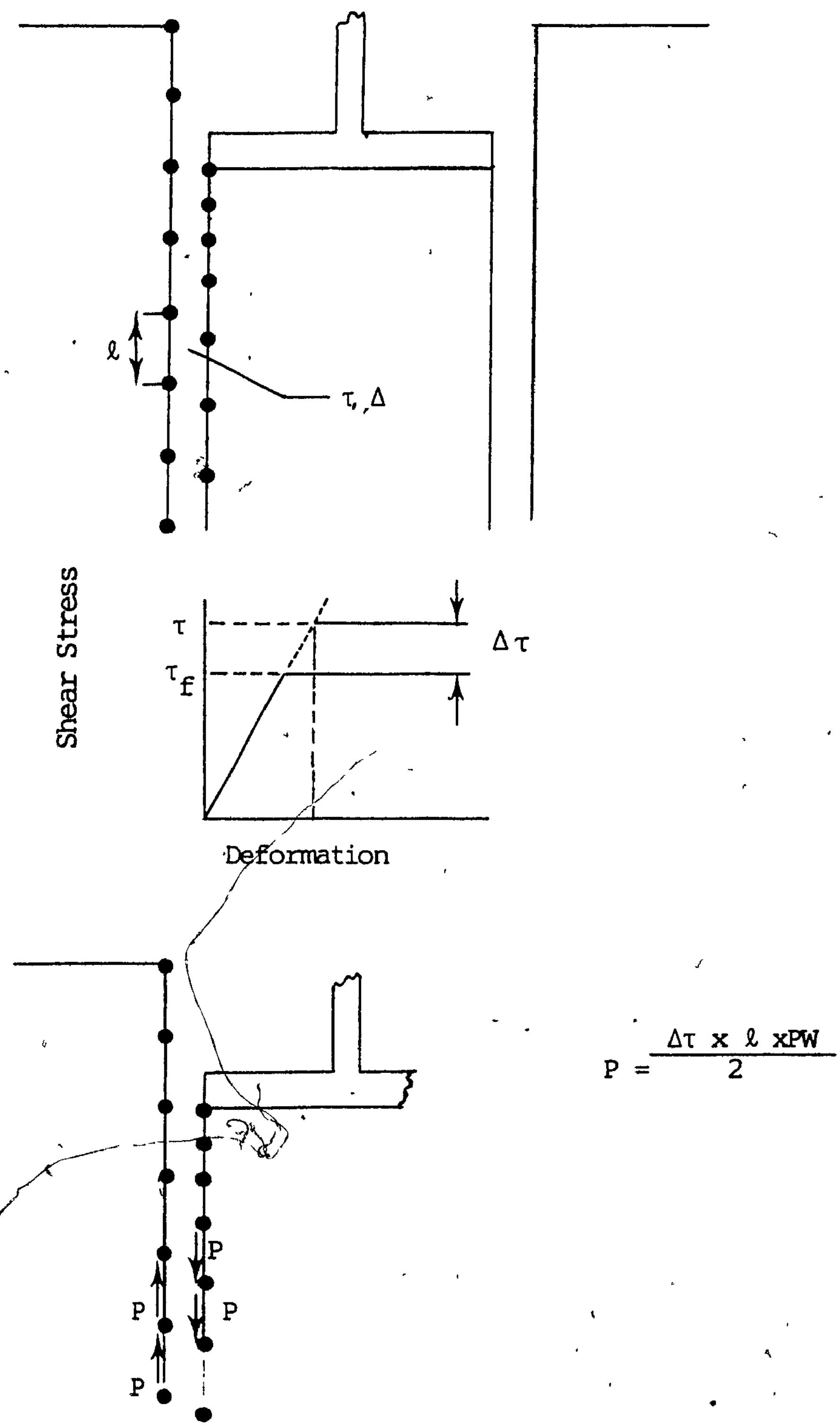

Fig. 2.18 Analysis for Excess Shear Stress Removal in Failed Joint Elements

CHAPTER 3

EXPERIMENTAL PROGRAM AND RESULTS

3.1 Introduction

The proposed method of analysis described in the previous chapter implies assumptions and approximations necessary to the formulation and solution of the present problem. In addition, the components of the proposed model require the following characteristics of the snow material:

1) compressibility as a function of density (axial stress-strain relationship for fully confined conditions),
2) shear stress-strain response as a function of density.

In view of the above, the experimental program carried out during the course of this study was designed to provide required material input parameters as well as for verification purposes of the proposed model and, by the same token, of the assumptions and approximations introduced in the solution procedure. As mentioned earlier, the objective of the present work is the numerical simulation of the load-deformation response of snow to rigid plate penetration with proper consideration of the dependence of material response on density distribution within the pressure bulb beneath the plate. Consequently, the experimental program consisted of three types of test:

1) plate penetration tests performed on snow of two different ages (i.e, different bonding strengths) at a given deformation rate. Results from these tests could then be compared to corresponding predicted values.
2) confined compression tests performed on the same types of snow at the same deformation rate as for plate penetration tests.
3) vane shear tests performed on the same types of snow and at approximately the same deformation rate as for plate penetration and confined compression tests. These tests were carried out for snow of different density so that results could then be used to represent the snow behaviour in shear for the range of densities considered.

3.2 Experimental Program

The three different types of tests and typical results are discussed in the following sections.

3.2.1 Preparation of Snow Samples

Artificial snow material was used in this study because of the critical need to replicate test samples of snow. It was felt that better control on snow properties would be achieved by generating snow in the laboratory. Snow was produced by crushing 3-day old ice with a pulverizing machine (Fig. 3.1) in a cold room of inside average temperature -13°C with fluctuations of ±3°C due to defrosting cycles. The ice crushing process was repeated three times in order to achieve a snow density of approximately 0.35 Mg/m^3.

In all, two types of snow, distinguished by the number of ageing days in the cold room, were used:

1) 4 day old snow (Age 4 days)
2) 30 day old snow (Age 30 days)

Snow samples were aged in the same cold room inside which the snow was produced. Ageing was observed to cause a density increase of the snow as shown in Fig. 3.2. Correspondingly, grain size distribution also varied with ageing time as depicted in Fig. 3.3.

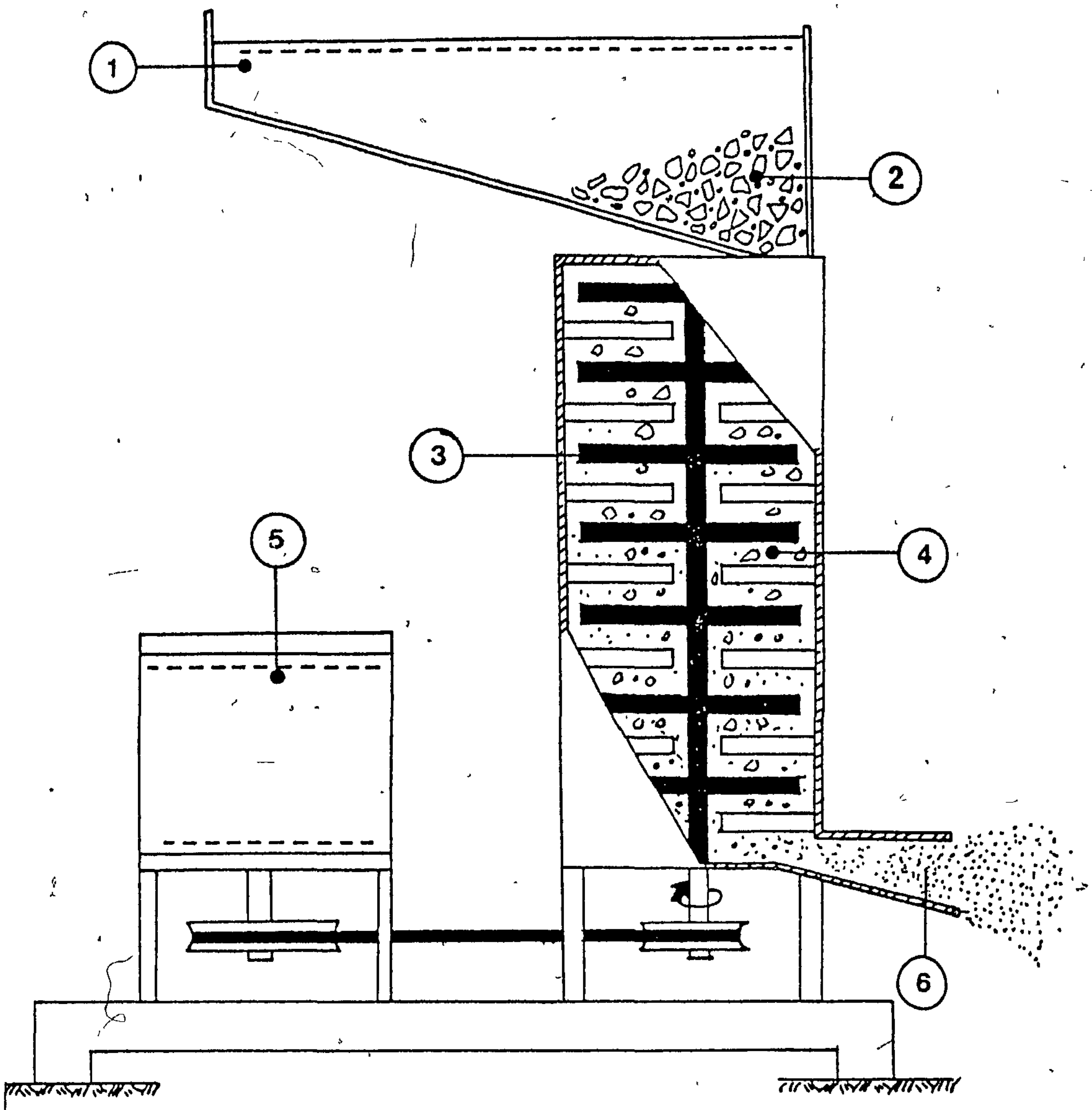

1. hopper
2. crushed ice
3. steel vane
4. drum
5. driving motor
6. artificial snow

Fig. 3.1 Artificial Snow Pulverizer

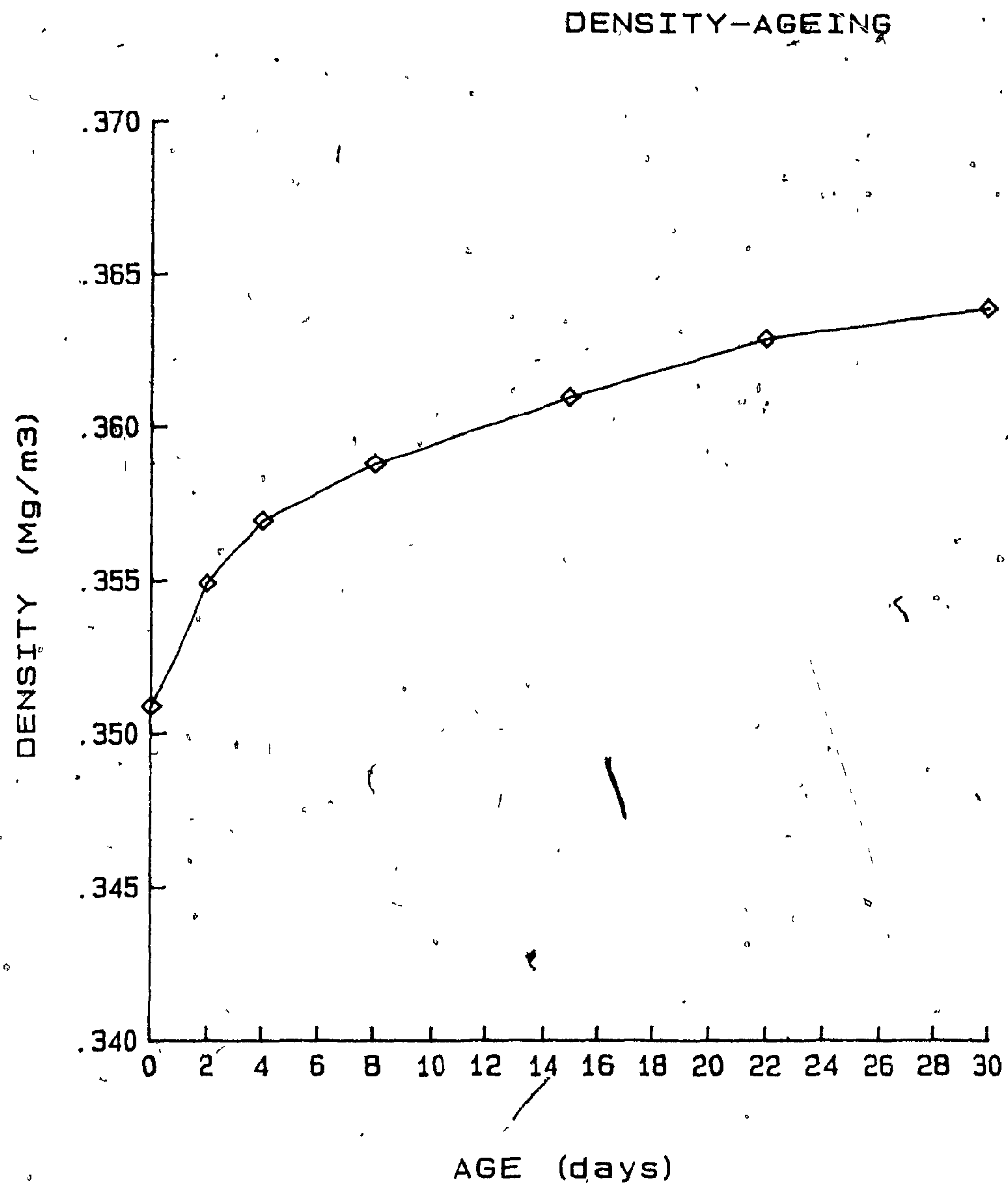

Fig. 3.2 Variation of Density with Ageing Time for Artificial Snow

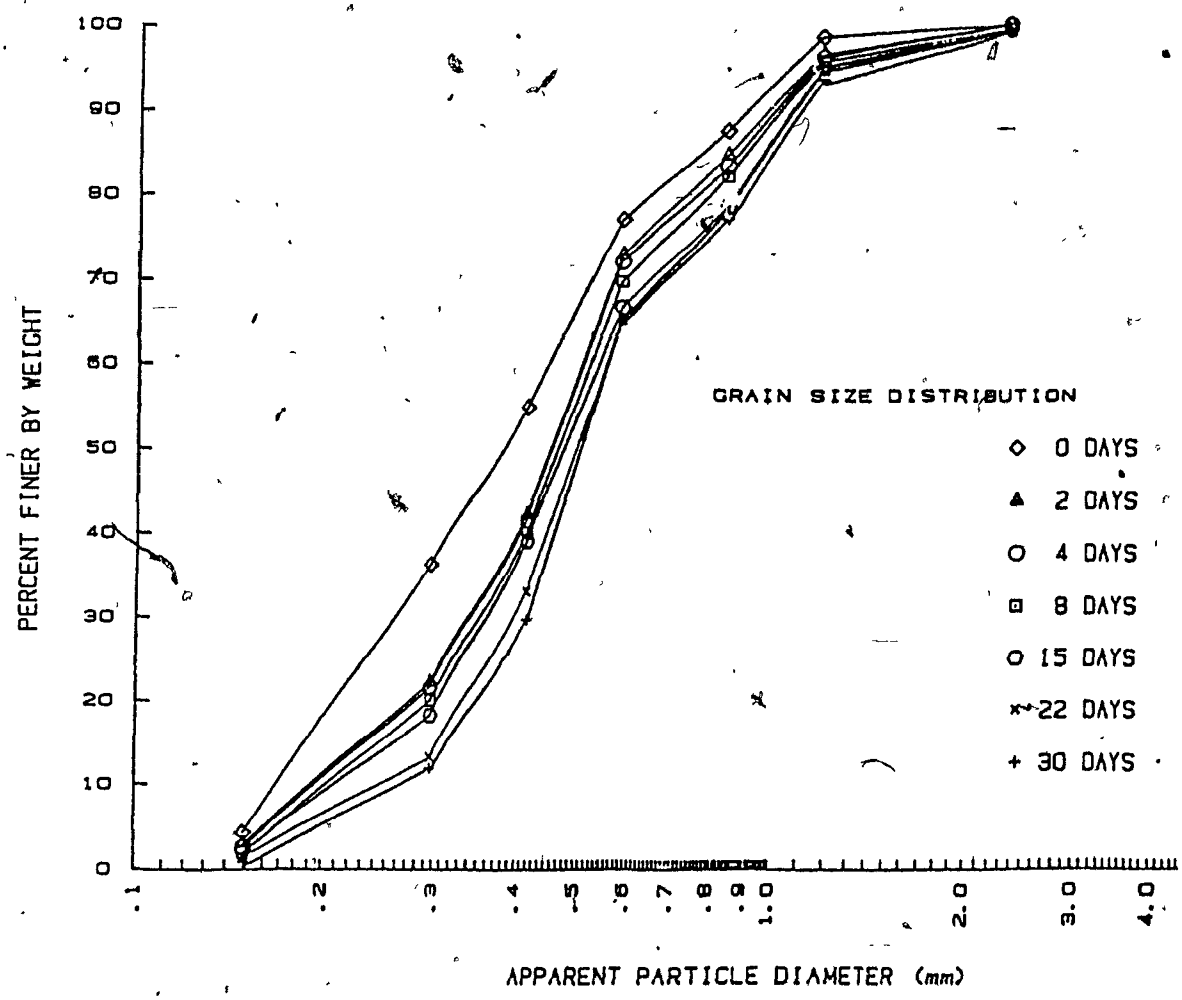

Fig. 3.3 Variation of Grain Size Distribution of Artificial Snow with Age

3.2.2 Confined Compression Testing

Confined compression tests basically consisted in compressing, at a specified deformation rate, cylindrical samples of snow from its initial density to a final specified density of approximately 0.60 Mg/m^3 while recording the load-deformation response. The rate of deformation used was 0.58 mm/sec.

The basic experimental apparatus for confined compression testing consisted of a compression testing machine driven by a 1/4 HP electric motor as shown in Fig. 3.4. A Kulite TC 2000 temperature compensated 500 lb (2224 N) load cell, having a calibration factor of 3.66 N/mV output and receiving input from a 10 V power source located outside the cold room, measured the load applied by the driving piston. Displacement of the piston was measured with a Pickering LVDT 7312-V2 displacement transducer having a calibration factor of 0.1 mm/mV output and being powered by a 6 V source. Both load and displacement were recorded on a two-channel Sanborn 320 chart recorder located outside the cold room. Tests were conducted using plexiglas cylinders of 38 mm inner diameter, 6 mm wall thickness and 178 mm height, perforated by small holes to allow for air extrusion during compression of snow samples.

Artificially prepared snow was deposited into the cylinders with a 2.4 mm size sieve from a height of 100 mm.

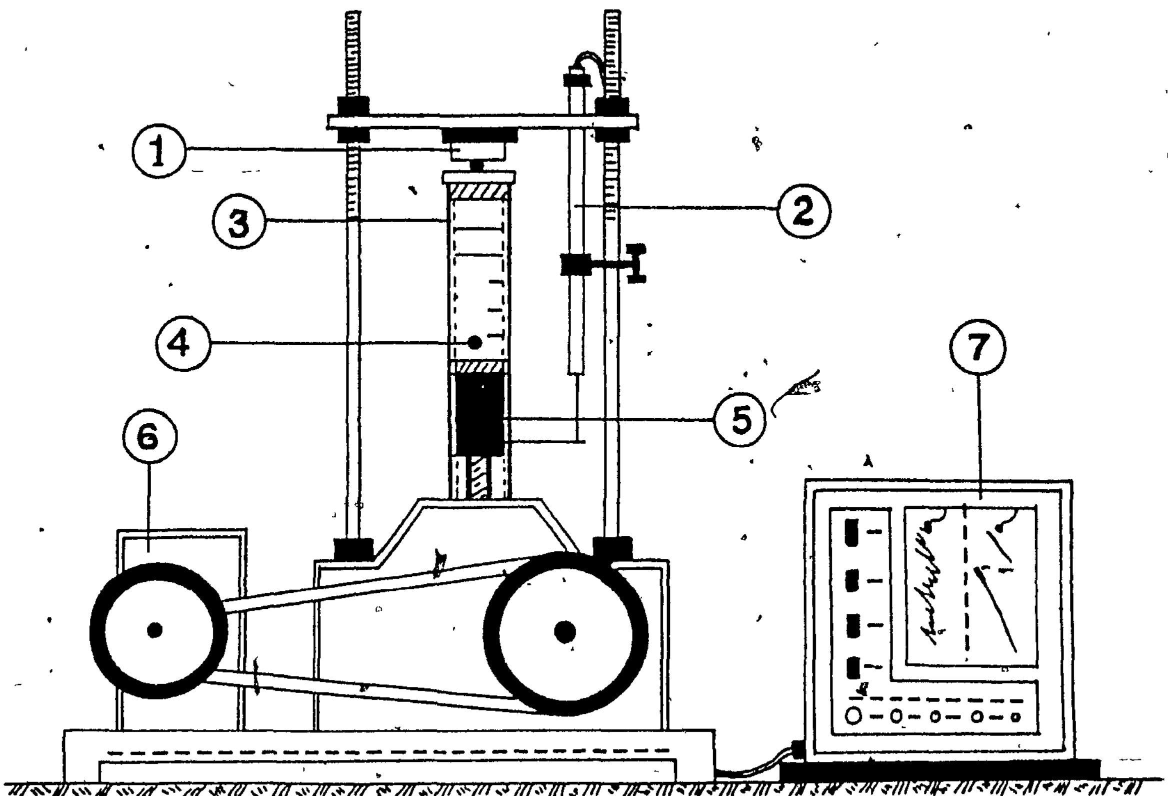

1. load cell
2. displacement transducer
3. casing
4. Snow Sample
5. driving piston
6. driving motor
7. recording system

Fig. 3.4 Apparatus Used for Confined Compression Test

The initial density of snow, determined using a Ohaus triple beam balance with a precision of 0.1 g, was more or less constant and equal to 0.35 Mg/m^3 ± 1.2%. Ageing of samples took place inside the cold room, as mentioned earlier, in thermally insulated boxes to avoid temperature change effects due to defrosting cycles. These boxes provided protection to the samples from air movement, humidity, light and other factors possibly influencing the ageing process.

Each individual test began by placing a cylinder containing a snow sample on the compression machine piston, just small enough to fit inside the cylinder. Friction between the piston and the interior wall of the cylinder was thus minimal. The compression machine was then started moving the piston upwards at a constant specified rate, thus compressing the snow. Friction between snow and the cylinder wall was negligibly small due to both the self-lubricating properties of the snow and the smoothness of the plexiglas material. As the piston moved, the load-displacement response was recorded on the chart recorder. The compression machine was stopped at piston penetration of approximately 76 mm, corresponding to a density of about 0.60 Mg/m^3. For the 30 day old snow samples, the machine was stopped somewhat before a piston penetration of 76 mm so as to allow an adequate margin of safety in reference to load cell capacity. Confined compression tests were repeated three times in order to check the reproduceability of results.

3.2.13. Shear Testing

The shear strength of snow was investigated through vane shear tests on snow compressed to a given density. More specifically, these tests were performed on the snow compressed during the plate penetration process. Once the desired maximum plate penetration was achieved, the plexiglas boxes were turned on their side and the front side wall removed. Samples were then extruded from the snow mass using thin walled aluminum tubes for determination of density. Density was calculated from the weight of the samples and the volume of the tubes. A portable hand vane was then utilized to determine the shear strength of the snow at approximately the same location from which the snow samples were taken (Fig. 3.5). The vane was inserted into the snow and turned very slowly (in order to approximately match the deformation rate selected for confined compression testing) until failure was observed. By repeating this procedure for many points inside and outside of the pressure bulb (highest density occurred near the plate and then decreased with distance), a relationship between shear strength and density could then be generated for snow of a given age.

It should be noted that during vane shear testing of snow, no stress normal to the surface of shear was externally applied. This is consistent with the real

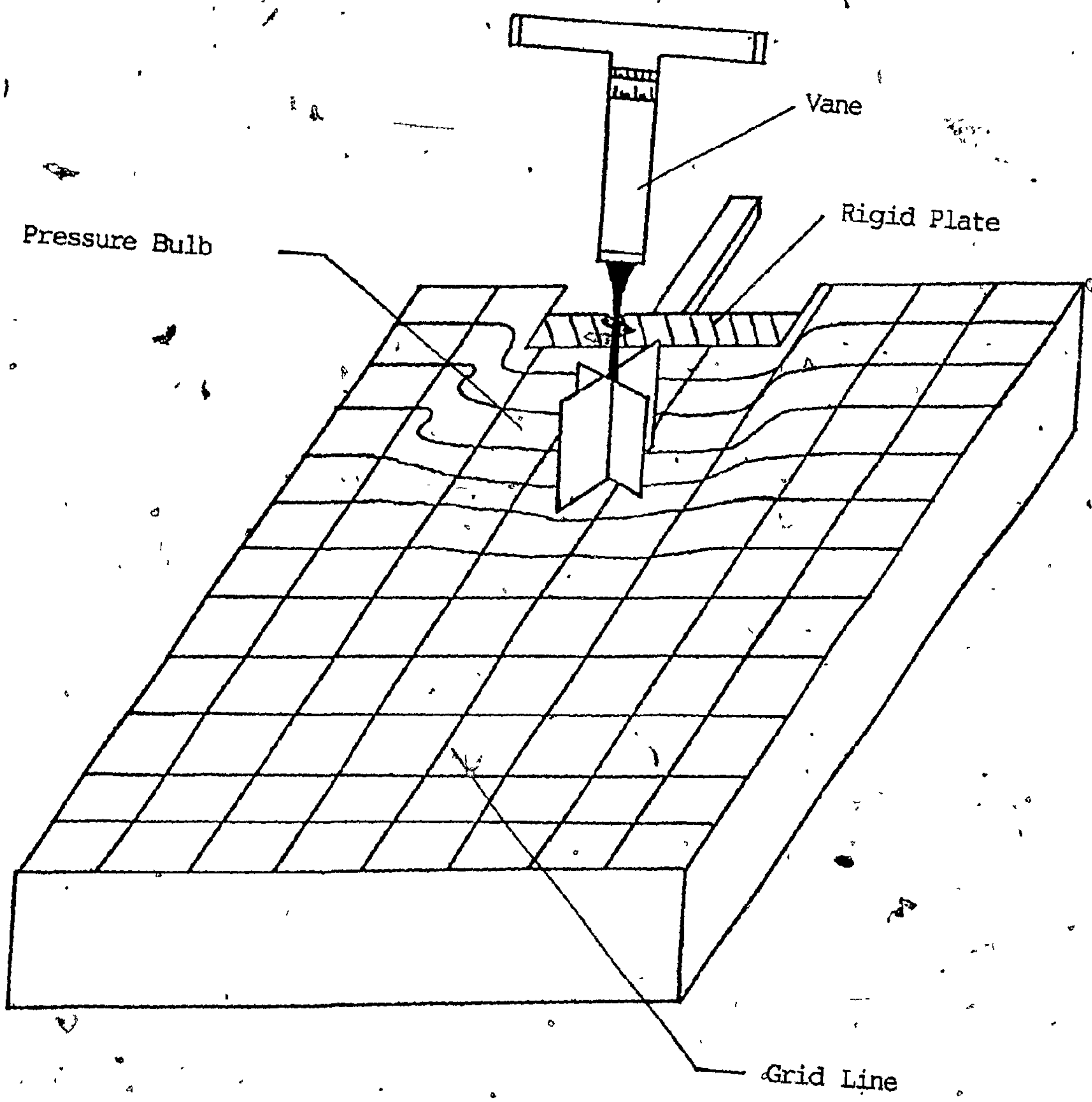

Fig. 3.5 Vane-Shear Test on Snow Previously Compressed by Plate Penetration

situation found during plate penetration tests during which no significant stresses normal to the planes of cutting shear are likely to develop due to the low Poisson's ratio of the material.

3.2.4. Plate Penetration Testing

Speed controlled plate penetration tests were performed on deep snow of approximate initial density 0.35 Mg/m^3 and aged for a specified number of days in the cold room. One of the objectives being to relate the behaviour of snow subjected to different loading conditions, it was thus necessary to test the same snow types at a deformation rate indentical to that used in confined compression and vane shear tests (i.e, 0.58 mm/sec).

The experimental apparatus designed and utilized in this series of tests is shown in Fig. 3.6. The loading system consisted of a moveable platform driven by a 3/4 HP DC motor located at the bottom of an aluminum frame of 1.75 m height, 0.90 m width and 0.46 m depth. A switch box enabled to have control of the deformation rate (i.e, the vertical speed of the platform) which could reach up to 30 mm/sec.

Plexiglas boxes, measuring 0.54 m in length, 0.79 m in depth and 0.1 m in width (outside dimensions), contained the snow samples for plate penetration testing.

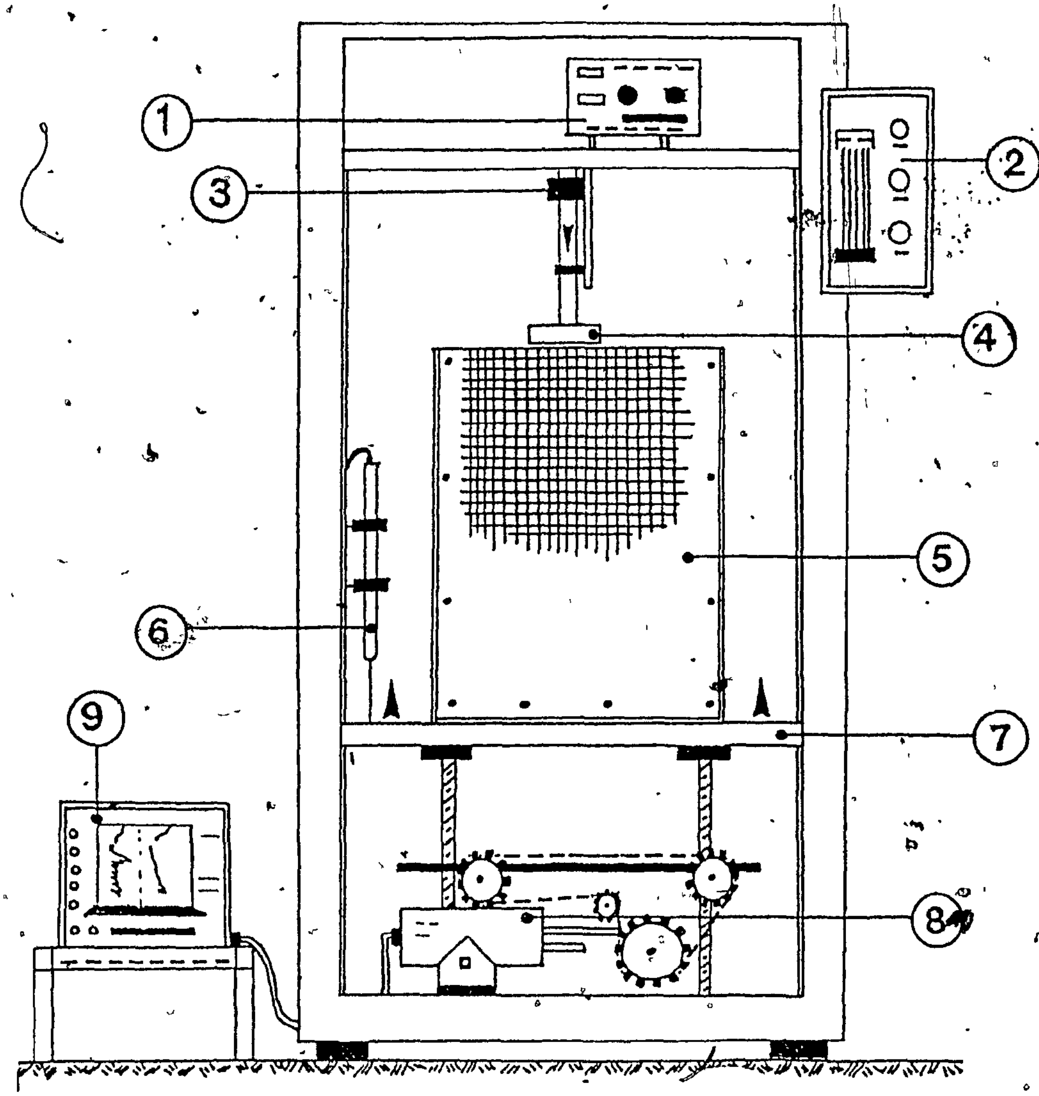

1. switch box
2. speed control unit
3. load cell
4. rigid plate
5. snow box
6. displacement transducer
7. moving platform
8. driving system
9. recording system

Fig. 3.6 Apparatus Used for Plate Penetration Tests

The length and depth of the boxes were chosen in relation to the loading plate length and maximum penetration depth so as to avoid side and bottom effects, respectively. In addition, the width of the boxes was such that the distance between the walls was just large enough to allow passage of the loading plate. A 71 mm x 71 mm square plate of 13 mm thickness was used.

The instrumentation (load cell, displacement transducer and chart recorder) which recorded the load-penetration relationship was the same as that used for the confined compression tests.

Test began by placing a given snow box on the platform and setting the deformation rate control switch to the position corresponding to the specified value of platform speed. Another switch started the moving platform upwards. The load cell and displacement transducer recorded the reaction force on the plate and the platform displacement (corresponding to the plate penetration in the snow), respectively, whose magnitudes appeared graphically on the chart recorder. Simultaneously, photographs of a grid, drawn on the snow during sample preparation using fine black sand, were taken at given time intervals thus recording the deformation patterns below the plate induced by the loading process.

3.3 Experimental Results and Discussion

Typical results from the three types of tests described in section 3.2 are shown and discussed in the following sections.

3.3.1 Confined Compression Response and Results

In a confined compression test, the material undergoes an axial deformation while lateral displacements are prevented. For a material with a relatively high Poisson's ratio, a lateral pressure develops and therefore the confining stress on the sample increases due to the restriction of lateral movement by the rigid wall of the plexiglas container. For soils, stress-strain behaviour is dependent on confining pressure and consequently, a confined compression test yields information of questionable value since the confining pressure varies throughout the test. However, when a material with a low Poisson's ratio, such as the snow types used in the present study, is tested in similar conditions, lateral deformations are minimal and thus lateral pressure is small in relation to the axial pressure. It can therefore be deduced that for such a material, the effect of confining pressure is insignificant.

Stress-strain relationships under confined compression conditions were obtained from test results simply by dividing the recorded load and piston displacement values by the cross-sectional area and original height of the sample, respectively. An example of a typical curve is illustrated in Fig. 3.7, showing a generally increasing slope, i.e. characteristic of a stiffening material, and the presence of microfractures also referred to as the "saw-tooth" effect and previously reported by Yong and Fukue (1977). This microfracturing behaviour is reflective of local failures caused by fracture of bonds between snow particles due to local stresses exceeding the bond strength. A resulting load transfer to other bonds occurs until their strength is in turn exceeded, due to stress superposition. A stress release is exhibited whenever bonds are broken and a subsequent stress build-up occurs as other bonds accept a share of the load transferred to them. The process, however, also causes packing of the snow particles which then offer more and more resistance to further compression. This effect seems to be dominant as the shape of the stress-strain curve, including both the bond fracture and densification mechanisms, is typically concave up thus implying that the material becomes stronger as load is increased, in spite of the increasing number of broken bonds. It can also be seen from the stress-strain curve that continued compression eventually produces a condition in which microfracturing eventually stops thus seeming to indicate that bond breakage becomes negligible after a

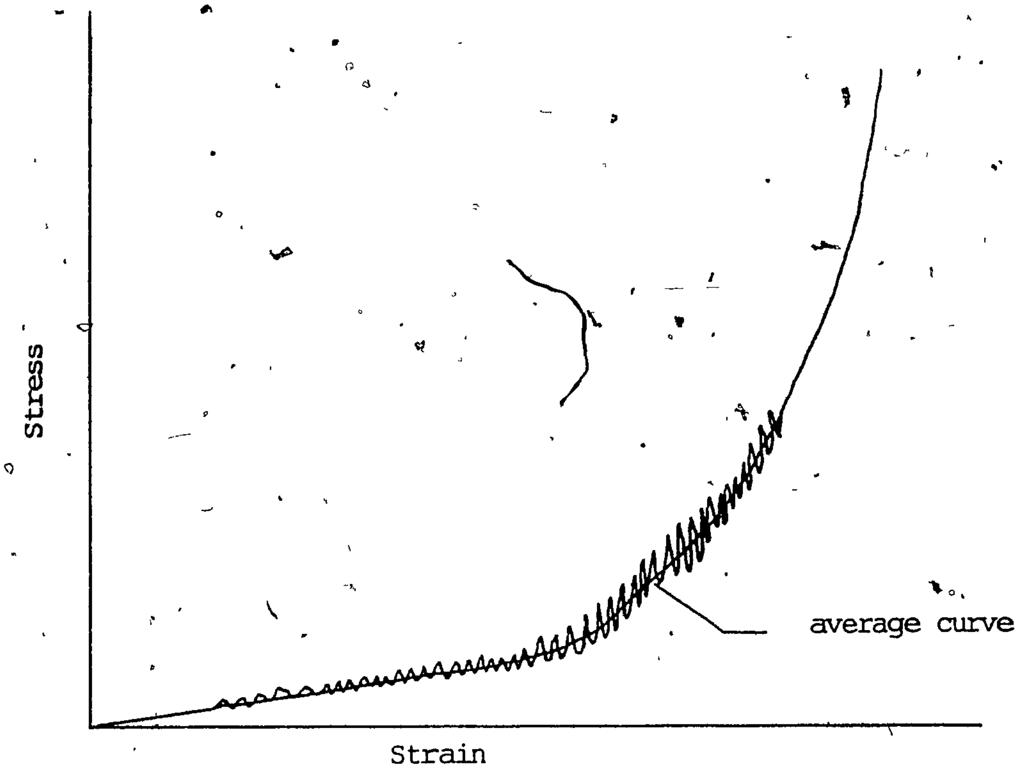

Fig. 3.7 Typical Curve From a Confined Compression Test

certain point. This condition arises when the snow material, having undergone a given volumetric strain, reaches the "threshold density", also discussed by Yong and Fukue (1977). Threshold density can be formally defined as the snow density at which no microfracturing will subsequently develop when the snow is subjected to speed controlled confined compression testing conditions and depends on the deformation rate. Beyond the volumetric strain corresponding to the threshold density, stress increases rapidly with respect to strain as microfracturing no longer occurs and as the degree of particle packing increases. Ultimately, further compression would produce a high density snow (0.60 Mg/m^3 and greater) with a higher Poisson's ratio and thus for which the confining stress during confined compression testing can no longer be disregarded. The analysis of the behaviour of such type of snow is however beyond the scope of the present study.

In the present work, results from confined compression tests are viewed simply as a characteristic to be inputted in the developed finite element model. The data describes the stress-strain behaviour in compression or compressibility of the snow material. The amplitude of the stress releases observed during tests were seen to be small with respect to the stress values themselves so that, consequently, the "saw-tooth" effect due to microfracturing is ignored as a parameter describing the stress-strain response. An average curve was thus fitted through the center of the recorded peaks and troughs, as shown in Fig. 3.7. The resulting stress-strain relationships obtained for the two snow types (i.e, age 4 and 30 days) are shown in Figs. 3.8 and 3.9 respectively. The same stress-strain data, presented differently in Fig. 3.10, schematically describes the effect of age on stress-strain response. Ageing of snow increases the degree of bonding and, as expected, the stress corresponding to a particular value of strain increases with the number of ageing days, thus demonstrating the higher resistance of older snow.

3.2.2 Response in Shear and Results

In a vane shear test, it is assumed that the snow is tested at essentially constant density. The fact that the failure plane is predetermined is consistent with the idealized version of the real situation of plate penetration in which the location of the shear plane is known (i.e, vertical planes through the edges of the plate). Although, in reality, the failure plane develops progressively as opposed to being established completely prior to loading as in the analytical model, it was felt that results from vane shear tests could be useful in the description of characteristics representing the behaviour of snow at points where the material is acting principally in pure shear (i.e. along the failure planes).

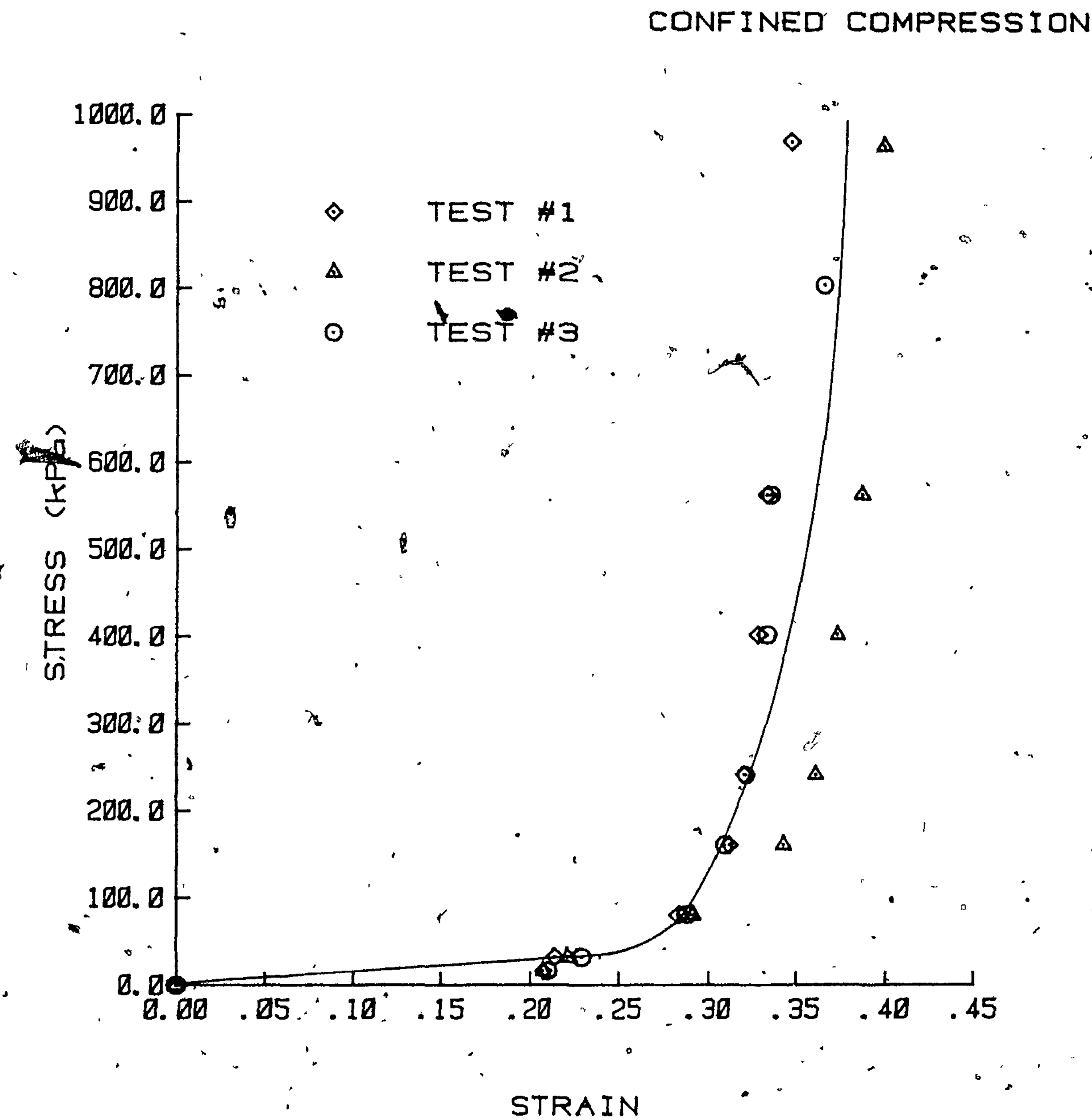

Fig. 3.8 Confined Compression Test Results - Age 4 Days

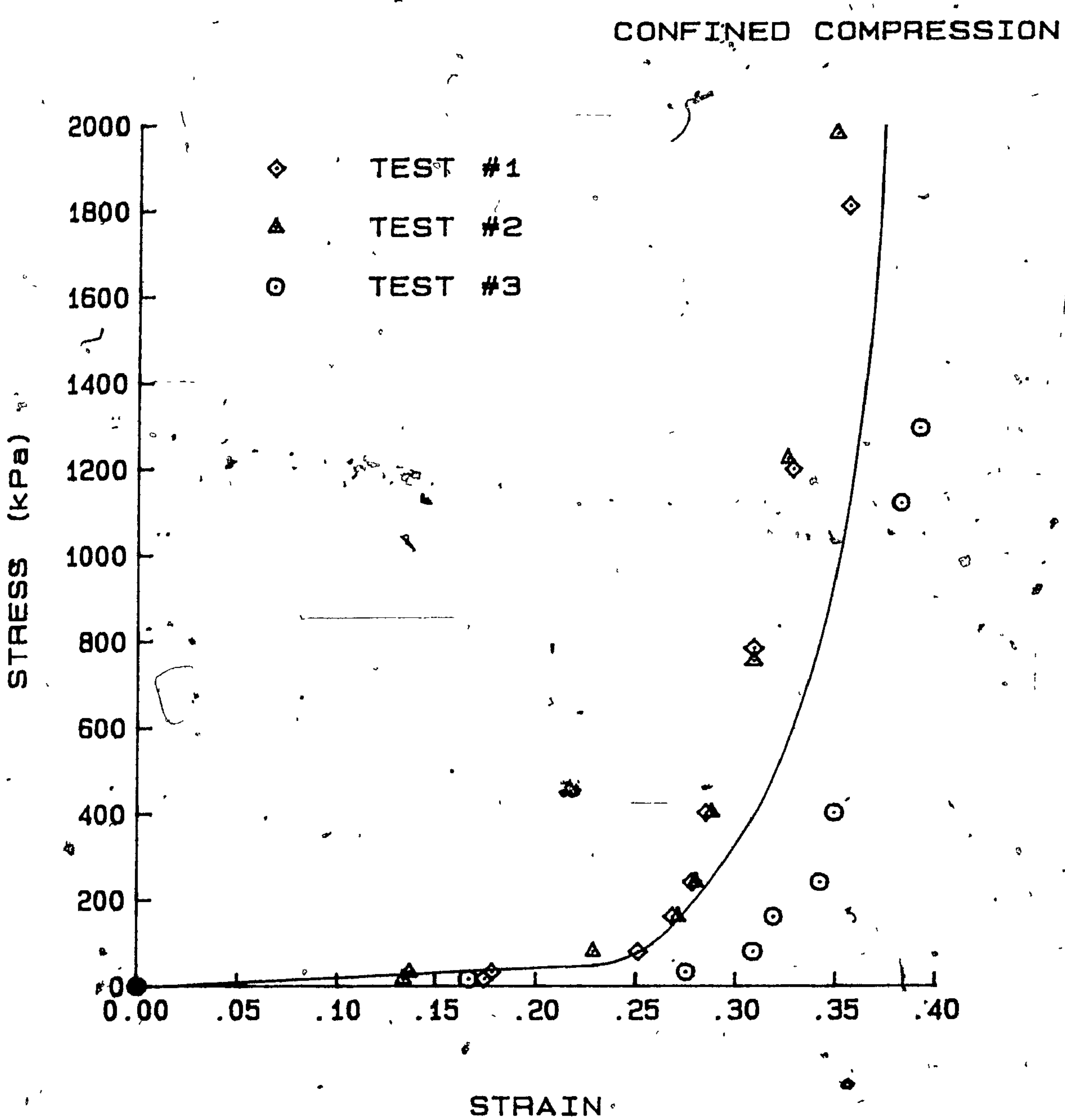

Fig. 3.9 Confined Compression Test Results - Age 30 Days

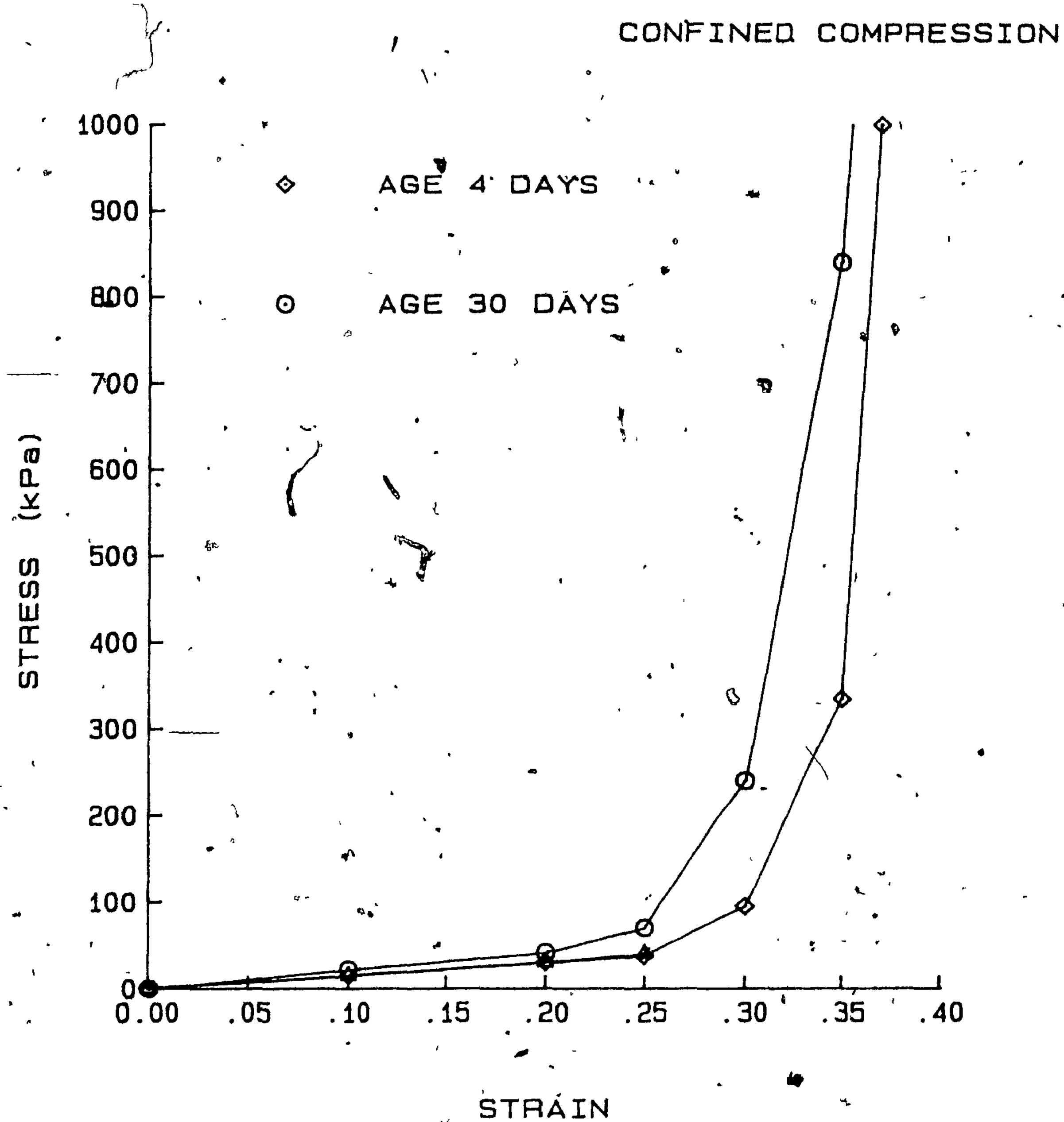

Fig. 3.10 Confined Compression Test Results - Age Effect

Results from vane shear tests essentially consisted of shear strength-density relationships, corresponding to the given deformation rate, for the two types of snow used. Shear strength of snow was computed from the vane reading and a calibration factor. Results, illustrating the effect of age, are graphically displayed on Fig. 3.11. A general pattern is observed according to which, as expected, shear strength of snow increases with density as well as with the number of ageing days. During the vane shear tests performed during the study, it was not possible to measure the shear resistance as a function of vane rotation since the recorded vane reading corresponded to the maximum shear stress developed (i.e, the shear strength). This, however, did not cause many problems in the formulation of the present model as the post-peak behaviour in shear was actually idealized in this study, and was discussed in more detail in Chapter 2 (section 2.2.β). Since the proposed model does require a stiffness parameter for snow in shear, which can only be obtained from a shear stress-deformation curve, such a number was thus assumed and considered as an additional parameter in the present study.

Shear tests thus provided means to determine the shear resistance of snow at a given density but other parameters describing the shear stress-deformation curves (required in the model as outlined in Chapter 2) had to be obtained from other sources due to limitations of the experimental facility.

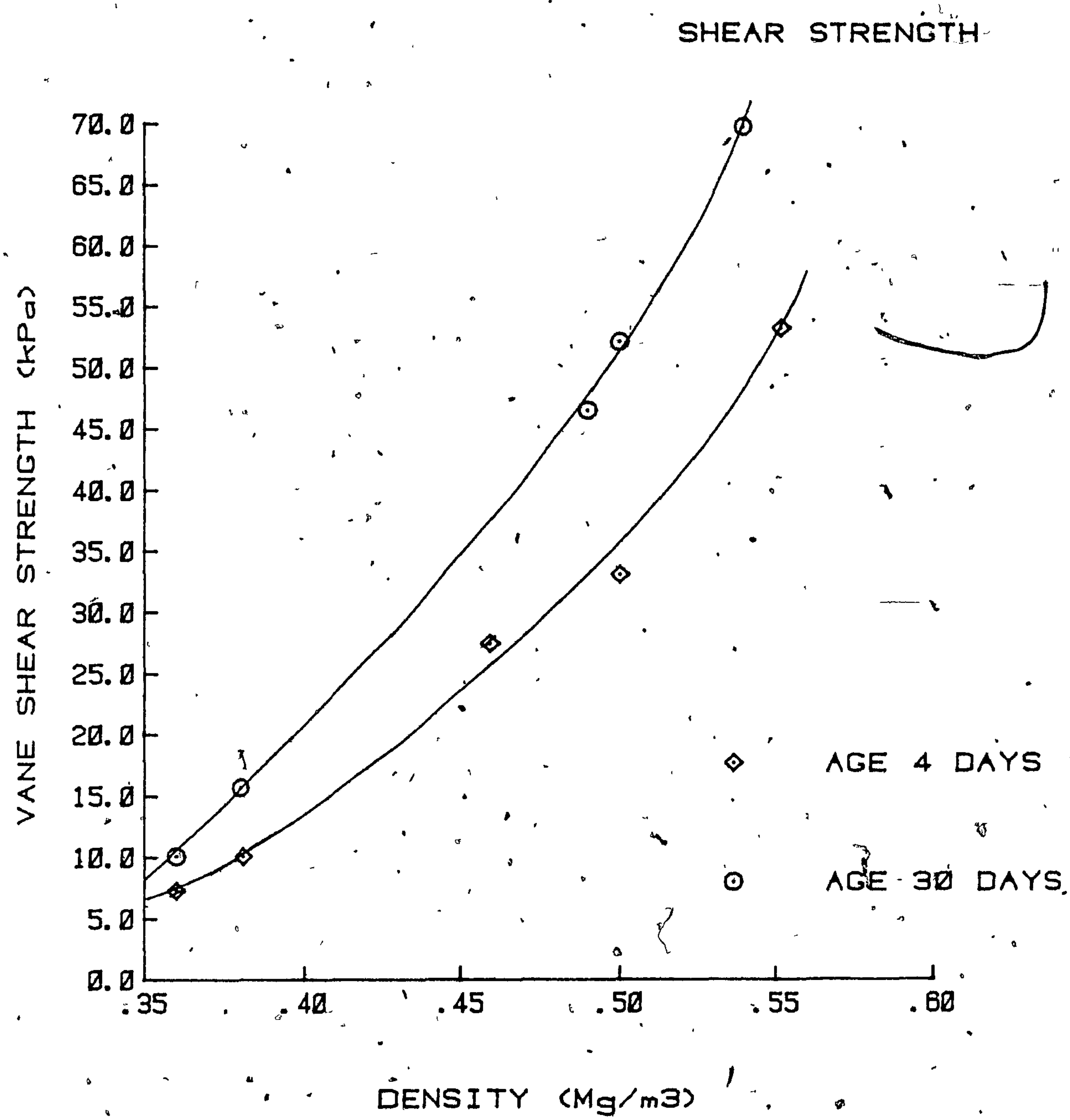

Fig. 3.11 Vane Shear Strength Results

3.3.3 Plate Penetration Response and Results

As mentioned earlier, a plate penetration test represents a loading situation in which both volume change and shear mechanisms occur simultaneously. As penetration of the plate in the snow sample progresses, a reaction load on the plate develops because of the resistance of the snow beneath the plate to undergo volume change and shear along the vertical planes of cutting shear passing through the edges of the plate. The recorded load-penetration response of a given snow type corresponding to a given penetration rate is therefore the result of the combined action of the two mechanisms mentioned above.

The load-penetration curves for ages 4 and 30 days are shown in Figs. 3.12 and 3.13. The "saw-tooth" effect, observed in confined compression tests, is also exhibited due to elements of snow within the stress bulb beneath the plate being subjected to a loading condition similar to that of confined compression as a result of the low Poisson's ratio of the material. As the plate penetrates deeper into the snow, more and more of these elements are involved in the volume change process, i.e the stress bulb extends deeper as penetration progresses. This reasoning seems to be supported by the fact that the amplitudes of stress releases increases with plate sinkage, due to a greater amount of snow material undergoing the bond breaking mechanism described in section 3.3.1.

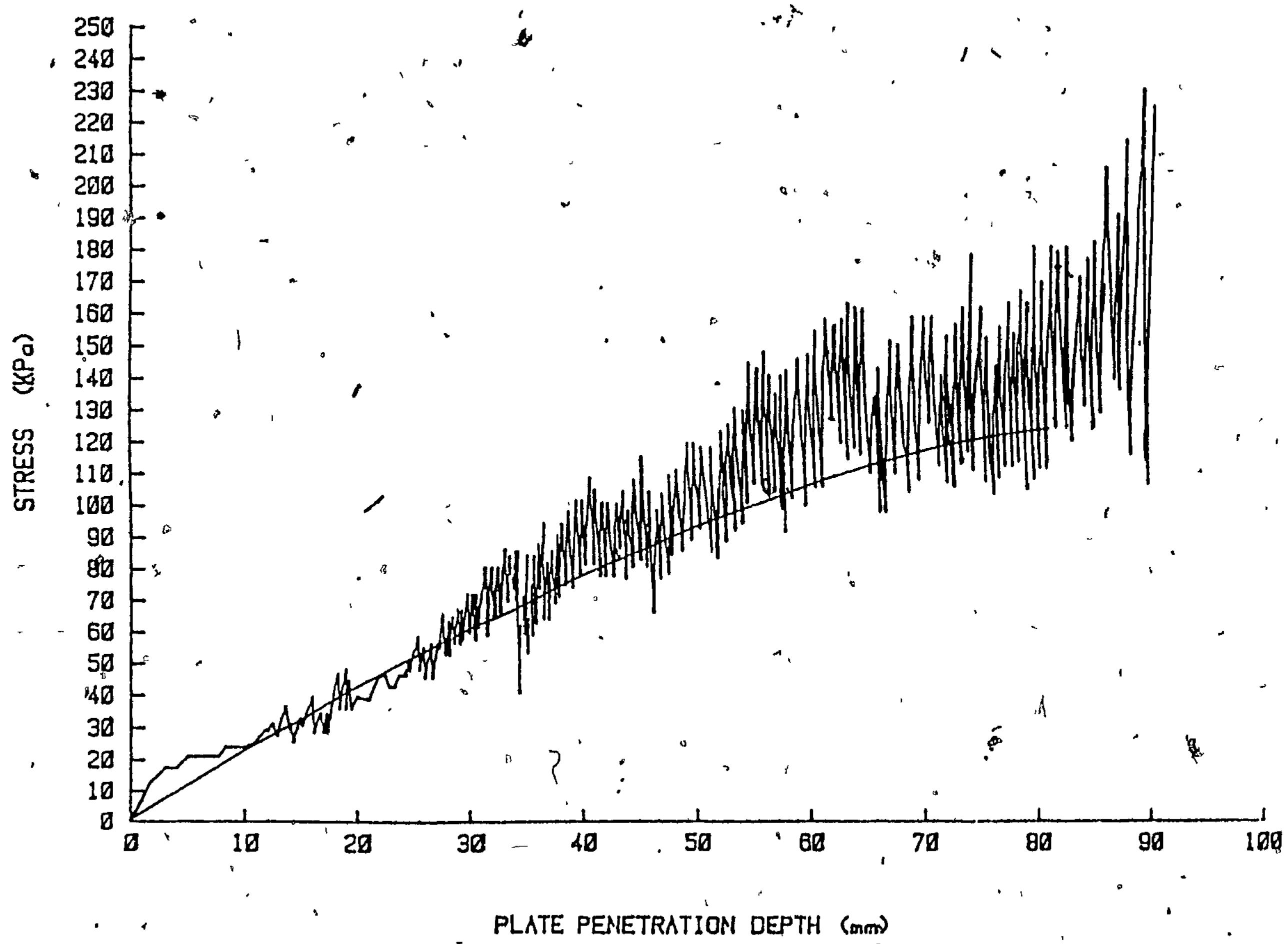

Fig. 3.12 Plate Penetration Test Results - Age 4 Days

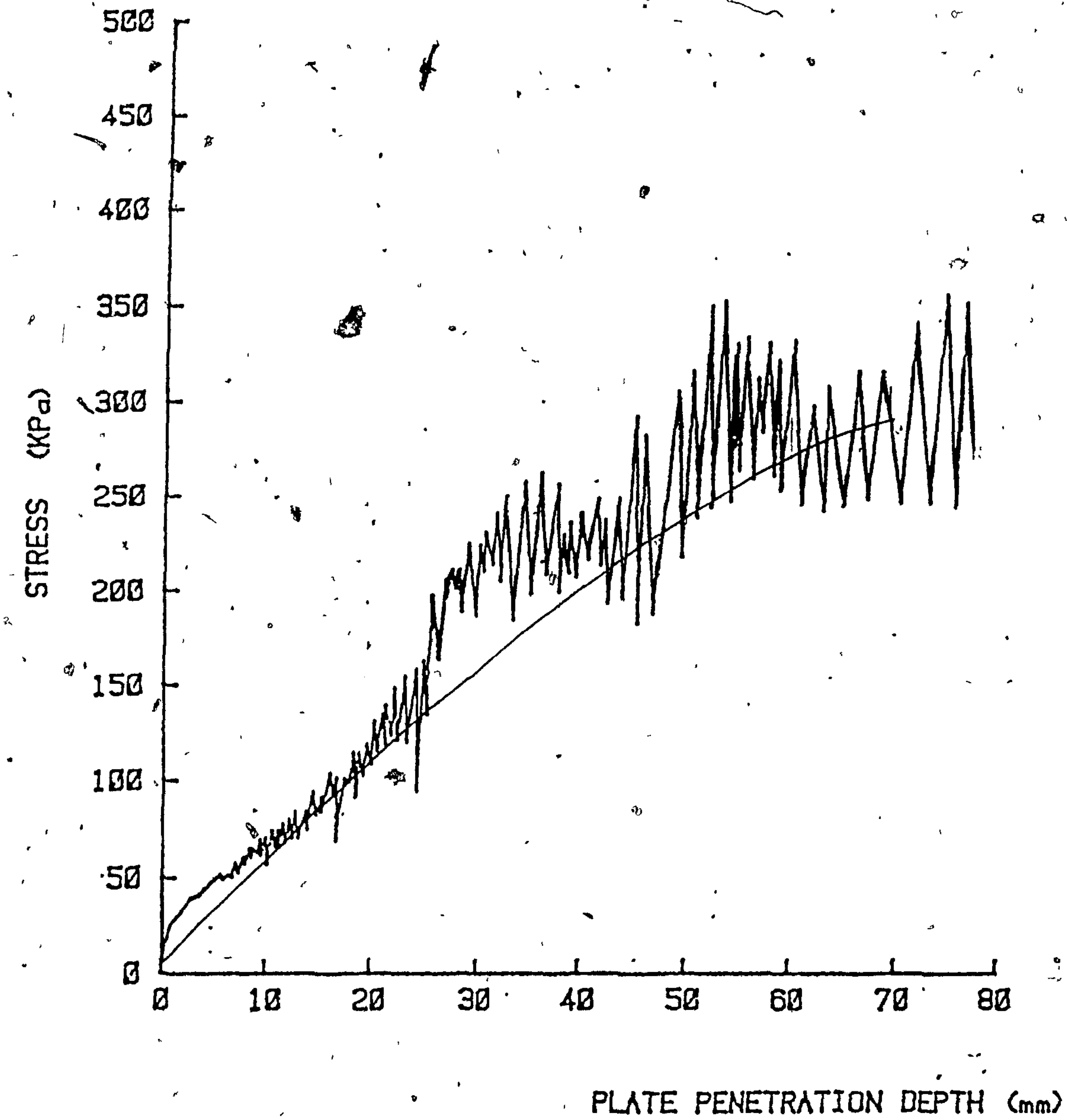

Fig. 3.13 Plate Penetration Test Results - Age 30 Days

As mentioned earlier, a plate load-penetration curve reflects the combined action of volume change and shearing mechanisms and, therefore, it can be expected that its shape is governed by the individual characteristics, describing the behaviour in volume change and pure shear, as obtained from confined compression and shear tests, respectively. The hypothesis discussed in Chapter 2 suggested that during plate penetration in deep snow, the depth of the pressure bulb beneath the plate is controlled by the magnitude of shear stresses supporting it along its sides. As the plate sinks into the snow, the shear strength of snow at any point along the planes of cutting shear could be exceeded depending on the density of the snow and cumulative shear stress at that point. It is therefore obvious that maximum stress bulb support in terms of side shear action occurs at the beginning of the plate penetration process and decreases as more snow material is stressed beyond its shear strength. Since the stiffness in shear of snow elements located along the planes of cutting shear is reduced to a negligible value after shear failure occurs, it thus becomes evident that the total stiffness of the system in shear decreases with increasing plate penetration. On the other hand, the volume change mechanism occurs simultaneously during which the density of snow within the stress bulb generally increases. As a result, and referring back to the stiffening behaviour of snow under compression loading, the resistance of the system to volume change increases (i.e, compressibility decreases). The shape of a given plate penetration curve therefore depends on two mechanisms with opposite effects, i.e softening effect in shear and stiffening effect in volume change. A plate load-penetration curve of the softening type (i.e, tangent slope decreases with increasing plate penetration) therefore represents a situation in which the cutting shear mechanism along the failure planes is dominant over the volume change action of the snow within the stress bulb beneath the plate. Similarly, a curve of the stiffening type (i.e, tangent slope increases with plate penetration) indicates that the volume change effect is more significant than the cutting shear effect. It is suspected that the first case applies to relatively old snow with a high degree of bonding (high shear strength) and low compressibility whereas the second case is typical of fresh or low age snow, characterized by a low shear strength and a hign compressibility. Following the same type of reasoning, a relatively linear plate load-penetration curve reflects the situation in which both volume change and shear mechanisms participate equally in the vertical support of the pressure bulb and thus tend to counteract one another. The validity of the above statements is demonstrated by the results of the plate penetration tests. The load-penetration curves from a test performed on 4 day old snow (Fig. 3.12) show that the response is essentially linear whereas results from the tests performed on older snow, aged 30 days, shows a strain softening behaviour (Fig. 3.13). The plate penetration behaviour for the two snow types considered is thus as expected. The curves fitted through the experimental plots in Figs. 3.12 and 3.13 serve as reference for comparative purposes with analytical predictions, as discussed in section 4.2.3.

CHAPTER 4

ANALYTICAL PREDICTION AND COMPARISON WITH EXPERIMENTAL RESULTS

4.1 General

This chapter is concerned with the results of the finite element model and its capacity to correctly simulate a constant rate rigid plate penetration process in deep snow. Results from confined compression and vane shear tests were used to define the compressibility and shear strength, respectively, of the material. The resulting curves defining material characteristics served as input to the model which predicted the plate stress-penetration relationship, displacement profiles, density profiles and depth of shear along the failure planes.

The validity of the proposed computer model relied on a favourable comparison between the experimentally observed and analytically predicted behaviour of the system. This involves simultaneously satisfying conditions of similarity between parameters describing the response of the real and simulated systems. Evidently, the list of such parameters may be very long and therefore a perfect simulation implies an exhaustive comparison of all the variables describing the behaviour of the system at anytime in addition to a flawless analytical formulation of the problem. Due to limitations of time and scope of the present study, only parameters judged most important and relatively easy to obtain through experiments are considered. As schematically described in Fig. 1.2 in the introductory chapter, the performance of the proposed model is evaluated in terms of the following descriptors of the behaviour of the system:

a) plate stress-penetration response

b) displacement profile

c) depth of shear

d) density profile

In the next section, an experimental vs predicted comparison is established for each of the above four items. The capability of the model to predict the load distribution beneath the rigid plate and the density at failure of shear elements along the failure planes is discussed in the subsequent section.

4.2 Comparison of Analytical and Experimental Results

The first subsection deals with the various techniques of data reduction which had to be developed during the course of the present study in order to obtain the required experimental data.

4.2.1. Data Reduction Techniques

Photographs of the distorting black sand grid (applied to the snow prior to loading) during plate penetration tests were the basis of analysis for generating displacement and density profiles as well as depth of shear as a function of plate penetration. The intersection of the grid lines of "nodes" were digitized using a plotter equipped with an eye piece which could be focused exactly on the node. A separate program was developed for the digitizing process and nodal coordinates, in terms of photograph dimensions, were thus obtained and stored in computer files. The measurement of the plate length on the photograph and a comparison to its real length allowed the computation of ~~a~~ scale factor so that the stored nodal coordinates could be translated to values describing actual dimensions. An additional Fortran program was written to treat the nodal coordinate files to obtain displacement and density profiles.

Displacement profile were obtained from the difference in nodal coordinates between a photograph corresponding to a given plate penetration and that of the initial undeformed grid. In the output of the program and in the analysis of results, the position of the nodes was always defined with respect to a point located at the center of the plate, along its bottom surface, before any penetration had occurred, i.e, on the original snow surface since the plate is just in contact with the snow at the beginning of the test. Displacement profiles, whether obtained experimentally or through analytical predictions, were always along vertical columns of nodes originally (prior to any plate penetration) located a given horizontal distance away from the plate center. In the case of profiles obtained from photographs, the grid lines were not originally exactly vertical and therefore an average of the horizontal coordinates of the nodes along a given column was used to define its original position with respect to the center of the plate.

Density profiles were generated using the same program from consideration of the change in area of square elements bounded by the grid lines. Division of these square elements into triangles facilitated the computation of area which was carried out as for the density calculation in the finite element model (Fig. 2.10). As for displacement, density profiles are also computed along vertical lines defined by the average horizontal coordinates of the centroids of the square elements.

The depth of full shear is defined hereafter as the depth beneath the plate (along the planes of cutting shear through the edges of the plate) at which the normalized shear deformation (i.e, ratio of shear deformation per unit length) is at least equal to 1 or, in other words, the depth until which an element of snow has sheared completely. In the illustrative example shown in Fig. 4.1, elements 1 to 3 have sheared completely whereas elements 4 to 7 have not. The depth of full shear defined above is thus referred as D_S on the same figure. This value is another basis for comparison between experimentally observed and analytically predicted plate penetration behaviour and proves to be useful as a check of the suitability of the input shear strength-density curve. The experimental values of D_S were obtained from the plate penetration test photographs of horizontal grid line deformations along the planes of cutting shear. The number of horizontal grid lines on either side of the failure plane(s) were counted and numbered following the example in Fig. 4.1. It was then possible to determine which shear elements, represented by pairs of vertical grid line segments bounded by nodes, failed completely as described earlier. Both planes of shear in the photograph were considered from which an average value of depth of shear was obtained. In terms of the present data reduction technique, elements for which the difference in elevation of the center of the two sides of the element was greater than the original length (obtained from the undeformed grid photograph) were considered completely failed. The distance from the center of the inner side (i.e, on the inside of the failure plane(s)) of the lowest completely failed element to the plate was taken as the depth of full shear D_S as shown in Fig. 4.1.

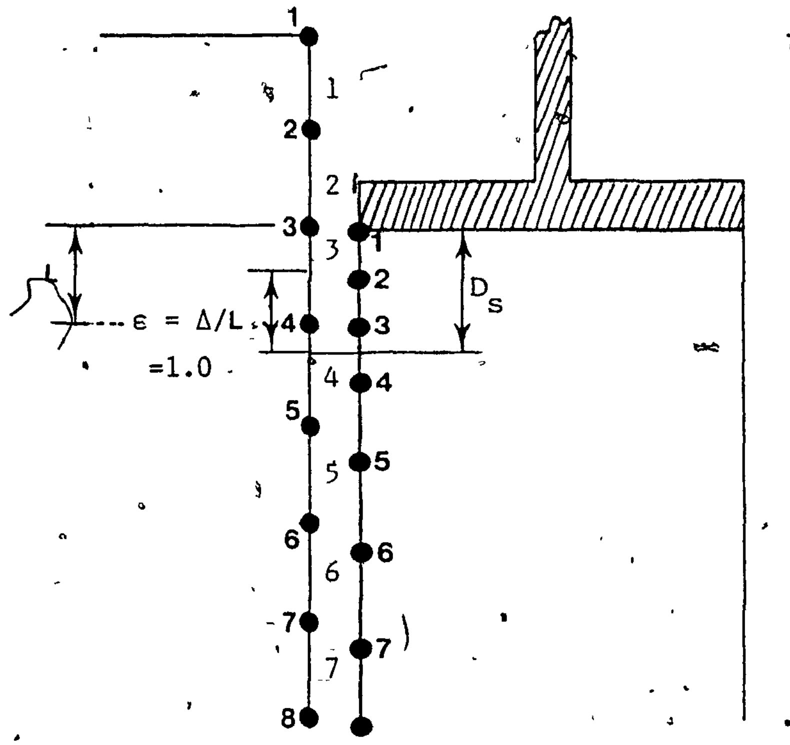

Fig. 4.1 Computation of Depth of Full Shear D_s

4.2.2 The Role of Shear Stiffness

As introduced earlier in chapter 2, the stiffness modulus in shear K_s is unavailable from the results of the performed set of experiments. This quantity is required in the model to characterize the behaviour of the snow as it fails along the two planes of cutting shear developed as plate penetration progresses. Essentially, the variable K_s defines the degree of shear deformation at which snow fails and thus can no longer accumulate additional shear stress.

Due to the absence of information about shear stiffness, the degree of sensitivity of the finite element model to this parameter was investigated. The developed computer program was run several times with different values of shear stiffness. The reaction of the model to a change in K_s, in terms of the four descriptors of plate penetration behaviour considered in this study and introduced in section 4.1, is discussed in the next few sections along with the comparison between experimental and predicted response.

4.2.3 Comparison of Experimental and Predicted Plate Penetration Curves

The plate penetration curves are expressed in terms of stress on the plate as a function of penetration. Plate stress is obtained by dividing the reaction load by the area of the plate. The stress-penetration relationships for 4 day old snow obtained from the plate test and predicted by the finite element model are depicted on the plot in Fig. 4.2 for comparison purposes. The experimental curve shown in the same figure is the same as that fitted through the experimental graph (section 3.3.3) which passes approximately half-way between the mean of the band of the test curve (Fig. 3.12) and the lower boundary of the same curve. The reason for the selection of such a reference curve is due to the fact that the finite element model predicts the plate load after stress releases caused by failing shear elements. In the actual case, the stress vibrations observed are produced by both the microfracturing of snow while compressed (discussed in Chapter 3) and the stress release effect mentioned above. It is therefore difficult to affirm that the lowest boundary of the plate penetration curve represents the behaviour after shear element stress releases since the microfracturing effect is also incorporated into the response with the result that it is impossible to separate the two components. Similarly,

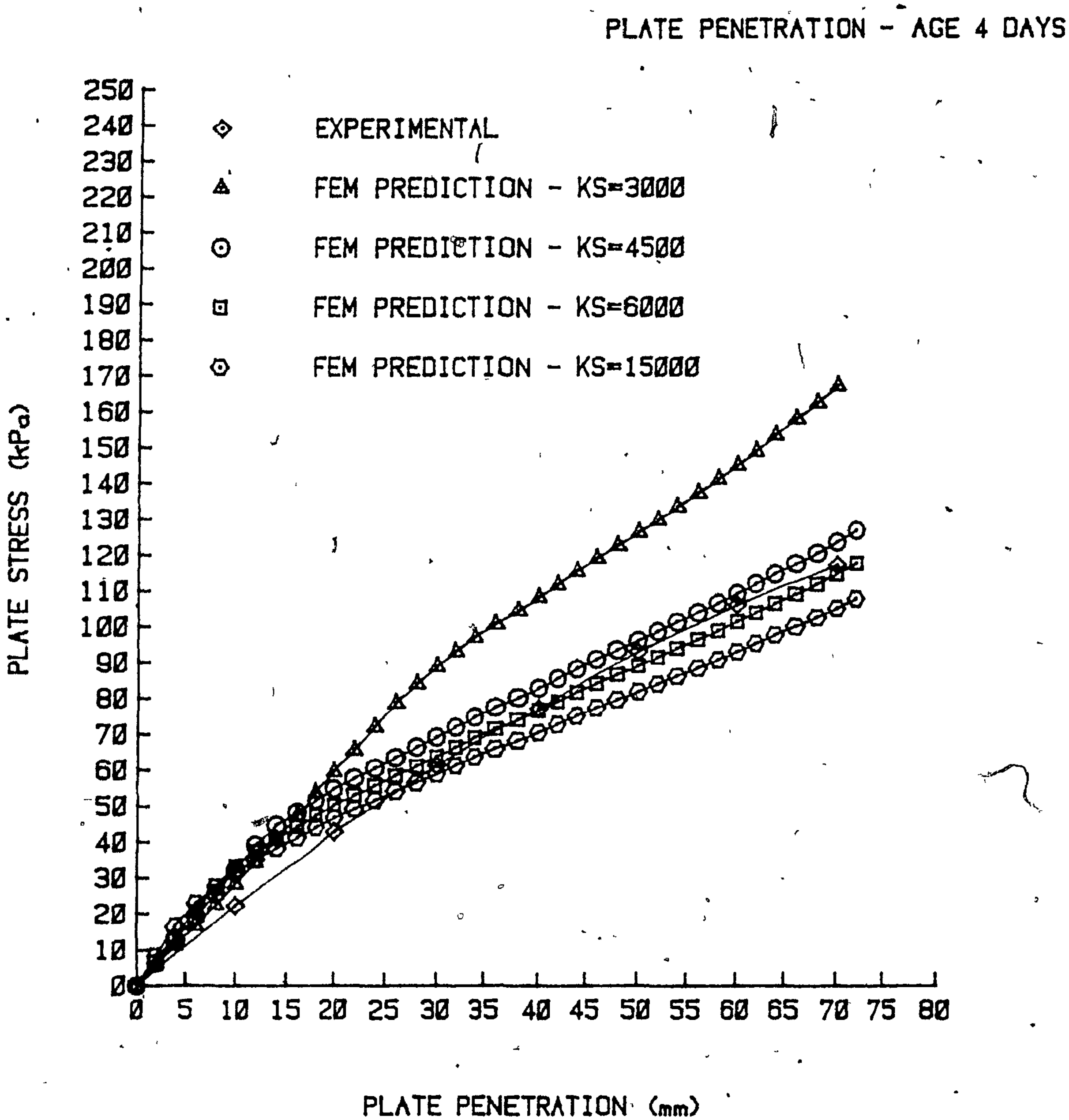

Fig. 4.2 Experimentally Obtained and Predicted Plate Penetration Curves - Age 4 Days

the mean of the same curve does not necessarily represent the response that can be compared to the finite element prediction because of the stress release effect although the latter is not suspected to cause large drops in plate stress. Therefore, due to the above arguments, a curve in the middle of the mean of the band and the lower boundary was selected as the reference experimental curve.

In the predicted response, the effect of shear stiffness is included. For the values of K_s considered, the agreement between experimental and finite element results is reasonable (see Fig. 4.2). The shape of both experimental and predicted curves is similar in that the relationships are characterized by a bi-linear type of behaviour such that the response is essentially linear, starting at a given slope, and then followed by a decrease in slope. It should also be noted that the predicted stress-penetration response is somewhat sensitive to the value of shear stiffness K_s and thus that different values of K_s generate different curves. In the set of curves shown in Fig. 4.2, the relationships pertaining to K_s=4500 and K_s=6000 seem to give the best results or closest agreement with the experimental curve. The curve corresponding to K_s=3000, overestimates the response whereas that for K_s=15000 tends to underestimate it. In general, the plot on Fig. 4.2 implies that an increase in K_s lowers the predicted curve whereas a decrease in K_s tends to raise it.

The reaction of the curve to a change in shear stiffness can be explained as follows; a low value of K_s implies a "ductile" behaviour of snow in shear so that elements of the material along the failure planes, and thus acting principally in shear, tolerate relatively large displacements before mobilizing the full shear strength. In such a case, if the value of K_s is too low in the model, the total shear stiffness of the system (i.e, the stiffness contributed to by the shear elements along the planes of shear) decreases too slowly, as compared to the real situation, since less elements have failed for a given plate penetration. Conversely, a high value of shear stiffness results into a "brittle" behaviour in shear such that failure occurs at a small shear deformation. A high value of K_s in the model causes a rapid progressive failure of shear elements resulting into a low value of the shear stiffness of the system starting at a small value of plate penetration and thus applying for most of the penetration process.

The corresponding plate stress-penetration curves for 30 day old snow are shown in Fig. 4.3. The agreement between experimental and predicted curves is not as good as for the 4 day old snow especially for the higher values of K_s (i.e, 9000 and 15000) but the curve corresponding to K_s =4500 yields relatively good results. Again, the predicted curves are bi-linear, but to a lesser degree than

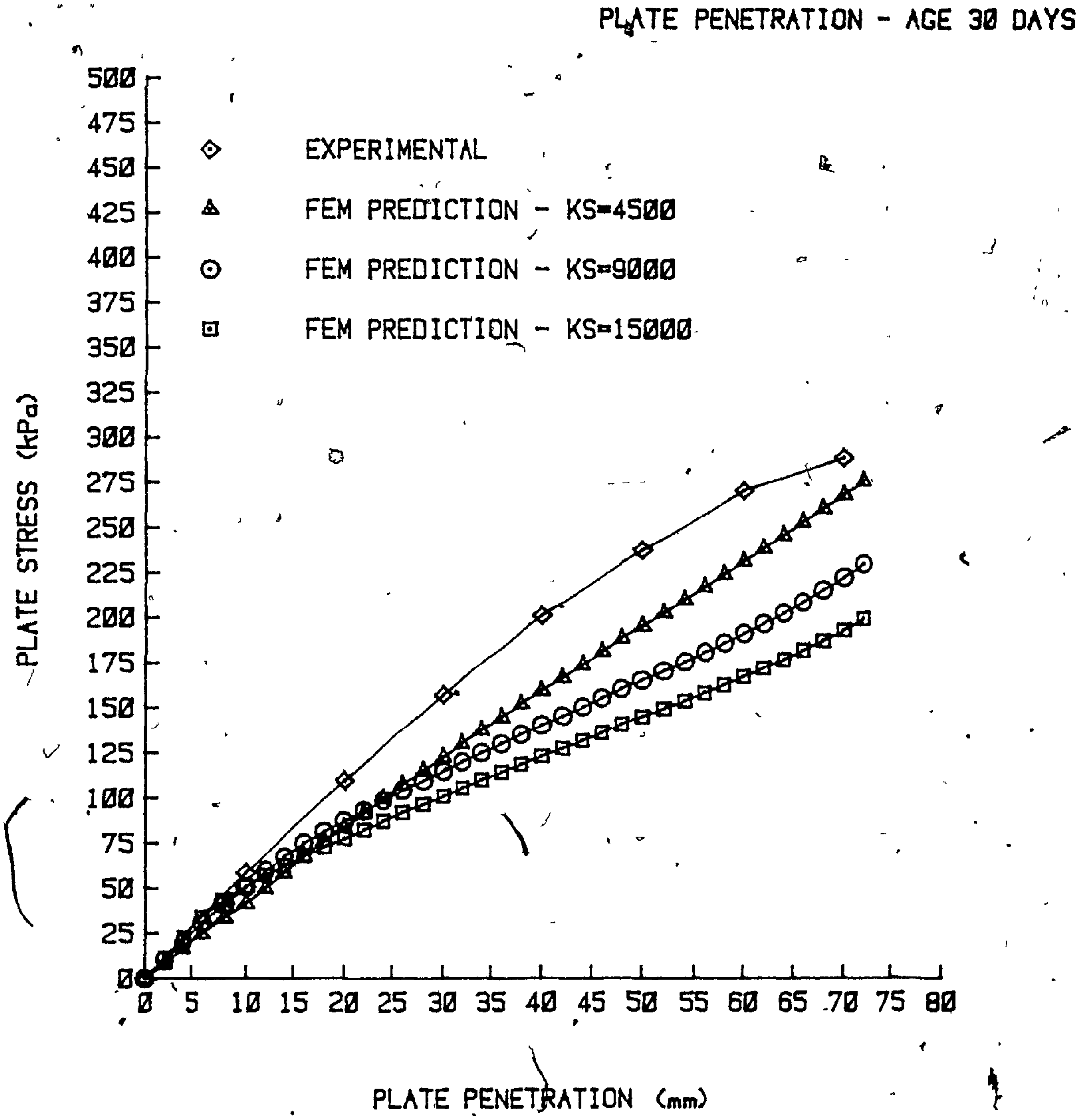

Fig. 4.3 Experimentally Obtained and Predicted Plate Penetration Curves - Age 30 Days

those for 4 day old snow. The analytical model is consistent in that its sensitivity parameter is similar to that for 4 day old snow; an increase in K_S results into a lower plate stress-penetration response and viceversa. It is also interesting to note that, as for 4 day old, predictions are quite good when the shear stiffness parameter K_S is 4500.

4.2.4 Predicted Distribution of Components of Total Plate Resistance

In the finite element model, provisions were made for determining the individual components of plate penetration resistance:

a) resistance due to shear along the planes of shear.

b) resistance due to compression of snow inside the pressure bulb, i.e, snow beneath the plate and bounded by the shearing planes.

c) resistance due to compression of snow outside the shearing planes.

The predicted distribution of the three components of plate penetration resistance for both types of snow is graphically displayed in Figs. 4.4 and 4.5 for the best predicted curves. For both types of snow, the greatest

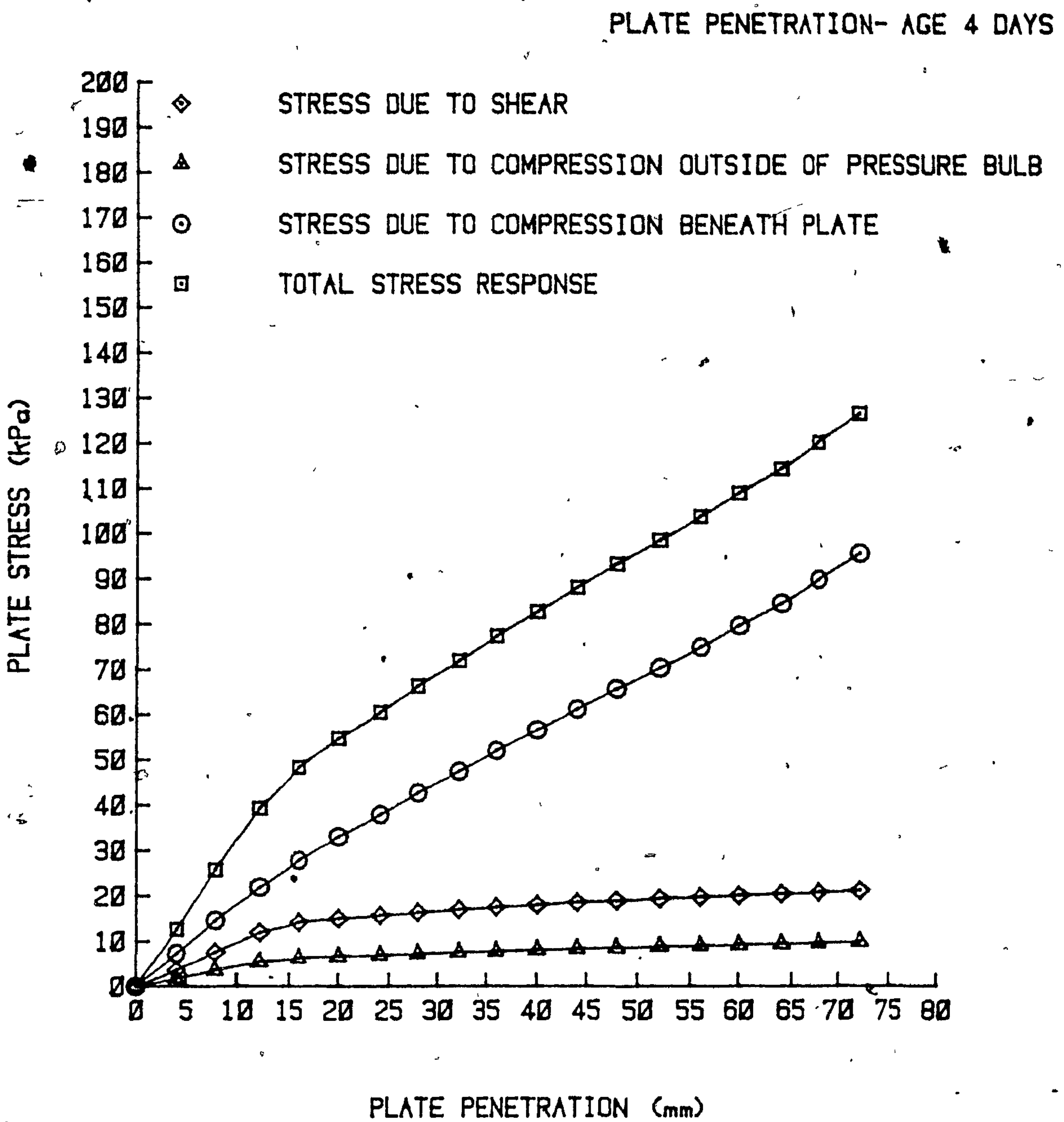

Fig. 4.4 Finite Element Prediction of Distribution of Components of Total Plate Resistance - Age 4 Days

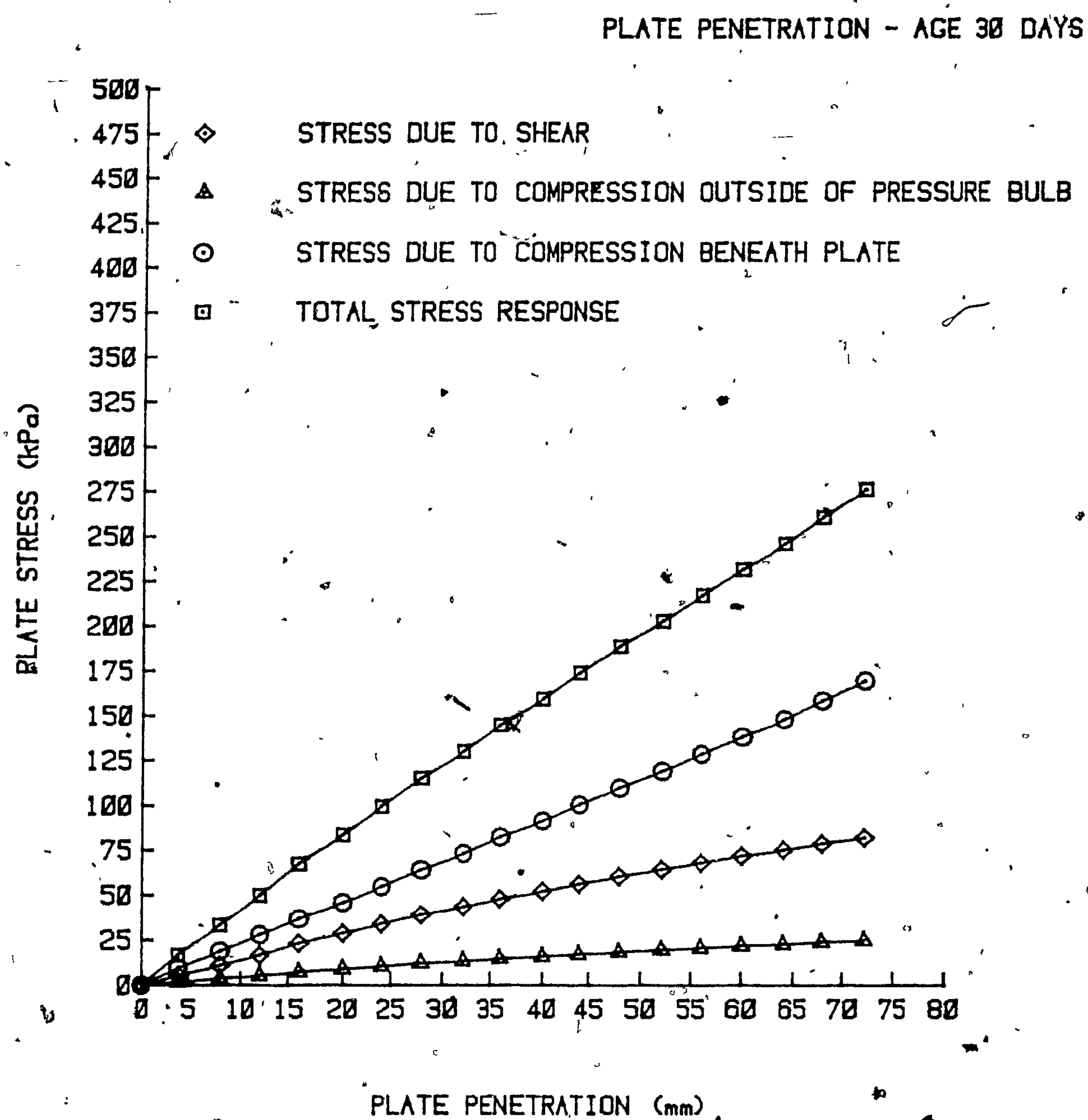

Fig. 4.5 Finite Element Prediction of Distribution of Components of Total Plate Resistance - Age 30 Days

component of plate resistance is that of compression beneath the plate followed by that due to shear along the failure planes. Compression outside of the shearing planes stays practically constant and contributes very little to the total plate resistance in both cases. The relative magnitudes pertaining to compression and shear vary with the age of the snow and with plate penetration. For 4 day old snow, the plate resistance due to shear is approximately half of that due to compression beneath the plate for low penetration values and decreases to about 20% of the latter value at the highest penetration. This is a result of less load being carried in shear as more shear elements have failed at higher plate penetration. In the case of 30 day old snow, the shear strength of the snow is higher and plate resistance due to shear contributes a greater percentage of the total response as shown in Fig. 4.5.

The above relative amounts of plate resistance due to compression and shear are consistent with results obtained by Metaxas (1984).

4.2.5 Comparison of Experimental and Predicted Displacement Fields

In this study, the similarity between experimentally obtained and predicted displacement fields is established in terms of vertical displacement profiles only. Observations during plate tests and grid line photographs showed that, by and large, horizontal displacements in the snow mass were negligible and could therefore be omitted from the comparative study.

The experimental and predicted cumulative vertical displacements under two points below the plate center for 4 day old snow at penetrations of 36 mm and 64 mm are shown in Figs: 4.6 and 4.7 respectively. Predicted vertical displacement profiles were obtained from the displacement of selected nodes originally located a given distance away from the plate according to the structure of the finite element mesh shown in Fig. 2.7. For both plate positions, the agreement between experimental and analytical values is good especially for points originally less than 1.5 plate lengths away from the original snow surface. Experimental and predicted values diverge from each other for some distance below and then seem to converge again. A similar comparison between vertical displacement profiles under a point some distance away from the plate center for the same plate penetrations is illustrated in Figs. 4.8 and 4.9 respectively. For a plate displacement of 36 mm, the agreement between experimental and predicted values is again very good for points originally located less than 1.5 plate lengths from the original snow surface. The above diverge-converge effect between experimental and predicted displacement values is also observed in this case. For a

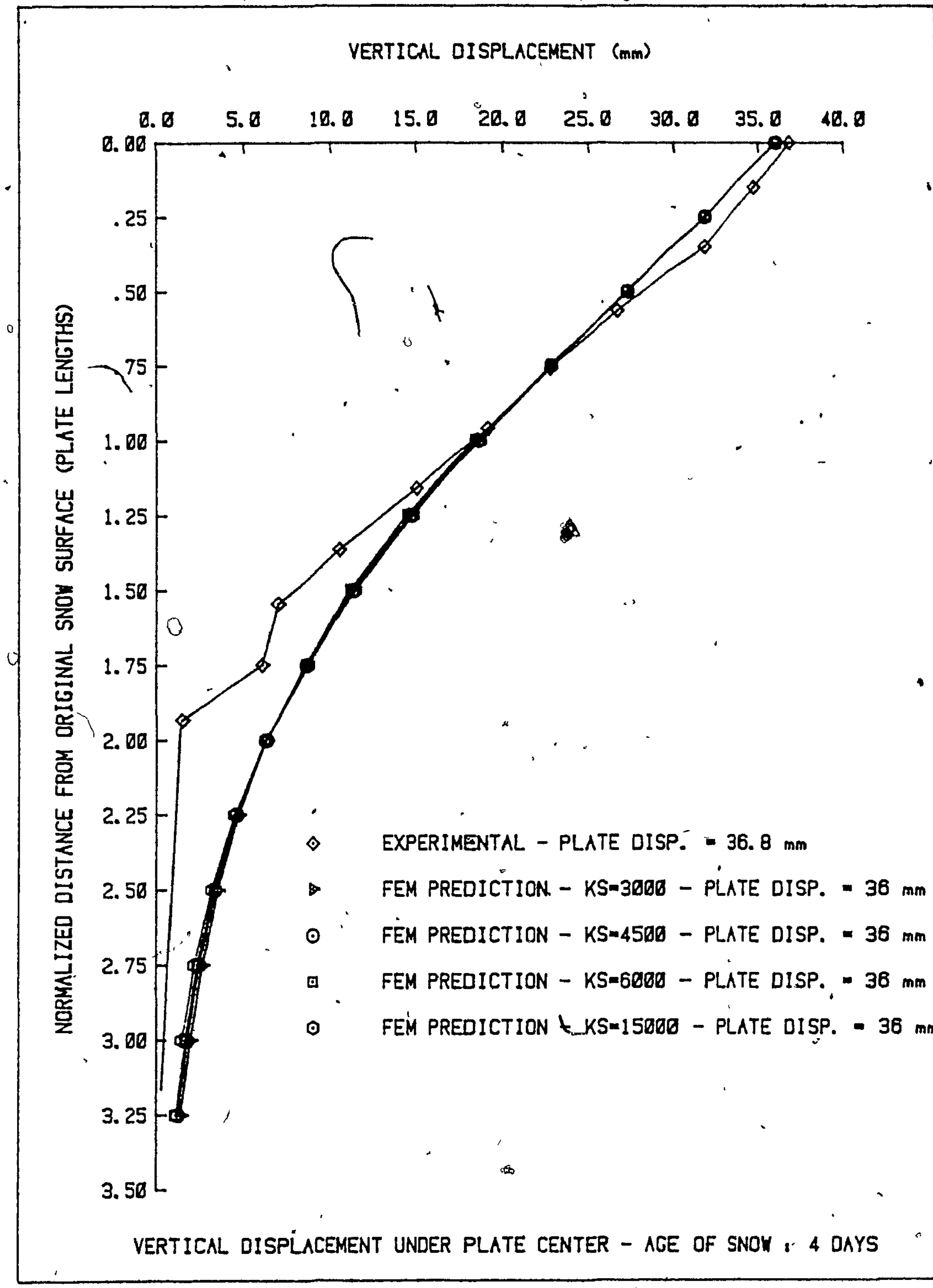

Fig. 4.6 Experimentally Obtained and Predicted Displacement Profiles Under Plate Center - Age 4 Days (Plate Pen. = 36 mm)

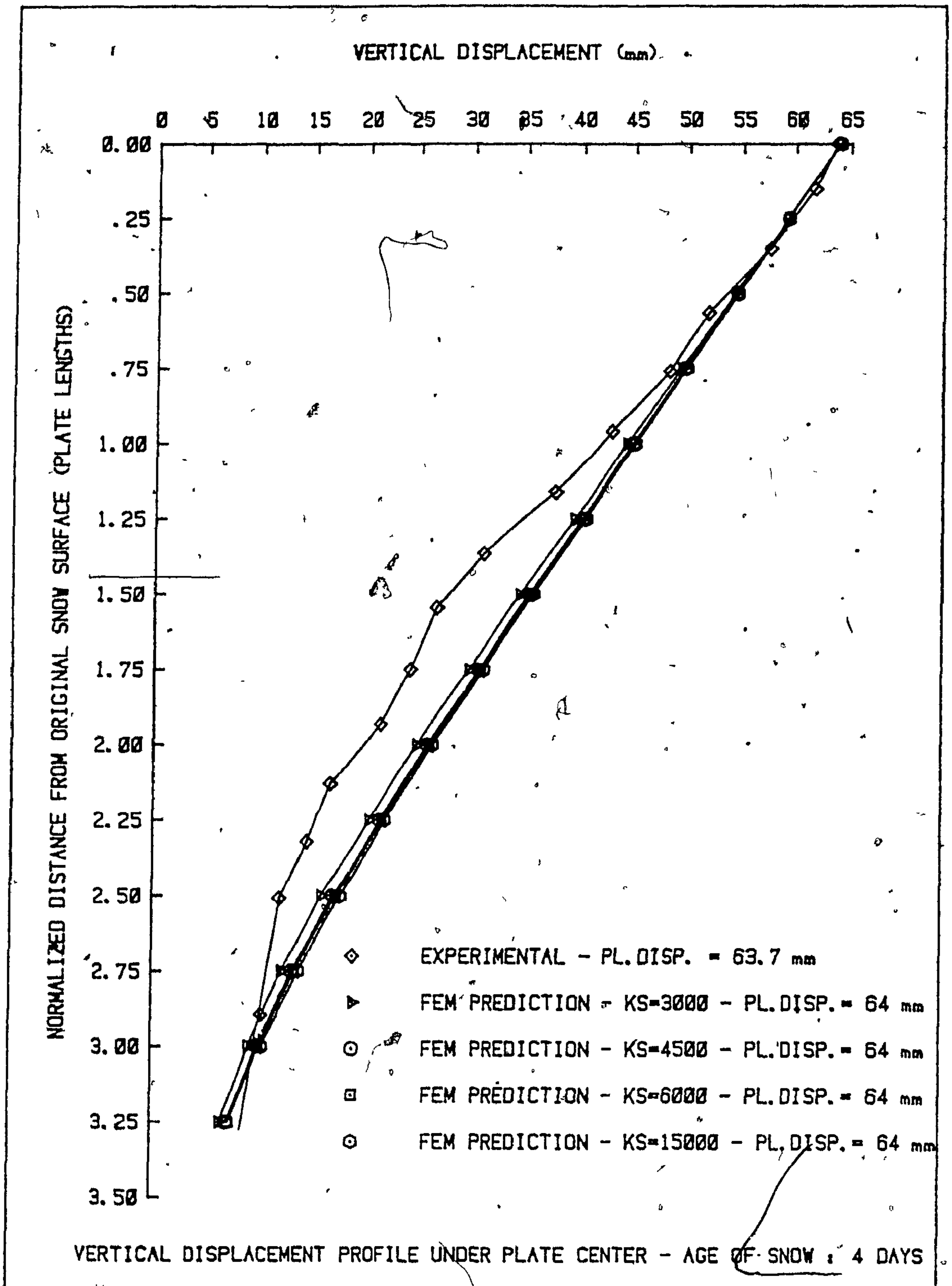

Fig. 4.7 Experimentally Obtained and Predicted Displacement Profiles Under Plate Center - Age 4 Days (Plate Pen. = 64 mm)

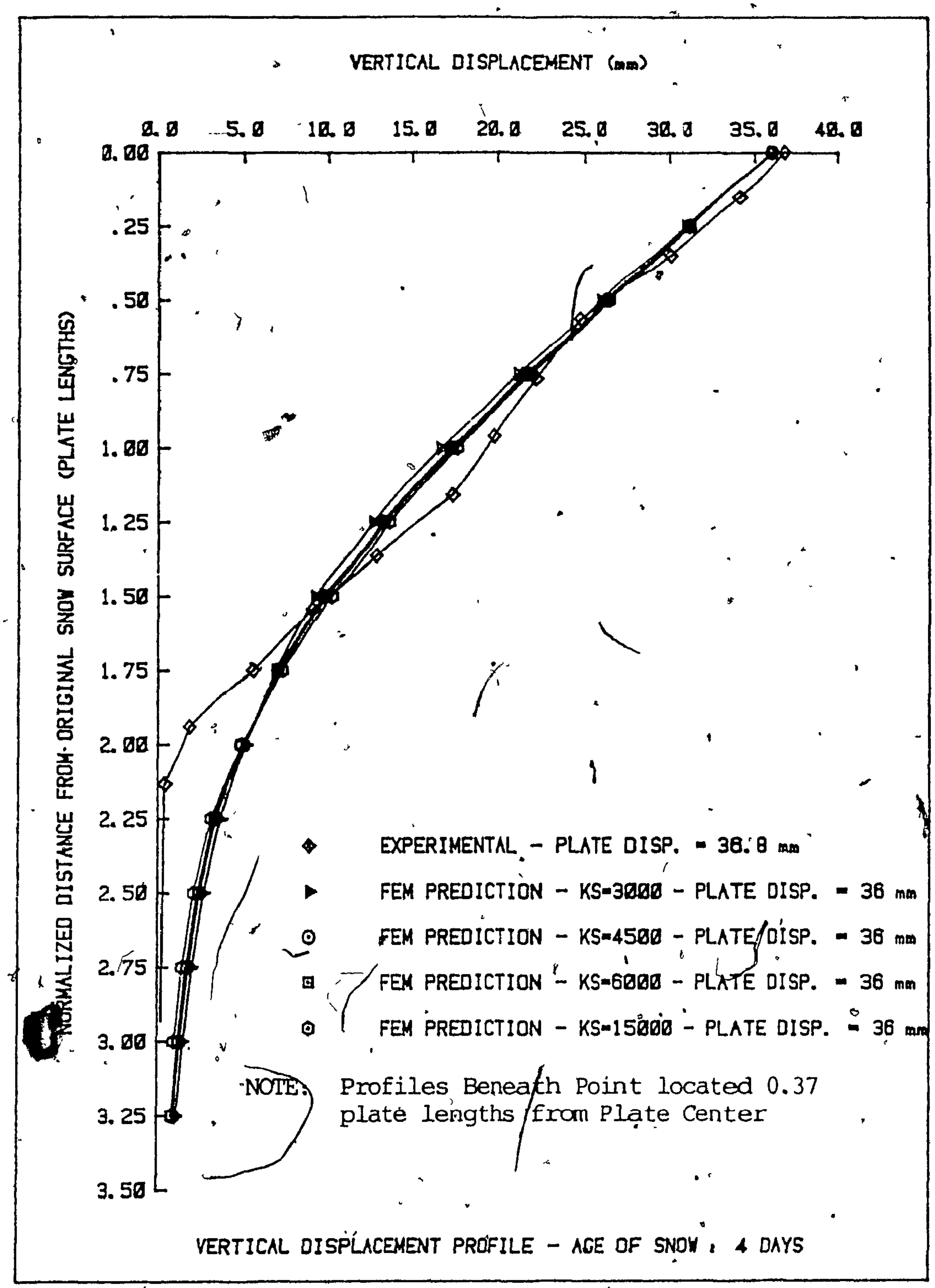

Fig. 4.8 Experimentally Obtained and Predicted Displacement Profiles
Age 4 Days - (Plate Pen. = 36 mm)

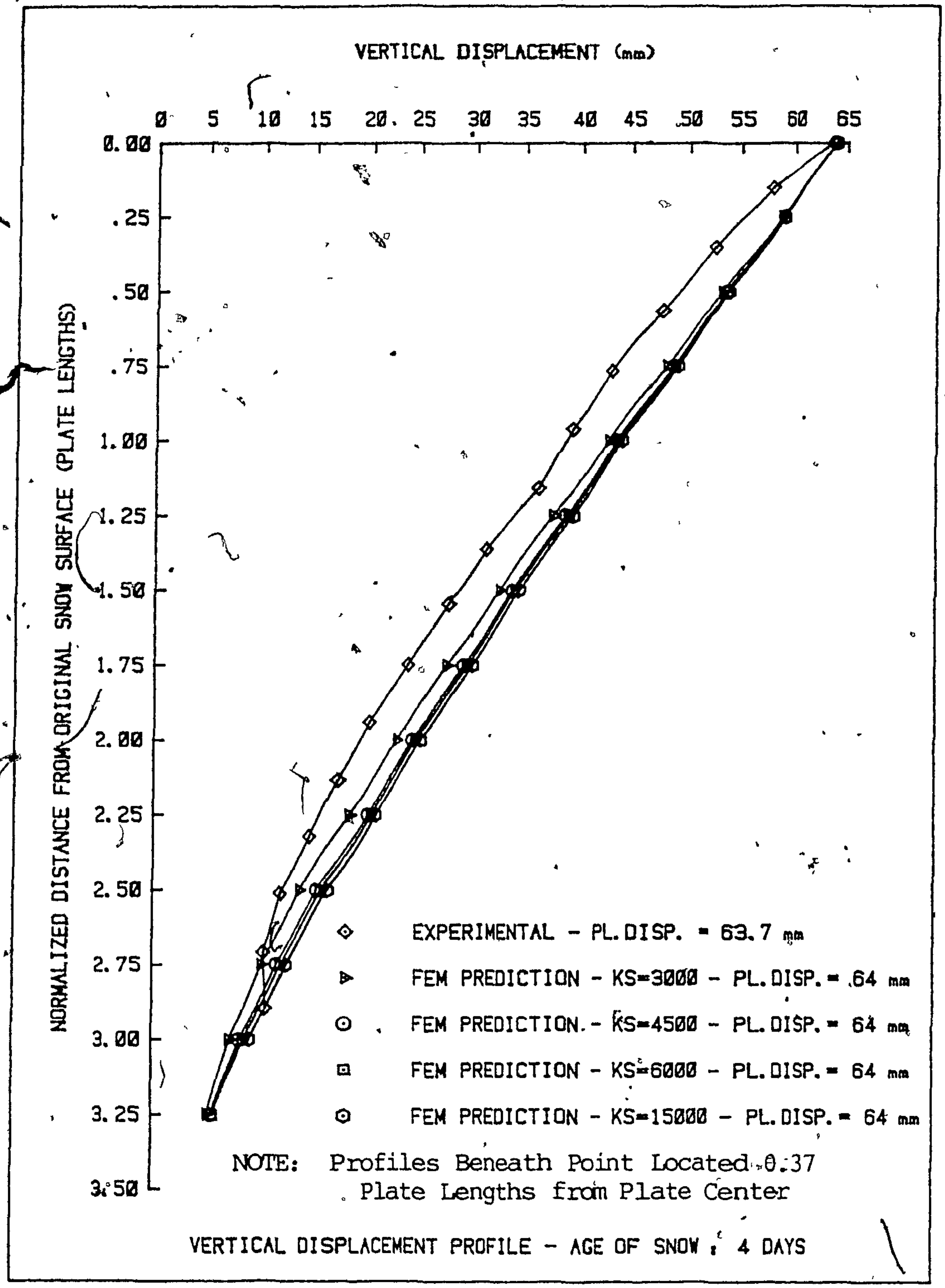

Fig. 4.9 Experimentally Obtained and Predicted Displacement Profiles Age 4 Days (Plate Pen. = 64 mm)

plate penetration of 64 mm, the discrepancy is more uniform all along the curve(s).

It should be noted that for a given plate penetration, both experimental and predicted displacement profiles are essentially linear up to a certain depth, thus implying an uniform vertical strain distribution, and are characterized by a change in gradient below that depth. The change in slope of the displacement profile is mainly due to the variation in stiffness of the system in shear. As discussed earlier, shear elements along the planes of cutting shear fail progressively so that for a given plate penetration, snow has failed above a certain point and has not below that same point. The stiffness of the system is thus lower above the given point and higher below so that displacements are also expected to be higher for the region of lower stiffness. As a result, the gradient of the displacement profile, or strain, is also expected to be higher for the less stiff snow and lower for the stiffer snow. The change of displacement gradient is particularly obvious in the profiles shown in Figs. 4.6 and 4.8. The above arguments thus seem to imply a relationship between the point of change in displacement gradient and the point above which the snow has failed completely, i.e, depth of full shear, introduced in section 4.2.1. This relationship is discussed in more detail in section 4.2.6.

The predicted displacement profiles in Figs. 4.6 to

4.9 also show their sensitivity to the shear stiffness parameter K_s, which in all cases, proves to be relatively small and, in any case, lower than that observed for the plate stress-penetration curves.

The displacement profiles obtained for 30 day old snow below two different points on the plate and for two plate penetrations are shown in Figs. 4.10 to 4.13. The agreement between experimental and predicted values can be seen to very good. As for 4 day old snow, the displacement profiles are linear for some depth and then feature a change in slope, the reasons for which have already been discussed in this section. Also, as for 4 day old snow, it appears that the shear stiffness parameter K_s has less effect on the resulting displacement profile than on plate penetration response.

4.2.6 Depth of Full Shear

The depth of full shear D_s (introduced in section 4.2.1) is a descriptor of the plate-snow system which quantifies the progressive shear failure mechanism generated by the plate penetration process. The predicted values of depth of full shear D_s are obtained from the finite element analysis which, for each increment, updates the values of total shear deformation for each joint element along the plane of shear. The depth of full shear value D_s is obtained by searching

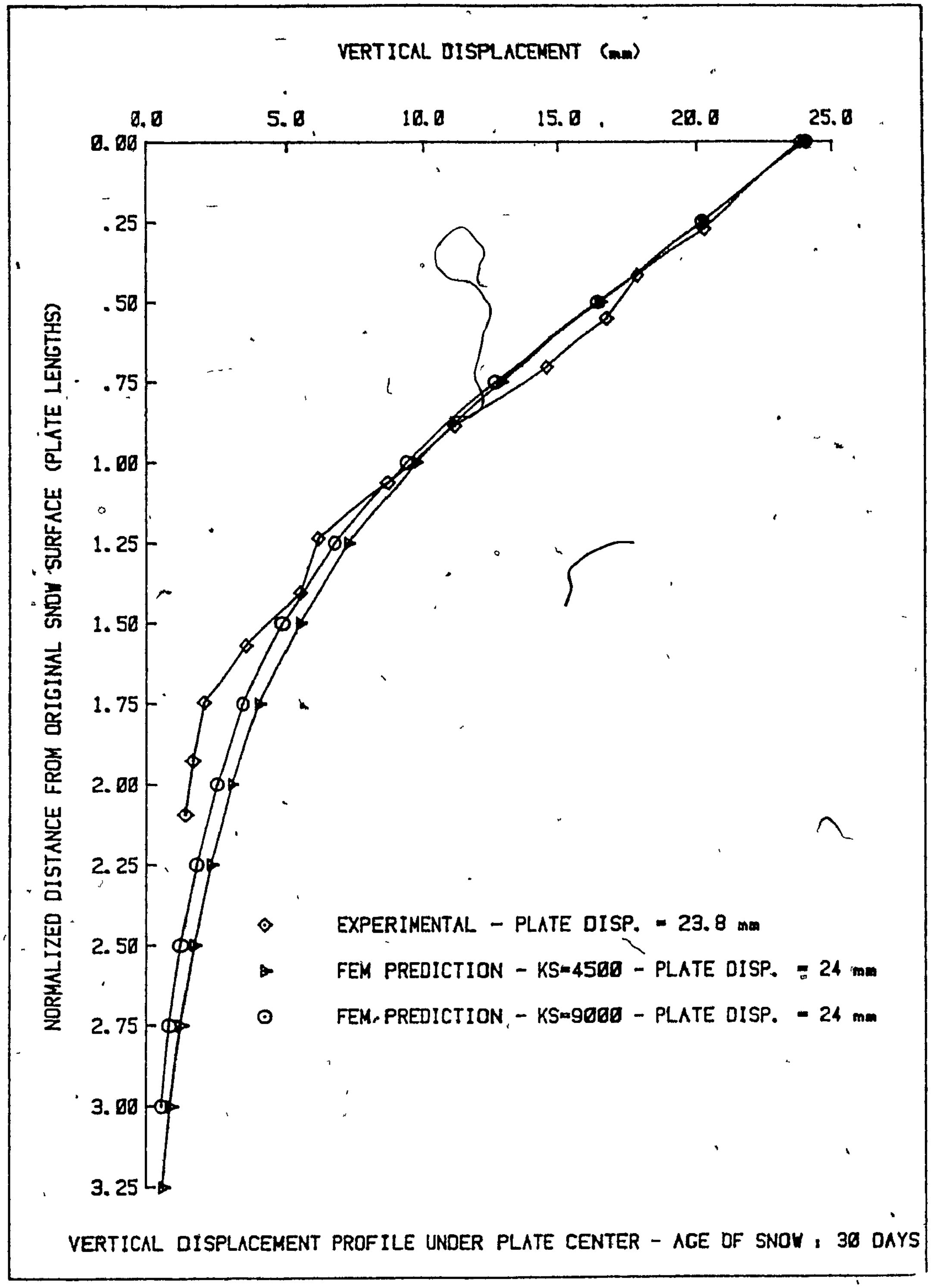

Fig. 4.10 Experimentally Obtained and Predicted Displacement Profiles Under Plate Center - Age 30 Days (Plate Pen. = 24 mm)

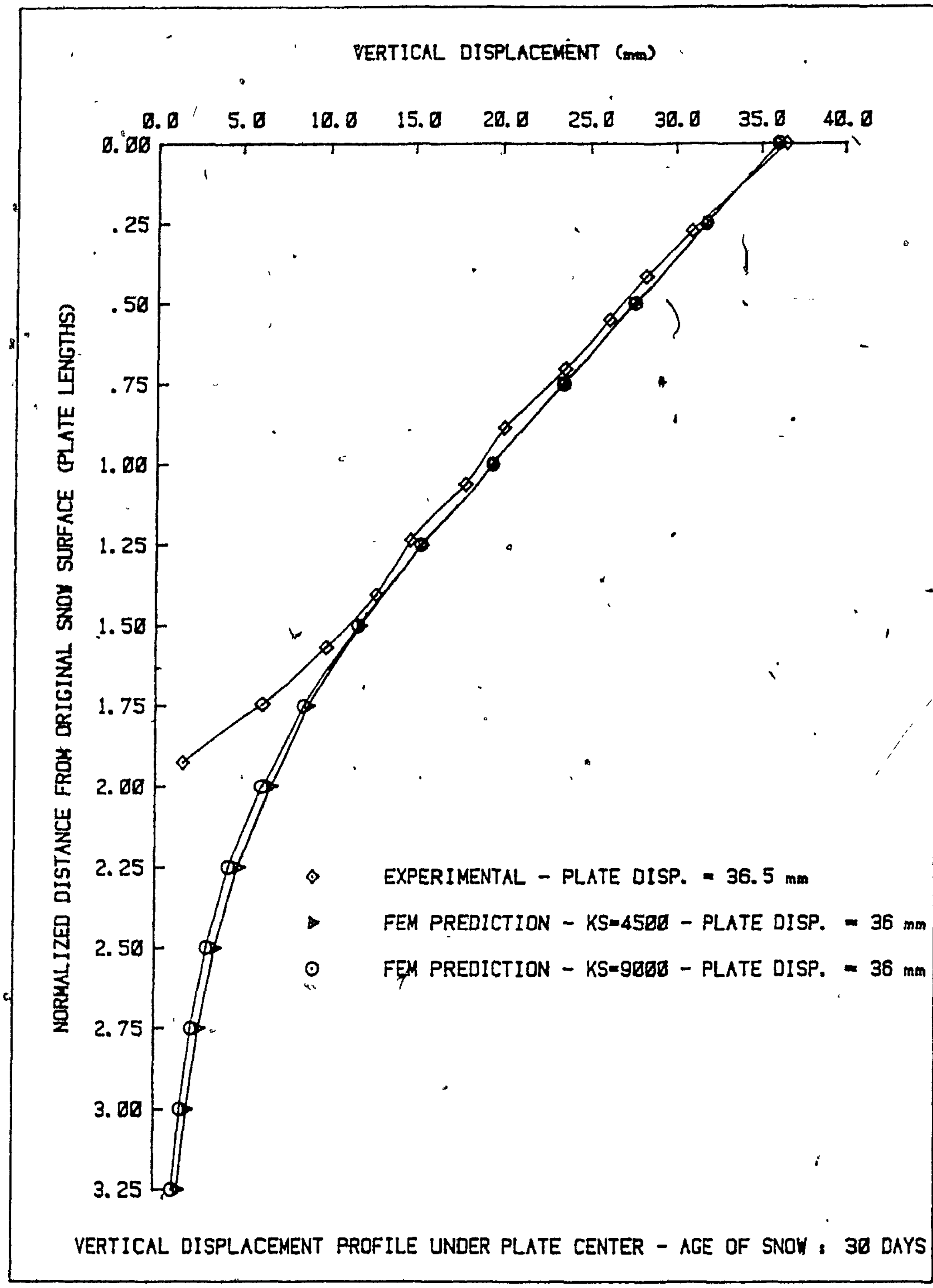

Fig. 4.11 Experimentally Obtained and Predicted Displacement Profiles Under Plate Center - Age 30 Days (Plate Pen. = 36 mm)

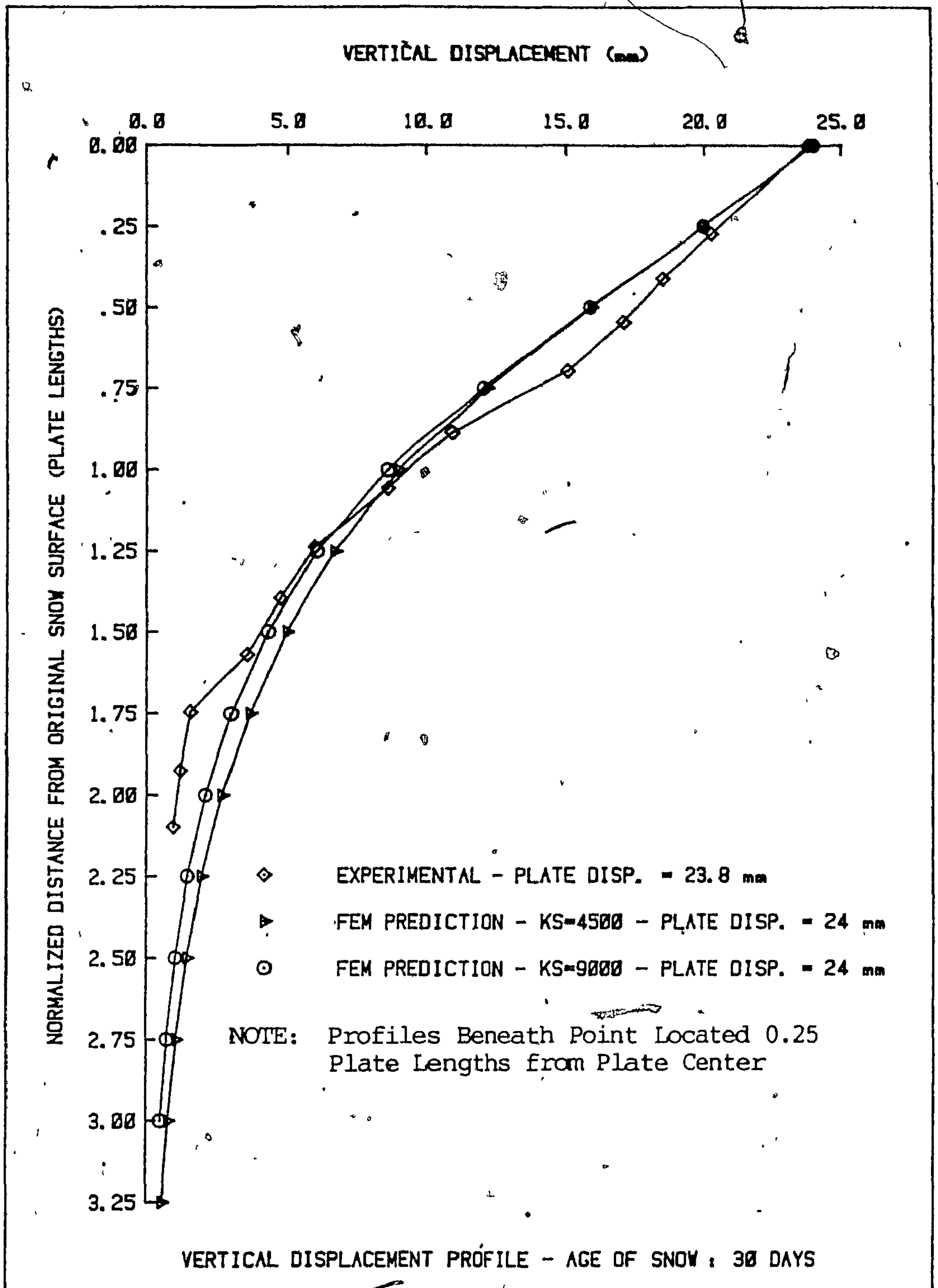

Fig. 4.12 Experimentally Obtained and Predicted Displacement Profiles
Age 30 Days (Plate Pen. = 24 mm)

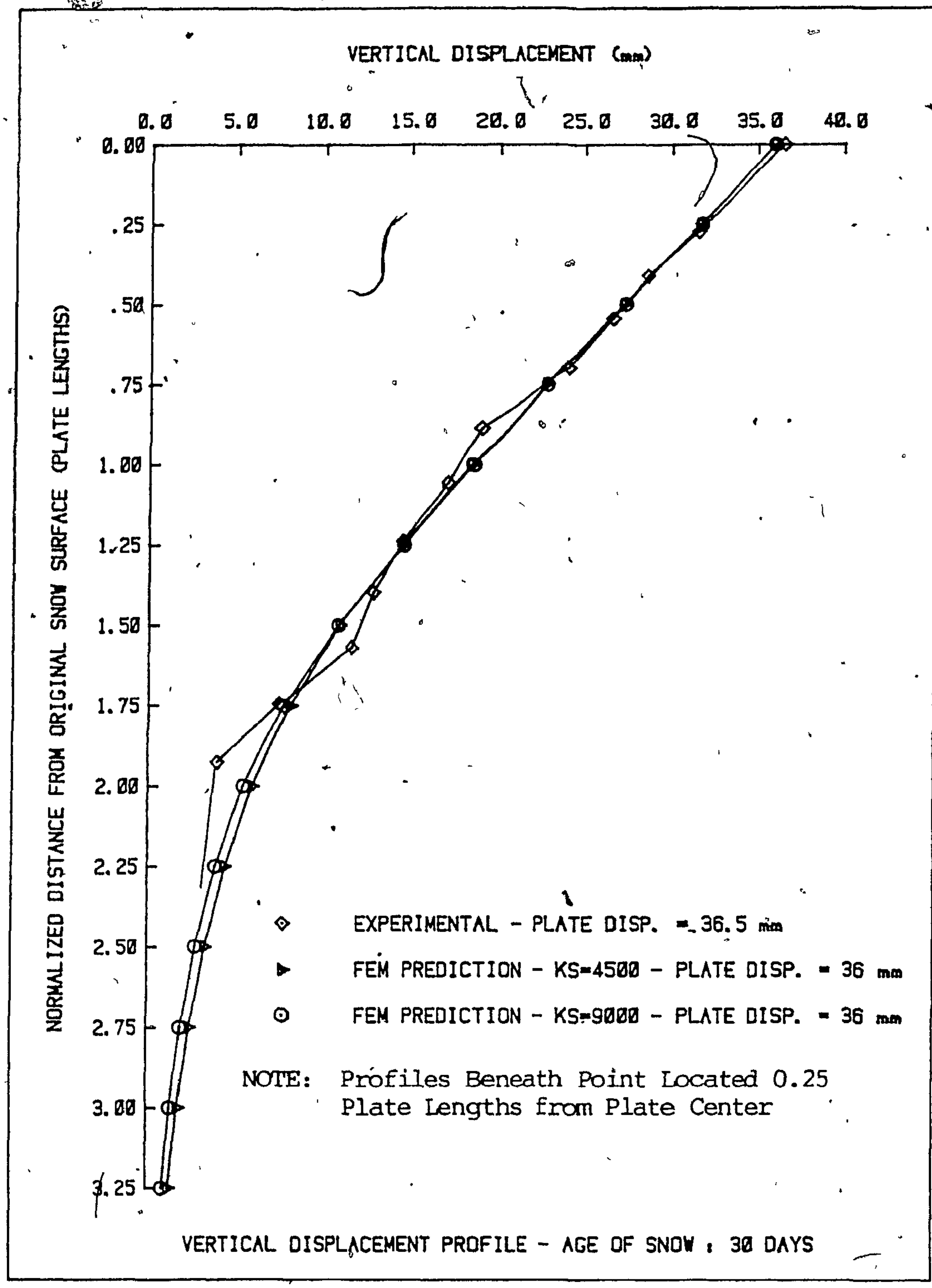

Fig. 4.13 Experimentally Obtained and Predicted Displacement Profiles Age 30 Days (Plate Pen. = 36 mm)

the deepest element for which the total shear deformation is greater or equal to the original depth.

For 4 day old snow, a comparison between experimental and predicted values of D_s for various values of the shear stiffness parameter K_s is presented in Table 4.1. The tabulated figures are consistent with the sensitivity analysis performed for the plate penetration response of the 4 day old snow in that there exists an optimum value of K_s which generates a shear depth value quite close to the experimental one obtained from plate penetration test photographs. As for the plate stress-penetration response, reasonable agreement between experimental and predicted values is obtained for the range of K_s values considered. Best results are obtained for values of K_s =4500 and K_s =3000. For the lower value of shear stiffness, the predicted shear depth implies that the failing mechanism along the planes of shear does not extend as deep as for the actual plate penetration test whereas the opposite applies for the higher K_s value thus indicating that the best prediction of D_s would be using a K_s value in between the above two values.

Depth of full shear values for 30 day old snow are shown in Table 4.2. For a plate penetration of 24 mm, the discrepancy between experimental and predicted values is considerable for both values of shear stiffness K_s considered whereas much better agreement is obtained for a plate penetration equal to 36 mm. Note that for 30 day old snow, the sensitivity analysis intentionally involves less values of the shear stiffness K_s since information about realistic values of K_s was already available from the computer runs for 4 day old snow.

The relationship between the point of change in gradient of the displacement profile and the depth of full shear, introduced in section 4.2.5, can now be verified. For the 4 day old snow, inspection of Figs. 4.6 and 4.8 show that for a plate displacement of 36 mm, the point of change of displacement gradient in the case of the actual experiment occurs at a depth of approximately 1.9 plate lengths whereas for the prediction, this value is about 1.5 plate lengths. From Table 4.1, the experimental value of depth of shear is 81 mm to which the plate penetration value of 37 mm must be added for a proper comparison with the values obtained from displacement profiles. The resulting value is therefore 118 mm or 1.67 plate lengths. Predicted values of depth of full shear from Table 4.1 corresponding to a plate displacement of 36 mm is about 95 mm which when added to the plate penetration value yields a value of 131 mm or 1.86 plate lengths. For a plate displacement of 64 mm, Figs. 4.7 and 4.9 indicate that the change in slope of the displacement profile, although not as obvious, occurs at a distance between 2.0 and 2.25 plate lengths for both the actual case and the prediction.

Table 4.1 shows experimental and predicted values of depth of full shear of 135 mm and about 165 mm respectively which, when adjusted for plate penetration, yield values of 199 mm (2.82 plate lengths) and 229.0 mm (3.24 plate lengths).

Similarly, in the case of 30 day old snow and for a plate penetration of 36 mm, Figs. 4.11 and 4.13 show that the change in gradient of the displacement profile occurs at a depth of approximately 1.75-2.0 plate lengths below the original snow surface. Consultation of Table 4.2 indicates experimental and predicted values of shear depth of 98 mm and approximately 90 mm, which when corrected for plate displacement, correspond to 134 mm (1.9 plate lengths) and 126 mm (1.8 plate lengths). For a plate displacement of 24 mm, the agreement between depth of full shear and point of change of displacement gradient is quite poor.

The above comparison between the point of change of displacement gradient and the depth of full shear is summarized in Table 4.3, and shows that in general there seems to exist a relationship between the two parameters.

	Plate Pen. mm	K_s	D_s mm
Experimental	36.8	-	80.6
Predicted	36.0	15000	97.4
"	36.0	9000	93.3
"	36.0	6000	93.1
"	36.0	4500	92.8
"	36.0	3000	73.7
Experimental	63.7	-	135.2
Predicted	64.0	15000	166.3
"	64.0	9000	166.4
"	64.0	6000	162.2
"	64.0	4500	158.2
"	64.0	3000	124.1

TABLE 4.1 Experimental and Predicted Depth of Full Shear - Age 4 Days

	Plate Pen. mm	K_s	D_s' mm
Experimental	23.8	-	34.5
Predicted	24.0	9000	52.7
"	24.0	4500	60.9
Experimental	36.5	-	97.8
Predicted	36.0	9000	88.9
"	36.0	4500	93.2

TABLE 4.2 Experimental and Predicted Depth of Full Shear - Age 30 Days

Age of snow (days)	Plate Penetration (mm)	Depth of Full Shear D_s (Plate Lengths)		Point of Change of Displacement Profile (Plate Lengths)	
		EXP.	PRED.	EXP.	PRED.
4	36	1.67	1.86	1.9	1.5
4	64	2.82	3.24	2.0 - 2.25	2.0 - 2.25
30	24	0.5	0.9	1.5 - 1.75	1.5 - 1.75
30	36	1.9	1.8	1.75 - 2.0	1.75 - 2.0

Table 4.3 Depth of Full Shear vs Point of Change of Displacement Gradient

4.2.7 Comparison between Experimental and Predicted Density Profiles

Density profiles derived from the change in area of square elements of the grid photographed during plate penetration tests and those predicted by the finite element model are displayed in Figs. 4.14 to 4.21 for both types of snow used. As shown in the plots, the experimental profiles feature a considerable scattering of the points although following more or less the same pattern as the predicted ones, i.e, density decrease with depth. The predicted density profiles are, of course, more clearly defined and in all cases, are characterized by a more or less constant value for some depth below the plate followed by a decrease to the initial density (prior to loading). This is therefore consistent with the predicted (and experimental) displacement profiles (section 4.2.5) which followed a similar pattern by which a linear displacement profile implied a constant degree of strain. Since, in the present loading situation, a relationship between vertical strain and density clearly exists, it is hence not surprising to observe a uniform density for some depth below the plate.

The agreement between experimental and density profiles can be said to be satisfactory in so far as the trends are similar on both cases. The scattering of experimental values, mainly due to the probably non-uniform density distribution of the snow deposit prior to loading,

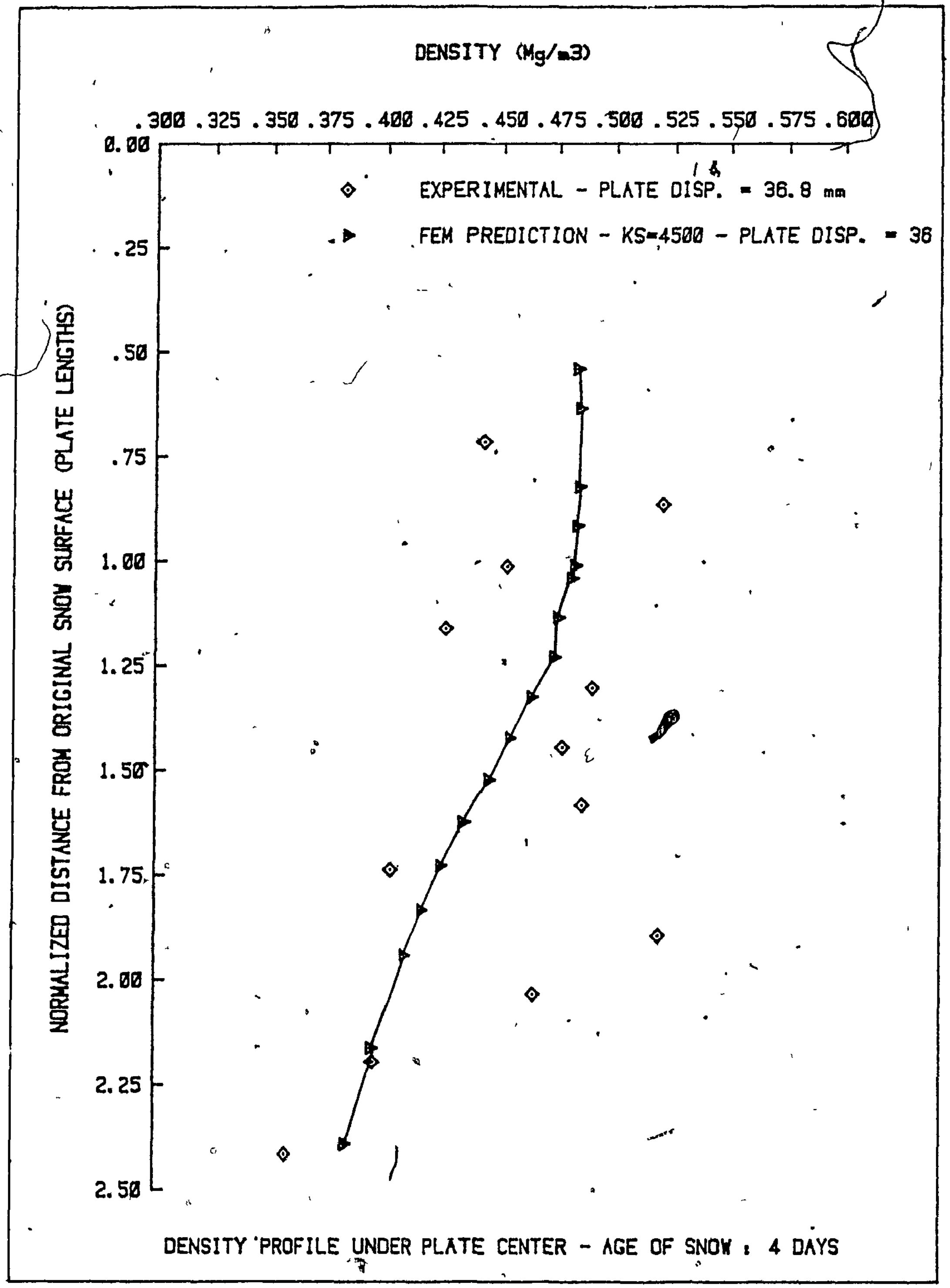

Fig. 4.14 Experimentally Obtained and Predicted Density Profiles Under Plate Center - Age 4 Days (Plate Pen. = 36 mm)

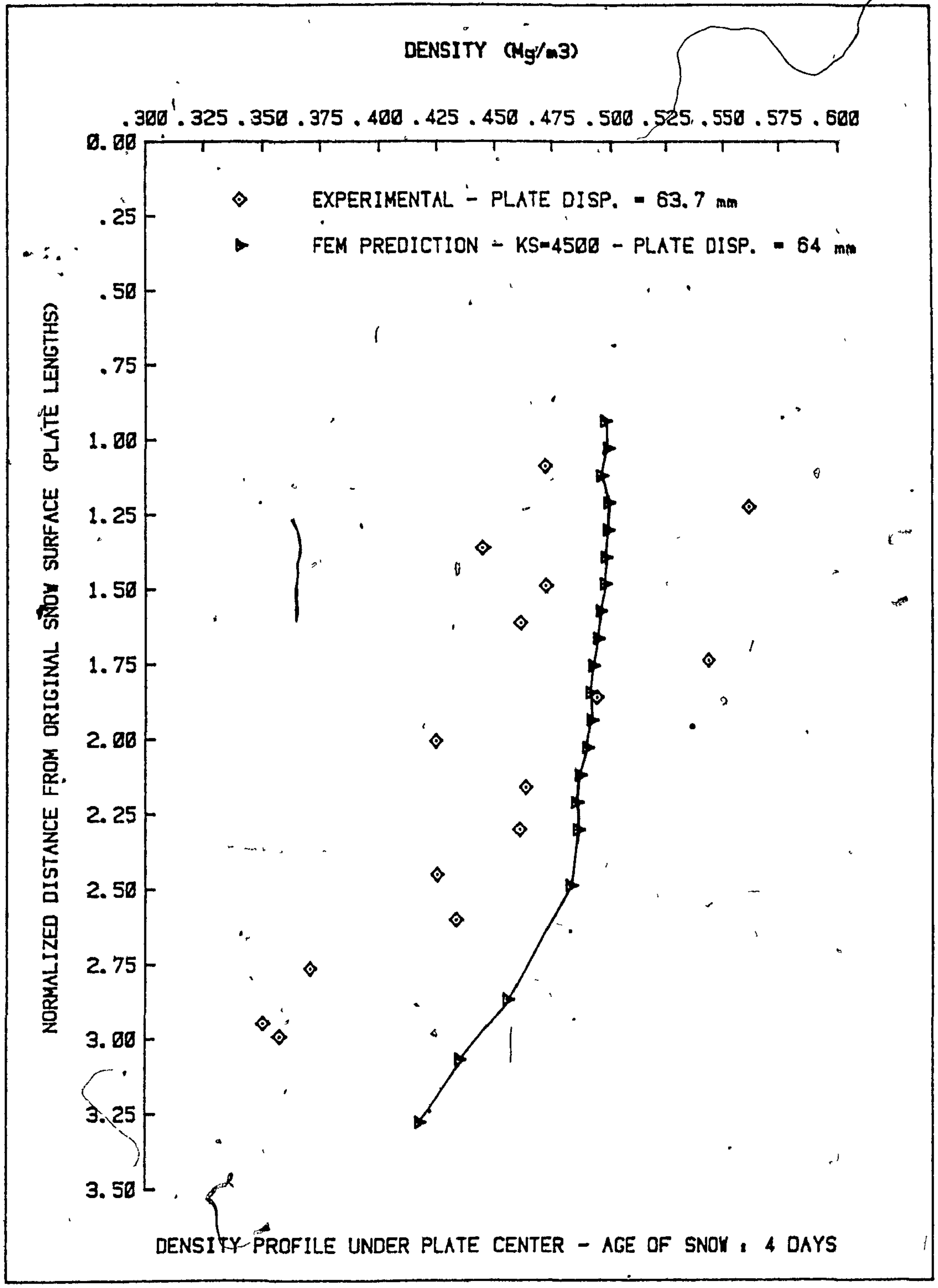

Fig. 4.15 Experimentally Obtained and Predicted Density Profiles Under Plate Center - Age 4 Days (Plate Pen. = 64 mm)

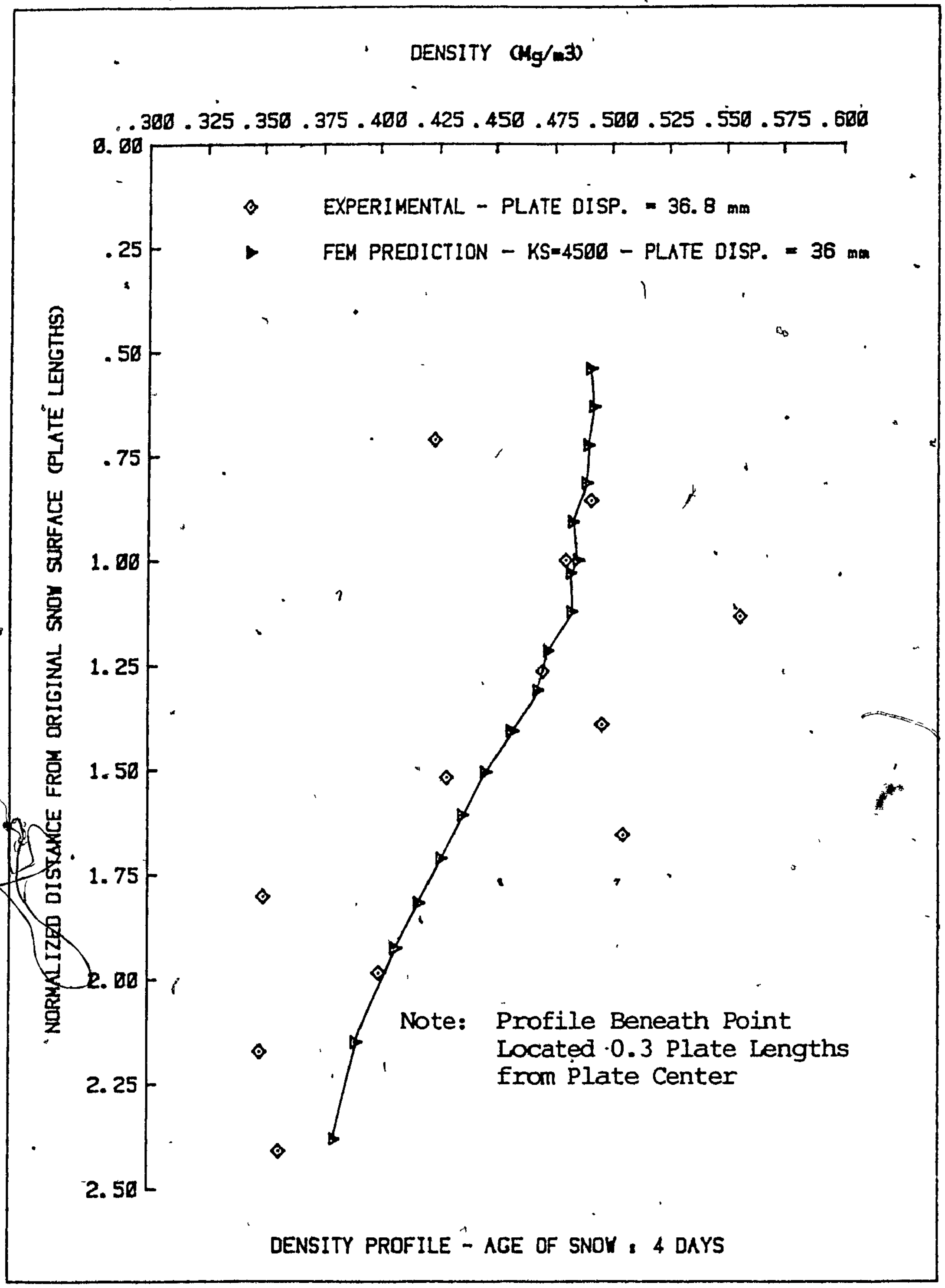

Fig. 4.16 Experimentally Obtained and Predicted Density Profiles
Age 4 Days (Plate Pen. = 36 mm)

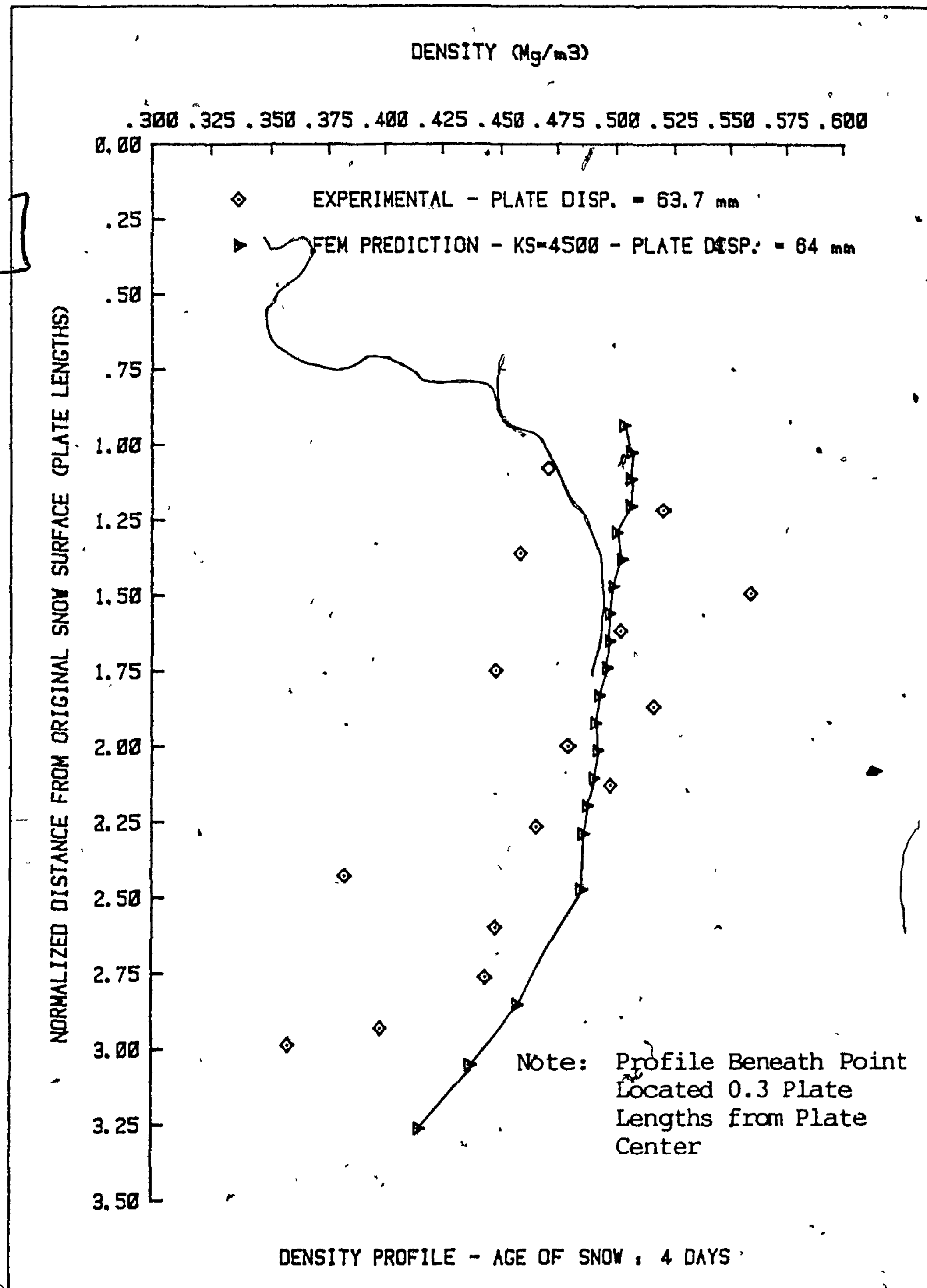

Fig. 4.17 Experimentally Obtained and Predicted Density Profiles
Age 4 Days (Plate Pen. = 64 mm)

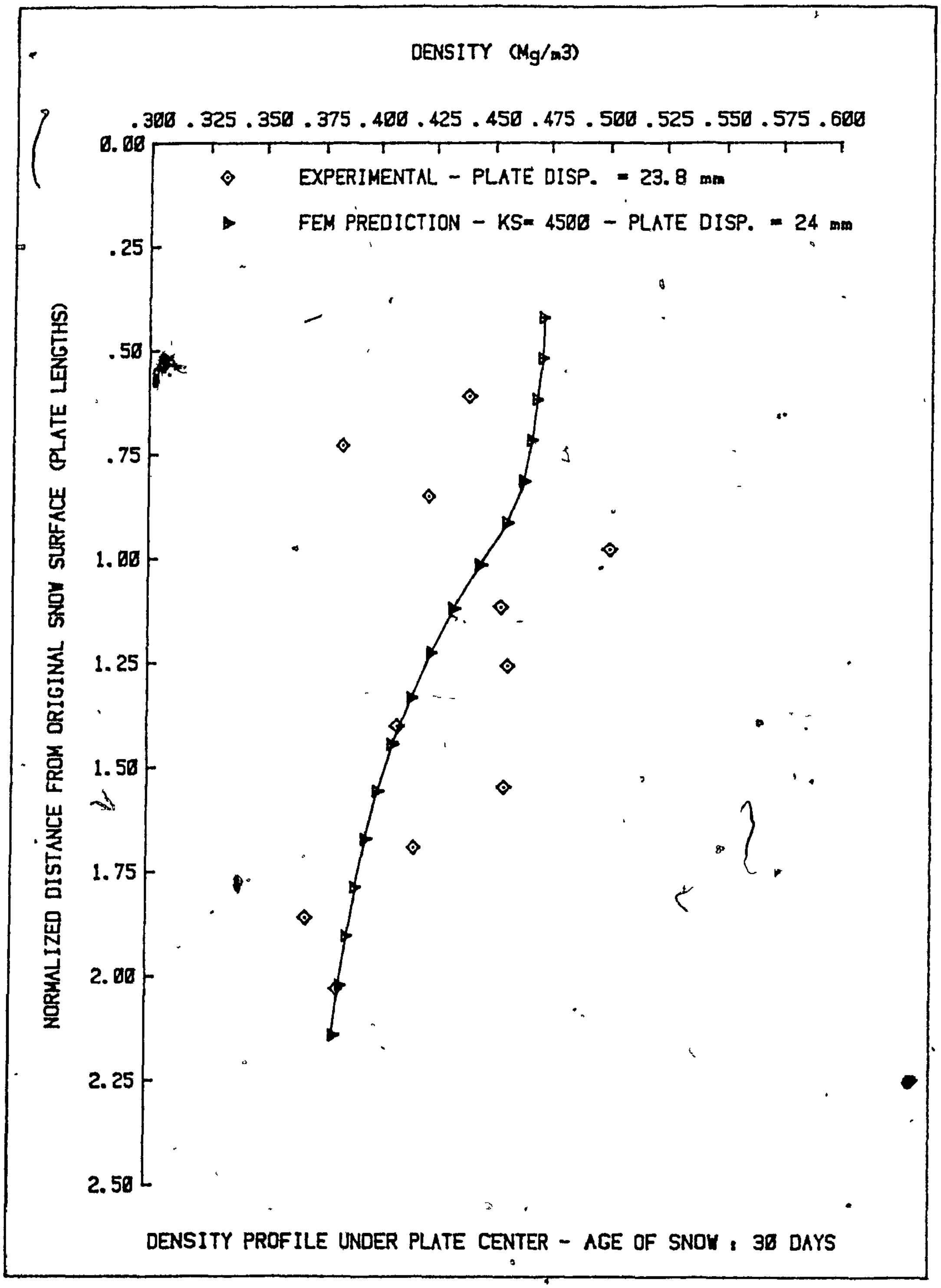

Fig. 4.18 Experimentally Obtained and Predicted Density Profiles Under Plate Center - Age 30 Days (Plate Pen. = 24 mm)

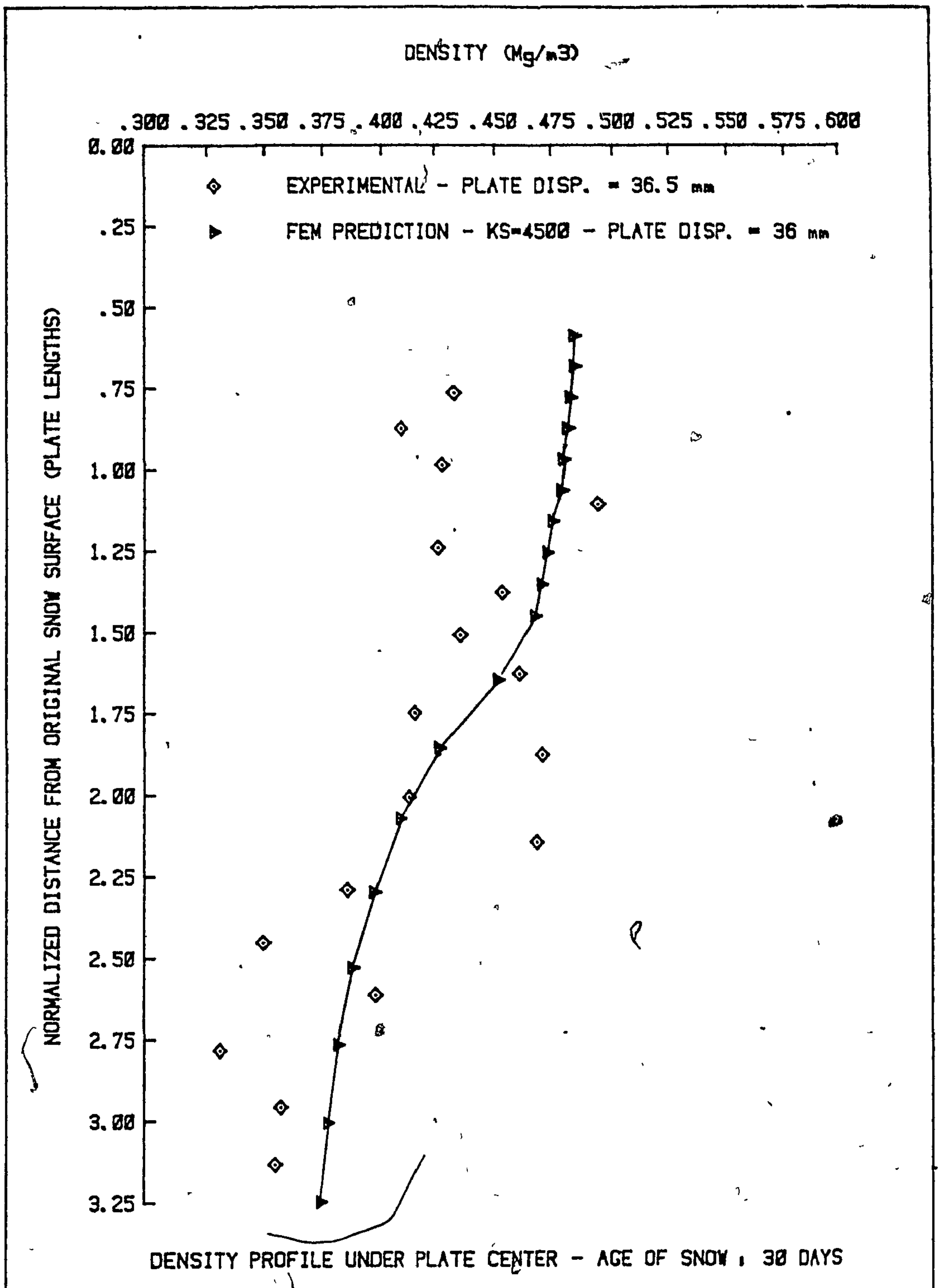

Fig. 4.19 Experimentally Obtained and Predicted Density Profiles Under Plate Center - Age 30 Days (Plate Pen. 36 mm)

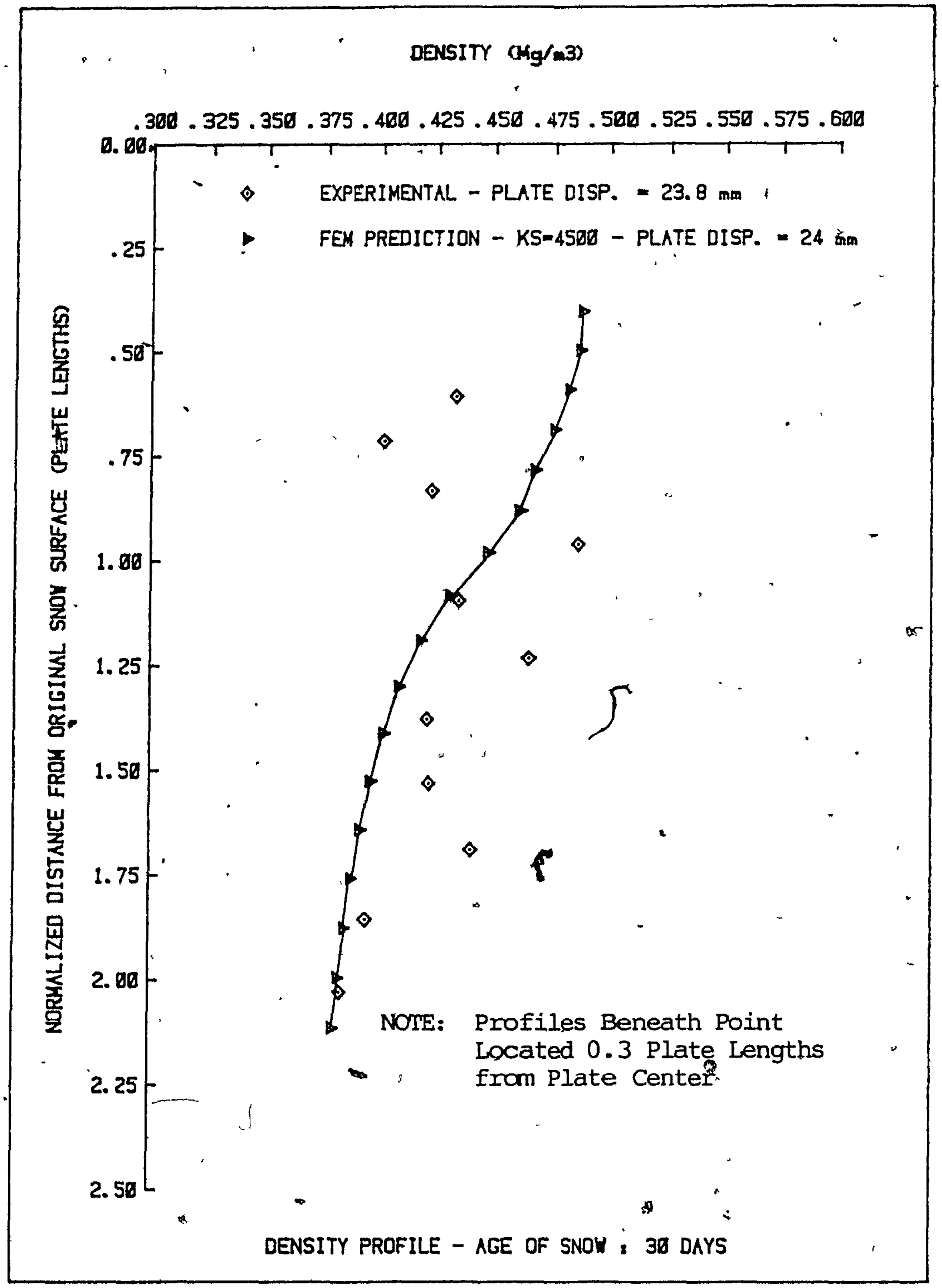

Fig. 4.20 Experimentally Obtained and Predicted Density Profiles - Age 30 Days (Plate Pen. = 24 mm)

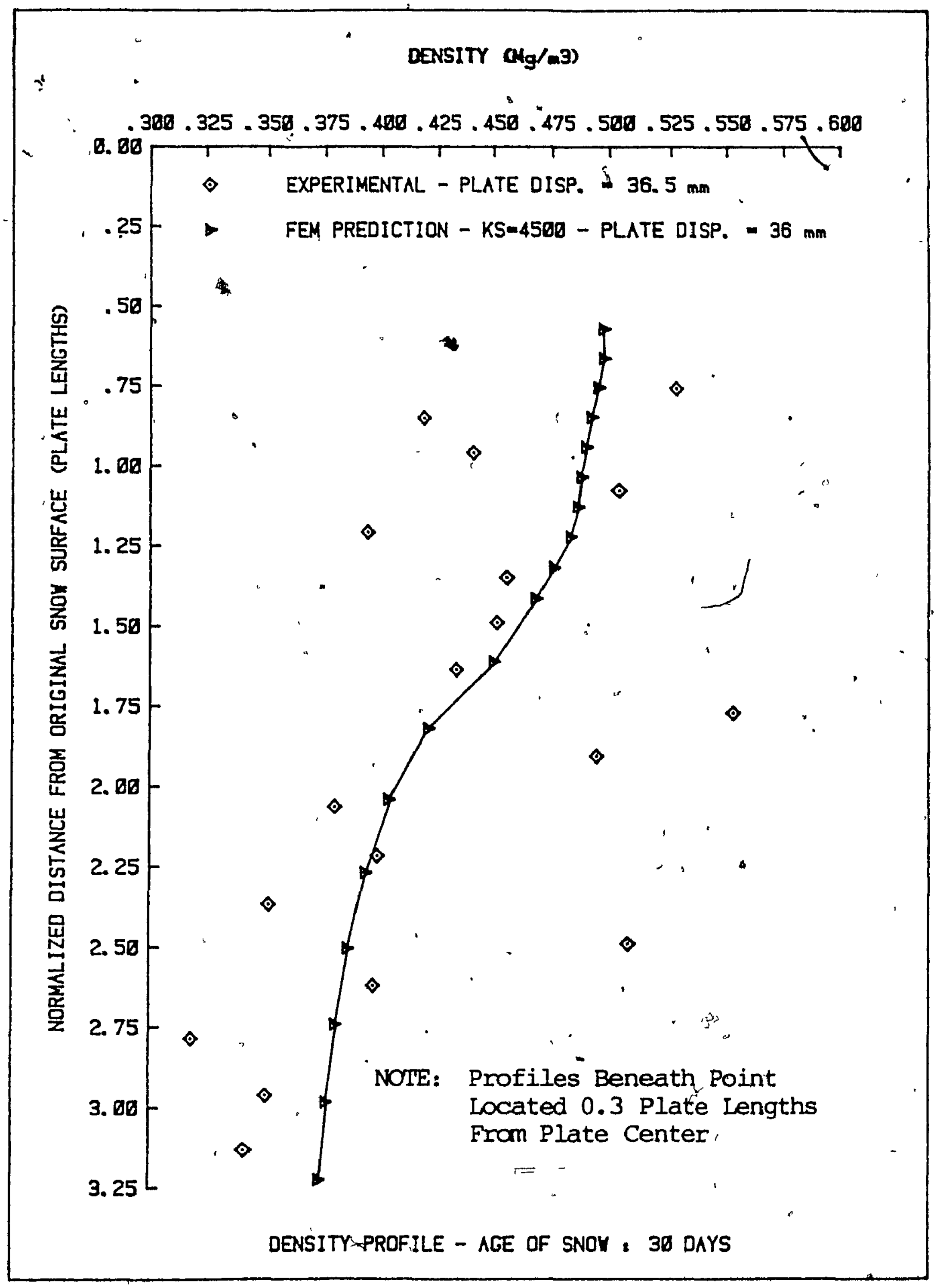

Fig. 4.21 Experimentally Obtained and Predicted Density Profiles - Age 30 Days (Plate Pen. = 36 mm)

does not allow an accurate comparison between individual, experimental and predicted density values along the profiles.

4.2.8 Predicted Load Distribution on the Plate

The developed model has the capability of predicting the load distribution on the plate as a function of plate penetration. Load at a given point along the plate is computed as the product of the reaction on a given node representing the plate-snow interface in the finite element mesh and the plate width since the problem is analyzed in terms of plane strain conditions.

The load distribution on the plate for several levels of plate penetration and for both types of snow used are shown in Figs. 4.22 and 4.23. In both cases, the distributions follow the same trend in that the portion of load carried increases from the center to the edges of the plate. Points near the plate center are subjected to reactions resulting from the resistance of the snow to undergo volume change. At or near the edges, the snow tends to simultaneously compress and shear along the failure planes so that an additional resisting force is involved. The predicted behaviour is therefore as expected.

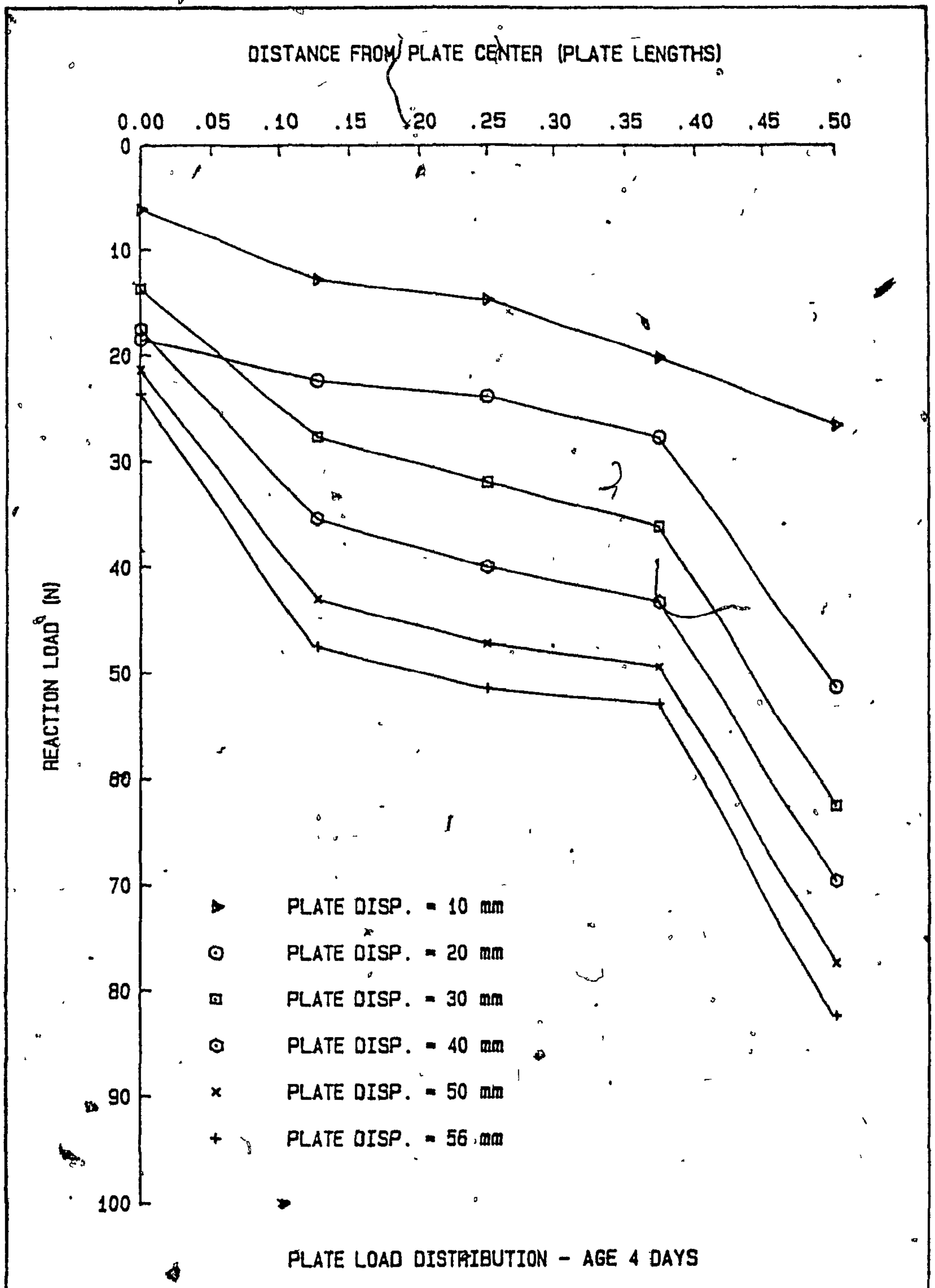

Fig. 4.22 Load Distribution on Plate - Age 4 Days (K_s = 4500)

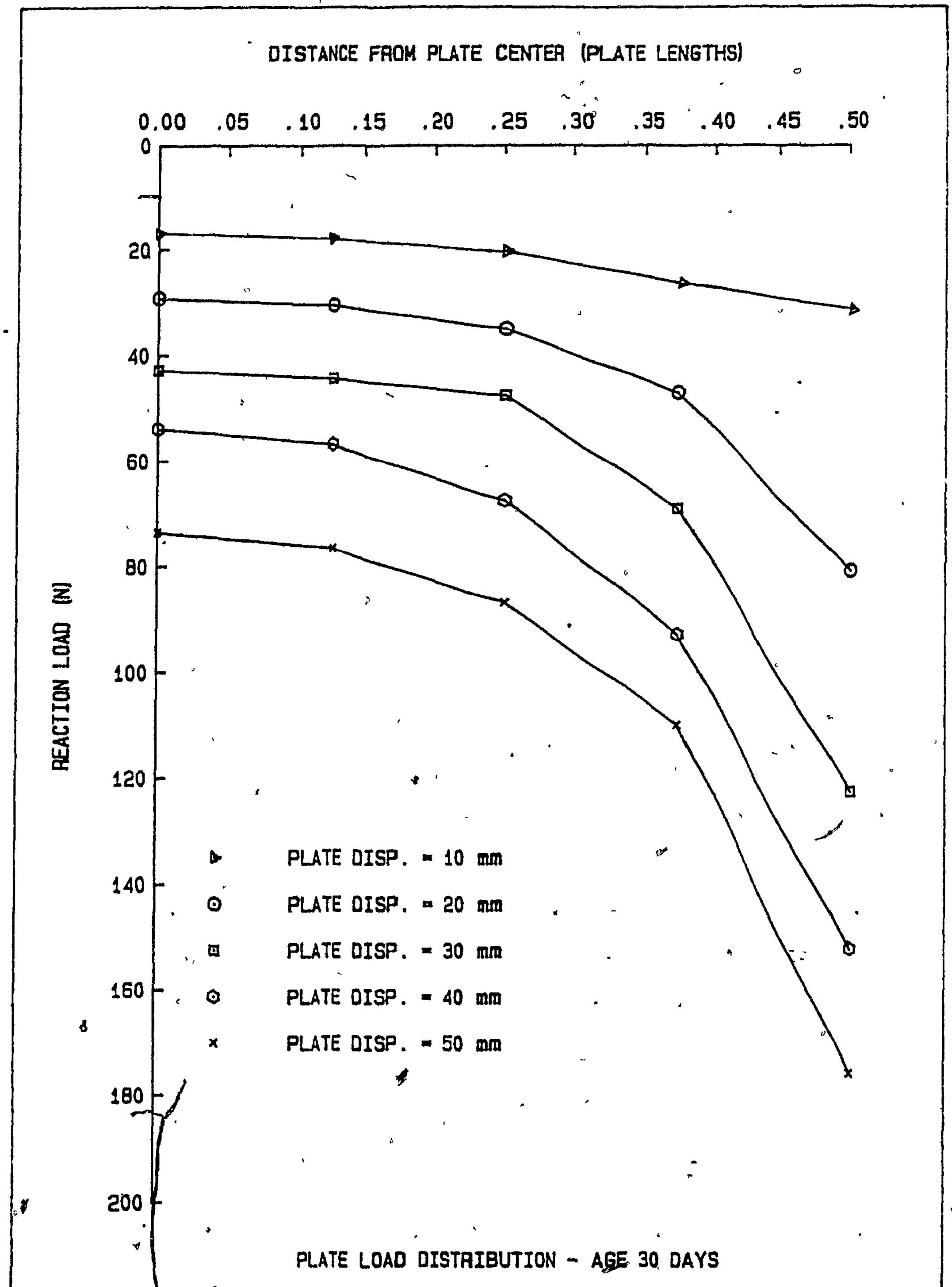

Fig. 4.23 Load Distribution on Plate - Age 30 Days (K_s = 4500)

4.2.9 Predicted Density at Failure of Shear Elements

As discussed in Chapter 2, joint or shear elements fail when the cumulative shear stress exceeds the shear strength at the density across the plane of shear of the element. Such density values are unknown quantities prior to any plate penetration and are generated by the model from the predicted displacement fields.

The density at failure of each joint element in the model and the corresponding distance from the original snow surface (i.e, original plate position) at which the failure process occurs is plotted in Figs. 4.24 and 4.25 for both types of snow. It can be observed that joint elements near the plate fail at a higher density than the rest especially in the case of the 4 day old snow (Fig. 4.24). This can be expected since at the beginning of the plate penetration process, support along the failure planes is higher due to that the failure process has not developed appreciably. Higher density in triangular elements near the failure planes can thus result.

For joint elements originally located at depths of 0.5 plate lengths and greater, density at failure stays practically constant and even more so for 4 day old snow. Comparison of Figs. 4.24 and 4.25 shows that the densities at failure for 30 day old snow are in general higher than those for 4 day old snow thus implying that the latter type of

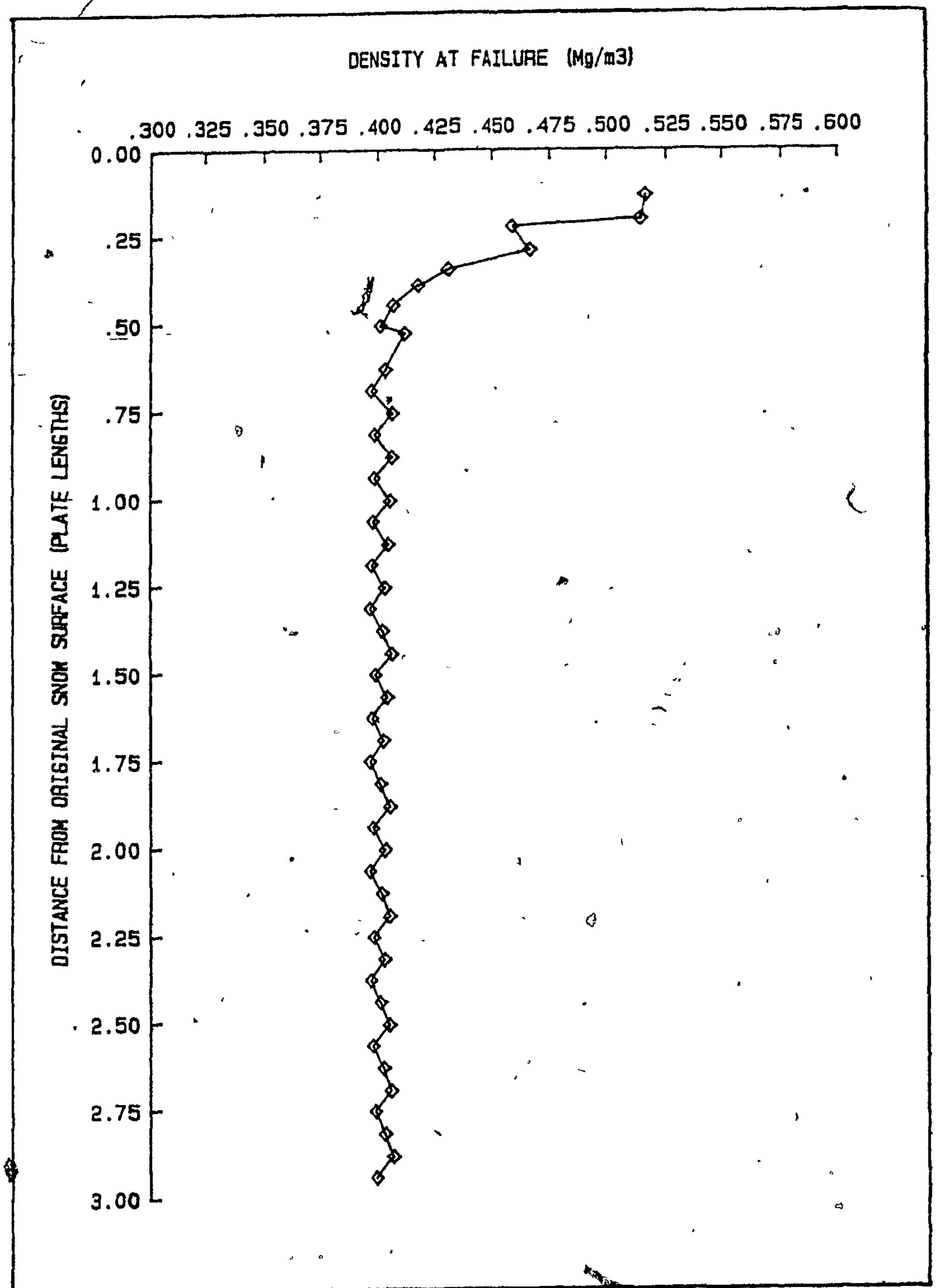

Fig. 4.24 Density at Failure of Shear Elements - Age 4 days
(K_s = 4500)

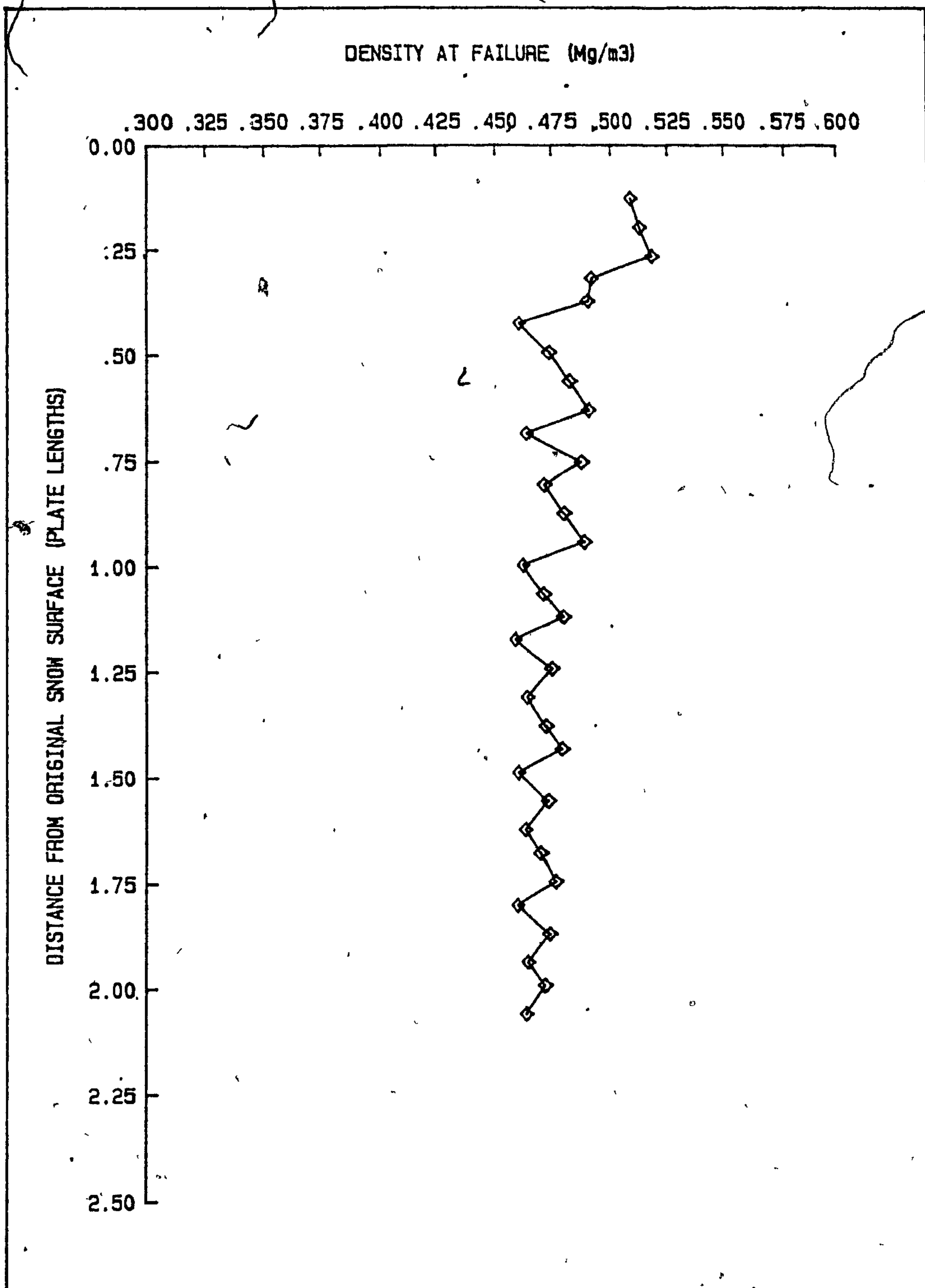

Fig. 4.25 Density at Failure of Shear Elements - Age 30 Days
(K_s = 4500)

snow fails earlier in the plate penetration process. This is to be expected since the shear strength of the lower age snow is lower as shown by the vane shear strength results presented in Chapter 3.

CHAPTER 5

CONCLUSIONS AND RECOMMENDATIONS FOR FURTHER RESEARCH

5.1 Conclusions

On the basis of the tests performed and the results of the developed predictive analytical model, the following conclusions may be drawn:

1. The compressibility of snow, as shown by confined compression tests, increased with density. A stiffening type of curve was obtained for all tests on both types of snow used. As expected, the response for 30 day old snow was stiffer due to the higher degree of sintering.

2. The shear strength of snow increased with age, due to the greater strength of bonds between particles, and with density, as demonstrated by results of vane shear tests.

3. The experimental plate stress-penetration curves were essentially bi-linear with a change of slope occurring relatively early in the penetration process. Significant stress vibration due to microfracturing was observed.

4. A method to model a highly compressible non-linear material which failed according to a punching shear type of mechanism was developed. The model includes the effect of non-linearity and strain hardening behaviour in compression as well as the effect of

shear stresses generated along the vertical sides of the pressure bulb. The maximum shear stress tolerated by a shear element was limited by its shear strength which in turn depended on density. Provisions were made to simulate this effect so that the model includes an algorithm by which excess shear stress in failing joint elements are redistributed within the snow mass. In so doing, the shear stress in any shear element never exceeds the value corresponding to the shear strength.

5. The plate resistance-penetration curves as predicted by the analytical model compared rather well with the experimentally obtained ones. The predicted response was somewhat sensitive to the single value of shear stiffness employed in the model but a value of 4500 for this parameter gave satisfactory results for both types of snow used. As expected, the predicted value for 30 day old snow is higher than that for 4 day old snow.

The good agreement between predicted and experimental plate stress-penetration curves demonstrates the ability of the proposed model to simulate the plate penetration mechanism. The success of the finite element method of analysis as a solution technique is indicative that the energy balance of the system is preserved. In terms of an energetics approach to the problem, the governing relationship describing the plate penetration process is that the work done on the system is equal to the total of the deformation energy of the snow, energy losses due to snow-plexiglas friction, strain energy of the plexiglas box which is not entirely rigid, etc. Comparison of experimental and predicted results based on the energy balance concept would simply involve integrating the experimental plate stress-penetration curve to obtain the total energy input and comparing the latter quantity to the strain energy associated the above process requires summation of the strain energy developed in each triangular and joint element in the finite element mesh over the number of plate displacement increments and excess shear stress analyses performed when applicable. Each increment of plate displacement or excess shear stress analysis is treated as a linear elastic problem in which, by the theorem of minimum potential energy used in the finite element formulation, the product of the reactions on the nodes representing the plate-snow interface, the incremental plate displacement and the plate width is equal to the stress-strain integration over the entire volume of snow considered. An experimental vs prediction comparison of the plate penetration energy balance is therefore superfluous since the compared values of energy are derived from results already available from i) the experimental plate stress-penetration curve, when computing the real energy input and ii) the finite element analysis performed for each plate displacement increment or excess shear stress analysis, when computing the total strain energy associated with snow deformation.

6. The predicted displacement depth profiles below the plate were, in general, in good agreement with the ones derived from experimental data. In both cases, the displacement profiles were found to be linear with a change of slope occurring at some depth more or less related to the degree of failure exhibited along the planes of cutting shear. Displacements and strains were found to be greater in the snow above the point of displacement gradient change. The displacement profile prediction was less sensitive than the plate penetration response to a change in shear stiffness.

7. The predicted values of depth of full shear, which are representative of the degree of failure along the planes of cutting shear were, in general, in relatively good agreement with those obtained from analysis of experimental data. The proposed relationships between these values and the point of displacement gradient change was established.

8. Density profiles as obtained experimentally yielded scattered results probably due to the initial non-uniform density distribution with depth and the non-homogeneity of the material. Predicted density profiles were smooth continuous curves whose shape was consistent with the predicted displacement profiles. Comparison of experimental

and predicted results was difficult due to the degree of scattering of experimental points but predicted curves, in general, fitted the points reasonably well.

9. The predicted load distribution on the plate was such that a greater portion of the reaction load was carried by the edges of the plate. This is mainly due to the additional resistance of the snow to shear along the failure planes. The effect was more pronounced for 4 day old snow. Due to technical difficulties, no experimental values were available for comparison purposes.

10. Densities at which shear elements failed along the planes of cutting shear converged to a practically constant value at a short distance from the plate. Again, no experimental data was available for comparison due to experimental difficulties.

11. Discrepancies between predicted and experimental values of paramaters describing the plate penetration mechanism were due to combined effects of the following:

a) Deposition of snow in the deep boxes was performed with care but nevertheless resulted in a non-homogeneous layer of non-uniform density. In addition, snow is not isotropic in reality.

b) The presence of some friction between the snow and the sides of the plexiglas boxes and that existing between the snow sample and the walls of the confined compression test cylinders.

c) The problem is not exactly plane strain since, in reality, stresses, strains, displacements, etc., also vary across the width of the plate.

d) The behaviour of snow in shear is possibly such that shear stiffness is not constant and may actually vary with density. The stress-deformation curve in shear may thus be non-linear. Also, during vane shear tests, snow is not sheared at an absolutely constant value of density due to the compressing action of the blades on the snow upon rotation of the vane.

e) The viscous nature of the material is such that response is quite sensitive to strain rate, particularly in the case of shear. An implicitly assumed uniform strain rate field generated in the snow may be an addition source of error.

f) The algorithm developed on the basis of the finite element method involves assumptions and idealizations, such as the handling of the large volume change behaviour of the material by a stress-strain curve updating procedure.

g) Good replication of snow samples is very difficult due to the thermodynamic activity of the material and its sensitivity to variation in surrounding conditions such as temperature, humidity, wind and light.

h) Similarly, the correspondence of snow produced for confined compression and plate penetration tests is questionable due to the different thermal isolation conditions.

12. The analysis of the present problem emphasizes on the prediction of the stress-penetration behaviour of a rigid plate in deep snow and, consequently on an investigation of the required material characteristics and parameters introduced in the solution procedure. Confined compression and vane test results proved to be legitimate and practical tests to obtain the compressibility and shear strength data demanded by the developed model. As mentioned in Chapter 2, the shear stiffness parameter is not obtained experimentally but rather is the focus of a sensitivity analysis of the model. Success in the modelling procedure lies in the selection of a narrow range of shear stiffness values such that experimental and predicted plate stress-penetration curves, displacement and density profiles, and depth of shear along the pair of planes of cutting shear agree relatively as well as can be expected considering the nature of the material itself and the assumptions and idealizations introduced in the developed predictive model. In the light of this, it can be said that the proposed model has satisfied the objectives of the study.

5.2 Recommendations For Further Research

1. The stress-deformation behaviour of snow in shear requires further investigation. The development of a constitutive law describing the stress-deformation response of snow under vane testing conditions appears to be an immediate priority.

2. A similar set of vane tests should be performed but using a rate controlled vane and recording the torque-rotation response. Values of shear stiffness would thus be obtained through an independent experiment. The resulting values, for different densities, could then be used in the present model and the effect on the predicted plate penetration responses could be investigated.

3. Further research is required to relate the plate stress-penetration response under plane strain conditions to that in three dimensions.

4. The present computer model can be extended to handle the dependence of shear stiffness on density simply by supplying an extra input curve and slightly modifying the main program and some subroutines.

5. The effect of plate dimensions should also be investigated. A different plate size implies a different distribution of compressive stresses within the pressure bulb and shear stresses along the failure planes.

REFERENCES

1. Ballard, G.E.H., and McGraw, R.W., (1965). A theory of snow failure. U.S. Cold Regions Research and Engineering Laboratory. Research Report 137.

2. Brown, R.L. (1979). Applications of Energitics to Vehicle Trafficability Problems. Proceedings of International Society of Terrain Vehicle Systems Workshop on Snow Traction Mechanics, Alta, Utah, 1979.

3. Fraser, C. (1978). Avalanches and Snow Safety. Scribner's Son, New-York, N.Y.

4. Fukue, M. (1977). Ph. D. Thesis, McGill University, Montreal.

5. Goodman, R.E., Taylor, R., and Brekke, T.L., A Model for the Mechanics of Jointed Rock, Journal of Soil Mechanics and Foundations Division, ASCE, Vol. 94, No. SM3, Proc. Paper 5937, May 1968, pp. 637-659.

6. Hanna, A.W. (1975) "Finite Element Analysis of Soil Cutting and Traction", Ph.D. Thesis, McGill University.

7. Harrison, W.L. (1975). Vehicle Performance over Snow: Mathematical Model Validation Study. CRREL, Technical Report 268.

8. Hobbs, P.V. (1973). Ice in The Atmosphere: a review of the present position. Physics and Chemistry of Ice (E. Whalley, S.J. Jones and L.W. Gold, eds). R. Sóc. Can., Ottawa, pp. 208-319.

9. Lo, K.Y. and Lee, C.F., (1973). Stress Analysis and Slope Stability in Strain Softening Materials, Geotechnique 23, No. 1, 1-11.

10. Metaxas, I., (1984). Master's Thesis, McGill University, Montreal.

11. Perla, R.I. and M.Martinelli Jr.(1976). Avalanche Handbook. Agric. Handbook, No. 489, U.S. Govt. Printing Office, Washington, D.C.

12. Yong, R.N. and Fukue, M. (1977). Performance of Snow in Confined Compression, Journal of Terramechanics, Vol, 14, No. 2, pp. 59 to 82.

13. Yong, R.N. (1979). Snow Traction Mechanics. Proceedings of International Society of Terrain-Vehicle Systems Worshop on Snow Traction Mechanics, Alta, Utah, 1979.

14. Yong, R.N. and Muro, T. (1981). Plate Loading and Vane-Cone Test Measurements for Fresh and Sintered Snow, Geotechnical Research Centre, McGill University, Montreal. Technical Report Submitted to the Defence Research Establishment Suffield, 32 p.

15. Yong, R.N. (1985). Derivation of Engineering Properties of Snow from Field Penetrometers, Geotechnical Research Centre, McGill University, Montreal. Technical Report Submitted to the Defence Research Establishment Suffield, 69 p.

16. Zienkiewicz, O.C., (1977) The Finite Element Method, 3rd. Ed., McGraw-Hill, London.

17. Zienkiewicz, O.C., Valliapan, S. and King, I.P. (1968). Stress Analysis of Rock as a 'No-Tension' Material, Geotechnique 18, No. 1, 56-66.

APPENDICES

APPENDIX A

PLATE TEST PHOTOGRAPHS

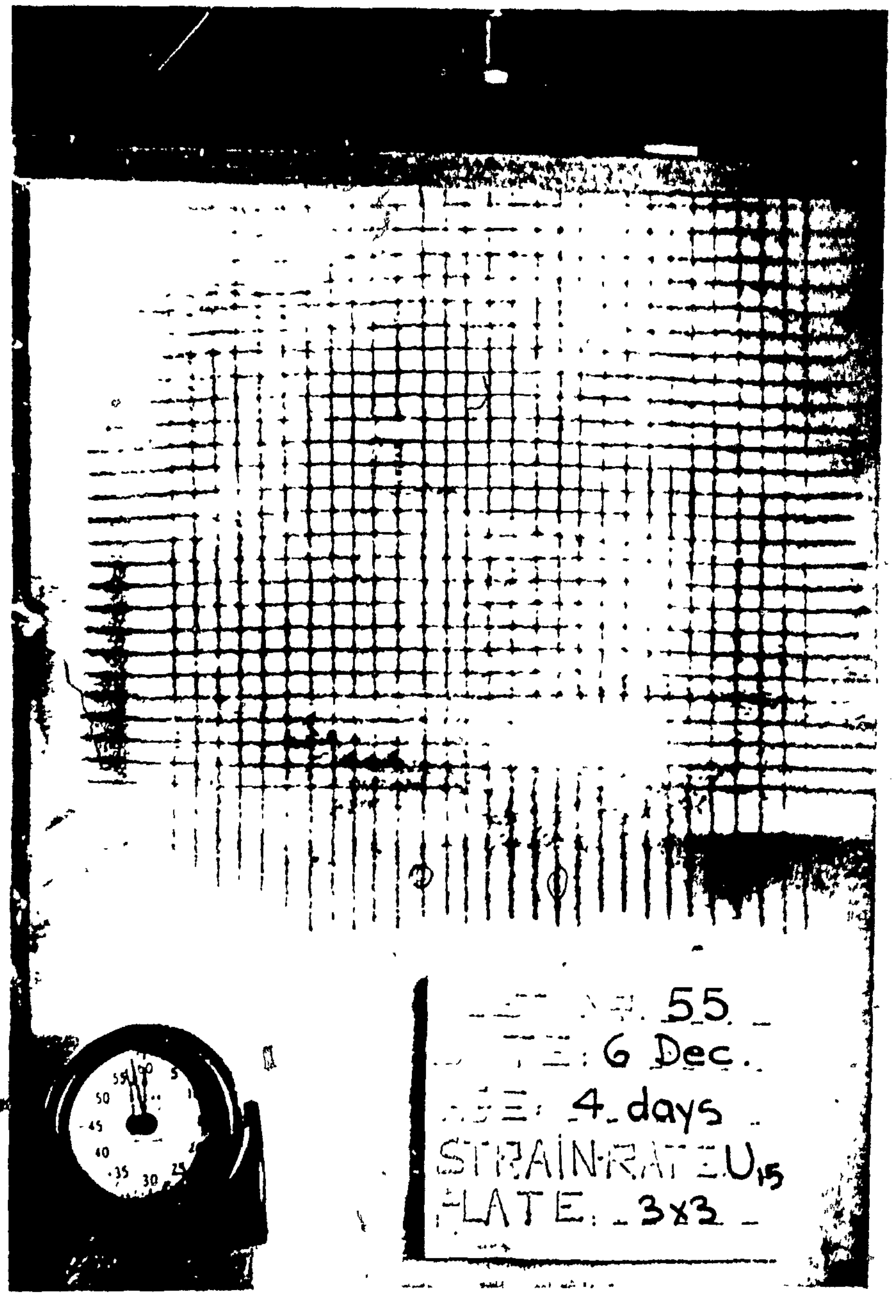

Photo # 1

Age 4 days
Plate Penetration = 0mm

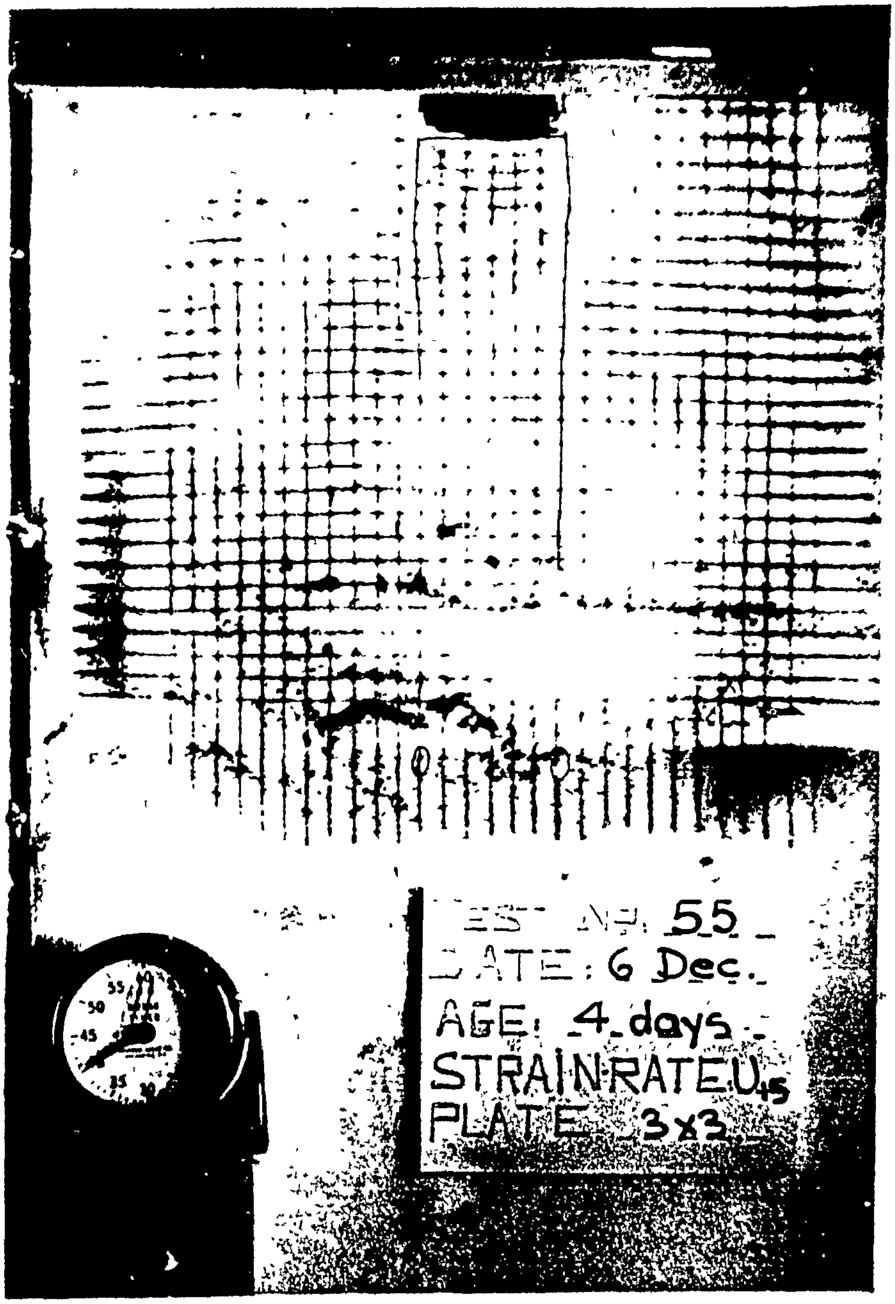

Photo # 2

Age 4 days
Plate Penetration = 36.8mm

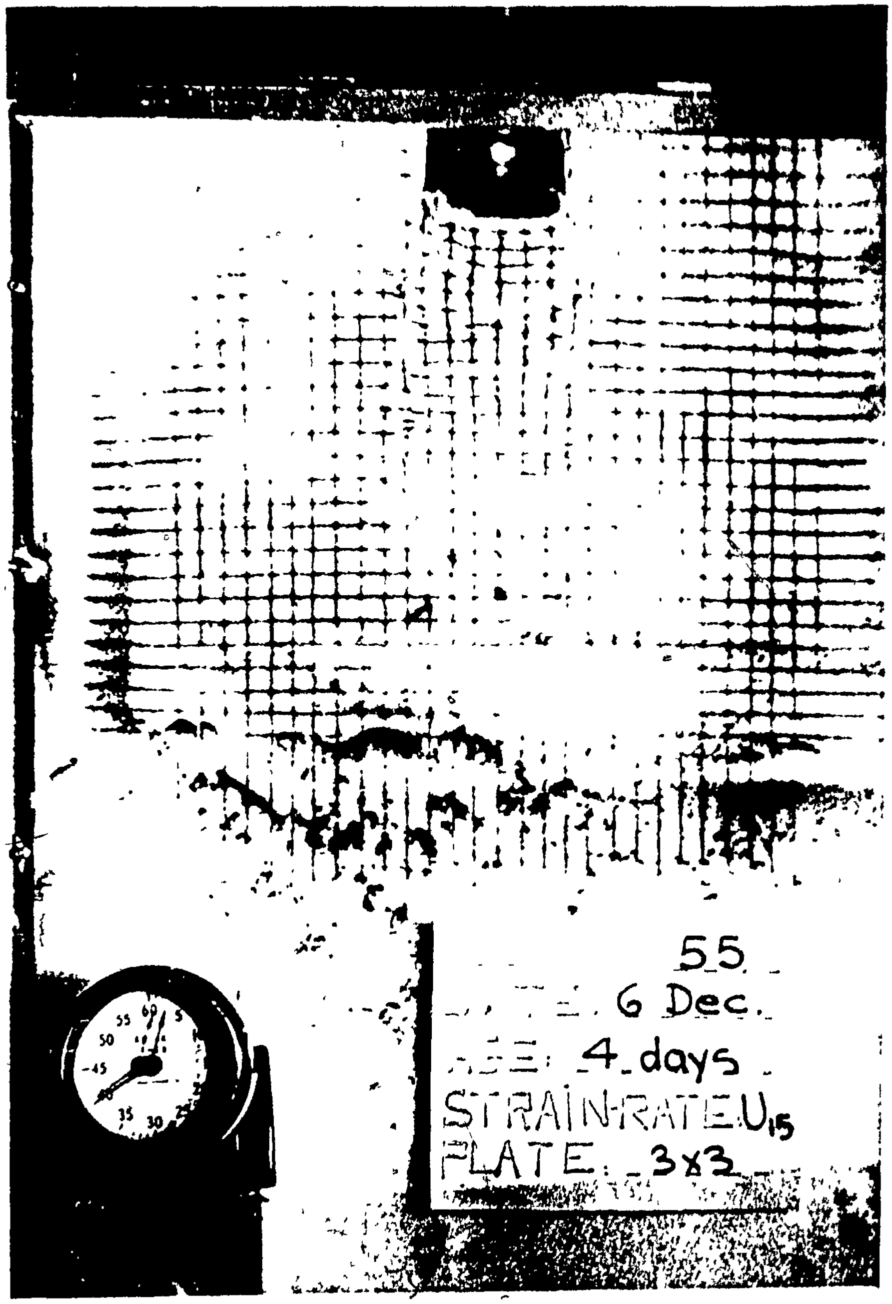

Photo # 3

Age 4 days
Plate Penetration =63.7 mm

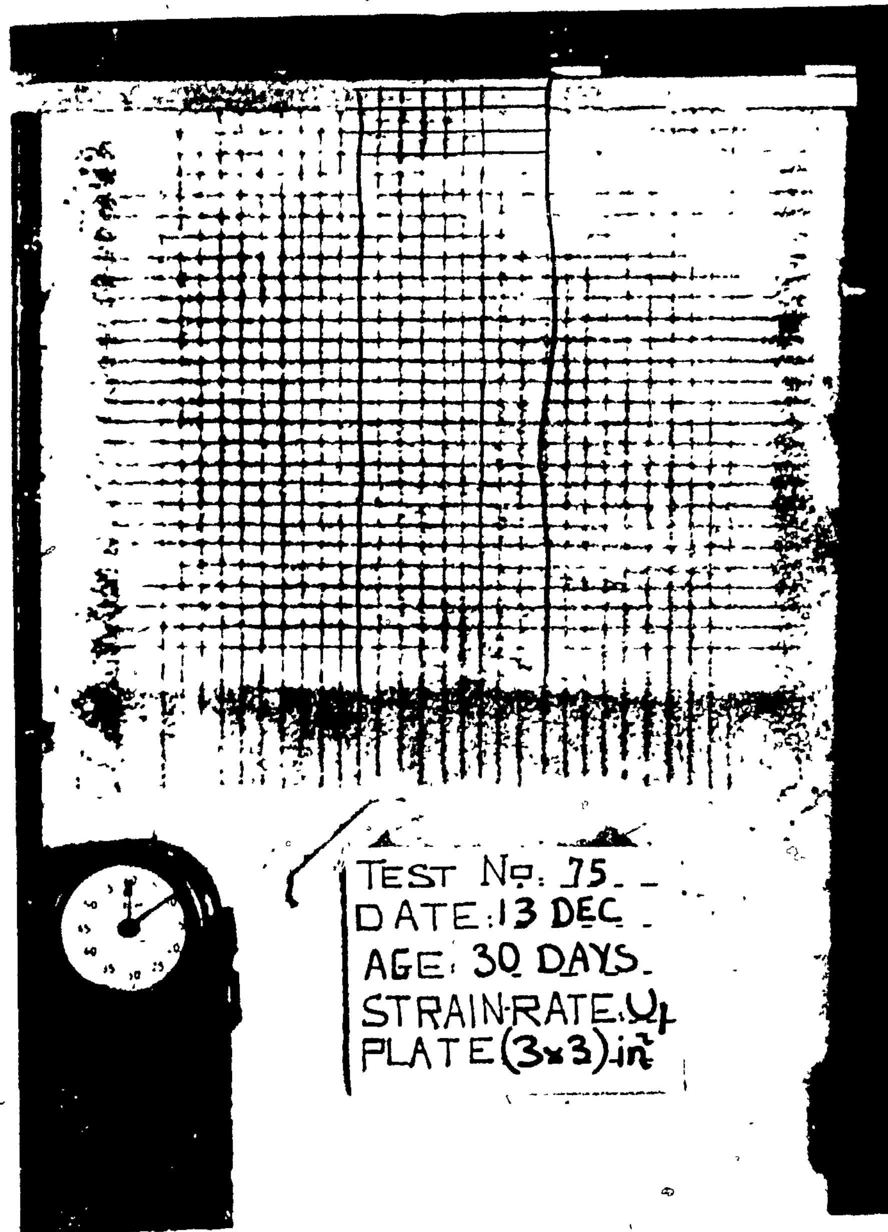

Photo #1

Age 30 days
Plate Penetration = 0mm

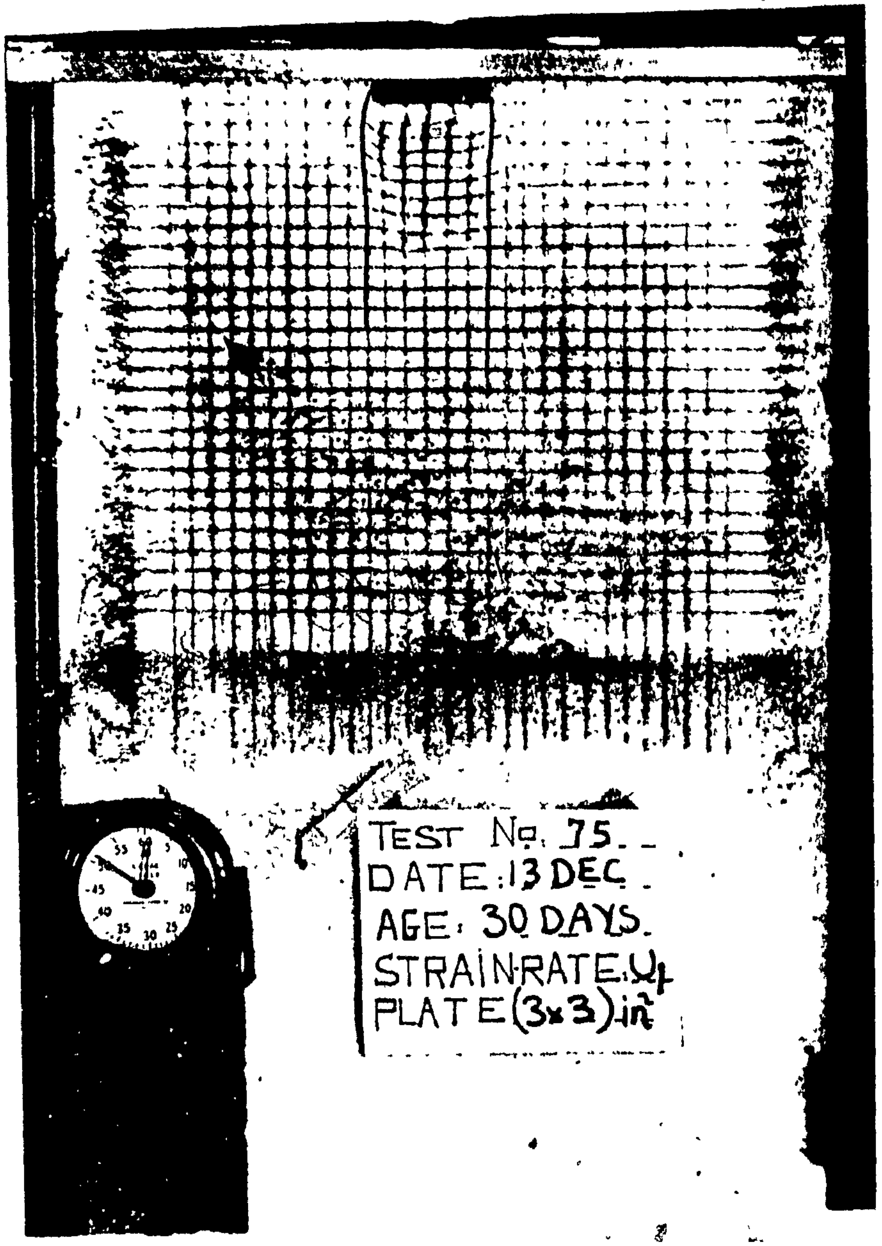

Photo # 2

Age 30 days
Plate Penetration = 23.8mm

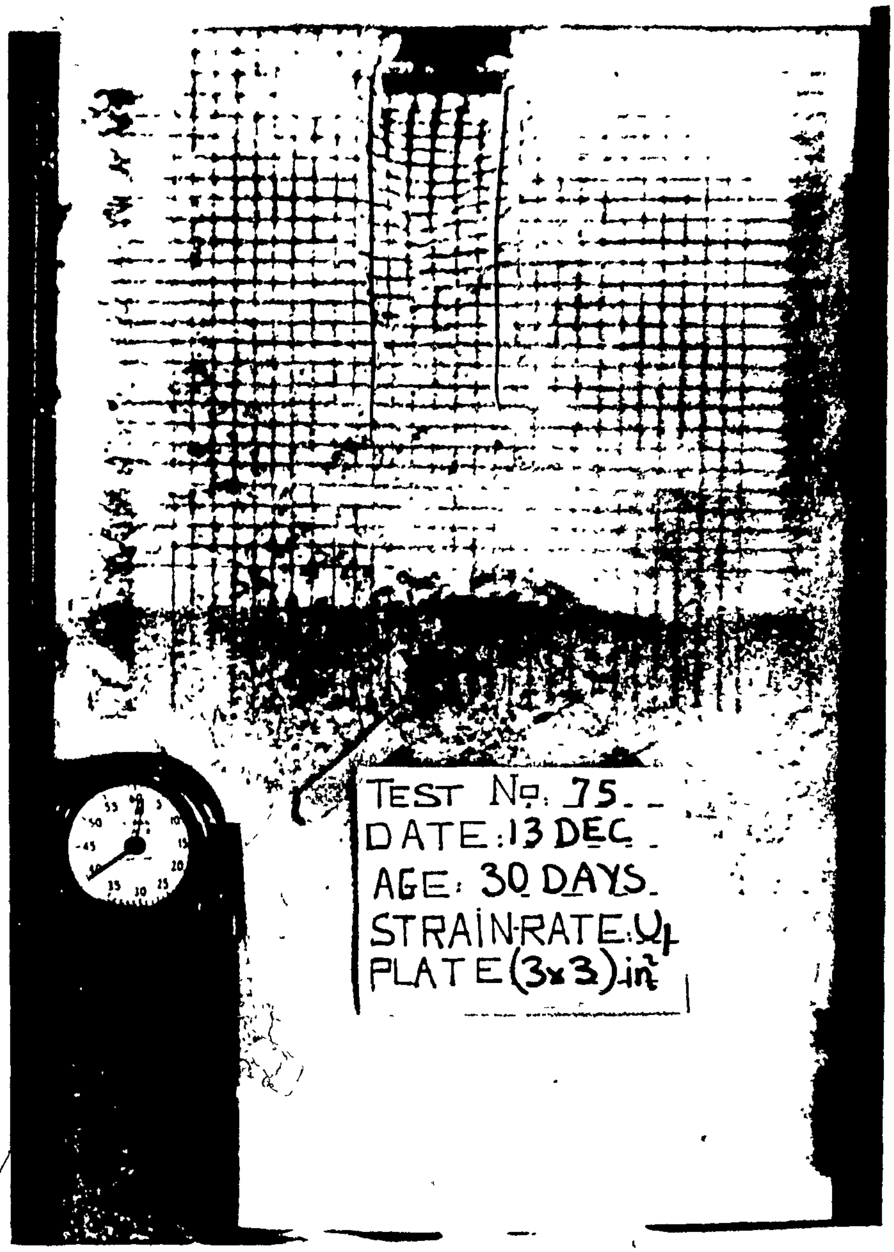

Photo # 3

Age 30 days
Plate Penetration = 36.5mm

APPENDIX B - Program Flowcharts

2.1 Main Program

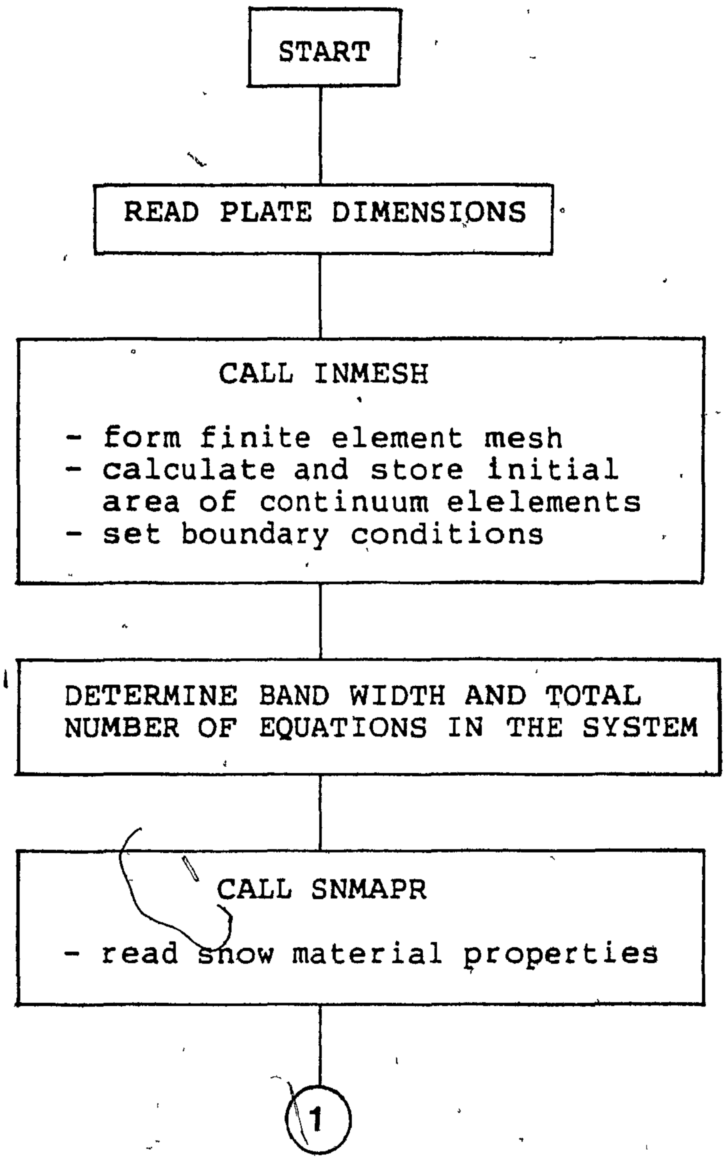

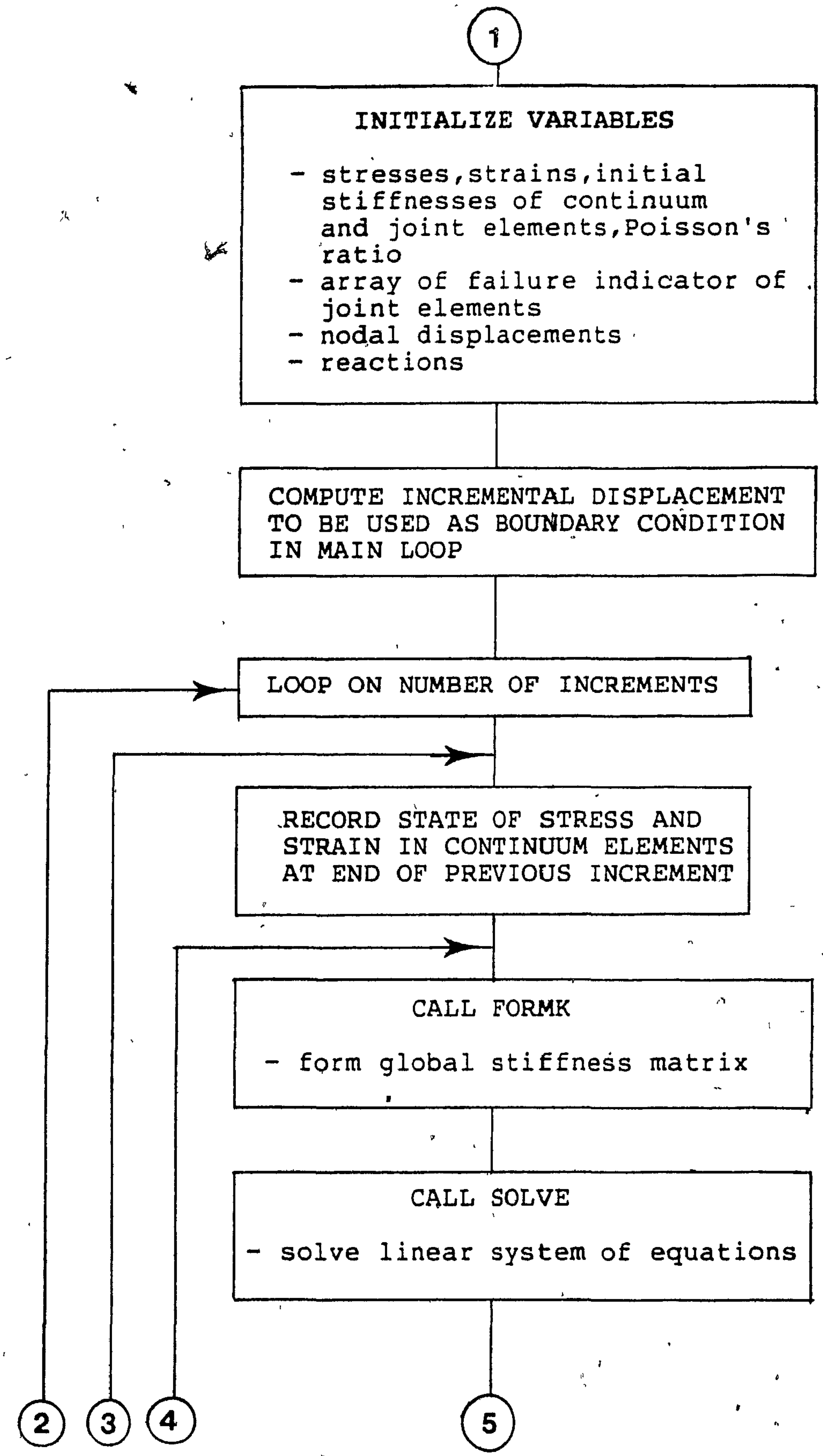
1
INITIALIZE VARIABLES
- stresses,strains,initial stiffnesses of continuum and joint elements,Poisson's ratio
- array of failure indicator of joint elements
- nodal displacements
- reactions
COMPUTE INCREMENTAL DISPLACEMENT TO BE USED AS BOUNDARY CONDITION IN MAIN LOOP
LOOP ON NUMBER OF INCREMENTS
RECORD STATE OF STRESS AND STRAIN IN CONTINUUM ELEMENTS AT END OF PREVIOUS INCREMENT
CALL FORMK
- form global stiffness matrix
CALL SOLVE
- solve linear system of equations
2
3
4
5

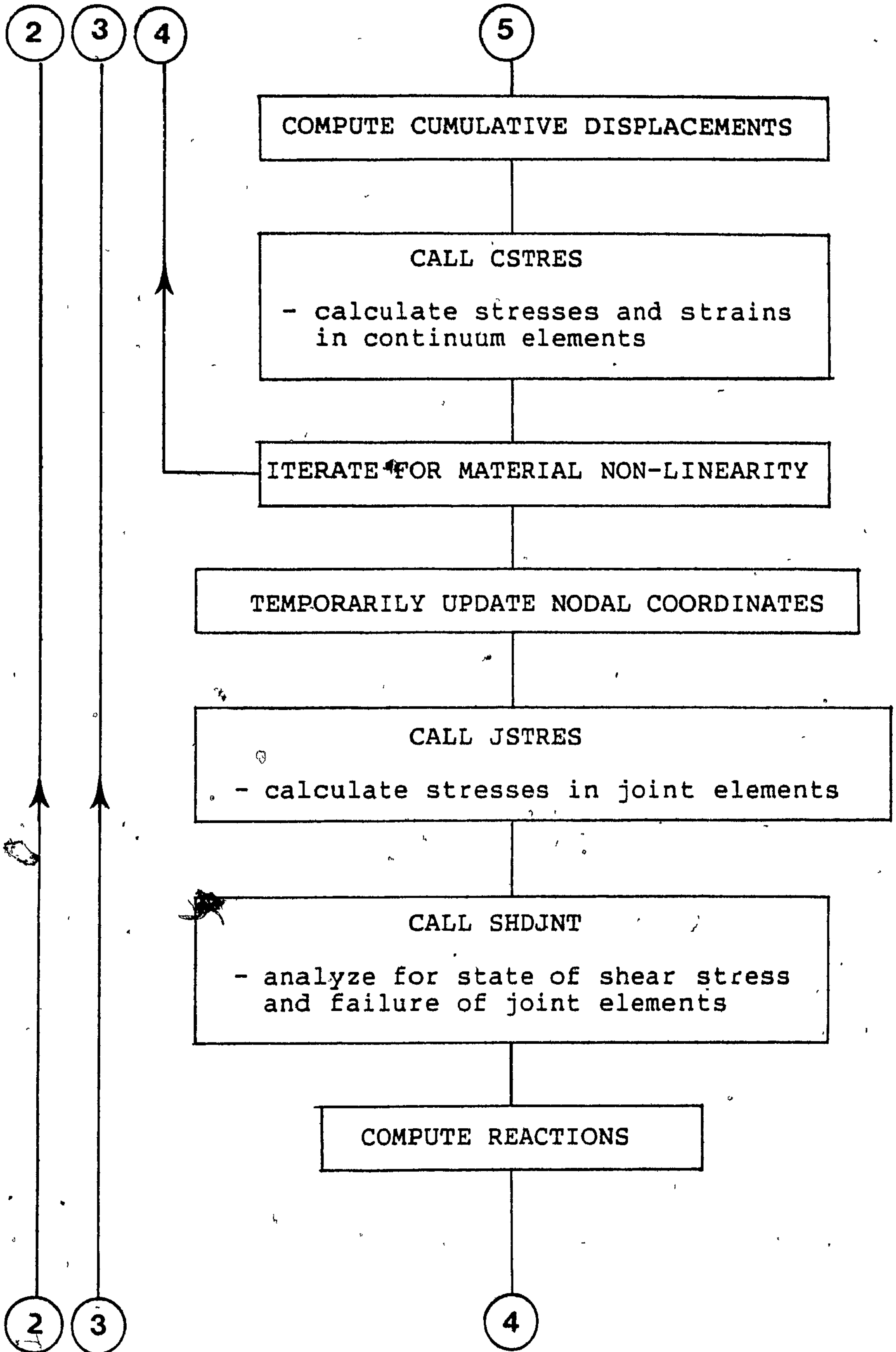
2
3
4
5
COMPUTE CUMULATIVE DISPLACEMENTS
CALL CSTRES
- calculate stresses and strains in continuum elements
ITERATE FOR MATERIAL NON-LINEARITY
TEMPORARILY UPDATE NODAL COORDINATES
CALL JSTRES
- calculate stresses in joint elements
CALL SHDJNT
- analyze for state of shear stress and failure of joint elements
COMPUTE REACTIONS
2
3
4

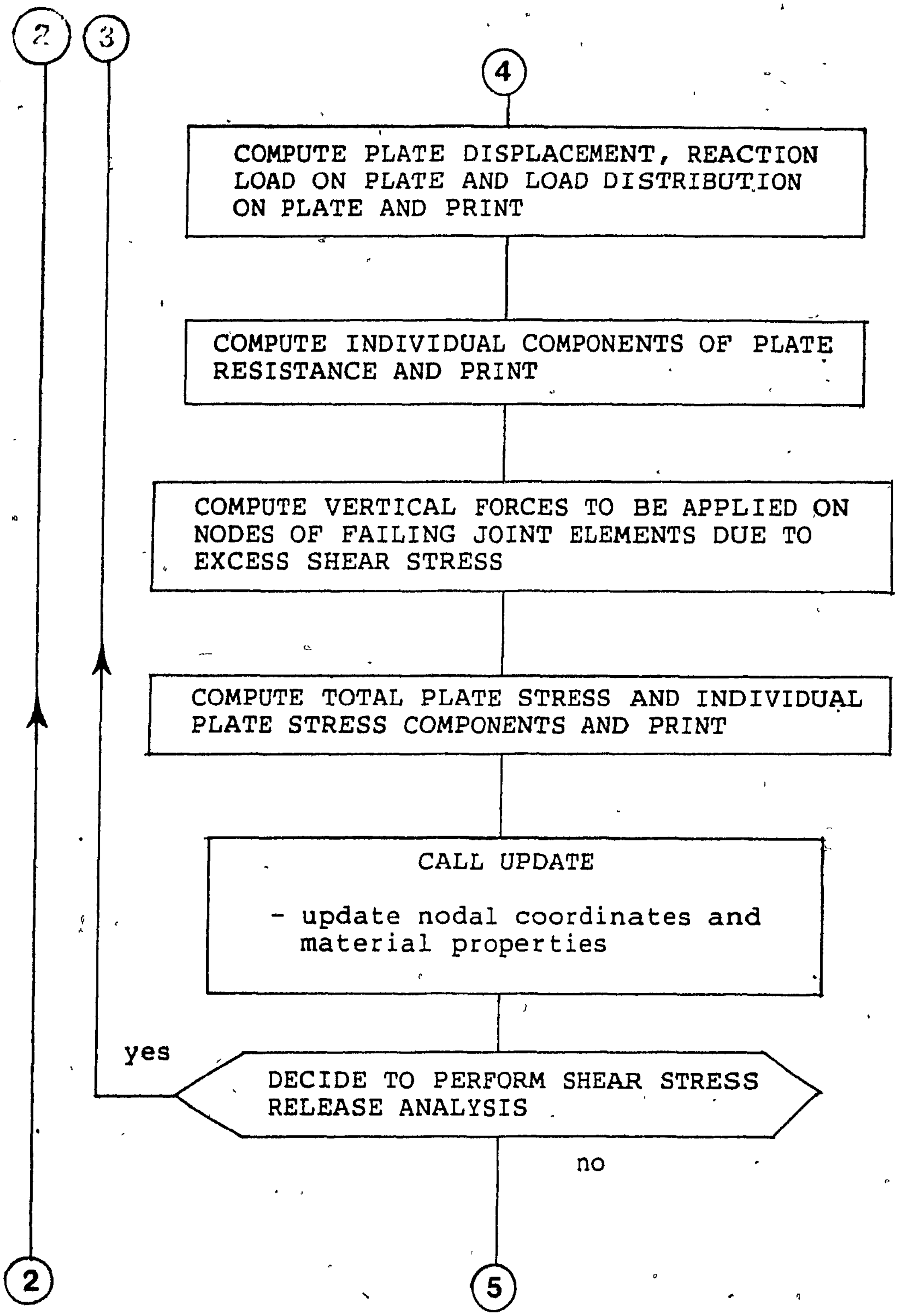
2
3
4
COMPUTE PLATE DISPLACEMENT, REACTION LOAD ON PLATE AND LOAD DISTRIBUTION ON PLATE AND PRINT
COMPUTE INDIVIDUAL COMPONENTS OF PLATE RESISTANCE AND PRINT
COMPUTE VERTICAL FORCES TO BE APPLIED ON NODES OF FAILING JOINT ELEMENTS DUE TO EXCESS SHEAR STRESS
COMPUTE TOTAL PLATE STRESS AND INDIVIDUAL PLATE STRESS COMPONENTS AND PRINT
CALL UPDATE
- update nodal coordinates and material properties
yes
DECIDE TO PERFORM SHEAR STRESS RELEASE ANALYSIS
no
2
5

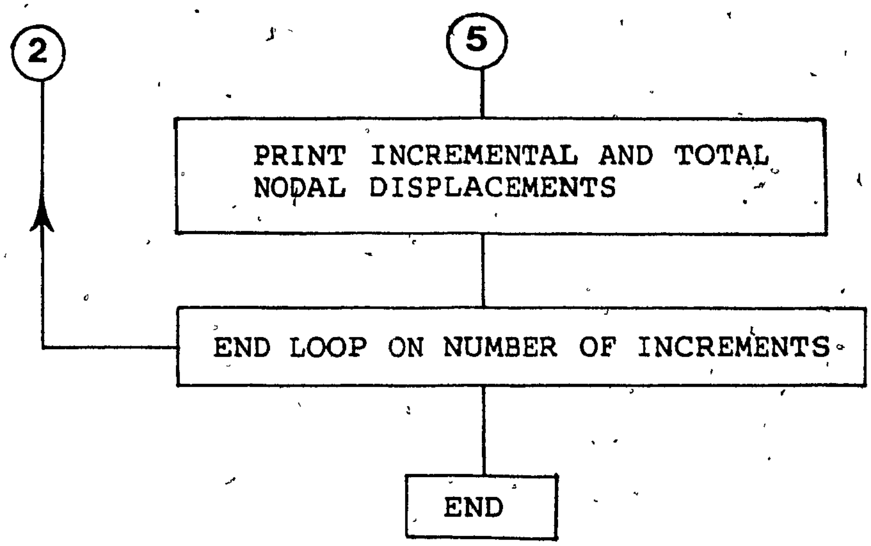
2
5
PRINT INCREMENTAL AND TOTAL NODAL DISPLACEMENTS
END LOOP ON NUMBER OF INCREMENTS
END

2.2 Subroutine INMESH

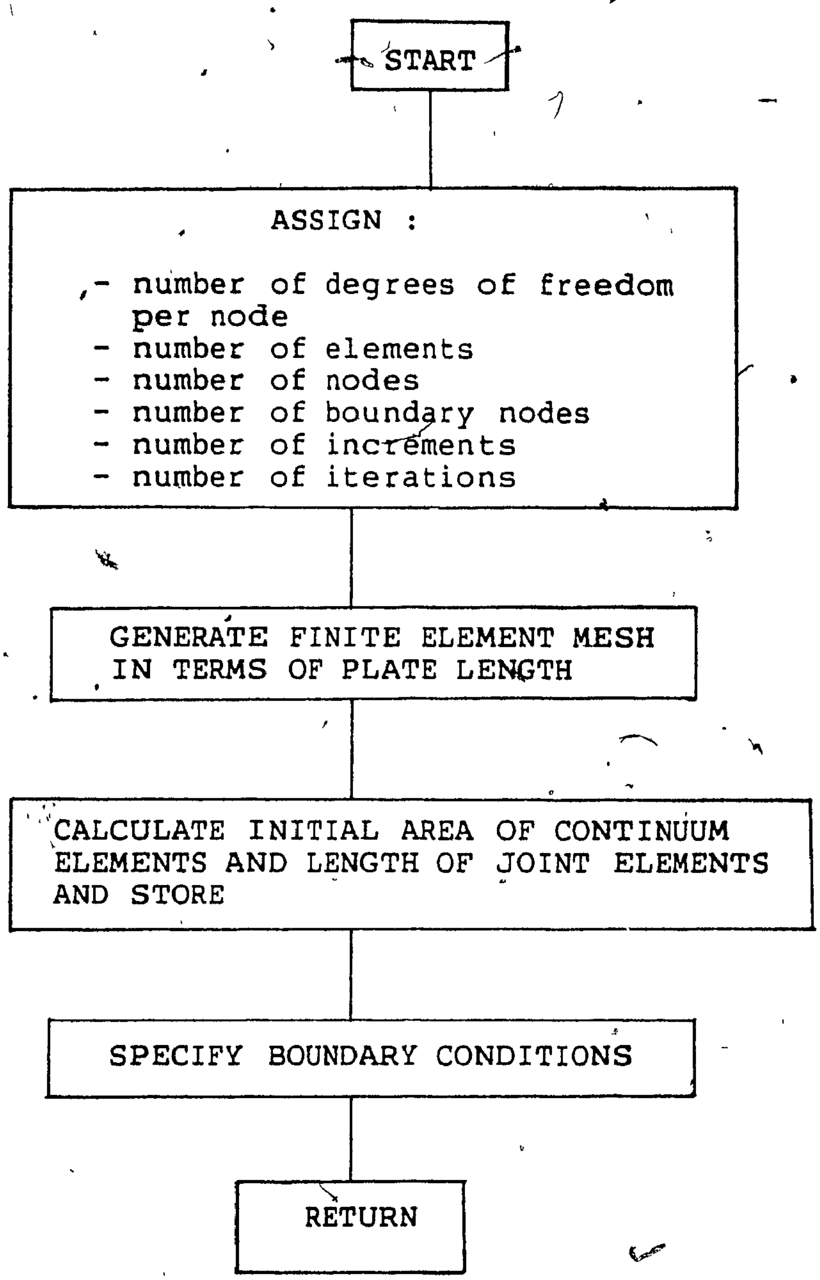

2.3 Subroutine SNMAPR

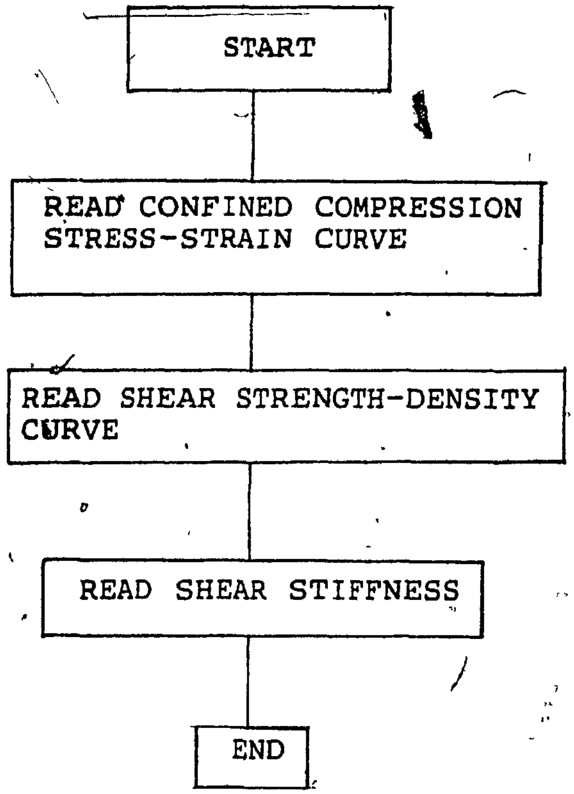

2.4 Subroutine FORMK

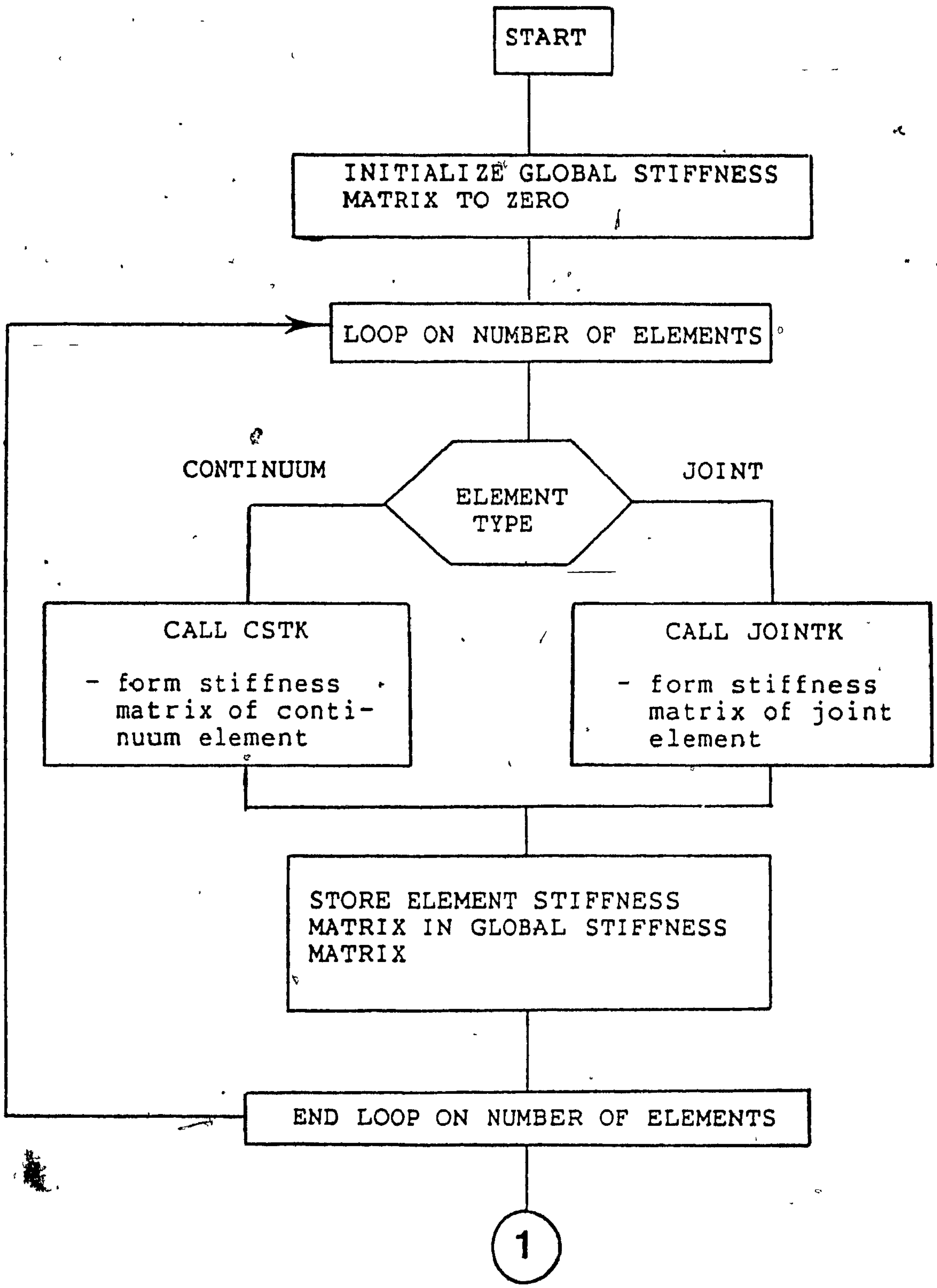

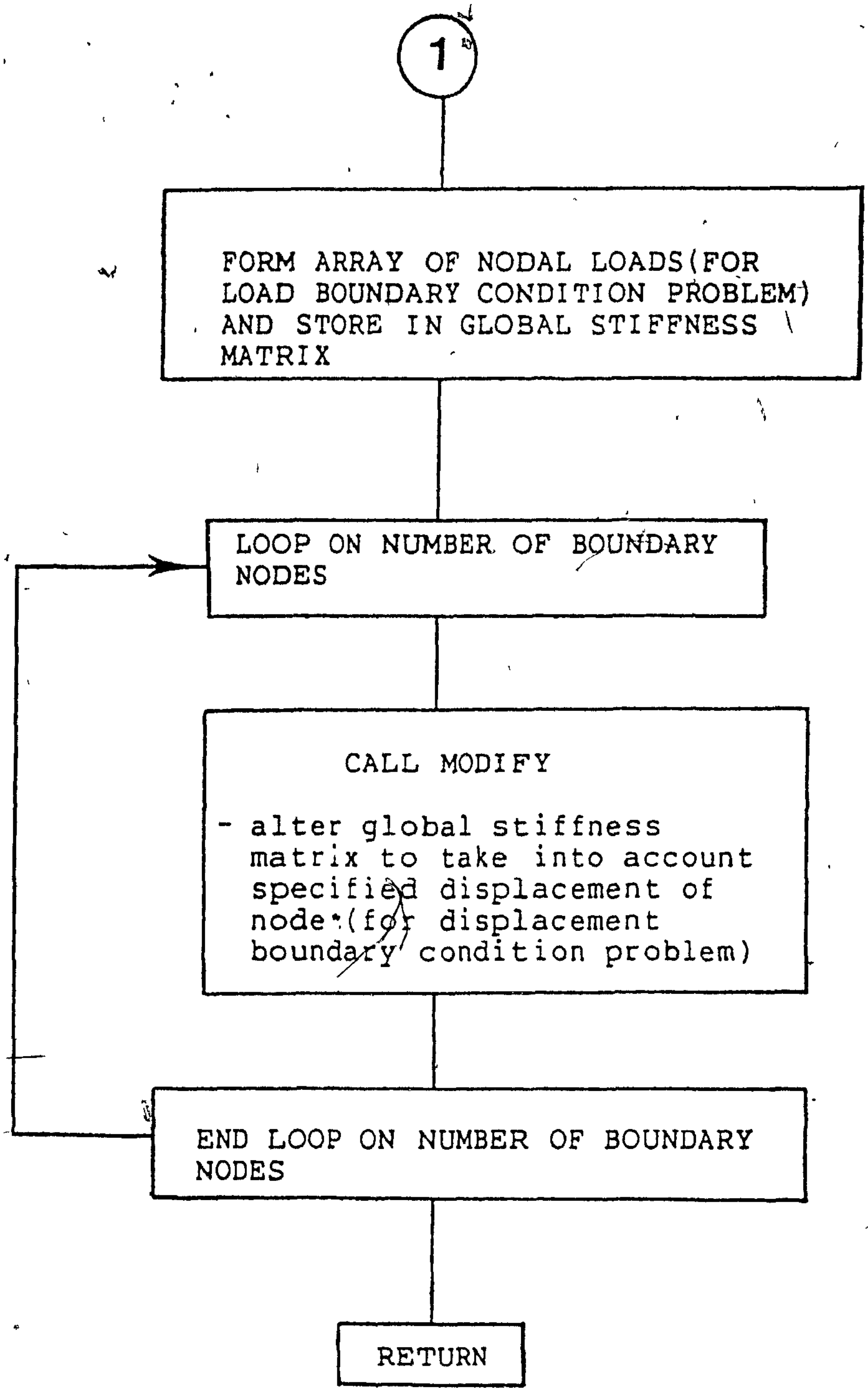
1
FORM ARRAY OF NODAL LOADS(FOR LOAD BOUNDARY CONDITION PROBLEM) AND STORE IN GLOBAL STIFFNESS MATRIX
LOOP ON NUMBER OF BOUNDARY NODES
CALL MODIFY
- alter global stiffness matrix to take into account specified displacement of node (for displacement boundary condition problem)
END LOOP ON NUMBER OF BOUNDARY NODES
RETURN

2.5 Subroutine CSTK

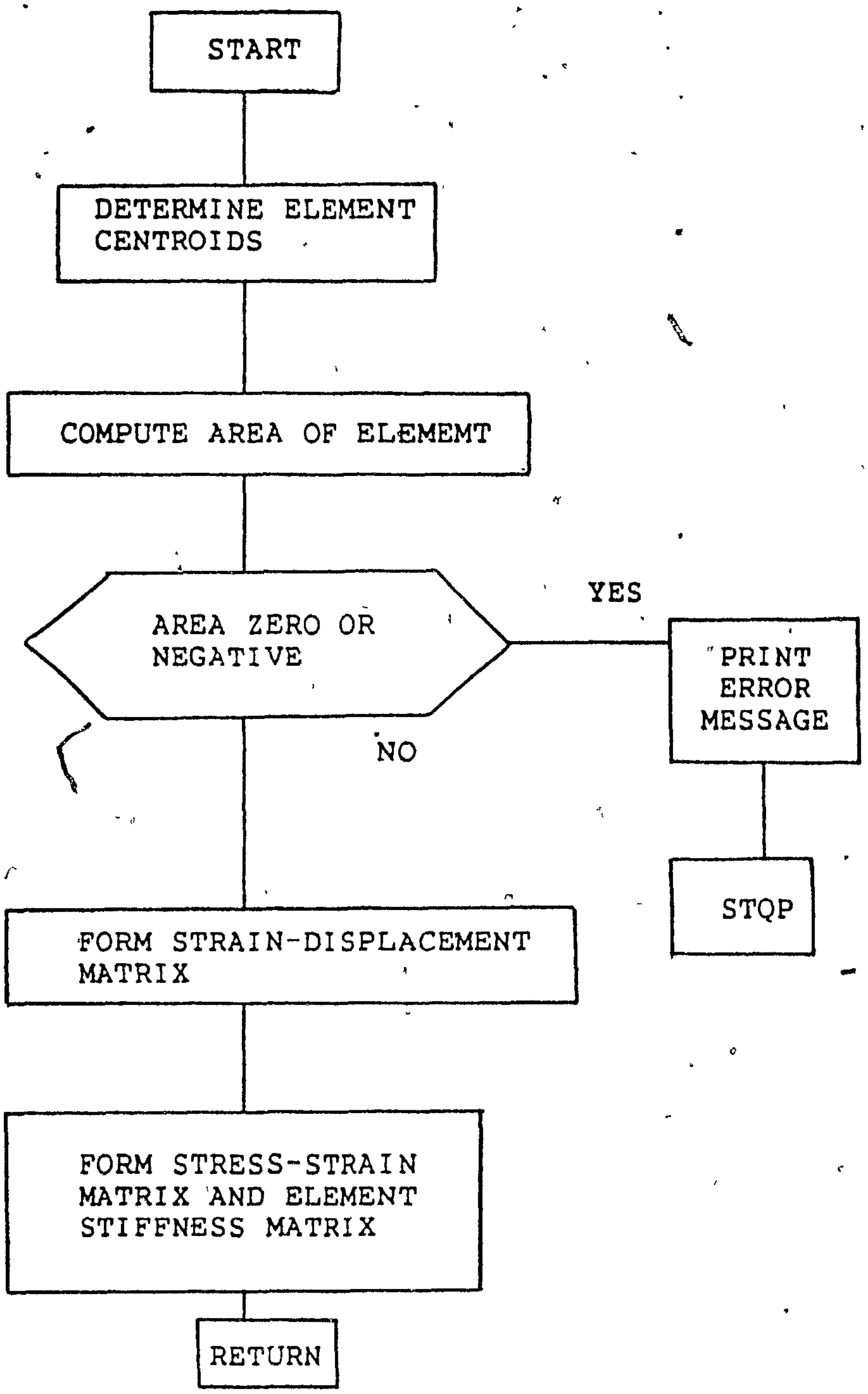

2.6 Subroutine JOINTK

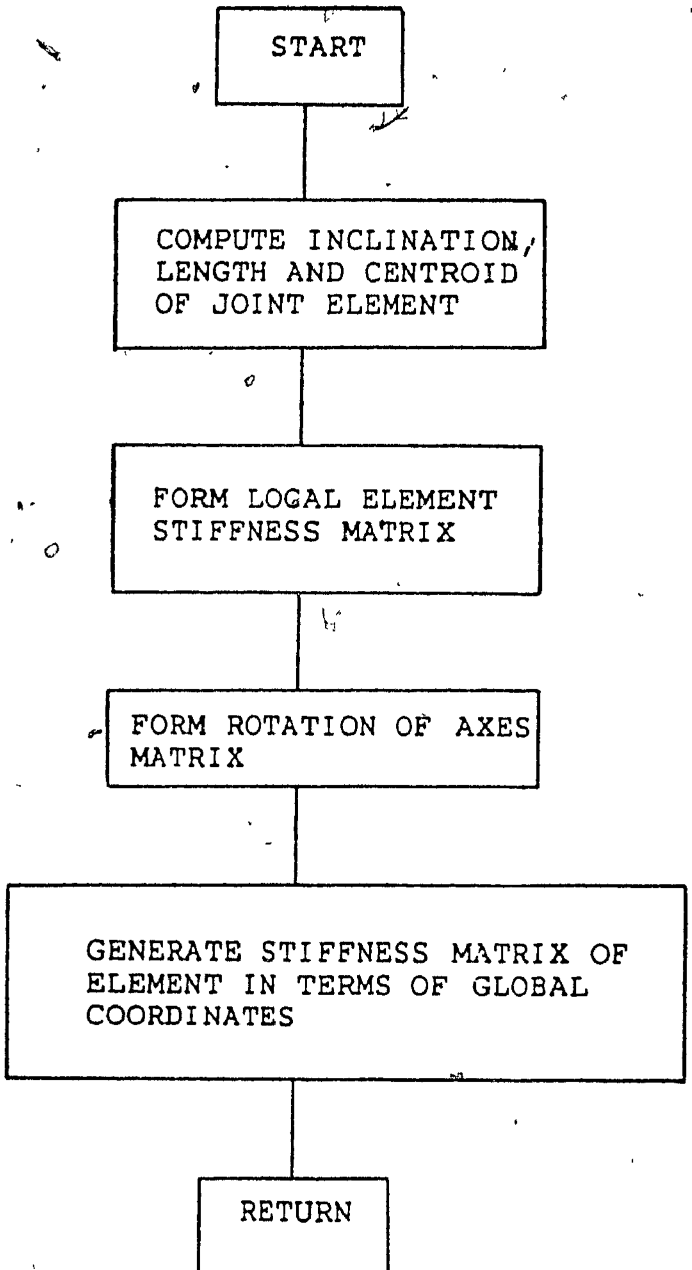

2.7 Subroutine MODIFY

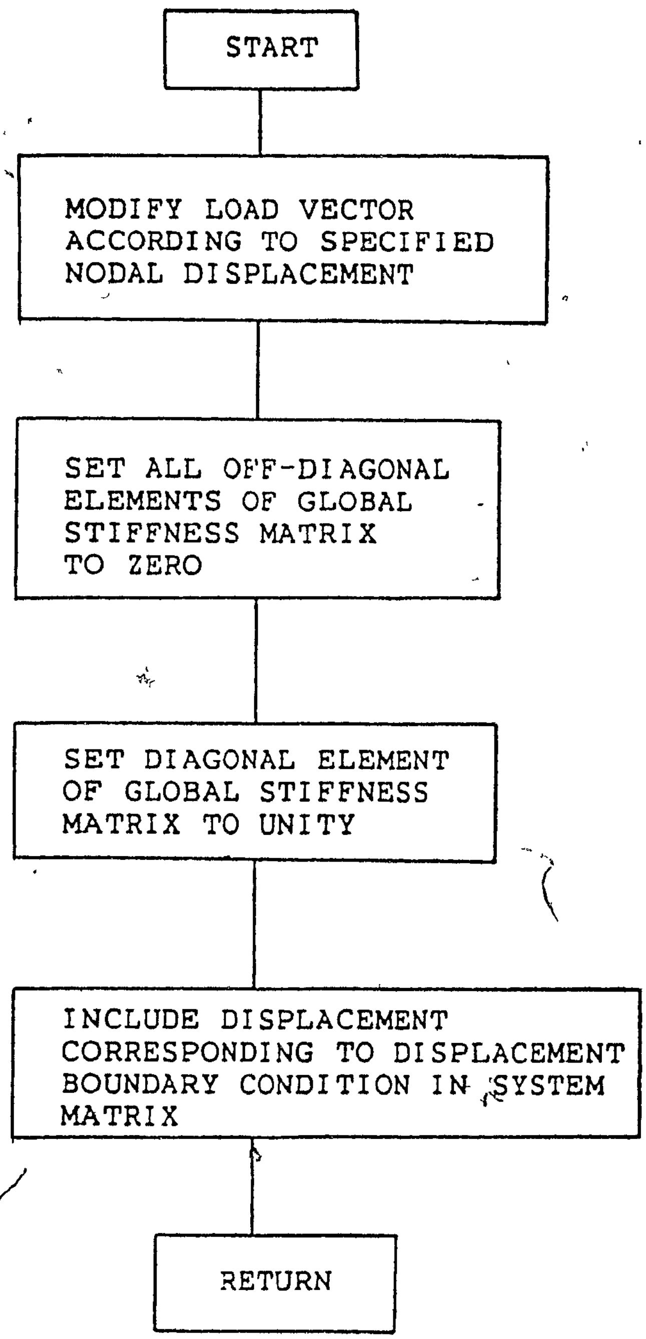

2.8 Subroutine SOLVE

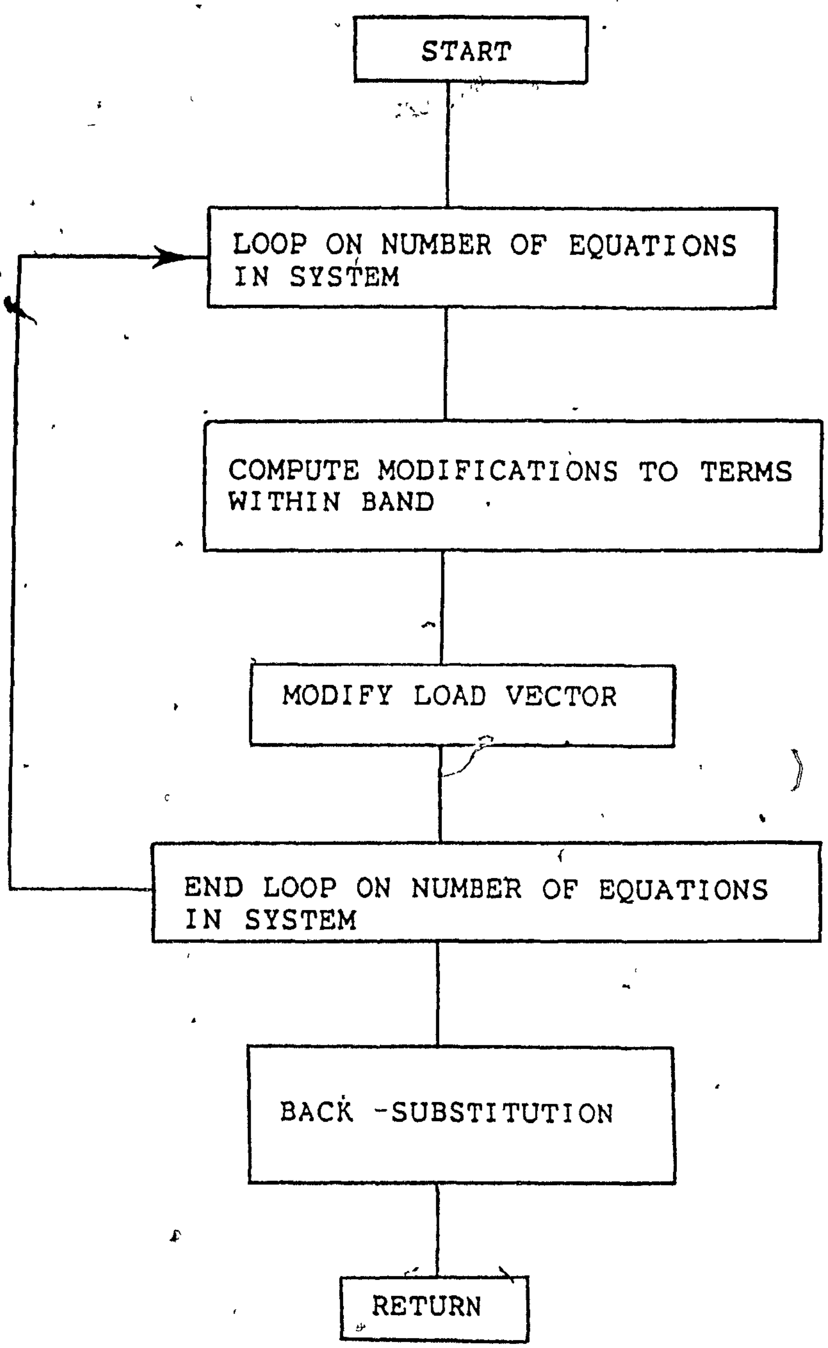

2.9 Subroutine CSTRES

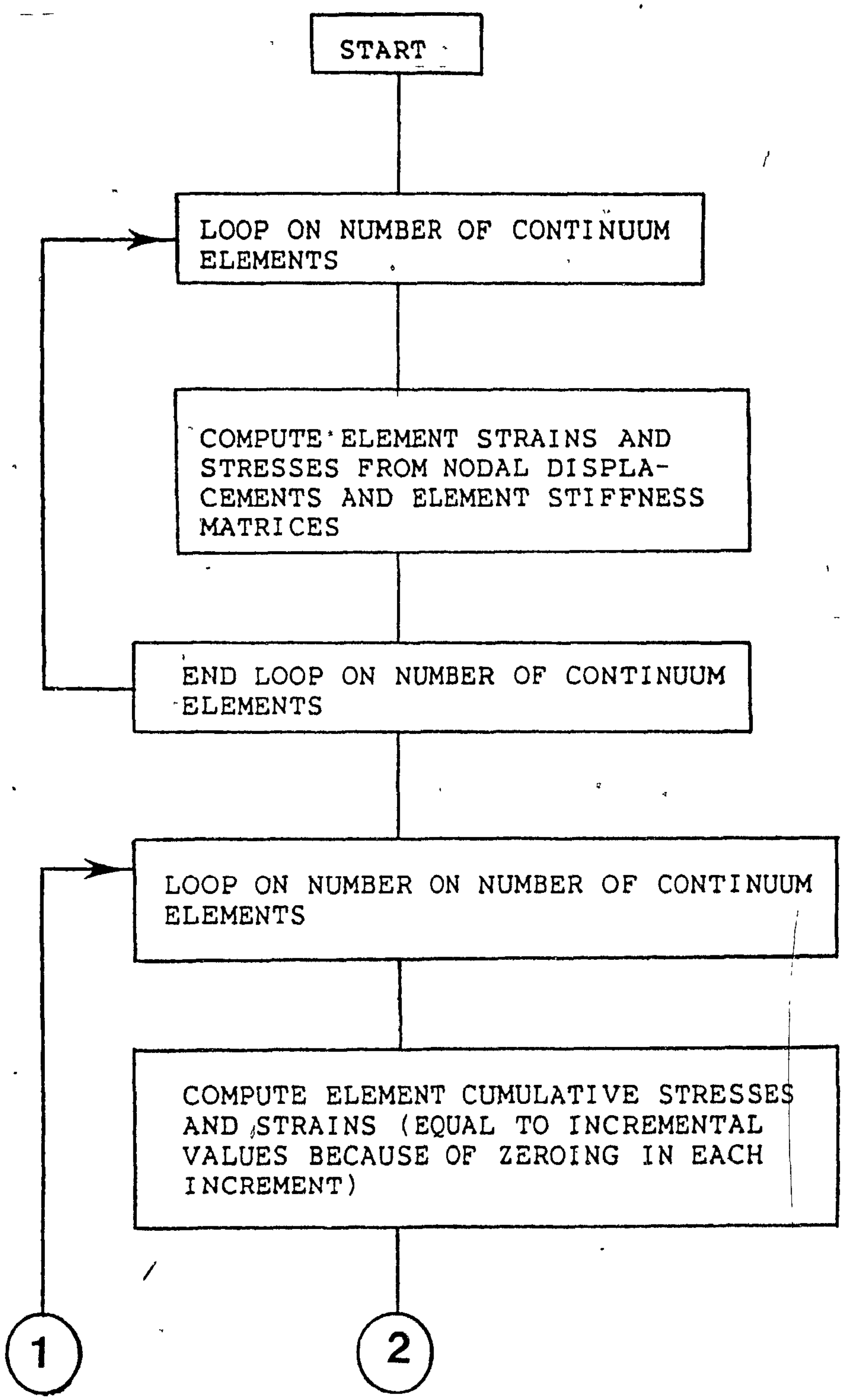

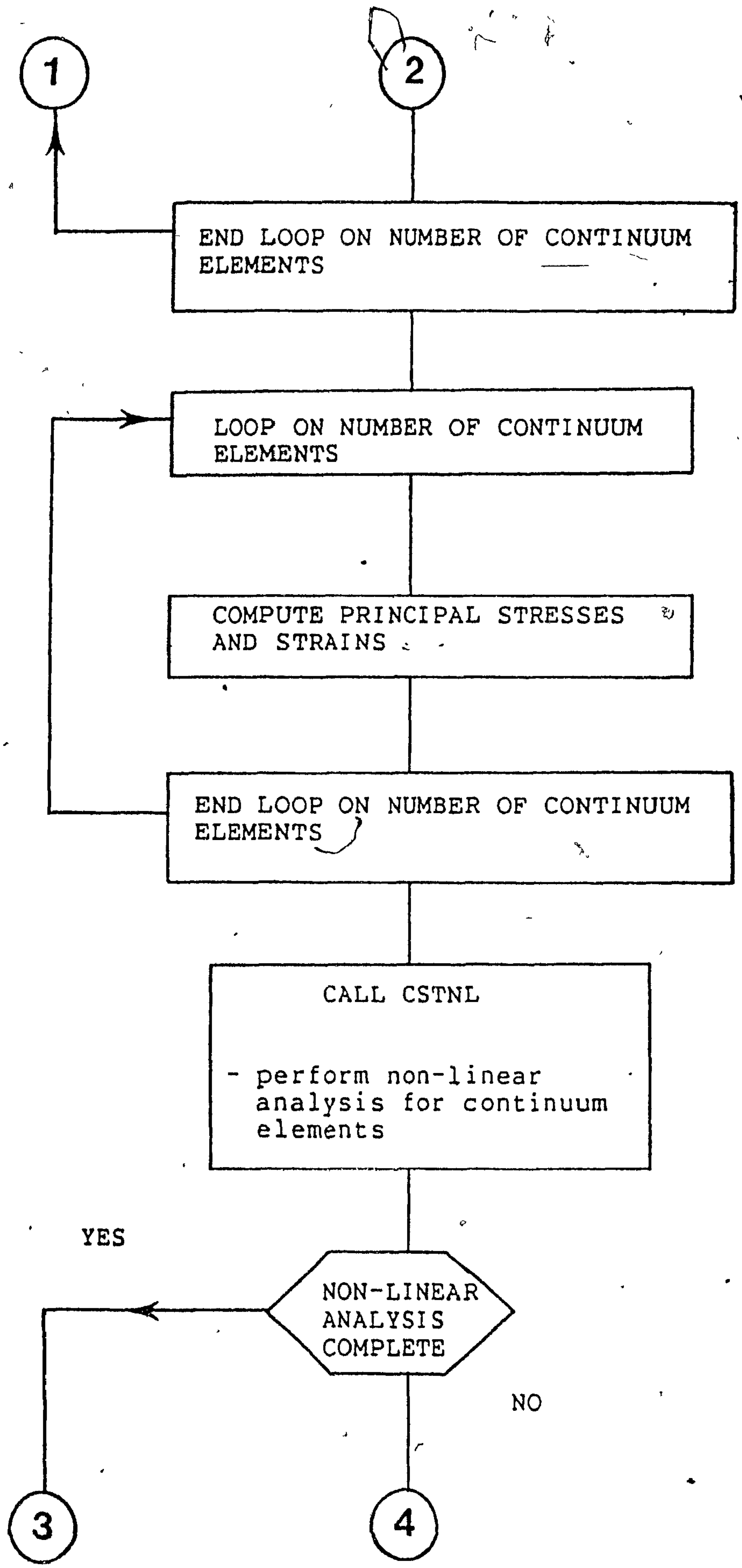
1
2
END LOOP ON NUMBER OF CONTINUUM ELEMENTS
LOOP ON NUMBER OF CONTINUUM ELEMENTS
COMPUTE PRINCIPAL STRESSES AND STRAINS
END LOOP ON NUMBER OF CONTINUUM ELEMENTS
CALL CSTNL
- perform non-linear analysis for continuum elements
YES
NON-LINEAR ANALYSIS COMPLETE
NO
3
4

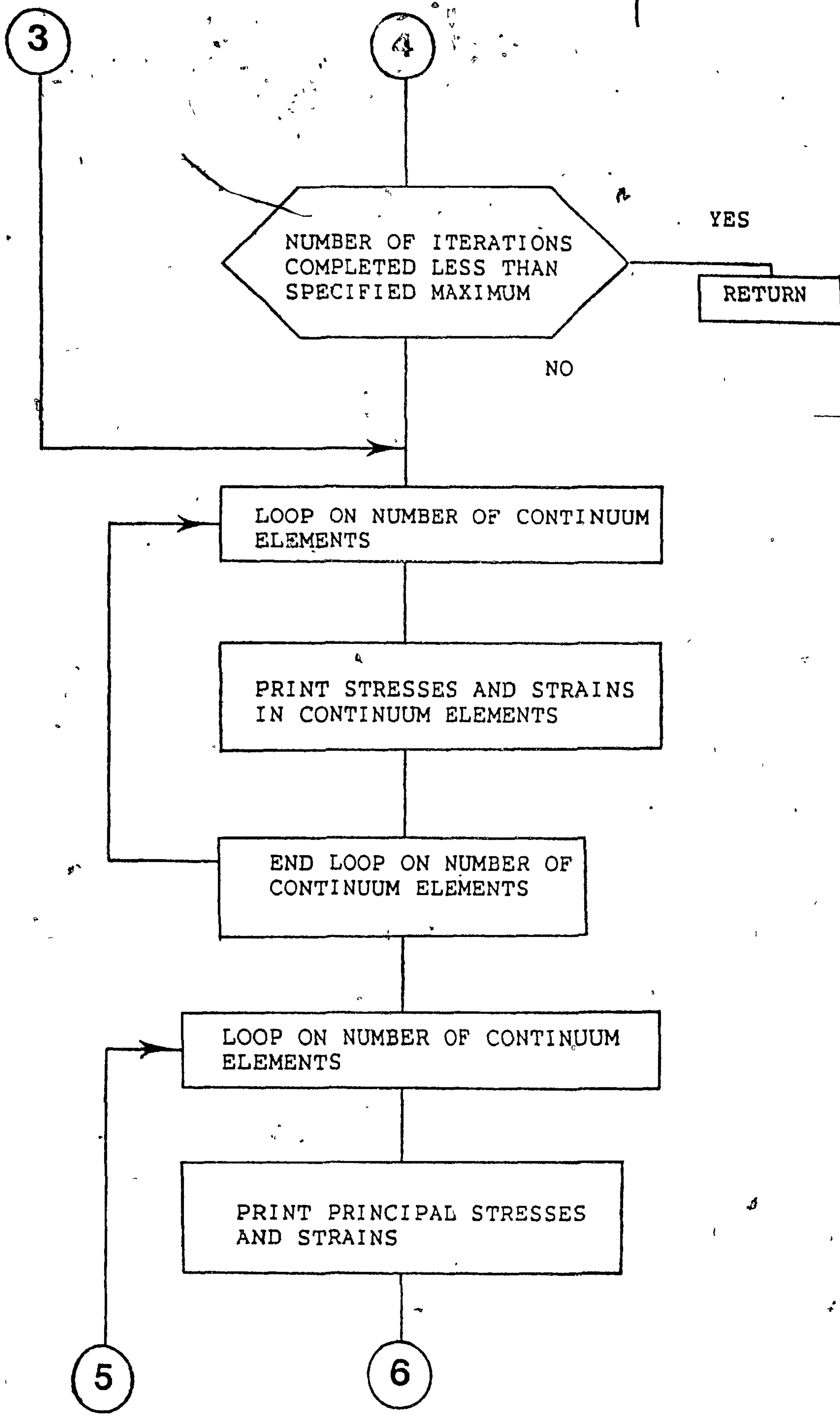
3
4
NUMBER OF ITERATIONS COMPLETED LESS THAN SPECIFIED MAXIMUM
YES
RETURN
NO
LOOP ON NUMBER OF CONTINUUM ELEMENTS
PRINT STRESSES AND STRAINS IN CONTINUUM ELEMENTS
END LOOP ON NUMBER OF CONTINUUM ELEMENTS
LOOP ON NUMBER OF CONTINUUM ELEMENTS
PRINT PRINCIPAL STRESSES AND STRAINS
5
6

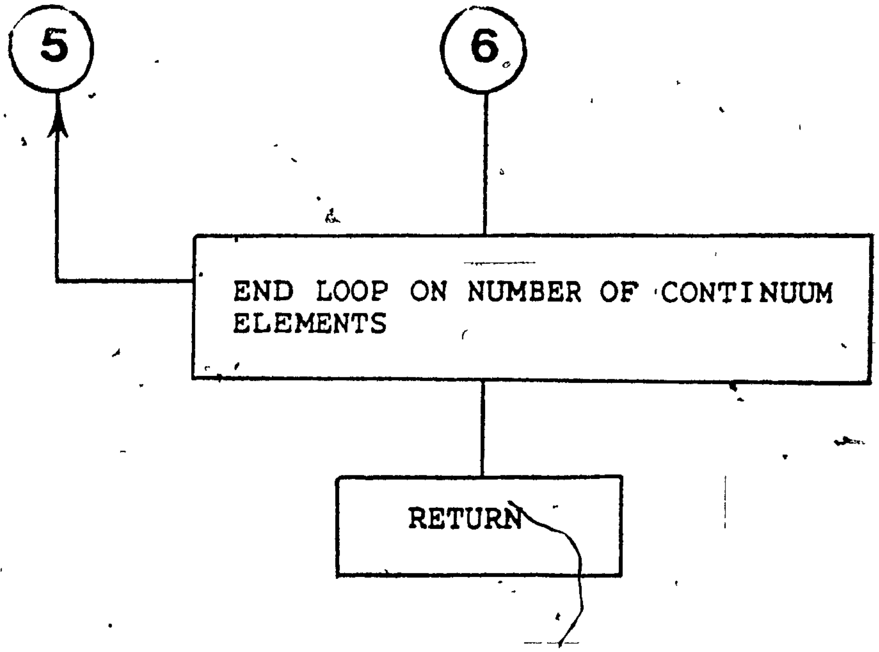
5
6
END LOOP ON NUMBER OF CONTINUUM ELEMENTS
RETURN

2.10 Subroutine CSTNL

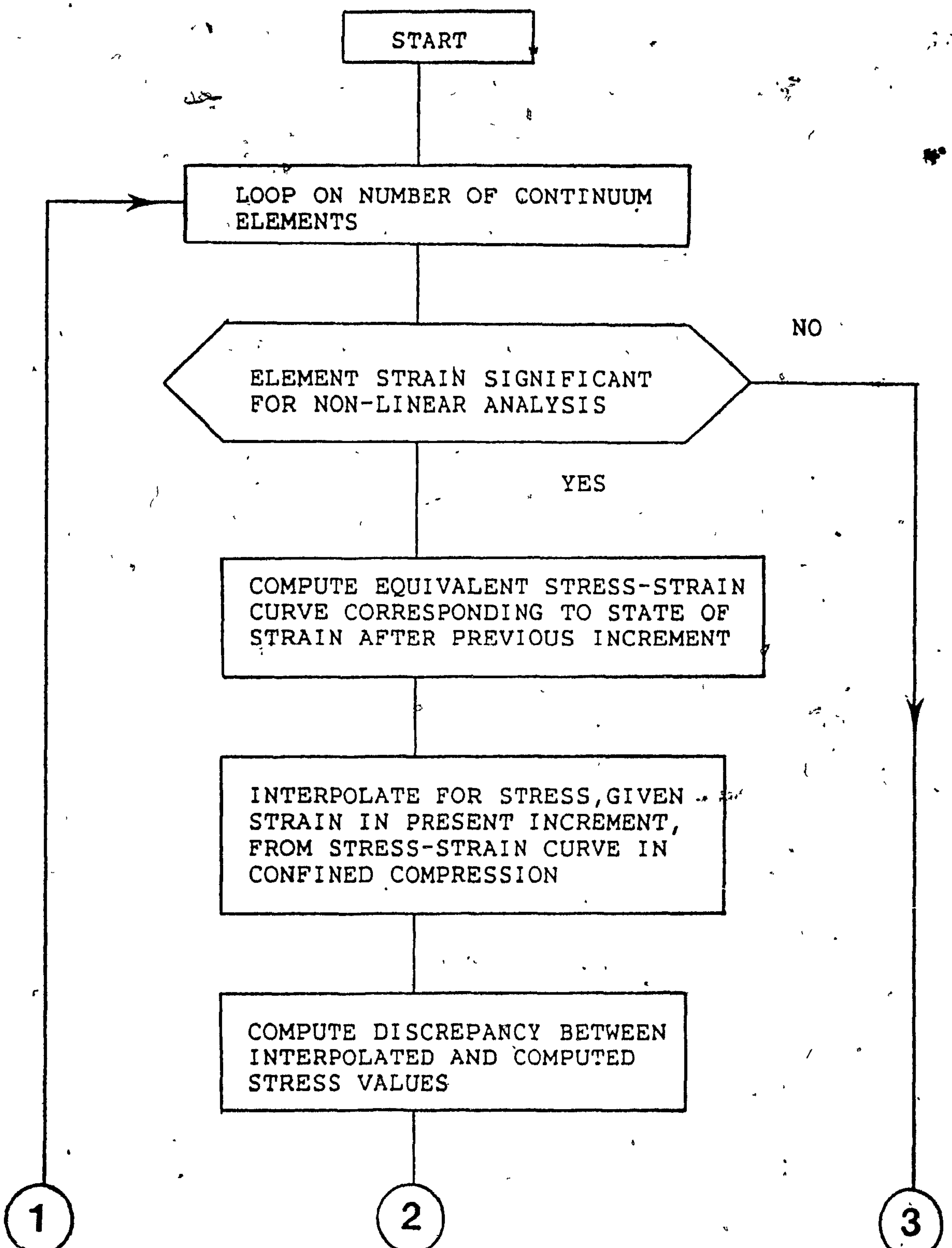

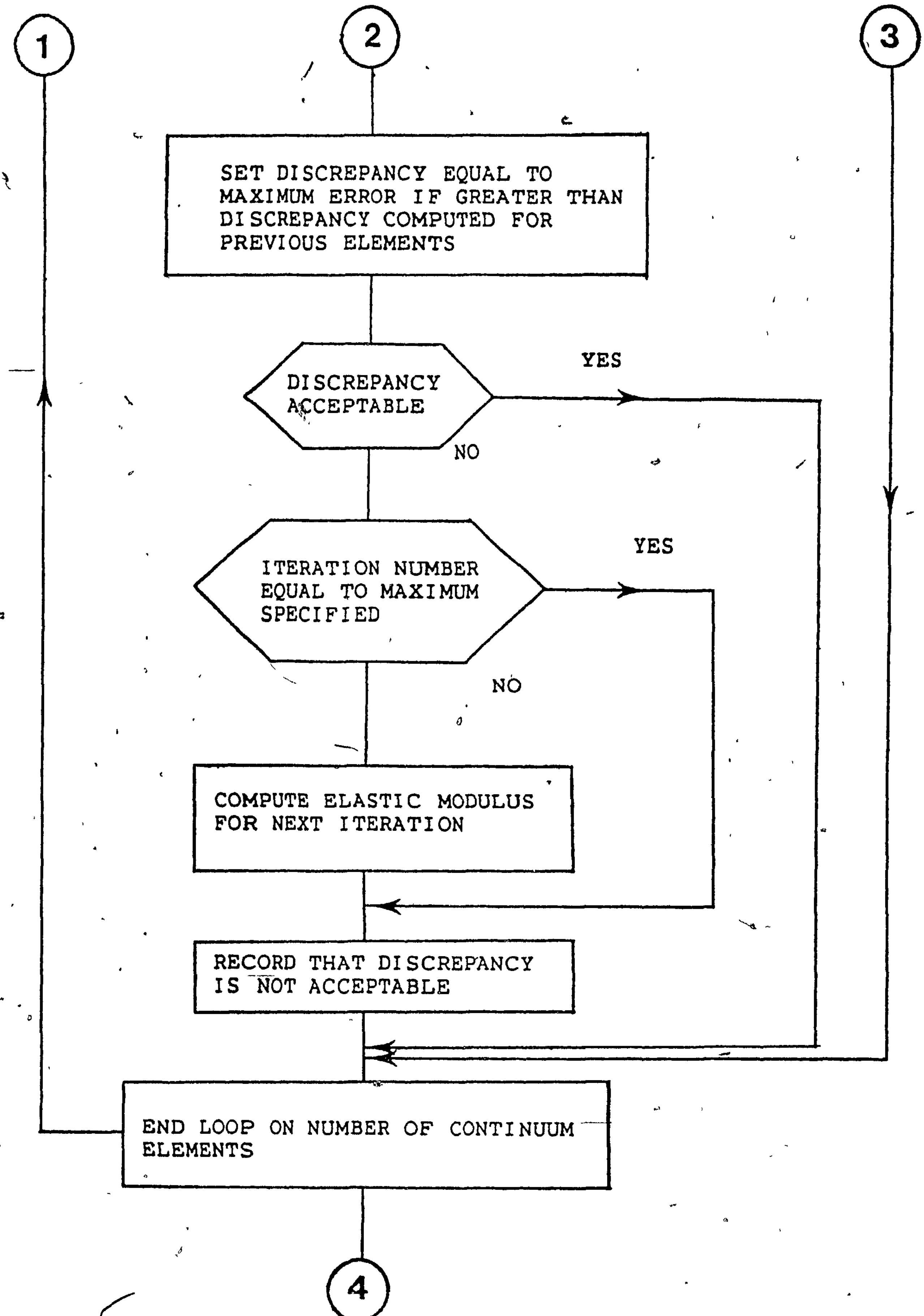
1
2
3
SET DISCREPANCY EQUAL TO MAXIMUM ERROR IF GREATER THAN DISCREPANCY COMPUTED FOR PREVIOUS ELEMENTS
DISCREPANCY ACCEPTABLE
YES
NO
ITERATION NUMBER EQUAL TO MAXIMUM SPECIFIED
YES
NO
COMPUTE ELASTIC MODULUS FOR NEXT ITERATION
RECORD THAT DISCREPANCY IS NOT ACCEPTABLE
END LOOP ON NUMBER OF CONTINUUM ELEMENTS
4

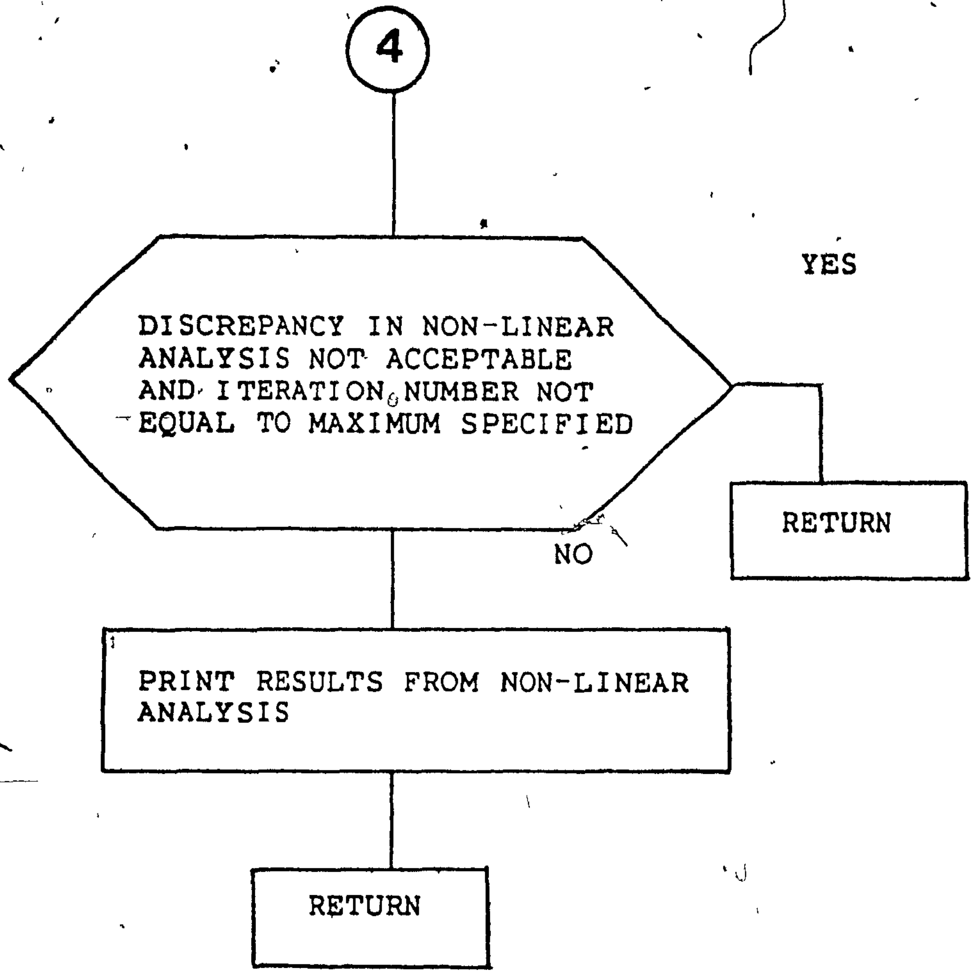
4
DISCREPANCY IN NON-LINEAR ANALYSIS NOT ACCEPTABLE AND ITERATION NUMBER NOT EQUAL TO MAXIMUM SPECIFIED
YES
RETURN
NO
PRINT RESULTS FROM NON-LINEAR ANALYSIS
RETURN

2.11 Subroutine SHDJNT

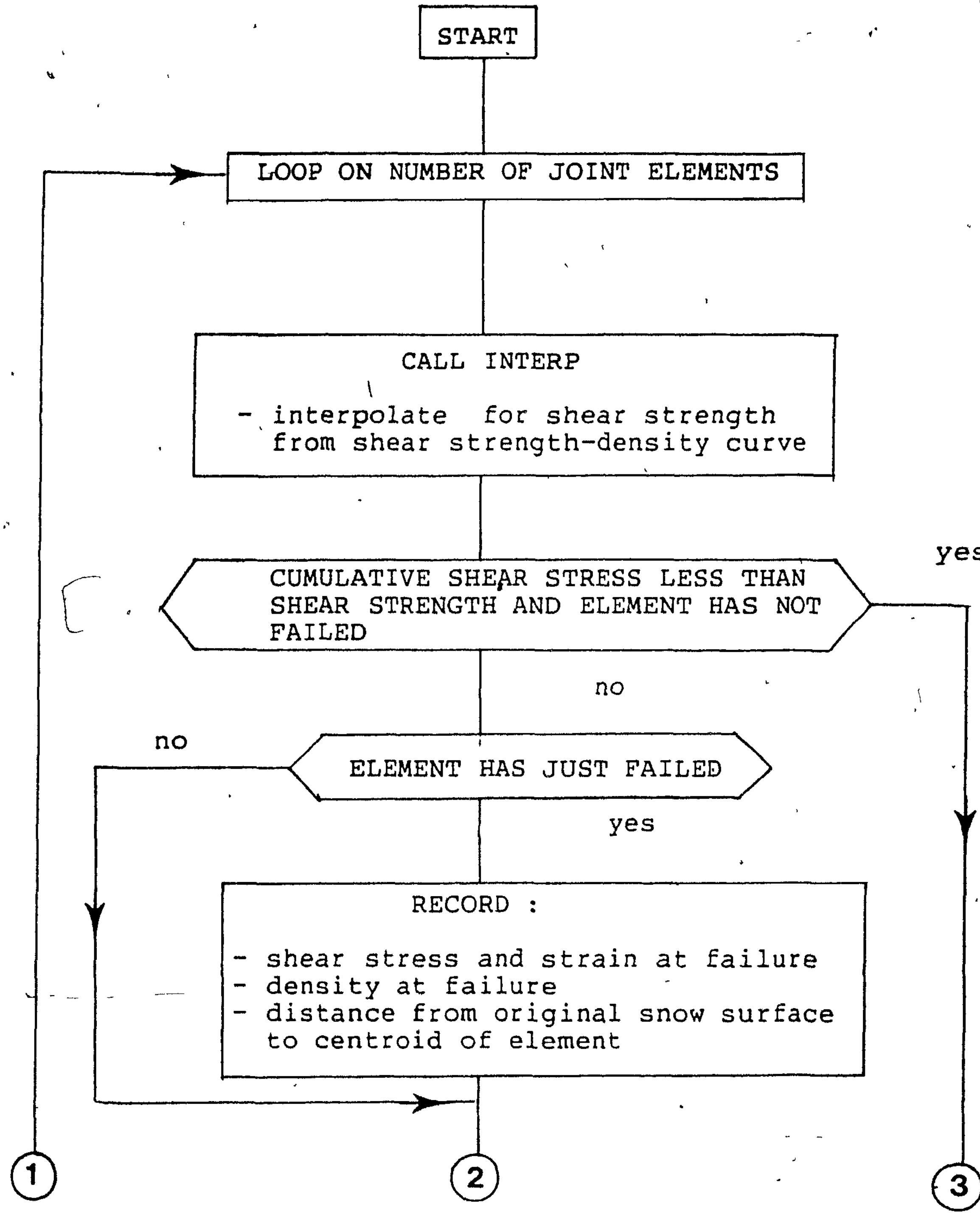

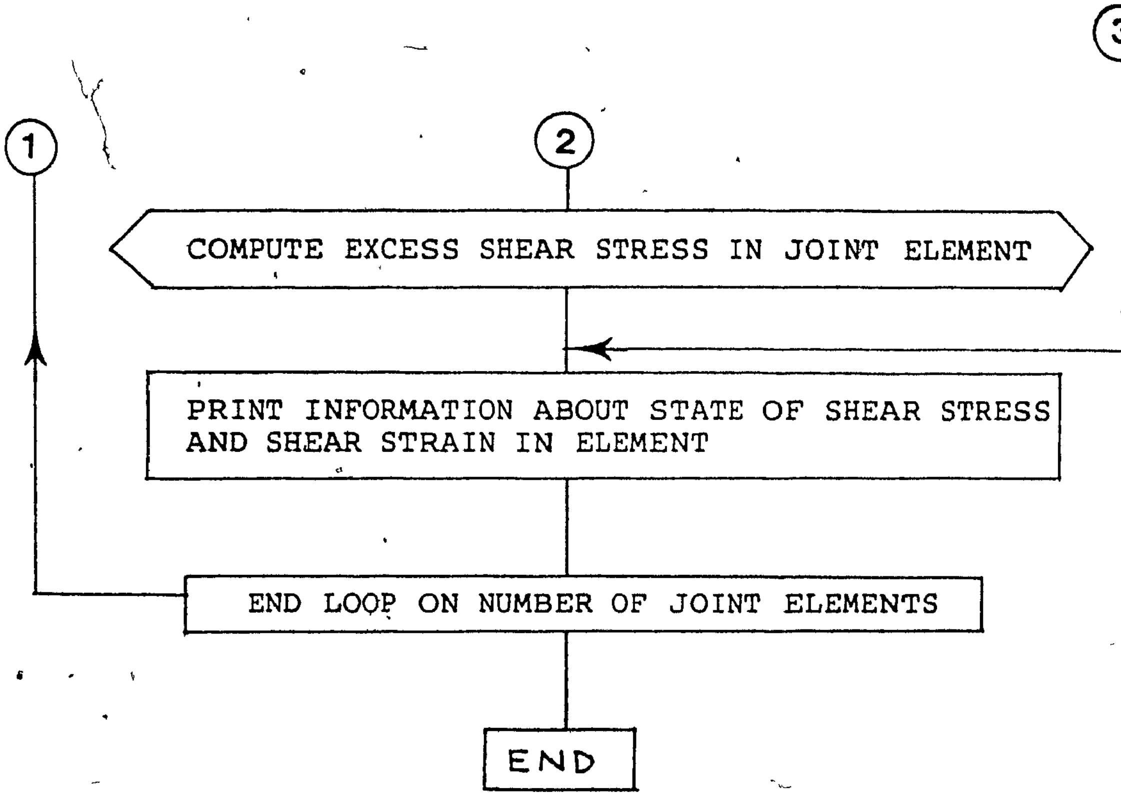
1
2
3
COMPUTE EXCESS SHEAR STRESS IN JOINT ELEMENT
PRINT INFORMATION ABOUT STATE OF SHEAR STRESS AND SHEAR STRAIN IN ELEMENT
END LOOP ON NUMBER OF JOINT ELEMENTS
END

2.12 Subroutine REAC

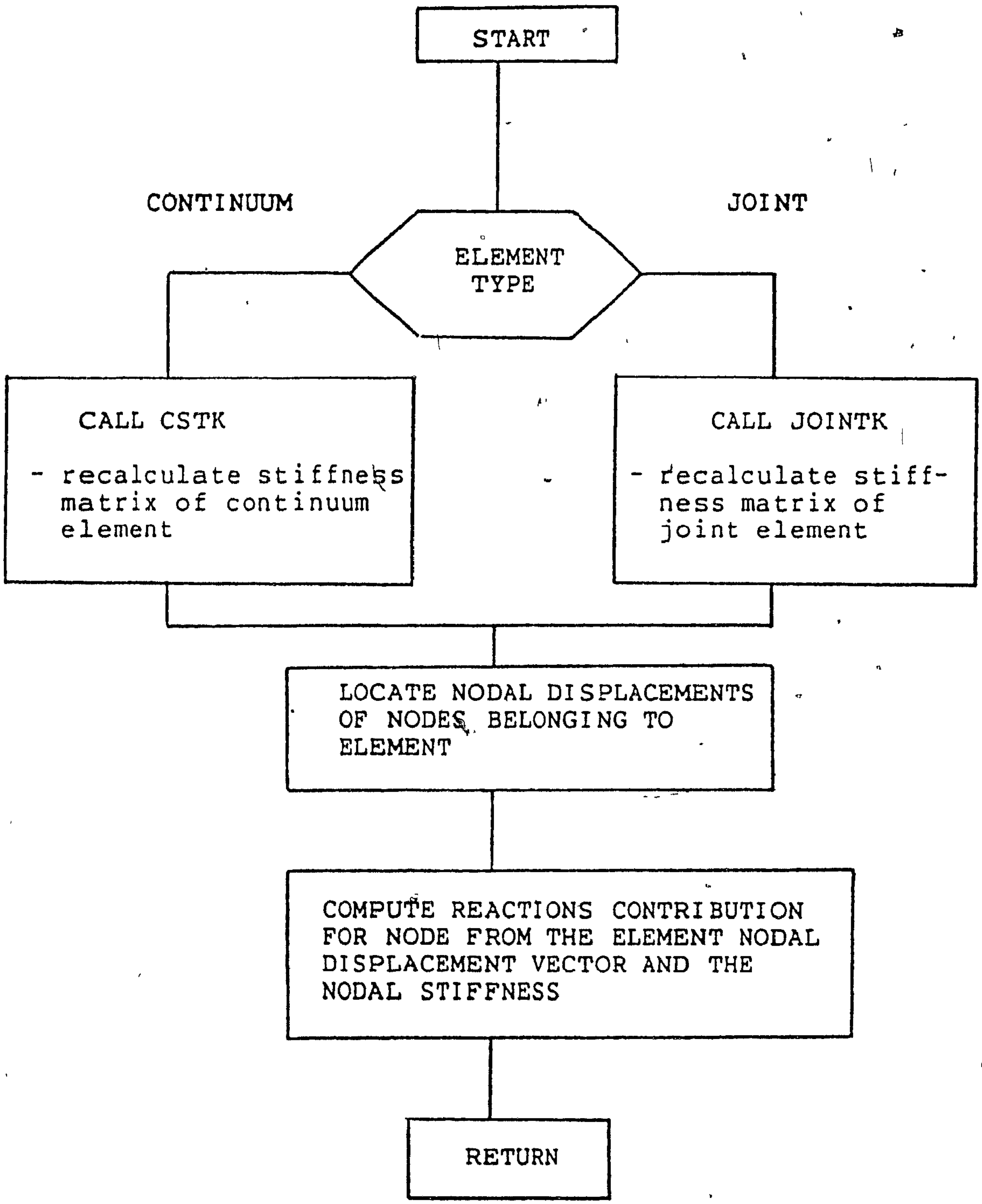

2.13 Subroutine DENSIT

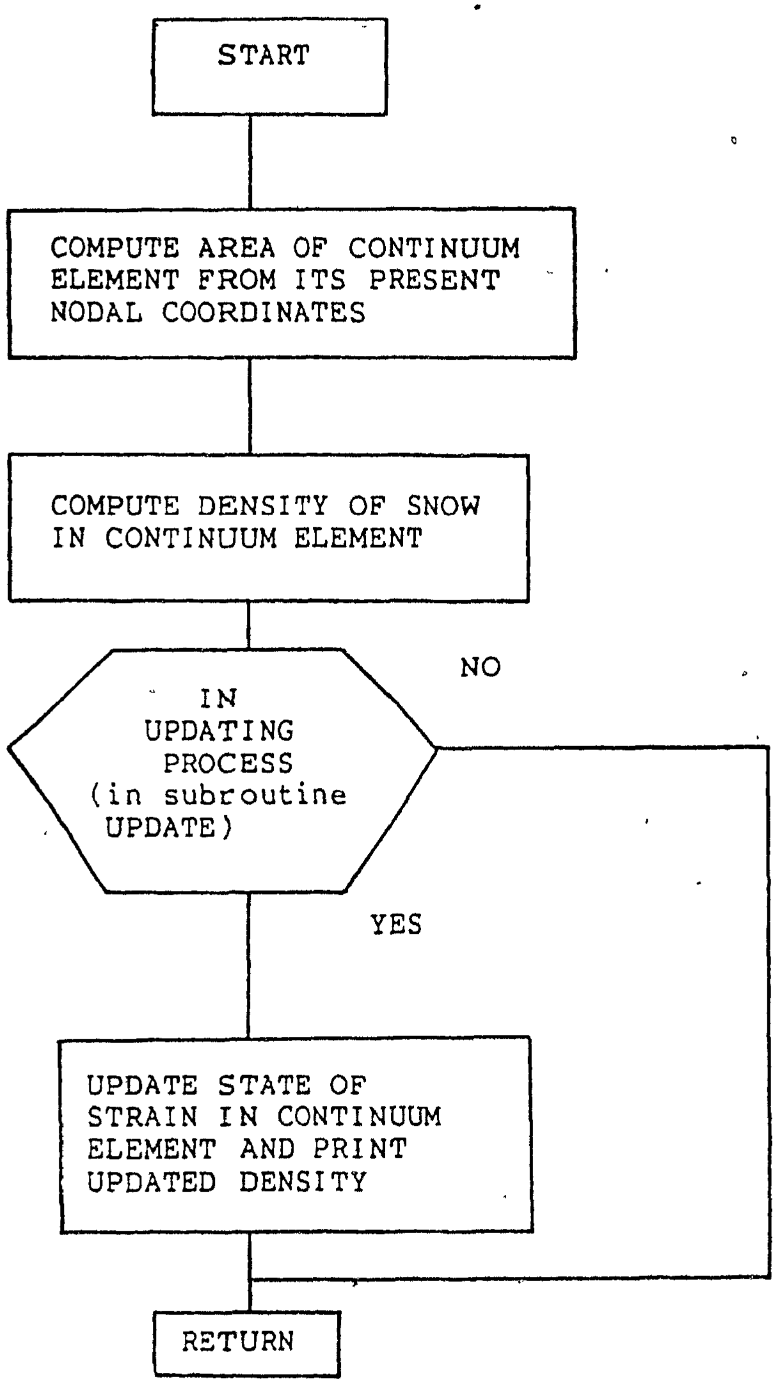

2.14 Subroutine UPDATE

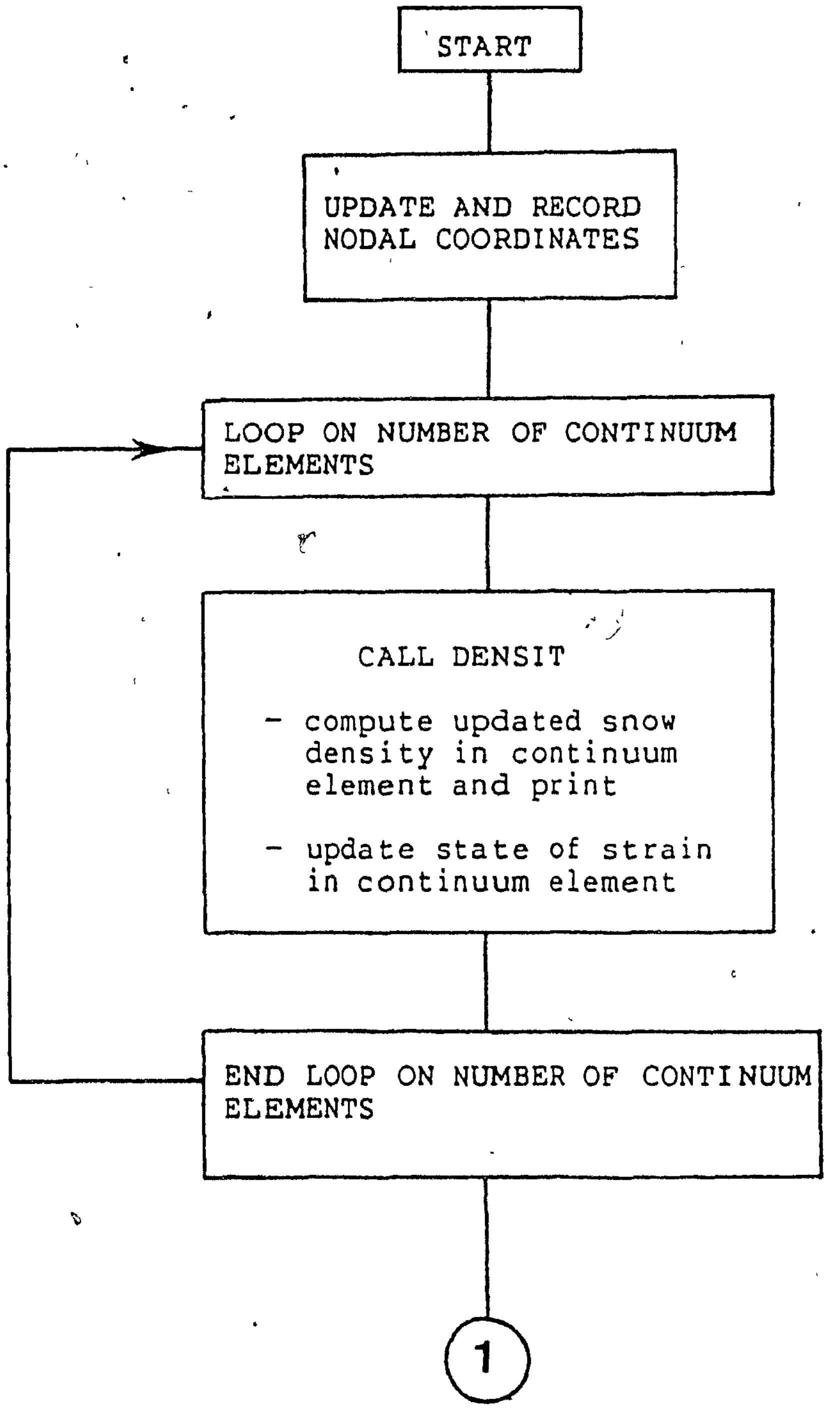

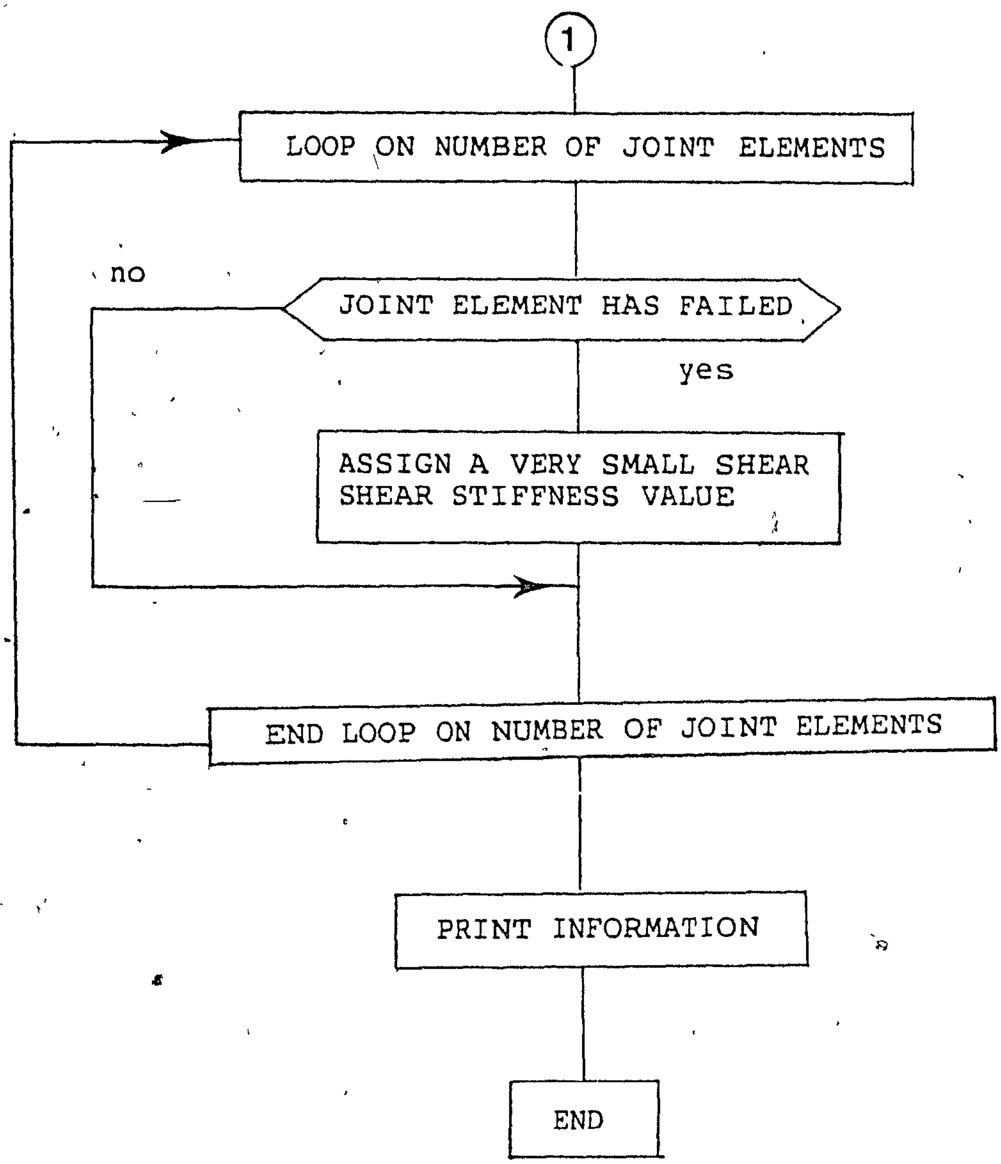
1
LOOP ON NUMBER OF JOINT ELEMENTS
no
JOINT ELEMENT HAS FAILED
yes
ASSIGN A VERY SMALL SHEAR
SHEAR STIFFNESS VALUE
END LOOP ON NUMBER OF JOINT ELEMENTS
PRINT INFORMATION
END

2.15 Subroutine INTERP

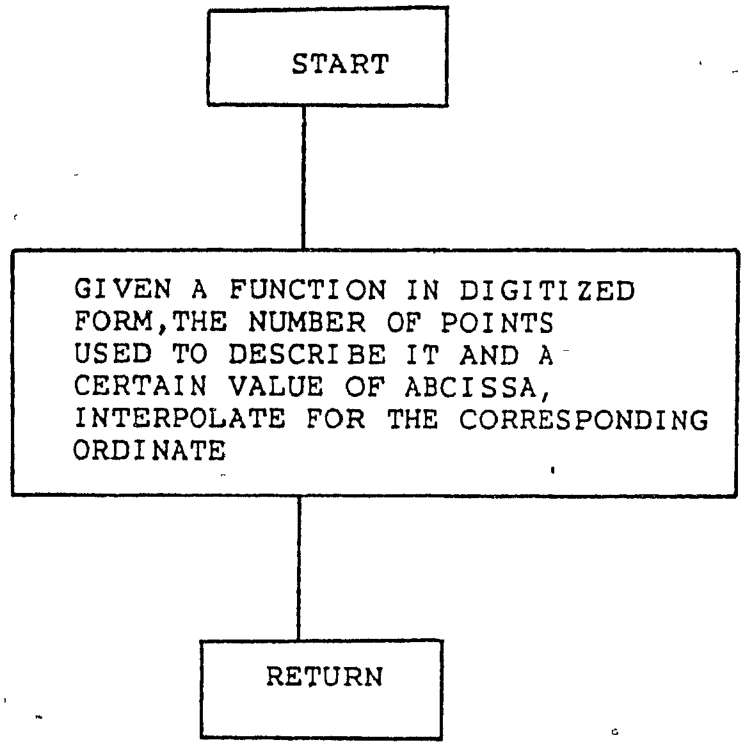

APPENDIX C

PROGRAM INPUT DATA

The input data to the finite element program developed during the course of this study is described below. All input is in S.I. units and must be entered using free format:

LINE 1 : Number of increments for which detailed output information
is provided

LINE 2 : Array containing numbers of increments for which detailed
information is provided

LINE 3 : Plate length (m) and width (m)

LINE 4 : Initial density of snow (Mg/m3)

LINE 5 : Number of points describing compressibility of the snow,
i.e, stress-strain curve from a confined compression test

LINE 6 TO line (6+NC-1) : Stress (kPa) and strain values (in order)
corresponding to a given point on the
above described compressibility curve.
(NC=number of points describing the curve).

LINE (6+NC) : Number of points describing the shear strength-density
curve obtained from vane shear tests

LINE (6+NC+1) to LINE (6+NC+NS) : Shear strength (kPa) and
Density (Mg/m3) values corresponding
to a given point on the above curve.
(NS=number of points on the curve)

LINE (6+NC+NS+1) : Shear stiffness parameter Ks (kN/m3)

APPENDIX D

PROGRAM OUTPUT

The output information produced by the program developed is summarized in the following lines:

a) dimensions of rigid plate

b) finite element mesh specifications

- horizontal and vertical coordinates of the nodes
- triangular and joint element connection array (i.e, nodes pertaining to each element)
- boundary conditions assigned to the mesh :
  - type of nodal restriction (numerical code)
  - horizontal displacement or force on node
  - vertical displacement or force on node

(Note: finite element mesh specifications are an output of the program due to that the mesh is generated inside the program)

c) input snow properties :

- compressibility curve
- shear strength-density curve
- shear stiffness paramater

d) finite element results: For each increment (plate displacement or excess shear stress analysis):

- number of performed iterations in non-linear analysis
- shear depth to plate sinkage ratio
- load distribution on plate
- density at failure for joint elements and corresponding distance from original snow surface (detailed information)
- results of stress analysis of joint elements (detailed information)
- plate load, stress and penetration coordinates and distribution of various components of plate resistance
- density distribution within snow mass (detailed information)
- incremental and cumulative nodal displacements

```
C                            S N O W   M O D E L
C                            -------------------
C
C                                ( THESIS )
C
C
C
C
C                              MAIN PROGRAM
C
C
      COMMON/CONTR/NP,NE,NB,NDF,NCN,NSZF,ITITL(50),IPRIN,SFLAG,FPL,DELPL
C
      COMMON/DATA/CORD(580,2),NOP(999,4),IMAT(1100),NBC(580),CODE(700),
     +UX(700),UY(700),T(1100),ORX(1100),ORY(1100),PRCORD(580,2)
C
      COMMON/STIFF/ESTIFM(12,12),A(3,6),B(3,6),SK(1100,92),AREA(1100),
     +C(1100),R(8),H(8),D(1100),AR(2000),AS(999,3,6),BS(999,3,6),NBAND
C
      COMMON/ANAL/NOINC,KOUNT,NITER,NOITER,CORDI(580,2)
C
      COMMON/STRES/DISTO(2,580),SIGTO(999,4),STRTO(999,3),SMAXTO(1100),
     +SMINTO(1100),ANGTO(1100),EANGTO(1100),EMAXTO(1100),EMINTO(1100),
     +FORCE(999,4),STR(999,3),PSIGTO(999,4),PSTRTO(999,3),PDISTO(2,580),
     +PEMINT(1100),PSMINT(1100),EXSH(1100)
C
      COMMON/JOINT/T1(8,8),BL(8,8),AL(1100),ANG(1100),DKS(1100),DKN(1000
     +),SD(2,2),W(999,2),P(999,2),V(999,2),AVP(999,2),CV(999,2),
     +CAVP(999,2),PCV(999,2),PCAVP(999,2),B1(8,8),IFAIL(1100),ALO(1100)
C
C
      COMMON/SNDATA/STRESS(40),STRAIN(40),SHEAR(40),DENSSH(40),
     +GAMMAO,NPTSCC,NPTSSH,STIFFS
      COMMON/ELAS/EE(1100),ENU(1100)
      EQUIVALENCE (DIS,C)
      DIMENSION DIS(2,580),AREAO(1100),PAREA(1100),TCORD(580,2),UYR(700)
     +,FSHSTE(1100),IAINCP(30),PLR(10)
      READ(5,*) NINCP
      READ(5,*) (IAINCP(I),I=1,NINCP)
      WRITE(6,*) (IAINCP(I),I=1,NINCP)
C ..READ AND PRINT PLATE LENGTH AND WIDTH
      READ(5,*) FPL,FPW
      WRITE(6,9) FPL,FPW
    9 FORMAT('1',///,10X,'MODEL - RIGID PLATE PENETRATION IN SNOW'/10X,3
     +9('-')/////5X,'PLATE LENGTH (M)',F15.6//5X,'PLATE WIDTH (M)',
     +F15.6)
      PREPL=0.0
      EC=0.0
      SUMPCS=0.0
      SUMPC=0.0
C
C
C  FORM FINITE ELEMENT MESH
      CALL INMESH(AREAO,YCTOP)
C
C  TOTAL NUMBER OF EQUATIONS IN SYSTEM
      NSZF=NP*NDF
C
```

```
C   DETERMINE BAND WIDTH
C   FIND LARGEST DIFFERENCE IN NODAL NUMBERS IN ANY ELEMENT
      JJ=0
      DO 350 N=1,NE
      DO 350 I=1,4
      DO 360 L=1,4
      KK=IABS(NOP(N,I)-NOP(N,L))
      IF(KK-JJ) 360,360,365
 365  JJ=KK
 360  CONTINUE
 350  CONTINUE
C
C   COMPUTE AND PRINT BAND WIDTH AS 2*JJ+NO. OF DEGREES OF FREEDOM
      NBAND=2*JJ+2
      WRITE(6,1000) NBAND
 1000 FORMAT(' ',///,5X,'BAND WIDTH',I10,///)
C
C   READ SNOW MATERIAL PROPERTIES
      CALL SNMAPR
C
C   INITIALIZE STRESSES,STRAINS AND STIFFNESSES
      DO 200 N=1,NE
      DO 500 I=1,4
      SIGTO(N,I)=0
      PSIGTO(N,I)=0
 500  CONTINUE
      DO 499 I=1,2
      PCV(N,I)=0
      PCAVP(N,I)=0
      CV(N,I)=0
      CAVP(N,I)=0
 499  CONTINUE
      DO 301 I=1,3
      STRTO(N,I)=0
      PSTRTO(N,I)=0
 301  CONTINUE
      SMAXTO(N)=0
      SMINTO(N)=0
      PSMINT(N)=0
      EMAXTO(N)=0
      EMINTO(N)=0
      PEMINT(N)=0
      EE(N)=STRESS(2)/STRAIN(2)
      ENU(N)=0.0
      DKN(N)=100000.
      DKS(N)=STIFFS
 200  CONTINUE
      DO 759 IKK=3,7
 759  PLR(IKK)=0.
C...INITIALIZE ARRAY OF INDICATORS OF FAILURES OF JOINT ELEMENTS
      DO 202 II=1,NE
      IFAIL(II)=0
 202  CONTINUE
C
C   INITIALIZE ALL NODAL DISPLACEMENTS
      DO 600 M=1,NP
      DO 600 J=1,2
      DISTO(J,M)=0
```

```
 600   CONTINUE
C
C   INITIALIZE ALL REACTIONS TO 0
       DO 437 J=1,NB
       M=NBC(J)
       N=2*M-1
       L=2*M
       AR(N)=0
       AR(L)=0
 437   CONTINUE
C
C   COMPUTE INCREMENTAL DISPLACEMENT TO BE USED AS BOUNDARY CONDITION
C
       DO 800 K=1,NB
       NN=NBC(K)
       UX(NN)=UX(NN)/NOINC
       UY(NN)=UY(NN)/NOINC
       UYR(NN)=UY(NN)
 800   CONTINUE
       DISINC=ABS(UY(6))
C
C   LOOP ON NUMBER OF INCREMENTS
C
       DO 700 IK=1,NOINC
       SFLAG=0.
       LCSRA=0
       DO 8000 K=1,NB
       NN=NBC(K)
 8000 UY(NN)=UYR(NN)
       IPRIN=0
       DO 547 IINC=1,NINCP
547    IF(IK.EQ IAINCP(IINC)) IPRIN=1
       WRITE(6,*) IPRIN
       IPUP=0
C...PRINT DISPLACEMENT INCREMENT NUMBER
       WRITE(6,991) IK
 991   FORMAT(' ',//,'------------------------------------------------
      +---'//5X,'INCR. NO ',I10,/)
C...DETERMINE STATE OF STRESS AND STRAIN OF CONTINUUM ELEMENTS
 711   IF(SFLAG.EQ.1.) WRITE(6,6258) LCSRA
 6258 FORMAT(' ',//,T10,'STRESS RELEASE CYCLE #',I5,//)
       DO 333 IPSS=1,NE
       IF(IMAT(IPSS).EQ 2) GO TO 333
       EQEMIN=PEMINT(IPSS)
       CALL INTERP(NPTSCC,EQEMIN,STRAIN,STRESS,SINT)
       PSMINT(IPSS)=SINT
 333   CONTINUE
C
C   FORM STIFFNESS MATRIX THEN SOLVE SIMULTANEOUS EQUATIONS
C
       NITER=0
701    NITER=NITER+1
       IF(IPRIN.NE.1) GO TO 844
C      DO 8003 K=1,NB
C      NN=NBC(K)
C      WRITE(6,*) NN,CODE(NN),UX(NN),UY(NN)
C8003 CONTINUE
 844   CALL FORMK
```

```
      CALL SOLVE
C   COMPUTE TOTAL DISPLACEMENTS
C   NODAL DISPLACEMENTS DUE TO INCREMENT ARE ADDED TO THOSE EXISTING
C   BEFORE TO OBTAIN TOTAL DISPLACEMENTS
C
      DO 280 M=1,NP
      DO 280 J=1,2
      IF(NITER.NE.1) GO TO 601
      PDISTO(J,M)=DISTO(J,M)
  601 DISTO(J,M)=PDISTO(J,M)+DIS(J,M)
  280 CONTINUE
C
C
C   CALCULATE STRESSES IN CONTINUUM ELEMENTS
C
612   CALL CSTRES(NLFLAG)
C   ITERATE FOR NONLINEARITY
      IF(NLFLAG.EQ.1.AND.NITER.NE.NOITER) GO TO 701
      WRITE(6,995) NITER
 995  FORMAT(' ',//,5X,'NUMBER OF  ITERATIONS',I10,///)
C
C. .TEMPORARILY UPDATE NODAL CORDINATES
      DO 606 N=1,NP
      TCORD(N,1)=CORD(N,1)+DIS(1,N)
      TCORD(N,2)=CORD(N,2)+DIS(2,N)
 606  CONTINUE
C. .COMPUTE STRESSES IN JOINT ELEMENTS
C
      CALL JSTRES
C
C CHECK STATE OF SHEAR STRESS IN JOINT ELEMENTS AND COMPARE WITH SHEAR
C STRENGTH OF SNOW
C
      CALL SHDJNT(IMAT,NOP,TCORD,AREAO,DIS,IPUP,FSHSTE,ORY)
C
C
C . DETERMINE REACTIONS
C
C
 8004 DO 436 I=1,NSZF
      AR(I)=0
 436  CONTINUE
      DO 438 L=1,NB
      M=NBC(L)
      DO 901 N1=1,NE
      IF(IMAT(N1).EQ 1) NCN=3
      IF(IMAT(N1).EQ.2) NCN=4
      DO 901 I=1,NCN
      IF(NOP(N1,I)-M) 901,705,901
  705 N=N1
      J=I
      IF(CODE(M)) 438,438,422
  422 CALL REAC(J,M,N)
  901 CONTINUE
  438 CONTINUE
C     IF(IPRIN EQ.1) WRITE(6,203)
C203  FORMAT(' ',////,5X,'REACTIONS AND LOAD-DISPLACEMENT COORDINATES OF
C    + PLATE'//5X,T2,'NODE',7X,'X-REACTION',11X,'Y-REACTION',/T17,'(KN)'
```

```
C     +,T37,'(KN)',//)
      SRX=0
      SRY=0
      DO 439 K=1,NB
      M=NBC(K)
      N=2*M-1
      L=2*M
      IF(CODE(M).NE 1) GO TO 501
      AR(N)=AR(N)-D(N)
      GO TO 503
  501 IF(CODE(M) EQ 2) GO TO 502
      AR(N)=AR(N)-D(N)
  502 AR(L)=AR(L)-D(L)
  503 CONTINUE
C .. PRINT INCREMENT REACTIONS
C     IF(IPRIN EQ.1) WRITE(6,201) M,AR(N),AR(L)
 201  FORMAT(I5,F16 6,5X,F16 6)
      SRX=SRX+AR(N)
      SRY=SRY+AR(L)
  439 CONTINUE
C     IF(IPRIN EQ 1) WRITE(6,440) SRX,SRY
 440  FORMAT(' ',///,1X,'TOTAL',2X,F15.8,5X,F15.8)
C
C.   COMPUTE PLATE DISPLACEMENT AND REACTION LOAD ON PLATE
C
      PDIS=DISINC*IK
C     WRITE(6,*) AR(6),AR(8),AR(10),AR(12),AR(14)
C...LOAD DISTRIBUTION ON PLATE
      SUMPLN=0 0
      DO 458 III=3,7
      II=2*III
      PLR(III)=PLR(III)+FPW*AR(II)
      SUMPLN=SUMPLN+PLR(III)
      WRITE(6,459) III,PLR(III)
459   FORMAT(' ',/,'REACTION ON NODE (KN)',I10,5X,'=',5X,F15.6)
 458  CONTINUE
      SUMPLN=2000 *SUMPLN
      WRITE(6,460) SUMPLN
 460  FORMAT(' ',///,'TOTAL REACTION LOAD ON PLATE (N)',F15 6,///)
C...
      DELPL=2000.*FPW*(AR(6)+AR(8)+AR(10)+AR(12)+AR(14))
      IF(SFLAG EQ.1 ) DELPL=DELPL+UY3
      PLOAD=PREPL+DELPL
C     EC=EC+0 5*(PLOAD+PREPL)*DISINC
      WRITE(6,961) DELPL
 961  FORMAT(' ',///,5X,'INCREMENTAL REACTION LOAD ON PLATE (N)',F15.6)
      WRITE(6,960) PLOAD,PDIS
 960  FORMAT(' ',///,5X,'TOTAL REACTION LOAD ON PLATE (N)',F15 6//5X,'PL
     +ATE DISPLACEMENT (M)',F15.6,///)
C...SEPARATE LOAD COMPONENTS INTO COMPRESSION AND SHEAR
      SUMES=0 0
      SUMEC=0 0
      N=0
      DO 512 I=1,70
      DO 512 J=1,11
      N=N+1
      IF(IMAT(N) EQ 2) GO TO 512
      DD = 0 0
```

```
      DO 204 I2 = 1,3
  204 DD = DD +  ( SIGTO(N,I2) * STRTO(N,I2) )
      DD = DD * AREA(N)
      IF(J LT 3) SUMES=SUMES+DD
      IF(J.GE.4) SUMEC=SUMEC+DD
512   CONTINUE
      IF(SFLAG.EQ.0.) GO TO 508
      SUMES=-SUMES
      SUMEC=-SUMEC
508   DPCS=2000.*SUMES*FPW/DISINC
      DPC=2000 *SUMEC*FPW/DISINC
      DS=DELPL-DPC-DPCS
      WRITE(6,222) DS,DPCS,DPC,DELPL
 222  FORMAT(' ',///,T10,'INCREMENTAL LOAD DUE TO SHEAR (N)',F15.6/,
     +T10,'INCREMENTAL LOAD DUE TO COMPRESSION OUTSIDE PRESSURE BULB (N)
     +',F15.6/T10,'INCREMENTAL LOAD DUE TO COMPRESSION INSIDE PRESSURE B
     +ULB  (N)',F15.6/T10,'INCREMENTAL LOAD ON PLATE (N)',F15.6,//)
      SUMPCS=SUMPCS+DPCS
      SUMPC=SUMPC+DPC
      SUMS=PLOAD-SUMPCS-SUMPC
      WRITE(6,223) SUMS,SUMPCS,SUMPC,PLOAD
 223  FORMAT(' ',///////,T10,'TOTAL LOAD DUE TO SHEAR (N)',F15.6/,
     +T10,'TOTAL LOAD DUE TO COMPRESSION OUTSIDE PRESSURE BULB (N)
     +',F15 6/T10,      'TOTAL LOAD DUE TO COMPRESSION INSIDE PRESSURE B
     +ULB  (N)',F15.6/T10,'TOTAL LOAD ON PLATE (N)',F15 6,//)
C   .COMPUTE  STRESS RELEASE FORCES DUE TO STRESS RELEASE IN
C    OVERSTRESSED JOINT ELEMENTS
      SLOAD=0 0
      DO 555 N=1,NP
 555  UY(N)=0.0
      DO 510 N=1,NE
      IF(IMAT(N).EQ.1) GO TO 510
      IF(IFAIL(N) EQ.0) GO TO 510
      RSREL=EXSH(N)*AL(N)*FPW*1000
      N1=NOP(N,1)
      N2=NOP(N,2)
      N3=NOP(N,3)
      N4=NOP(N,4)
      UY(3)=0.0
      UY(N1)=UY(N1)+RSREL/(2 *FPW*1000.)
      IF(N.EQ.3) UY3=-UY(N1)*2000.*FPW
C     WRITE(6,4445) UY3
C4445  FORMAT(' ',/,T5,'UY3',F15 6)
      UY(N2)=UY(N2)+RSREL/(2.*FPW*1000.)
      UY(N3)=UY(N3)-RSREL/(2.*FPW*1000.)
      UY(N4)=UY(N4)-RSREL/(2 *FPW*1000.)
      SFLAG=1.
      CAVP(N,1)=CAVP(N,1)+EXSH(N)
C     IF(IPRIN.EQ.1) WRITE(6,4444) N,EXSH(N),AL(N),FPW,RSREL,PPLOAD
C4444 FORMAT(' ','N',I5,5X,'EXSH(N)',F15.6,5X,'AL(N)',F10.6,5X,'FPW',
C    +F10.6,5X,'RSREL',F15.6,5X,'PPLOAD',F15.6,/)
C     IF(IPRIN.EQ.1) WRITE(6,*)N,N1,UY(N1),N2,UY(N2),N3,UY(N3),N4,UY(N4)
 510  CONTINUE
      DO 8001 N=3,7
      UY(N)=0.0
 8001 CONTINUE
      CLOAD=PLOAD-SLOAD
      FACTOR=1000 *FPL*FPW
```

```
      PSTRES=PLOAD/FACTOR
      PS1=SUMS/FACTOR
      PS2=SUMPCS/FACTOR
      PS3=SUMPC/FACTOR
      WRITE(6,521) PS1,PS2,PS3,PSTRES
  521 FORMAT(' ',///,5X,'PLATE STRESS CARRIED IN SHEAR (KPA)',F15.6/
     +,5X,'PLATE STRESS CARRIED IN COMPRESSION OUTSIDE PRESSURE BULB (KP
     +A)',F15.6/5X,'PLATE STRESS CARRIED IN COMPRESSION INSIDE PRESSURE
     +BULB (KPA)',F15.6/5X,'PLATE STRESS (KPA)',F15.6,///)
      PREPL=PLOAD
C  UPDATE NODAL COORDINATES AND MATERIAL PROPERTIES
      CALL UPDATE(AREAO,PAREA,PDIS,YCTOP)
      LCSRA=LCSRA+1
      WRITE(6,9000) SFLAG,LCSRA,DELPL,PLOAD
 9000 FORMAT(' ',/5X,'SFLAG',F6.3/5X,'LCSRA',I5/5X,'DELPL',F10 3/5X,
     +'PLOAD',F10.3)
      IF(SFLAG.EQ.1 AND LCSRA EQ.1) GO TO 711
      IF(SFLAG.EQ.1.0.AND.LCSRA LE.3.AND.DELPL.LT 0.AND ABS(DELPL).GT.0.
     +05*PLOAD) GO TO 711
C. .PRINT NODAL DISPLACEMENTS
      IF(IPRIN.NE.1)  GO TO 700
      WRITE(6,603)
  603 FORMAT(///,5X,'NODAL DISPLACEMENTS',///7X,'NODE',T23,'X',T38,'Y',
     +T50,'XTOTAL',T65,'YTOTAL',T81,'ORIG HOR.DISTANCE',T106,'ORIG.VERT.
     +DISTANCE')
      WRITE(6,710)
  710 FORMAT(' ',T22,'(M)',T37,'(M)',T52,'(M)',T67,'(M)',T81,'FROM PLATE
     + CENTER',T106,'FROM PLATE CENTER'/T87,'(PL#S)',T113,'(PL#S)',//)
      DO 604 M=1,NP
      RX=(CORDI(7,1)-CORDI(M,1))/FPL
      RY=CORDI(M,2)/FPL
      WRITE(6,605) M,(DIS(J,M),J=1,2),(DISTO(J,M),J=1,2),RX,RY
  605 FORMAT(' ',I9,1X,4(5X,F10.6),T85,F9.6,T111,F10.3)
  604 CONTINUE
  700 CONTINUE
      STOP
      END
C
C
      SUBROUTINE INMESH(AREAO,YCTOP)
C
      COMMON/CONTR/NP,NE,NB,NDF,NCN,NSZF,ITITL(50),IPRIN,SFLAG,FPL,DELPL
C
      COMMON/DATA/CORD(580,2),NOP(999,4),IMAT(1100),NBC(580),CODE(700),
     +UX(700),UY(700),T(1100),ORX(1100),ORY(1100),PRCORD(580,2)
C
      COMMON/STIFF/ESTIFM(12,12),A(3,6),B(3,6),SK(1100,92),AREA(1100),
     +C(1100),R(8),H(8),D(1100),AR(2000),AS(999,3,6),BS(999,3,6),NBAND
C
      COMMON/ANAL/NOINC,KOUNT,NITER,NOITER,CORDI(580,2)
C
      COMMON/STRES/DISTO(2,580),SIGTO(999,4),STRTO(999,3),SMAXTO(1100),
     +SMINTO(1100),ANGTO(1100),EANGTO(1100),EMAXTO(1100),EMINTO(1100),
     +FORCE(999,4),STR(999,3),PSIGTO(999,4),PSTRTO(999,3),PDISTO(2,580),
     +PEMINT(1100),PSMINT(1100),EXSH(1100)
C
      COMMON/JOINT/T1(8,8),BL(8,8),AL(1100),ANG(1100),DKS(1100),DKN(1000
     +),SD(2,2),W(999,2),P(999,2),V(999,2),AVP(999,2),CV(999,2),
```

```
     +CAVP(999,2),PCV(999,2),PCAVP(999,2),B1(8,8),IFAIL(1100),ALO(1100)
C
C
      COMMON/SNDATA/STRESS(40),STRAIN(40),SHEAR(40),DENSSH(40),
     +GAMMAO,NPTSCC,NPTSSH,STIFFS(40),NPTSDK,DENSK(40)
      COMMON/ELAS/EE(1100),ENU(1100)
C
      DIMENSION AREAO(1100),NFR1(180),NFR2(180),NBBN(4)
      DATA NFR1/1,1,9,8,8,2,1,2,9,9,3,3,10,9,2,4,3,4,10,10,5,4,11,10,10,
     +6,4,12,11,11,7,4,5,12,12,8,5,6,12,12,9,6,13,12,12,10,6,14,13,13,
     +11,6,7,14,14/
      DATA NFR2/12,8,9,15,15,13,9,16,15,15,14,10,17,16,9,15,10,18,17,17,
     +16,10,11,18,18,17,11,12,18,18,18,12,19,18,18,19,12,20,19,19,20,12,
     +13,20,20,21,13,14,20,20,22,14,21,20,20/
      DATA NBBN/1,2,3,7/
C. ASSIGN NUMBER OF DEGREES OF FREEDOM PER NODE
C  ASSIGN MAXIMUM NUMBER OF INCREMENTS AND ITERATIONS
      NDF=2
      NOINC=36
      NOITER=12
      PDMAX=0.072
      NP=0
C...... .GENERATE MESH IN TERMS OF PLATE LENGTH
C.  NODES
      DO 10 J=1,71
      DO 10 I=1,7
      NP=NP+1
      CORD(NP,1)=(I-1)*FPL/8.
      CORD(NP,2)=(J-1)*FPL/16.
      CORDI(NP,1)=CORD(NP,1)
      CORDI(NP,2)=CORD(NP,2)
      WRITE(6,222) NP,CORD(NP,1),CORD(NP,2)
222   FORMAT(' ',T2,I3,T10,F15.6,T26,F15.6)
 10   CONTINUE
      YCTOP=CORD(1,2)
C...ELEMENTS
      DO 200 I=1,35
      DO 21 II=1,2
      IK=0
      DO 21 J=1,11
      IK=IK+1
      IF(II EQ.1) N=NFR1(IK)+(I-1)*22
      IF(II EQ.2) N=NFR2(IK)+(I-1)*22
      DO 300 K=1,4
      IK=IK+1
      IF(II.EQ.1) NOP(N,K)=NFR1(IK)+(I-1)*14
      IF(II.EQ 2) NOP(N,K)=NFR2(IK)+(I-1)*14
 300  CONTINUE
      IMAT(N)=1
      IF(J.EQ.3) IMAT(N)=2
 860  FORMAT(' ',T11,6I10)
 21   CONTINUE
 200  CONTINUE
      NE=N
      DO 888 N=1,NE
      WRITE(6,860) N,(NOP(N,KKK),KKK=1,4),IMAT(N)
 888  CONTINUE
C...CALCULATE INITIAL AREA OF ELEMENTS , INITAL LENGTH OF JOINT ELEMENTS
```

```
C   AND STORE
      DO 400 N=1,NE
      IF(IMAT(N).EQ.2) GO TO 41
      I=NOP(N,1)
      J=NOP(N,2)
      K=NOP(N,3)
      AJ=CORD(J,1)-CORD(I,1)
      AK=CORD(K,1)-CORD(I,1)
      BJ=CORD(J,2)-CORD(I,2)
      BK=CORD(K,2)-CORD(I,2)
      AREAO(N)=(AJ*BK-AK*BJ)/2.
C     WRITE(6,*) N,AREAO(N)
      GO TO 400
 41   I=NOP(N,1)
      J=NOP(N,2)
      ALO(N)=SQRT((CORD(J,2)-CORD(I,2))**2+(CORD(J,1)-CORD(I,1))**2)
 400  CONTINUE
C.. BOUNDARY CONDITIONS
      DO 806 I=1,NP
      CODE(I)=0
      UX(I)=0
      UY(I)=0
 806  CONTINUE
      CODE(1)=3 0
      CODE(2)=1.0
      CODE(3)=3 0
      UY(3)=PDMAX
      NBC(1)=1
      NBC(2)=2
      NBC(3)=3
      NB=3
      DO 807 N=4,6
      NB=NB+1
      NBC(NB)=N
      CODE(N)=2.0
      UY(N)=PDMAX
 807  CONTINUE
      NB=NB+1
      CODE(7)=3.0
      UY(7)=PDMAX
      NBC(NB)=7
      DO 809 I=1,69
      DO 810 J=1,4
      NB=NB+1
      NBC(NB)=NBBN(J)+I*7
      NN=NBC(NB)
      CODE(NN)=1.0
      IF(J.EQ.1) CODE(NN)=3.0
 810  CONTINUE
 809  CONTINUE
      DO 811 K=1,7
      NB=NB+1
      NBC(NB)=NBC(NB-1)+1
      NN=NBC(NB)
      CODE(NN)=3.0
 811  CONTINUE
      DO 812 I=1,NB
      NN=NBC(I)
```

```
      WRITE(6,*) NN,CODE(NN),UX(NN),UY(NN)
  812 CONTINUE
      RETURN
      END
C
      SUBROUTINE SNMAPR
C
      COMMON/CONTR/NP,NE,NB,NDF,NCN,NSZF,ITITL(50),IPRIN,SFLAG,FPL,DELPL
C
      COMMON/DATA/CORD(580,2),NOP(999,4),IMAT(1100),NBC(580),CODE(700),
     +UX(700),UY(700),T(1100),ORX(1100),ORY(1100),PRCORD(580,2)
C
      COMMON/STIFF/ESTIFM(12,12),A(3,6),B(3,6),SK(1100,92),AREA(1100),
     +C(1100),R(8),H(8),D(1100),AR(2000),AS(999,3,6),BS(999,3,6),NBAND
C
      COMMON/ANAL/NOINC,KOUNT,NITER,NOITER,CORDI(580,2)
C
      COMMON/STRES/DISTO(2,580),SIGTO(999,4),STRTO(999,3),SMAXTO(1100),
     +SMINTO(1100),ANGTO(1100),EANGTO(1100),EMAXTO(1100),EMINTO(1100),
     +FORCE(999,4),STR(999,3),PSIGTO(999,4),PSTRTO(999,3),PDISTO(2,580),
     +PEMINT(1100),PSMINT(1100),EXSH(1100)
C
      COMMON/JOINT/T1(8,8),BL(8,8),AL(1100),ANG(1100),DKS(1100),DKN(1000
     +),SD(2,2),W(999,2),P(999,2),V(999,2),AVP(999,2),CV(999,2),
     +CAVP(999,2),PCV(999,2),PCAVP(999,2),B1(8,8),IFAIL(1100),ALO(1100)
C
C
      COMMON/SNDATA/STRESS(40),STRAIN(40),SHEAR(40),DENSSH(40),
     +GAMMAO,NPTSCC,NPTSSH,STIFFS
      COMMON/ELAS/EE(1100),ENU(1100)
C
C
C  SUBROUTINE TO ENTER SNOW PROPERTIES
C
C
C  READ AND PRINT INPUT DATA
C
      WRITE(6,20)
   20 FORMAT(' ',//////,5X,'SNOW PROPERTIES'/5X,15('-'),///)
C  READ INITIAL SNOW DENSITY
      READ(5,*) GAMMAO
      WRITE(6,10) GAMMAO
   10 FORMAT(' ',///,5X,'INITIAL SNOW DENSITY (MG/M3)',F15.6)
C...CONFINED COMPRESSION DATA
      READ(5,*) NPTSCC
      WRITE(6,2)
    2 FORMAT(//,5X,'CONFINED COMPRESSION   STRESS-STRAIN',///,T15,'STRES
     +S',T30,'STRAIN'/T16,'(KPA)',///)
      DO 30 I=1,NPTSCC
      READ(5,*) STRESS(I),STRAIN(I)
      WRITE(6,31) STRESS(I),STRAIN(I)
   31 FORMAT(' ',5X,2F15.6)
   30 CONTINUE
C  .DIRECT SHEAR DATA
      READ(5,*) NPTSSH
      WRITE(6,5)
    5 FORMAT(///,5X,'SHEAR STRENGTH-DENSITY',///T10,'SHEAR STRENGTH',T29
     +,'DENSITY'/T15,'(KPA)',T29,'(MG/M3)',///)
```

```
      DO 50 I=1,NPTSSH
      READ(5,*) SHEAR(I),DENSSH(I)
      WRITE(6,31) SHEAR(I),DENSSH(I)
 50   CONTINUE
C . SHEAR STIFFNESS
      READ(5,*) STIFFS
      WRITE(6,12) STIFFS
 12   FORMAT(//,1X,'SHEAR STIFFNESS/UNIT LENGTH  (KN/M3)',F15.6,///)
      RETURN
      END
C
C
      SUBROUTINE FORMK
C
      COMMON/CONTR/NP,NE,NB,NDF,NCN,NSZF,ITITL(50),IPRIN,SFLAG,FPL,DELPL
C
      COMMON/DATA/CORD(580,2),NOP(999,4),IMAT(1100),NBC(580),CODE(700),
     +UX(700),UY(700),T(1100),ORX(1100),ORY(1100),PRCORD(580,2)
C
      COMMON/STIFF/ESTIFM(12,12),A(3,6),B(3,6),SK(1100,92),AREA(1100),
     +C(1100),R(8),H(8),D(1100),AR(2000),AS(999,3,6),BS(999,3,6),NBAND
C
      COMMON/ANAL/NOINC,KOUNT,NITER,NOITER,CORDI(580,2)
C
      COMMON/STRES/DISTO(2,580),SIGTO(999,4),STRTO(999,3),SMAXTO(1100),
     +SMINTO(1100),ANGTO(1100),EANGTO(1100),EMAXTO(1100),EMINTO(1100),
     +FORCE(999,4),STR(999,3),PSIGTO(999,4),PSTRTO(999,3),PDISTO(2,580),
     +PEMINT(1100),PSMINT(1100),EXSH(1100)
C
      COMMON/JOINT/T1(8,8),BL(8,8),AL(1100),ANG(1100),DKS(1100),DKN(1000
     +),SD(2,2),W(999,2),P(999,2),V(999,2),AVP(999,2),CV(999,2),
     +CAVP(999,2),PCV(999,2),PCAVP(999,2),B1(8,8),IFAIL(1100),ALO(1100)
C
      COMMON/ELAS/EE(1100),ENU(1100)
C
C
C                   FORMS STIFFNESS MATRIX
C
      DIMENSION XE(3,2)
C
C                   ZERO STIFFNESS MATRIX
C
      DO 300 N=1,NSZF
      C(N)=0 0
      D(N)=0 0
      DO 300 M = 1,NBAND
  300 SK(N,M)=0.
C
C                   SCAN ELEMENTS
C
      DO 400 N=1,NE
      IF(IMAT(N) EQ 1) CALL CSTK(N)
      IF(IMAT(N) EQ.2) CALL JOINTK(N)
C
C                   RETURNS ESTIFM AS STIFFNESS MATRIX
C
C                   STORE ESTIFM IN SK
C                   FIRST ROWS
```

```
C
      IF(IMAT(N).EQ.1) NCN=3
      IF(IMAT(N).EQ.2) NCN=4
      DO 360 JJ=1,NCN
      NROWB=(NOP(N,JJ)-1)*NDF
      IF(NROWB)360,305,305
  305 DO 350 J=1,NDF
      NROWB=NROWB+1
      I=(JJ-1)*NDF+J
C
C                    THEN COLUMNS
C
      DO330 KK=1,NCN
      NCOLB=(NOP(N,KK)-1)*NDF
      DO 320 K=1,NDF
      L = (KK-1)*NDF + K
      NCOL = NCOLB + K + 1 -NROWB
C                SKIP STORING IF BELOW BAND
C
      IF(NCOL)320,320,310
  310 SK(NROWB,NCOL)=SK(NROWB,NCOL)+ESTIFM(I,L)
  320 CONTINUE
  330 CONTINUE
  350 CONTINUE
  360 CONTINUE
  400 CONTINUE
C                  ADDITION OF CONCENTRATED  FORCES
      DO 297 I=1,NB
      N=NBC(I)
      K=2*N
      IF(CODE(N)-1.) 295,295,296
  296 IF(CODE(N) EQ 2.) GO TO 301
  298 IF(CODE(N)-3 ) 425,297,425
  295 C(K)=C(K)+UY(N)
      IF(CODE(N) NE.0.0) GO TO 297
  301 C(K-1)=C(K-1)+UX(N)
      GO TO 297
  425 WRITE(6,426) N
      STOP
  426 FORMAT(5X,'ERROR IN CODE NUMBER-NODE-EXECUTION TERMINATED',I4)
  297 CONTINUE
C
C
C                  TRANSFER LOAD VECTOR TO D
C
      DO 601 I=1,NSZF
      D(I)=C(I)
  601 CONTINUE
  602 CONTINUE
C                  DISPLACEMENT BOUNDARY CONDITIONS
C
      DO 401 J=1,NB
      M=NBC(J)
      U=UX(M)
      N=2*M-1
      IF(CODE(M)) 401,401,311
  311 IF(CODE(M)-1 0) 401,325,331
  331 IF(CODE(M) EQ.2 ') GO TO 335
```

```
      IF(CODE(M)-3.) 401,340,401
  325 CALL MODIFY(SK,C,NSZF,NBAND,N,U)
      GO TO 401
  340 CALL MODIFY(SK,C,NSZF,NBAND,N,U)
  335 U=UY(M)
      N=N+1
      CALL MODIFY(SK,C,NSZF,NBAND,N,U)
  401 CONTINUE
      RETURN
      END
C
C
      SUBROUTINE CSTK(N)
C
      COMMON/CONTR/NP,NE,NB,NDF,NCN,NSZF,ITITL(50),IPRIN,SFLAG,FPL,DELPL
C
      COMMON/DATA/CORD(580,2),NOP(999,4),IMAT(1100),NBC(580),CODE(700),
     +UX(700),UY(700),T(1100),ORX(1100),ORY(1100),PRCORD(580,2)
C
      COMMON/STIFF/ESTIFM(12,12),A(3,6),B(3,6),SK(1100,92),AREA(1100),
     +C(1100),R(8),H(8),D(1100),AR(2000),AS(999,3,6),BS(999,3,6),NBAND
C
      COMMON/ANAL/NOINC,KOUNT,NITER,NOITER,CORDI(580,2)
C
      COMMON/STRES/DISTO(2,580),SIGTO(999,4),STRTO(999,3),SMAXTO(1100),
     +SMINTO(1100),ANGTO(1100),EANGTO(1100),EMAXTO(1100),EMINTO(1100),
     +FORCE(999,4),STR(999,3),PSIGTO(999,4),PSTRTO(999,3),PDISTO(2,580),
     +PEMINT(1100),PSMINT(1100),EXSH(1100)
C
      COMMON/JOINT/T1(8,8),BL(8,8),AL(1100),ANG(1100),DKS(1100),DKN(1000
     +),SD(2,2),W(999,2),P(999,2),V(999,2),AVP(999,2),CV(999,2),
     +CAVP(999,2),PCV(999,2),PCAVP(999,2),B1(8,8),IFAIL(1100),ALO(1100)
C
      COMMON/ELAS/EE(1100),ENU(1100)
C
C
C   CONTINUUM ELEMENT STIFFNESS MATRIX
C
C
C                     DETERMINE ELEMENT CONNECTIONS
C
      I=NOP(N,1)
      J=NOP(N,2)
      K=NOP(N,3)
      ORX(N)=(CORD(I,1)+CORD(J,1)+CORD(K,1))*0 333333
      ORY(N)=(CORD(I,2)+CORD(J,2)+CORD(K,2))*0.333333
C
C                     SET UP LOCAL COORDINATE SYSTEM
C
      AJ=CORD(J,1)-CORD(I,1)
      AK=CORD(K,1)-CORD(I,1)
      BJ=CORD(J,2)-CORD(I,2)
      BK=CORD(K,2)-CORD(I,2)
      AREA(N)=(AJ*BK-AK*BJ)/2
221   IF(AREA(N).LE 0.) GO TO 220
C
C                     FORM STRAIN DISP  MATRIX
C
```

```
      A(1,1)=BJ-BK
      A(1,2)=0.
      A(1,3)=BK
      A(1,4)=0.
      A(1,5)=-BJ
      A(1,6)=0
      A(2,1)=0
      A(2,2)=AK-AJ
      A(2,3)=0
      A(2,4)=-AK
      A(2,5)=0.
      A(2,6)=AJ
      A(3,1)=AK-AJ
      A(3,2)=BJ-BK
      A(3,3)=-AK
      A(3,4)=BK
      A(3,5)=AJ
      A(3,6)=-BJ
      DO 10 I = 1,3
      DO 10 J = 1,6
      AS(N,I,J) = A(I,J)
   10 CONTINUE
C
C                        FORM STRESS STAIN MATRIX
C
      COMM=EE(N)/((1.+ENU(N))*(1.-ENU(N)*2.)*AREA(N))
      ESTIFM(1,1)=COMM*(1.-ENU(N))
      ESTIFM(1,2)=COMM*ENU(N)
      ESTIFM(3,1)=0.
      ESTIFM(3,2)=0.
      ESTIFM(3,3)=EE(N)/(2.*(1.+ENU(N))*AREA(N))
      ESTIFM(1,3)=0.
      ESTIFM(2,1)=ESTIFM(1,2)
      ESTIFM(2,2)=ESTIFM(1,1)
      ESTIFM(2,3)=0.
C
C                        B IS THE STRESS BACKSUBSTITUTION
C
    4 DO 205 I = 1,3
      DO 205 J=1,6
      B(I,J)=0.
      DO 205 K=1,3
  205 B(I,J)=B(I,J)+ESTIFM(I,K)/2.*A(K,J)
      DO 20 I = 1,3
      DO 20 J = 1,6
      BS(N,I,J) = B(I,J)
   20 CONTINUE
C
C                        ESTIFM IS STIFFNESS MATRIX
C
      DO 210 I=1,6
      DO 210 J=1,6
      ESTIFM(I,J)=0.
      DO 210 K=1,3
  210 ESTIFM(I,J)=ESTIFM(I,J)+B(K,I)/2.*A(K,J)
      RETURN
C
C                        ERROR EXIT FOR BAD CONNECTIONS
```

```
C
 220 WRITE(6,100) N
 100 FORMAT('ZERO OR NEGATIVE AREA ELEMENT NO',I4/'EXECUTION TERMINATED
    1')
      WRITE(6,*) AJ,BK,AK,BJ
      STOP
      END
C
C
      SUBROUTINE JOINTK(N)
C
C  JOINT ELEMENT STIFFNESS MATRIX
C
      COMMON/CONTR/NP,NE,NB,NDF,NCN,NSZF,ITITL(50),IPRIN,SFLAG,FPL,DELPL
C
      COMMON/DATA/CORD(580,2),NOP(999,4),IMAT(1100),NBC(580),CODE(700),
     +UX(700),UY(700),T(1100),ORX(1100),ORY(1100),PRCORD(580,2)
C
      COMMON/STIFF/ESTIFM(12,12),A(3,6),B(3,6),SK(1100,92),AREA(1100),
     +C(1100),R(8),H(8),D(1100),AR(2000),AS(999,3,6),BS(999,3,6),NBAND
C
      COMMON/ANAL/NOINC,KOUNT,NITER,NOITER,CORDI(580,2)
C
      COMMON/STRES/DISTO(2,580),SIGTO(999,4),STRTO(999,3),SMAXTO(1100),
     +SMINTO(1100),ANGTO(1100),EANGTO(1100),EMAXTO(1100),EMINTO(1100),
     +FORCE(999,4),STR(999,3),PSIGTO(999,4),PSTRTO(999,3),PDISTO(2,580),
     +PEMINT(1100),PSMINT(1100),EXSH(1100)
C
      COMMON/JOINT/T1(8,8),BL(8,8),AL(1100),ANG(1100),DKS(1100),DKN(1000
     +),SD(2,2),W(999,2),P(999,2),V(999,2),AVP(999,2),CV(999,2),
     +CAVP(999,2),PCV(999,2),PCAVP(999,2),B1(8,8),IFAIL(1100),ALO(1100)
C
      COMMON/ELAS/EE(1100),ENU(1100)
C
C
      I=NOP(N,1)
      J=NOP(N,2)
      K=NOP(N,3)
      L=NOP(N,4)
      IF(CORD(I,1).EQ.CORD(J,1)) GO TO 11
      ANG(N)=ATAN((CORD(J,2)-CORD(I,2))/(CORD(J,1)-CORD(I,1)))
      GO TO 12
  11  ANG(N)=90.0/57.29578
  12  CONTINUE
      AL(N)=SQRT((CORD(J,2)-CORD(I,2))**2+(CORD(J,1)-CORD(I,1))**2)
      ORX(N)=(CORD(I,1)+CORD(J,1)+CORD(K,1)+CORD(L,1))/4.
      ORY(N)=(CORD(I,2)+CORD(J,2)+CORD(K,2)+CORD(L,2))/4.
C
C  ESTIFM IS STIFFNESS MATRIX
C
      DO 3 I=1,8
      DO 3 J=1,8
  3   ESTIFM(I,J)=0.0
      ESTIFM(1,1)=DKS(N)*AL(N)/3.
      ESTIFM(1,3)=ESTIFM(1,1)/2.
      ESTIFM(1,5)=-ESTIFM(1,3)
      ESTIFM(1,7)=-ESTIFM(1,1)
      ESTIFM(2,2)=DKN(N)*AL(N)/3.
```

```
      ESTIFM(2,4)=ESTIFM(2,2)/2.
      ESTIFM(2,6)=-ESTIFM(2,4)
      ESTIFM(2,8)=-ESTIFM(2,2)
      ESTIFM(3,3)=ESTIFM(1,1)
      ESTIFM(3,5)=-ESTIFM(1,1)
      ESTIFM(3,7)=-ESTIFM(1,1)/2.
      ESTIFM(4,4)=ESTIFM(2,2)
      ESTIFM(4,6)=-ESTIFM(2,2)
      ESTIFM(4,8)=-ESTIFM(2,2)/2.
      ESTIFM(5,5)=ESTIFM(1,1)
      ESTIFM(5,7)=ESTIFM(1,1)/2.
      ESTIFM(6,6)=ESTIFM(2,2)
      ESTIFM(6,8)=ESTIFM(2,2)/2.
      ESTIFM(7,7)=ESTIFM(1,1)
      ESTIFM(8,8)=ESTIFM(2,2)
C     WRITE(6,40)
      DO 4 K=1,7
      K1=K+1
      DO 4 J=K1,8
    4 ESTIFM(J,K)=ESTIFM(K,J)
C
C  DETERMINE TRANSFORMATION MATRIX
C
      E=COS(ANG(N))
      S=SIN(ANG(N))
      DO 5 I=1,8
      DO 5 J=1,8
    5 T1(I,J)=0.0
      DO 6 I=1,8
      J=I
    6 T1(I,J)=E
      DO 7 I=1,7,2
      J=I+1
    7 T1(I,J)=S
      DO 8 I=2,8,2
      J=I-1
    8 T1(I,J)=-S
C
C  TRANSFORM STIFFNESS TO GLOBAL AXES
C
      DO 9 I=1,8
      DO 9 J=1,8
      BL(I,J)=0.0
      DO 9 L=1,8
    9 BL(I,J)=BL(I,J)+ESTIFM(I,L)*T1(L,J)
      DO 10 I=1,8
      DO 10 J=1,8
      ESTIFM(I,J)=0.0
      DO 10 L=1,8
   10 ESTIFM(I,J)=ESTIFM(I,J)+BL(L,I)*T1(L,J)
      RETURN
      END
C
C
      SUBROUTINE MODIFY(SK,B,NUEQ,NBAND,N,U)
C                 SUBROUTINE MODIFY MODIFIES THE STIFFNESS MATRIX
C                 SO AS TO ACCOUNT FOR THE SPECIFIED DISPLACEMENTS
C
```

```
      DIMENSION B(1100),SK(1100,92)
      DO 240 M = 2,NBAND
      K=N-M+1
      IF(K) 210,210,220
  220 B(K)=B(K)-SK(K,M)*U
      SK(K,M)=0.0
  210 K=N+M-1
      IF(NUEQ - K)240,230,230
  230 B(K)=B(K)-SK(N,M)*U
      SK(N,M)=0.0
  240 CONTINUE
      SK(N,1)=1.0
      B(N)=U
      RETURN
      END
C
C
      SUBROUTINE SOLVE
C
      COMMON/CONTR/NP,NE,NB,NDF,NCN,NSZF,ITITL(50),IPRIN,SFLAG,FPL,DELPL
C
      COMMON/DATA/CORD(580,2),NOP(999,4),IMAT(1100),NBC(580),CODE(700),
     +UX(700),UY(700),T(1100),ORX(1100),ORY(1100),PRCORD(580,2)
C
      COMMON/STIFF/ESTIFM(12,12),A(3,6),B(3,6),SK(1100,92),AREA(1100),
     +C(1100),R(8),H(8),D(1100),AR(2000),AS(999,3,6),BS(999,3,6),NBAND
C
      COMMON/ANAL/NOINC,KOUNT,NITER,NOITER,CORDI(580,2)
C
      COMMON/STRES/DISTO(2,580),SIGTO(999,4),STRTO(999,3),SMAXTO(1100),
     +SMINTO(1100),ANGTO(1100),EANGTO(1100),EMAXTO(1100),EMINTO(1100),
     +FORCE(999,4),STR(999,3),PSIGTO(999,4),PSTRTO(999,3),PDISTO(2,580),
     +PEMINT(1100),PSMINT(1100),EXSH(1100)
C
      COMMON/JOINT/T1(8,8),BL(8,8),AL(1100),ANG(1100),DKS(1100),DKN(1000
     +),SD(2,2),W(999,2),P(999,2),V(999,2),AVP(999,2),CV(999,2),
     +CAVP(999,2),PCV(999,2),PCAVP(999,2),B1(8,8),IFAIL(1100),ALO(1100)
C
      COMMON/ELAS/EE(1100),ENU(1100)
C
C
C          SPECIFICATION STATMENTS
C
C
C                         REDUCE MATRIX
C
C     DO 900 I=1,40
C     WRITE(6,700) (SK(I,J),J=1,40)
C700  FORMAT(' ',10F10.6,/)
C900  CONTINUE
      DO 300 N = 1,NSZF
      I = N
      DO 290 L = 2,NBAND
      I = I + 1
      IF(SK(N,L))240,290,240
  240 G =SK(N,L)/SK(N,1)
      J = 0
      DO 270 K = L,NBAND
```

```
      J = J + 1
      IF(SK(N,K))260,270,260
  260 SK(I,J)=SK(I,J) - G*SK(N,K)
  270 CONTINUE
  280 SK(N,L) = G
C
C
C                       AND LOAD VECTOR
C                       FOR EACH EQUATION
      C(I)=C(I)-G*C(N)
  290 CONTINUE
  300 C(N)=C(N)/SK(N,1)
C
C
C                       BACK-SUBSTITUTION
      N=NSZF
  350 N = N - 1
      IF(N)500,500,360
  360 L = N
      DO 400 K = 2,NBAND
      L = L + 1
      IF(SK(N,K))370,400,370
  370 C(N)=C(N)-SK(N,K)*C(L)
  400 CONTINUE
      GO TO 350
  500 CONTINUE
      RETURN
      END
C
C
      SUBROUTINE CSTRES(NLFLAG)
C
      COMMON/CONTR/NP,NE,NB,NDF,NCN,NSZF,ITITL(50),IPRIN,SFLAG,FPL,DELPL
C
      COMMON/DATA/CORD(580,2),NOP(999,4),IMAT(1100),NBC(580),CODE(700),
     +UX(700),UY(700),T(1100),ORX(1100),ORY(1100),PRCORD(580,2)
C
      COMMON/STIFF/ESTIFM(12,12),A(3,6),B(3,6),SK(1100,92),AREA(1100),
     +C(1100),R(8),H(8),D(1100),AR(2000),AS(999,3,6),BS(999,3,6),NBAND
C
      COMMON/ANAL/NOINC,KOUNT,NITER,NOITER,CORDI(580,2)
C
      COMMON/STRES/DISTO(2,580),SIGTO(999,4),STRTO(999,3),SMAXTO(1100),
     +SMINTO(1100),ANGTO(1100),EANGTO(1100),EMAXTO(1100),EMINTO(1100),
     +FORCE(999,4),STR(999,3),PSIGTO(999,4),PSTRTO(999,3),PDISTO(2,580),
     +PEMINT(1100),PSMINT(1100),EXSH(1100)
C
      COMMON/JOINT/T1(8,8),BL(8,8),AL(1100),ANG(1100),DKS(1100),DKN(1000
     +),SD(2,2),W(999,2),P(999,2),V(999,2),AVP(999,2),CV(999,2),
     +CAVP(999,2),PCV(999,2),PCAVP(999,2),B1(8,8),IFAIL(1100),ALO(1100)
C
      COMMON/ELAS/EE(1100),ENU(1100)
C
      DIMENSION DIS(2,580)
      EQUIVALENCE(DIS,C)
C
C
C                       CALCULATE ELEMENT STRAINS
```

```
      DO 200 N =1,NE
      IF(IMAT(N) EQ.2) GO TO 200
      DO 260 I =1,3
      M=NOP(N,I)
      IF(M.EQ 0)GO TO 260
      K = (I - 1)*NDF
      DO 240 J =1,NDF
      IJ = J + K
  240 R(IJ) = DIS(J,M)
  260 CONTINUE
      IA = K + NDF
      DO 500 I=1,4
  500 FORCE(N,I)=0.
      DO 300 I = 1,3
      STR(N,I)=0.
      DO 300 J = 1,IA
      STR(N,I) = STR(N,I) + (AS(N,I,J)*R(J))/(2.*AREA(N))
  300 FORCE(N,I) = FORCE(N,I) + BS(N,I,J)*R(J)
      FORCE(N,4)=FORCE(N,4)+ENU(N)*(FORCE(N,1)+FORCE(N,2))
  200 CONTINUE
C
C                   CUMULATIVE STRESSES AND STRAINS
C
      DO 801 N=1,NE
      IF(IMAT(N).EQ.2) GO TO 801
      DO 290 I=1,3
      IF(NITER.NE 1) GO TO 802
C     PSTRTO(N,I)=STRTO(N,I)
      PSTRTO(N,I)=0
  802 STRTO(N,I)=PSTRTO(N,I)+STR(N,I)
  290 CONTINUE
      DO 304 I=1,4
      IF(NITER.NE 1) GO TO 803
C     PSIGTO(N,I)=SIGTO(N,I)
      PSIGTO(N,I)=0
  803 SIGTO(N,I)=PSIGTO(N,I)+FORCE(N,I)
  304 CONTINUE
  801 CONTINUE
C
C                   TOTAL PRINCIPAL STRESSES AND STRAINS AND DIRECTIONS
C
      DO 301 N=1,NE
      IF(IMAT(N) EQ.2) GO TO 301
      C1=(SIGTO(N,1)+SIGTO(N,2))/2.
      D1=SQRT(((SIGTO(N,2)-SIGTO(N,1))/2 )**2+SIGTO(N,3)**2)
      SMAXTO(N)=C1+D1
      SMINTO(N)=C1-D1
      IF(SIGTO(N,2) EQ.SMINTO(N)) GO TO 701
      ANGTO(N)=57 29578*ATAN(SIGTO(N,3)/(SIGTO(N,2)-SMINTO(N)))
      GO TO 702
  701 ANGTO(N)=90 0
  702 CONTINUE
      E1=(STRTO(N,1)+STRTO(N,2))/2.
      F1=SQRT(((STRTO(N,2)-STRTO(N,1))/2 )**2+(STRTO(N,3)/2.)**2)
      EMAXTO(N)=E1+F1
      EMINTO(N)=E1-F1
      IF(STRTO(N,2).EQ.EMINTO(N)) GO TO 703
      EANGTO(N)=57.29578*ATAN((STRTO(N,3)/2.)/(STRTO(N,2)-EMINTO(N)))
```

```
      GO TO 704
  703 EANGTO(N)=90.0
  704 CONTINUE
C
C                   PERFORM NON-LINEAR ANALYSIS
C
  301 CONTINUE
      CALL CSTNL(NLFLAG)
      IF(NLFLAG EQ.1.AND NITER.NE.NOITER) RETURN
C40   WRITE(6,299)
C299  FORMAT('1',5X,'STRESSES AND STRAINS IN CST ELEMENTS',///)
C     WRITE(6,298)
C298  FORMAT(' ',T2,'ELEM',T14,'SIG 1',T29,'SIG 3',T44,'TXY',T59,
C    +'SIG 2',T75,'E 1',T90,'E 3',T104,'EXY',//)
C     SLIM=0.01*FORCE(NE,2)
C     DO 302 N=1,NE
C     IF(IMAT(N) EQ.2) GO TO 302
C     IF(ABS(FORCE(N,2)).GT.SLIM)
C    +WRITE(6,303) N,(FORCE(N,I),I=1,4),(STR(N,I),I=1,3)
C303  FORMAT(' ',I5,7(5X,F10.5))
C302  CONTINUE
C     WRITE(6,310)
C310  FORMAT('1',5X,'TOTAL STRESSES AND STRAINS IN CST ELEMENTS',///)
C     WRITE(6,298)
C     DO 305 N=1,NE
C     IF(IMAT(N).EQ 2) GO TO 305
C     WRITE(6,303) N,(SIGTO(N,I),I=1,4),(STRTO(N,I),I=1,3)
C305  CONTINUE
C     WRITE(6,307)
C307  FORMAT('1',5X,'PRINCIPAL STRESSES AND STRAINS',///)
C     WRITE(6,308)
C308  FORMAT(' ',T4,'ELEM',T16,'SIGMAX',T31,'SIGMIN',T47,'EMAX',T62,
C    +'EMIN'/T17,'(KPA)',T32,'(KPA)',//)
C     SLIM=0 01*ABS(SMINTO(NE))
C     DO 309 N=1,NE
C     IF(IMAT(N).EQ.2) GO TO 309
C     SHMAX=(SMAXTO(N)-SMINTO(N))/2
C     IF(ABS(SMINTO(N)) GT.SLIM)
C    +WRITE(6,303) N,SMAXTO(N),SMINTO(N),EMAXTO(N),EMINTO(N)
C     TSTRO(N)=TSTRO(N)+EMINTO(N)
C309  CONTINUE
C311  CONTINUE
      RETURN
      END
C
C
      SUBROUTINE REAC(J,M,N)
C
      COMMON/CONTR/NP,NE,NB,NDF,NCN,NSZF,ITITL(50),IPRIN,SFLAG,FPL,DELPL
C
      COMMON/DATA/CORD(580,2),NOP(999,4),IMAT(1100),NBC(580),CODE(700),
     +UX(700),UY(700),T(1100),ORX(1100),ORY(1100),PRCORD(580,2)
C
      COMMON/STIFF/ESTIFM(12,12),A(3,6),B(3,6),SK(1100,92),AREA(1100),
     +C(1100),R(8),H(8),D(1100),AR(2000),AS(999,3,6),BS(999,3,6),NBAND
C
      COMMON/ANAL/NOINC,KOUNT,NITER,NOITER,CORDI(580,2)
C
```

```
      COMMON/STRES/DISTO(2,580),SIGTO(999,4),STRTO(999,3),SMAXTO(1100),
     +SMINTO(1100),ANGTO(1100),EANGTO(1100),EMAXTO(1100),EMINTO(1100),
     +FORCE(999,4),STR(999,3),PSIGTO(999,4),PSTRTO(999,3),PDISTO(2,580),
     +PEMINT(1100),PSMINT(1100),EXSH(1100)
C
      COMMON/JOINT/T1(8,8),BL(8,8),AL(1100),ANG(1100),DKS(1100),DKN(1000
     +),SD(2,2),W(999,2),P(999,2),V(999,2),AVP(999,2),CV(999,2),
     +CAVP(999,2),PCV(999,2),PCAVP(999,2),B1(8,8),IFAIL(1100),ALO(1100)
C
      DIMENSION U(10),TEMP(10)
C
C                    RECALCULATE STIFFNESS MATRIX FOR ELEMENT N
C
      IF(IMAT(N).EQ.2) GO TO 504
      CALL CSTK(N)
      J1=2*NOP(N,1)-1
      J2=2*NOP(N,1)
      K1=2*NOP(N,2)-1
      K2=2*NOP(N,2)
      L1=2*NOP(N,3)-1
      L2=2*NOP(N,3)
      U(1)=C(J1)
      U(2)=C(J2)
      U(3)=C(K1)
      U(4)=C(K2)
      U(5)=C(L1)
      U(6)=C(L2)
      IF(CODE(M).NE 1.) GO TO 501
      I=2*J-1
      K=2*NOP(N,J)-1
C     AR(K)=0
      SUM=0.0
      DO 425 L=1,6
  425 SUM=SUM+ESTIFM(I,L)*U(L)
      AR(K)=AR(K)+SUM
      GO TO 503
  501 IF(CODE(M).EQ 2.) GO TO 502
      I=2*J-1
      K=2*NOP(N,J)-1
      SUM=0 0
      DO 426 L=1,6
  426 SUM=SUM+ESTIFM(I,L)*U(L)
      AR(K)=AR(K)+SUM
  502 I=2*J
      K=2*NOP(N,J)
      SUM=0.0
      DO 427 L=1,6
  427 SUM=SUM+ESTIFM(I,L)*U(L)
      AR(K)=AR(K)+SUM
  503 CONTINUE
      GO TO 3
 504  CALL JOINTK(N)
      I1=2*NOP(N,1)-1
      I2=2*NOP(N,1)
      J1=2*NOP(N,2)-1
      J2=2*NOP(N,2)
      K1=2*NOP(N,3)-1
      K2=2*NOP(N,3)
```

```
      L1=2*NOP(N,4)-1
      L2=2*NOP(N,4)
      U(1)=C(I1)
      U(2)=C(I2)
      U(3)=C(J1)
      U(4)=C(J2)
      U(5)=C(K1)
      U(6)=C(K2)
      U(7)=C(L1)
      U(8)=C(L2)
      IF(CODE(M).NE.1) GO TO 1
      I=2*J-1
      K=2*NOP(N,J)-1
      SUM=0.0
      DO 2 L=1,8
 2    SUM=SUM+ESTIFM(I,L)*U(L)
      AR(K)=AR(K)+SUM
      GO TO 3
 1    IF(CODE(M).EQ 2 ) GO TO 4
      I=2*J-1
      K=2*NOP(N,J)-1
      SUM=0 0
      DO 5 L=1,8
 5    SUM=SUM+ESTIFM(I,L)*U(L)
      AR(K)=AR(K)+SUM
 4    I=2*J
      K=2*NOP(N,J)
      SUM=0 0
      DO 6 L=1,8
 6    SUM=SUM+ESTIFM(I,L)*U(L)
      AR(K)=AR(K)+SUM
 3    CONTINUE
      RETURN
      END
C
C
      SUBROUTINE UPDATE(AREAO,PAREA,PDIS,YCTOP)
      COMMON/CONTR/NP,NE,NB,NDF,NCN,NSZF,ITITL(50),IPRIN,SFLAG,FPL,DELPL
      COMMON/DATA/CORD(580,2),NOP(999,4),IMAT(1100),NBC(580),CODE(700),
     +UX(700),UY(700),T(1100),ORX(1100),ORY(1100),PRCORD(580,2)
      COMMON/STIFF/ESTIFM(12,12),A(3,6),B(3,6),SK(1100,92),AREA(1100),
     +C(1100),R(8),H(8),D(1100),AR(2000),AS(999,3,6),BS(999,3,6),NBAND
      COMMON/ANAL/NOINC,KOUNT,NITER,NOITER,CORDI(580,2)
      COMMON/STRES/DISTO(2,580),SIGTO(999,4),STRTO(999,3),SMAXTO(1100),
     +SMINTO(1100),ANGTO(1100),EANGTO(1100),EMAXTO(1100),EMINTO(1100),
     +FORCE(999,4),STR(999,3),PSIGTO(999,4),PSTRTO(999,3),PDISTO(2,580),
     +PEMINT(1100),PSMINT(1100),EXSH(1100)
      COMMON/JOINT/T1(8,8),BL(8,8),AL(1100),ANG(1100),DKS(1100),DKN(1000
     +),SD(2,2),W(999,2),P(999,2),V(999,2),AVP(999,2),CV(999,2),
     +CAVP(999,2),PCV(999,2),PCAVP(999,2),B1(8,8),IFAIL(1100),ALO(1100)
      COMMON/SNDATA/STRESS(40),STRAIN(40),SHEAR(40),DENSSH(40),
     +GAMMAO,NPTSCC,NPTSSH,STIFFS
      COMMON/ELAS/EE(1100),ENU(1100)
C
      DIMENSION DIS(2,580),AREAO(1100),PAREA(1100)
      EQUIVALENCE(DIS,C)
C
C   UPDATE AND RECORD NODAL COORDINATES
```

```
      DO 100 N=1,NP
      CORD(N,1)=CORD(N,1)+DIS(1,N)
      CORD(N,2)=CORD(N,2)+DIS(2,N)
      PRCORD(N,1)=CORD(N,1)
      PRCORD(N,2)=CORD(N,2)
  100 CONTINUE
C   COMPUTE NEW DENSITY FOR CONTINUUM ELEMENTS AND
C   UPDATED SHEAR STRESS AND STIFFNESS IN JOINT ELEMENTS
      IF(IPRIN.EQ 1) WRITE(6,610)
  610 FORMAT(' ',////,T5,'DENSITY AND STATE OF STRAIN IN CONTINUUM ELEME
     +NTS',///T14,'ELEM',T22,'INITIAL AREA',T37,'PRESENT AREA',T55,'DENS
     +ITY',T66,'EQUIV AX.STRAIN',T86,'SHEAR STIFFNESS',T106,'SHEAR STRES
     +S'/T28,'(M2)',T42,'(M2)',T55,'(MG/M3)',T89,'(KN/M3)',T111,'(KPA)',
     +///)
      IPUP=1
      DO 200 J=1,NE
      IF(IMAT(J).EQ 2) GO TO 201
      CALL DENSIT(CORD,J,AREAO,PAREA,DENS,IPUP)
      GO TO 200
  201 IF(IFAIL(J).LT.1) GO TO 200
      DKS(J)=0.0001
      IF(IPRIN EQ.1) WRITE(6,202) J,DKS(J),CAVP(J,1)
  202 FORMAT(' ',T6,I10,T88,F9.3,T108,F9.4)
  200 CONTINUE
      RETURN
      END
      SUBROUTINE DENSIT(SCORD,N,AREAO,PAREA,DENS,IPUP)
      COMMON/CONTR/NP,NE,NB,NDF,NCN,NSZF,ITITL(50),IPRIN,SFLAG,FPL,DELPL
      COMMON/DATA/CORD(580,2),NOP(999,4),IMAT(1100),NBC(580),CODE(700),
     +UX(700),UY(700),T(1100),ORX(1100),ORY(1100),PRCORD(580,2)
      COMMON/SNDATA/STRESS(40),STRAIN(40),SHEAR(40),DENSSH(40),
     +GAMMAO,NPTSCC,NPTSSH,STIFFS
      COMMON/STRES/DISTO(2,580),SIGTO(999,4),STRTO(999,3),SMAXTO(1100),
     +SMINTO(1100),ANGTO(1100),EANGTO(1100),EMAXTO(1100),EMINTO(1100),
     +FORCE(999,4),STR(999,3),PSIGTO(999,4),PSTRTO(999,3),PDISTO(2,580),
     +PEMINT(1100),PSMINT(1100),EXSH(1100)
      COMMON/ANAL/NOINC,KOUNT,NITER,NOITER,CORDI(580,2)
      DIMENSION SCORD(580,2),AREAO(1100),PAREA(1100)
C.  COMPUTE PRESENT AREA OF CST ELEMENT
      I=NOP(N,1)
      J=NOP(N,2)
      K=NOP(N,3)
      AJ=SCORD(J,1)-SCORD(I,1)
      AK=SCORD(K,1)-SCORD(I,1)
      BJ=SCORD(J,2)-SCORD(I,2)
      BK=SCORD(K,2)-SCORD(I,2)
      OX=(SCORD(I,1)+SCORD(J,1)+SCORD(K,1))*0 333333
      OY=(SCORD(I,2)+SCORD(J,2)+SCORD(K,2))*0 333333
      XRAT=(CORD(7,1)-OX)/FPL
      YRAT=OY/FPL
      PAREA(N)=(AJ*BK-AK*BJ)/2.
C.  COMPUTE DENSITY IN CST ELEMENT
      DENS=(AREAO(N)/PAREA(N))*GAMMAO
C.  COMPUTE EQUIVALENT TOTAL AXIAL STRAIN
      IF(IPUP EQ.0) RETURN
      PEMINT(N)=1-GAMMAO/DENS
      IF(DENS.LT GAMMAO) PEMINT(N)=0
      IF(IPRIN EQ.1)
```

```
      +WRITE(6,1) N,AREAO(N),PAREA(N),DENS,PEMINT(N),XRAT,YRAT
 1     FORMAT(' ',5X,I10,4F15.6,5X,'X.DIST (PL#S)',F10.6,5X,'Y DIST (PL#S
      +)',F10 6)
       RETURN
       END
       SUBROUTINE SHDJNT(IMAT,NOP,TCORD,AREAO,DIS,IPUP,FSHSTE,ORY)
       COMMON/CONTR/NP,NE,NB,NDF,NCN,NSZF,ITITL(50),IPRIN,SFLAG,FPL,DELPL
       COMMON/SNDATA/STRESS(40),STRAIN(40),SHEAR(40),DENSSH(40),
      +GAMMAO,NPTSCC,NPTSSH,STIFFS
       COMMON/STRES/DISTO(2,580),SIGTO(999,4),STRTO(999,3),SMAXTO(1100),
      +SMINTO(1100),ANGTO(1100),EANGTO(1100),EMAXTO(1100),EMINTO(1100),
      +FORCE(999,4),STR(999,3),PSIGTO(999,4),PSTRTO(999,3),PDISTO(2,580),
      +PEMINT(1100),PSMINT(1100),EXSH(1100)
       COMMON/JOINT/T1(8,8),BL(8,8),AL(1100),ANG(1100),DKS(1100),DKN(1000
      +),SD(2,2),W(999,2),P(999,2),V(999,2),AVP(999,2),CV(999,2),
      +CAVP(999,2),PCV(999,2),PCAVP(999,2),B1(8,8),IFAIL(1100),ALO(1100)
       DIMENSION IMAT(1100),TCORD(580,2),FSHSTA(1100)
       DIMENSION NOP(999,4),ORY(1100),DENSF(1100),DISTF(1100)
       DIMENSION AREAO(1100),PAREA(1100),DIS(2,580),FSHSTE(1100)
C...COMPUTE  DENSITY ACROSS JOINT ELEMENTS
       IF(IPRIN EQ.1) WRITE(6,3)
 3     FORMAT(' ',////,T5,'CHECK FAILURE OF JOINT ELEMENTS'///T3,'J.EL',
      +T8,'T.EL',T16,'L',T21,'UPDT AV.DS',T33,'SH.RES.',T42,'SH.STIF.',
      +T52,'PREV STRE',T64,'SH STRE',T75,'TOT.STRE',T86,'FAILURE STRAIN',
      +T110,'TOT STRAIN'/
      +T15,'(M)',T22,'(MG/M3)',T34,'(KPA)',T43,'(KN/M3)',T53,'(KPA)',T63,
      +'(KPA)',T77,'(KPA)',///)
       DO 20 N=1,NE
       IF(IMAT(N) EQ 1) GO TO 20
       IA=N+1
       IB=N-1
C   .COMPUTE AVERAGE DENSITY ACROSS PLANE OF SHEAR OF JOINT ELEMENT
C    FROM DEFORMATIONS OF PRESENT INCREMENT
       CALL DENSIT(TCORD,IA,AREAO,PAREA,DENS1,IPUP)
C      CALL DENSIT(TCORD,IB,AREAO,PAREA,DENS2,IPUP)
       D2=DENS1
       IF(D2 LT.GAMMAO) D2=GAMMAO
C...INTERPOLATE FROM SHEAR STRENGTH-DENSITY CURVE TO GET SHEAR STRENGTH
       CALL INTERP(NPTSSH,D2,DENSSH,SHEAR,SHINT)
C...IS JOINT ELEMENT SHEARING ?
       SHSTRA=V(N,1)/ALO(N)
       SHSTRE=AVP(N,1)
       PRESTA=PCV(N,1)
       PRESTE=PCAVP(N,1)
       STRTO(N,1)=CV(N,1)/ALO(N)
C. .COMPARE CUMULATIVE SHEAR STRESS TO SHEAR STRENGTH AND PRINT INFO
       IF(ABS(CAVP(N,1)) LE SHINT.AND.IFAIL(N).LT.1) GO TO 50
       IFAIL(N)=IFAIL(N)+1
       IF(IFAIL(N).NE.1) GO TO 60
       FSHSTA(N)=SHINT/DKS(N)/ALO(N)
       FSHSTE(N)=SHINT
       DENSF(N)=D2
       DISTF(N)=ORY(N)/FPL
C    COMPUTE EXCESS SHEAR STRESS IN JOINT ELEMENT
 60    I=NOP(N,1)
       J=NOP(N,2)
       K=NOP(N,3)
       L=NOP(N,4)
```

```
      CENT=(TCORD(I,2)+TCORD(J,2)+TCORD(K,2)+TCORD(L,2))/4.
      SRAT=(CENT-DISTO(2,6))/DISTO(2,6)
C     WRITE(6,*) N,CENT,DISTO(2,5),SRAT
C     ARG=-4.0*3.14159265*(ABS(STRTO(N,1))-FSHSTA(N))
      EXSH(N)=ABS(CAVP(N,1))-FSHSTE(N)
      IF(CAVP(N,1).GT.0) EXSH(N)=-EXSH(N)
      IF(IPRIN.EQ.1)
     +WRITE(6,5) N,IA,AL(N),D2,SHINT,DKS(N),PRESTE,AVP(N,1),CAVP(N,1),
     +FSHSTA(N),STRTO(N,1)
      IF(IFAIL(N).GE.1) WRITE(6,666) N,DENSF(N),DISTF(N)
 666  FORMAT(' ',/,'JOINT ELEMENT NO',I10,10X,'DENSITY AT FAILURE (MG/M3
     +)',F15.6,10X,'DISTANCE FROM PLATE (PL S)',F15.6)
      GO TO 20
 50   IF(IPRIN.EQ.1)
     +WRITE(6,4) N,IA,AL(N),D2,SHINT,DKS(N),PRESTE,AVP(N,1),CAVP(N,1)
 4    FORMAT(' ',2I5,F7.4,F10.6,F11.4,F10 4,F11.6,F10.6,F12.6)
 5    FORMAT(' ',2I5,F7.4,F10.6,F11.4,F10 4,F11.6,F10.6,F12.6,'    SH',4X
     +,F12.6,T113,F10.6)
      IF(IFAIL(N).GE.1) WRITE(6,666) N,DENSF(N),DISTF(N)
 20   CONTINUE
      WRITE(6,100) SRAT
 100  FORMAT(' ',///,5X,'SHEAR DEPTH TO PLATE SINKAGE RATIO',F15 6)
      RETURN
      END
      SUBROUTINE INTERP(NPTS,X,XX,YY,Y)
      DIMENSION XX(40),YY(40),SL(40)
C. .INTERPOLATION SUBROUTINE
C     WRITE(6,*) NPTS
      DO 2  I=2,NPTS
      SL(I-1)=(YY(I)-YY(I-1))/(XX(I)-XX(I-1))
C     WRITE(6,*) SL(I-1),YY(I),YY(I-1),XX(I),XX(I-1)
 2    CONTINUE
      IF(X NE XX(NPTS)) GO TO 5
      Y=YY(NPTS)
      RETURN
 5    DO 3  I=2,NPTS
      IF(X.GE.XX(I-1).AND.X.LT.XX(I)) GO TO 4
 3    CONTINUE
 4    Y=YY(I-1)+SL(I-1)*(X-XX(I-1))
C     WRITE(6,*) Y,YY(I-1),SL(I),X,XX(I-1)
      RETURN
      END
      SUBROUTINE CSTNL(NLFLAG)
      COMMON/CONTR/NP,NE,NB,NDF,NCN,NSZF,ITITL(50),IPRIN,SFLAG,FPL,DELPL
      COMMON/STRES/DISTO(2,580),SIGTO(999,4),STRTO(999,3),SMAXTO(1100),
     +SMINTO(1100),ANGTO(1100),EANGTO(1100),EMAXTO(1100),EMINTO(1100),
     +FORCE(999,4),STR(999,3),PSIGTO(999,4),PSTRTO(999,3),PDISTO(2,580),
     +PEMINT(1100),PSMINT(1100),EXSH(1100)
      COMMON/SNDATA/STRESS(40),STRAIN(40),SHEAR(40),DENSSH(40),
     +GAMMAO,NPTSCC,NPTSSH,STIFFS
      COMMON/DATA/CORD(580,2),NOP(999,4),IMAT(1100),NBC(580),CODE(700),
     +UX(700),UY(700),T(1100),ORX(1100),ORY(1100),PRCORD(580,2)
      COMMON/ANAL/NOINC,KOUNT,NITER,NOITER,CORDI(580,2)
      COMMON/ELAS/EE(1100),ENU(1100)
      DIMENSION STRE(40),STRA(40),PRE(999),ERRMAX(999),ERRORP(999),
     +SRSIP(999)
      NLFLAG=0
      TOLERR=5.0
```

```
      ERROR=0.0
      ERRHI=0.0
      DO 200 N=1,NE
      ERRMAX(N)=0 0
      ERRORP(N)=0 0
200   CONTINUE
      DO 1 N=1,NE
      IF(IMAT(N).EQ.2) GO TO 1
      PRE(N)=EE(N)
      STRINT=ABS(EMINTO(N))
      IF(ABS(PEMINT(N)).LT.0 1.OR.ABS(EMINTO(N)).LT 0.0001) GO TO 100
C ..COMPUTE STRESS-STRAIN CURVE WITH RESPECT TO PREVIOUS EQUIVALENT
C   PRINCIPAL STRESS AND STRAIN
      DO 11 I=1,NPTSCC
      STRE(I)=STRESS(I)-ABS(PSMINT(N))
      STRA(I)=STRAIN(I)-ABS(PEMINT(N))
11    CONTINUE
C...CHECK FOR NON-LINEARITY
      CALL INTERP(NPTSCC,STRINT,STRA,STRE,SIGINT)
      ERRORP(N)=100*((ABS(SMINTO(N))-ABS(SIGINT))/ABS(SIGINT))
      ERROR=ABS(ERRORP(N))
      IF(ERROR.GT ERRHI) ERRHI=ERROR
      ERRMAX(N)=ERRHI
      SRSIP(N)=SIGINT
      IF(ERRHI LE.TOLERR) GO TO 1
C. .COMPUTE ELASTIC MODULUS FOR NEXT ITERATION
      IF(NITER NE NOITER) EE(N)=SIGINT/STRINT
      NLFLAG=1
      GO TO 1
100   ERRORP(N)=0 0
      ERRMAX(N)=ERRHI
1     CONTINUE
      IF(NLFLAG.EQ.1 AND NITER.NE NOITER) RETURN
      IF(IPRIN.EQ.0.OR SFLAG.EQ.1.) RETURN
      WRITE(6,10)
10    FORMAT(' ',////,T22,'NON LINEAR ANALYSIS',///,T6,'N',T10,'PEMINTO'
     +,T20,'PSMINTO',T31,'EMINTO',T41,'SMINTO',T48,'SIGINT',T58,'ERROR',
     +T68,'MAX.ERROR',T80,'E USED',T92,'E NEW',T104,'EMAXTO',T114,
     +'SMAXTO'/T21,'(KPA)',T42,'(KPA)',T49,'(KPA)',T81,'(KPA)',T92,
     +'(KPA)',T105,'(KPA)',T115,'(KPA)',///)
      DO 300 N=1,NE
      IF(IMAT(N).EQ.2) GO TO 300
      IF(ABS(PEMINT(N)).GE.0 1)
     +WRITE(6,20) N,PEMINT(N),PSMINT(N),EMINTO(N),SMINTO(N),
     +SRSIP(N),ERRORP(N),ERRMAX(N),PRE(N),EE(N),EMAXTO(N),SMAXTO(N)
      IF(ABS(PEMINT(N)).LT 0 1)
     +WRITE(6,22) N,PEMINT(N),PSMINT(N),EMINTO(N),SMINTO(N),
     +ERRORP(N),ERRMAX(N),PRE(N),EE(N),EMAXTO(N),SMAXTO(N)
20    FORMAT(' ',I5,11F10.5)
22    FORMAT(' ',I5,4F10.5,10X,6F10.5)
300   CONTINUE
      RETURN
      END
      SUBROUTINE JSTRES
      COMMON/CONTR/NP,NE,NB,NDF,NCN,NSZF,ITITL(50),IPRIN,SFLAG,FPL,DELPL
C
      COMMON/DATA/CORD(580,2),NOP(999,4),IMAT(1100),NBC(580),CODE(700),
     +UX(700),UY(700),T(1100),ORX(1100),ORY(1100),PRCORD(580,2)
```

```
C
      COMMON/STIFF/ESTIFM(12,12),A(3,6),B(3,6),SK(1100,92),AREA(1100),
     +C(1100),R(8),H(8),D(1100),AR(2000),AS(999,3,6),BS(999,3,6),NBAND
C
      COMMON/ANAL/NOINC,KOUNT,NITER,NOITER,CORDI(580,2)
      COMMON/JOINT/T1(8,8),BL(8,8),AL(1100),ANG(1100),DKS(1100),DKN(1000
     +),SD(2,2),W(999,2),P(999,2),V(999,2),AVP(999,2),CV(999,2),
     +CAVP(999,2),PCV(999,2),PCAVP(999,2),B1(8,8),IFAIL(1100),ALO(1100)
      DIMENSION DIS(2,580)
      EQUIVALENCE (DIS,C)
C      IF(IPRIN.EQ.1) WRITE(6,6000)
C      IF(IPRIN.EQ.1) WRITE(6,604)
      DO 301 N=1,NE
      IF(NOP(N,3).EQ.NOP(N,4)) GO TO 301
C
C                      FORM STRESS-STRAIN MATRIX
C
      DO 1 I=1,2
      DO 1 J=1,2
 1    SD(I,J)=0.0
      SD(1,1)=DKS(N)
      SD(2,2)=DKN(N)
      DO 7 I=1,2
 7    V(N,I)=0:0
C
C  DETERMINE TRANSFORMATION MATRIX
      E=COS(ANG(N))
      S=SIN(ANG(N))
      DO 13 I=1,8
      DO 13 J=1,8
 13   T1(I,J)=0.0
      DO 14 I=1,8
      J=I
 14   T1(I,J)=E
      DO 15 I=1,7,2
      J=I+1
 15   T1(I,J)=S
      DO 16 I=2,8,2
      J=I-1
 16   T1(I,J)=-S
C
C  ELEMENT NODAL DISPLACEMENTS
C
      DO 260 I=1,4
      M=NOP(N,I)
      IF(M EQ.0) GO TO 260
      K=(I-1)*NDF
      DO 240 J=1,NDF
      IJ=J+K
 240  R(IJ)=DIS(J,M)
 260  CONTINUE
C
C              DISPLACEMENTS WITH RESPECT TO ELEMENT LOCAL AXES
C
      DO 12 I=1,8
      H(I)=0.0
      DO 12 IJ=1,8
 12   H(I)=H(I)+T1(I,IJ)*R(IJ)
```

```
      X=-AL(N)/2.
      DO 1000 II=1,2
C
C             FORM STRAIN-DISPLACEMENT MATRIX
C
      F=1 -2 *X/AL(N)
      G=1.+2 *X/AL(N)
      DO 2 I=1,2
      DO 2 J=1,8
    2 B1(I,J)=0.0
      B1(1,1)=-F/2
      B1(1,3)=-G/2.
      B1(1,5)=G/2
      B1(1,7)=F/2.
      B1(2,2)=-F/2
      B1(2,4)=-G/2
      B1(2,6)=G/2.
      B1(2,8)=F/2.
C
C              FORM RELATIVE DISPLACEMENT VECTOR
C
      DO 3 I=1,2
      W(N,I)=0 0
      DO 3 J=1,8
    3 W(N,I)=W(N,I)+B1(I,J)*H(J)
C
C       AVERAGE RELATIVE DISPLACEMENT
C
      DO 11 I = 1,2
   11 V(N,I)=V(N,I)+W(N,I)
C
C  FIND SHEAR AND NORMAL STRESSES
C
      DO 4 I = 1,2
      P(N,I)=0 0
      DO 4 J=1,2
 4    P(N,I)=P(N,I)+SD(I,J)*W(N,J)
 1000 X=X+AL(N)
C
C       FIND AVERAGE SHEAR AND NORMAL STRESSES ACROSS THE ELEMENT
C
      DO 10 I=1,2
 10   V(N,I)=V(N,I)/2
      DO 6 I=1,2
      AVP(N,I) = 0.0
      DO 6 J=1,2
  6   AVP(N,I) = AVP(N,I) + SD(I,J) * V(N,J)
      ANG(N)=ANG(N)*(360 /(2.0*3.141593))
C     IF(IPRIN.EQ.1) WRITE(6,4000) N,ANG(N),AL(N),ORX(N),ORY(N),V(N,1),
C    +V(N,2),AVP(N,1),AVP(N,2)
 301  CONTINUE
C
C             CUMULATIVE AVERAGE STRESSES AND DISPLACEMENTS
C
C     IF(IPRIN EQ 1) WRITE(6,5000)
C     IF(IPRIN.EQ 1) WRITE(6,605)
      DO 2000 N=1,NE
      IF(NOP(N,3) EQ NOP(N,4)) GO TO 2000
```

```
      DO 9 I=1,2
      PCV(N,I)=CV(N,I)
      PCAVP(N,I)=CAVP(N,I)
      CV(N,I) = CV(N,I) + V(N,I)
      CAVP(N,I) = CAVP(N,I) + AVP(N,I)
 9    CONTINUE
 601  DO 17 I=1,2
      CV(N,I) = PCV(N,I) + V(N,I)
      CAVP(N,I)=PCAVP(N,I)+AVP(N,I)
 17   CONTINUE
C     IF(IPRIN.EQ.1) WRITE(6,300) N,CV(N,1),CV(N,2),CAVP(N,1),CAVP(N,2),
C    +DKS(N),DKN(N)
4000  FORMAT('0',I5,4F10.3,2F15.7,2F14.6)
300   FORMAT('0',I5,4F15.7,F15.7,E15.5)
2000  CONTINUE
6000  FORMAT('1',5X,'TABLE 9 - STRESSES AND DISPLACEMENTS IN JOINT ELEME
     +NTS'/)
5000  FORMAT(//,5X,'TABLE 10 - CUMULATIVE STRESSES AND DISPLACEMENTS IN
     + JOINT ELEMENTS'/)
604   FORMAT('0',5X,'N',4X,'ANGLE',4X,'LENGTH',6X,'CENTROID',12X,'AVERAG
     +E DISPLACEMENT',13X,'AVERAGE STRESS'/32X,'X',9X,'Y',9X,'SHEAR',9X,
     +'NORMAL',10X,'SHEAR',9X,'NORMAL')
605   FORMAT('0',4X,'N',5X,'CUMULATIVE DISPLACEMENTS',4X,'CUMULATIVE STR
     +ESSES',10X,'STIFFNESS VALUES'/12X,'SHEAR',10X,'NORMAL',9X,'SHEAR',
     +10X,'NORMAL',8X,'SHEAR',11X,'NORMAL')
      RETURN
      END
```